

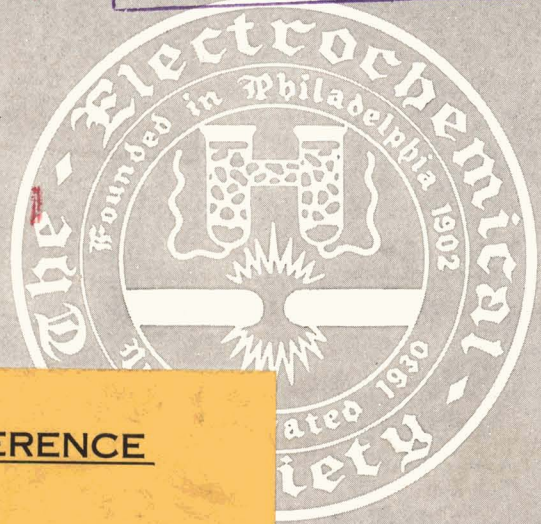
JOURNAL OF THE  
**Electrochemical  
Society**

Vol. 108, No. 11

November 1961

แผนกห้องสมุด คณะวิทยาศาสตร์  
กระทรวงอุตสาหกรรม

MERCK SHARP & DOHME  
RESEARCH LABORATORIES  
NOV 1961  
LIBRARY, RARWAY, N. J.



FOR REFERENCE

This Journal Must Be Kept On File  
In The Library Until

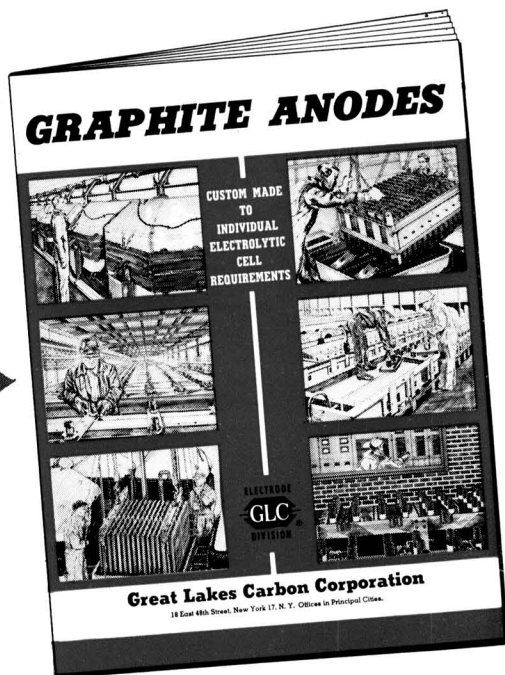
DEC 15 1961



CO., Inc.  
460

Handwritten initials or signature.

# GET YOUR FREE COPY OF THIS INFORMATIVE, ILLUSTRATED BROCHURE



Everyone connected with electrolytic cell operations should have a copy of our new brochure GRAPHITE ANODES. It contains a wealth of useful information.

Here you will find tables of standard sizes and grades of square and rectangular anodes for diaphragm and mercury cells...reasons why anodes custom made to individual cell requirements are more economical and efficient...a brief review of our special anode production and machining facilities...and an explanation of our technical exchange program which has helped our customers lower cell operating costs.

**Write us for a copy of GRAPHITE ANODES—  
it is yours for the asking.**



**GREAT LAKES CARBON CORPORATION**

18 EAST 48TH STREET, NEW YORK 17, N. Y.



## EDITORIAL STAFF

C. L. Faust, Chairman, Publication Committee  
Cecil V. King, Editor  
Norman Hackerman, Technical Editor  
Ruth G. Sterns, Managing Editor  
U. B. Thomas, News Editor  
H. W. Salzberg, Book Review Editor  
Natalie Michalski, Assistant Editor

## DIVISIONAL EDITORS

W. C. Vosburgh, Battery  
Milton Stern, Corrosion  
R. T. Foley, Corrosion  
Louis J. Frisco, Electric Insulation  
Seymour Senderoff, Electrodeposition  
H. C. Froelich, Electronics  
Ephraim Banks, Electronics  
Ernest Paskell, Electronics—Semiconductors  
D. R. Frankl, Electronics—Semiconductors  
Sherlock Swann, Jr., Electro-Organic  
Stanley Wawzonek, Electro-Organic  
John M. Blocher, Jr., Electrothermics and Metallurgy  
J. H. Westbrook, Electrothermics and Metallurgy  
N. J. Johnson, Industrial Electrolytic  
C. W. Tobias, Theoretical Electrochemistry  
A. J. deBethune, Theoretical Electrochemistry  
R. M. Hurd, Theoretical Electrochemistry

## ADVERTISING OFFICE

ECS  
1860 Broadway, New York 23, N. Y.

## ECS OFFICERS

Henry B. Linford, President  
Columbia University, New York, N. Y.  
F. L. LaQue, Vice-President  
National Nickel Co., Inc.,  
New York, N. Y.  
W. J. Hamer, Vice-President  
National Bureau of Standards,  
Washington, D. C.  
Lyle I. Gilbertson, Vice-President  
Air Reduction Co., Murray Hill, N. J.  
Ernest G. Enck, Treasurer  
Felicity Farm,  
Gwynedd Valley, Pa.  
Ivor E. Campbell, Secretary  
National Steel Corp., Weirton, W. Va.  
Robert K. Shannon, Executive Secretary  
National Headquarters, The ECS,  
1860 Broadway, New York 23, N. Y.

Manuscripts submitted to the Journal should be sent, in triplicate, to the Editorial Office at 1860 Broadway, New York 23, N. Y. They should conform to the revised Instructions to Authors, last published on pp. 145C-146C of the July 1961 issue. Manuscripts so submitted become the property of The Electrochemical Society and may not be published elsewhere, in whole or in part, unless permission is requested of and granted by the Editor.

The Electrochemical Society does not maintain a supply of reprints of papers appearing in its Journal. A photoprint copy of any particular paper, however, may be obtained by corresponding direct with the Engineering Societies Library, 345 E. 47 St., New York, N. Y.

Inquiries re positive microfilm copies of volumes should be addressed to University Microfilms, Inc., 313 N. First St., Ann Arbor, Mich.

Walter J. Johnson, Inc., 111 Fifth Ave., New York 3, N. Y., have reprint rights to out-of-print volumes of the Journal, and also have available for sale back volumes and single issues, with the exception of the current calendar year. Anyone interested in securing back copies should correspond direct with them.

# Journal of the Electrochemical Society

NOVEMBER 1961

VOL. 108 • NO. 11

## CONTENTS

### Editorial

Water! ..... 240C

### Technical Papers

- Cathodic Reduction of Oxide Scales on Cr and Fe-25 Cr Alloy.  
*D. Caplan and M. Cohen* ..... 1005
- The Kinetics of Oxidation and Nitridation of Lithium, Calcium, Strontium, and Barium. *M. S. Chandrasekharaiah and J. L. Margrave* ..... 1008
- Impedance Phenomena in Molten Salts. *G. J. Hills and K. E. Johnson* ..... 1013
- Measurement of Stress in Very Thin Electrodeposits. *H. Watkins and A. Kolk* ..... 1018
- Electrical Characteristics of Anodized Niobium Foil and Sintered Pellets. *R. B. Hand, H. W. Ling, and T. L. Kolski* ..... 1023
- Effects of Interaction among Particles in Electroluminescent Layers. *A. T. Halpin and P. Goldberg* ..... 1028
- A Photosensitive Single Crystal p-n Junction in Lead Selenide. *M. F. Kimmitt and A. C. Prior* ..... 1034
- Single Crystal Photoconductive Detectors in Lead Selenide. *D. G. Coates, W. D. Lawson, and A. C. Prior* ..... 1038
- A Metallographic Investigation of the Damaged Layer in Abraded Germanium Surfaces. *E. N. Pugh and L. E. Samuels* ..... 1043
- The Semiconducting Properties of CdSb. *F. Ermanis and E. Miller* ..... 1048
- Molten Carbonate Electrolytes: Physical Properties, Structure, and Mechanism of Electrical Conductance. *G. J. Janz and M. R. Lorenz* ..... 1052
- Electronic Commutator Method for Determining  $E^\circ$  of Formation of Fused Halides. *A. P. Wilde and R. L. Seifert* ..... 1059
- Simultaneous Solution of Voltage and Mass Balances in Electrolytic Cells. *E. A. Grens, II, and C. W. Tobias* ..... 1063

### Technical Notes

- Rhenium-Tungsten-Carbon Interactions. *R. F. Havell and Y. Baskin* ..... 1068
- On the Electrodeposition of Arsenic and Its Role in Corrosion Prevention. *G. Wranglén* ..... 1069
- A Method for the Deposition of  $\text{SiO}_2$  at Low Temperatures. *J. Klerer* ..... 1070
- On the Preparation of the Nitrides of Aluminum and Gallium. *A. Addamiano* ..... 1072

### Technical Features

- The DSK System of Fuel Cell Electrodes. *E. W. Justi and A. W. Winsel* ..... 1073
- Materials Problems in Cesium Thermionic Converters. *L. Yang and F. D. Carpenter* ..... 1079

Current Affairs ..... 245C-252C

Published monthly by The Electrochemical Society, Inc., from Manchester, N. H., Executive Offices, Editorial Office and Circulation Dept., and Advertising Office at 1860 Broadway, New York 23, N. Y., combining the JOURNAL and TRANSACTIONS OF THE ELECTROCHEMICAL SOCIETY. Statements and opinions given in articles and papers in the JOURNAL OF THE ELECTROCHEMICAL SOCIETY are those of the contributors, and The Electrochemical Society assumes no responsibility for them. Subscription to members as part of membership service; subscription to nonmembers \$24.00. Single copies \$1.70 to members—\$2.25 to nonmembers. Copyright 1961 by The Electrochemical Society, Inc. Entered as second-class matter at the Post Office at Manchester, N. H. under the Act of August 24, 1912.

239C

กษณพจนนชคตสวคทกนณ



## Water!

*F*RESH water consumption in the United States has been estimated at about 320,000,000,000 gallons per day out of a dependable supply of 515,000,000,000 gallons. Whether these figures are accurate or not, within the next few decades the "dependable supply" will have to be revised sharply upward, or water will have to be used much more economically, or both.

An obvious way to augment the supply is by distillation of saline water, and this can be done economically in certain cases, as on naval vessels. In the little Sheikdom of Kuwait, where a hole in the ground may fill up with oil but hardly with water, modern distillation plants provide some 5,000,000 gallons per day, replacing the more expensive and inadequate transport of fresh water by ship of 15 years ago.

The U. S. Government is providing about \$10,000,000 per year to build exploratory plants for distillation and other methods of water recovery. At present, the objective is not to produce water at the lowest cost—this would require very large plants designed to operate at highest efficiency—but rather to gain experience which will point the way and be useful later.

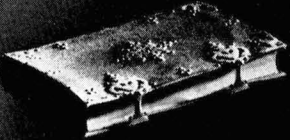
Evidently, such experience is vitally needed; everything must be learned the hard way. The distillation plant at Freeport, Texas, costing \$1,250,000, designed to run for 20 years, with a capacity of 1,000,000 gallons per day, went into operation ("on stream") last June and was proudly dedicated on June 21. On August 1, the plant had to be shut down; 1700 steel plugs had been put into heat exchanger tubes made of other metals. We are not told whether this was a planned test procedure, but we think the plumber was just up to his usual tricks. We had personal experience with a copper hot water tank, installed with iron plugs in the extra holes.

Other methods of increasing the nation's usable water supply ought to be explored. A tremendous amount of good rain water drains uselessly to the ocean, carrying away millions of tons of topsoil and often causing devastating floods. Big dams on big rivers, creating huge reservoirs, look good to politicians—and are useful, too; perhaps thousands of little dams on little streams could be equally, or even more, valuable. The government pays farmers to take fields out of production; why not pay them to conserve water at the same time? Ohio's treatment of the Miami River valley has been very satisfactory. Originally designed for flood control, it has provided wild life refuges, hunting and fishing, camp and recreation sites, as well as a stable water supply for city and industry.

Israel has considered the possibility of leading water from the Mediterranean into the Dead Sea to raise its level a few feet and increase its area. Would this change the climate of the region by allowing more evaporation, producing more rainfall? Well, Israel is in the wrong part of the world, politically, to attempt such experimentation. One wonders if it would be feasible to lead Pacific Ocean water into California's Death Valley to flood at least the lowest parts. Would this eventually affect the climate and the fresh water supply of surrounding areas? And would evaporation leave a concentrate from which chemicals could more easily be extracted?

—CVK





## THE DIARY THAT IMPRISONED PROGRESS

Nearly two centuries ago, Karl Gauss, "Prince of Mathematicians," kept a diary which was destined to become one of the most significant documents in the history of mathematics.

In his diary Gauss jotted down the results of elaborate calculations that had led him to fundamental discoveries in mathematics. But he never published these discoveries, and many of them remained undisclosed during his lifetime.

It wasn't until almost 50 years after Gauss's death that his diary was found and published. Much time and talent, meanwhile, had been spent in duplicating Gauss's efforts. Mathematical progress had been needlessly slowed.

In contrast, today's scientists and engineers are alert to the importance of sharing their findings through publication. In fact, the number of definitive papers published

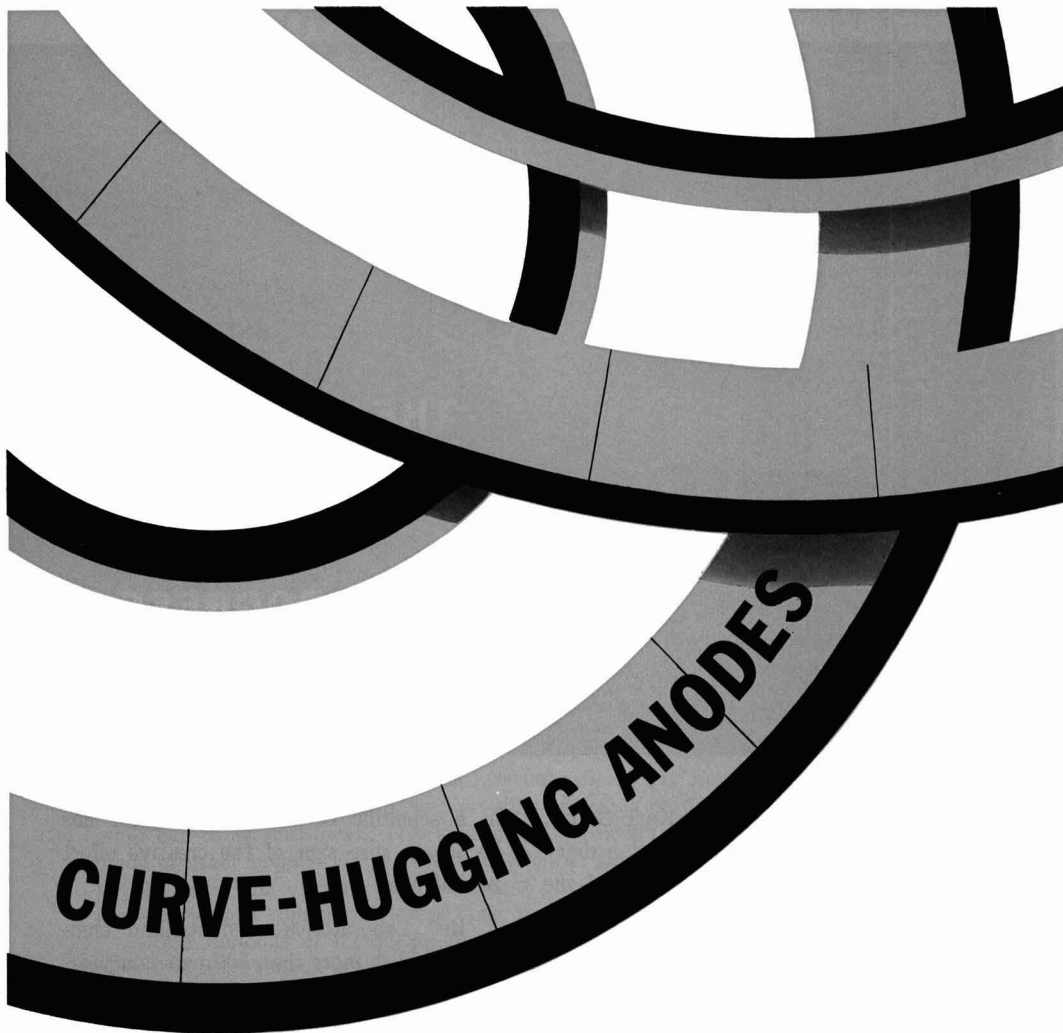
in a scientific or technological field has become a sure sign of the creative effort in that field.

Bell Laboratories scientists and engineers publish more than 800 papers a year, reporting new observations and new thinking in the arts and sciences that serve communications. They have also authored more than 50 technical books, many of which have become standard works of reference. The steady stream of new information that comes out of Bell Laboratories again reflects the scope and depth of the creativity that works to improve Bell System communications.

### BELL TELEPHONE LABORATORIES



World center of communications research and development



## **for faster, more uniform roto cylinder plating**

For plating cylinders faster and more uniformly, Anaconda now shapes Plus-4® (phosphorized copper anodes) to fit the rotogravure cylinder being plated.

This design offers possible cost savings and improved cylinder quality. For example, users of these special-shaped anodes report:

- very uniform deposits which help to cut finishing costs.
- more uniform solution of the anode which reduces scrap.

For further information, write for literature describing Curved Plus-4's, and Publication C-5 on Regular Plus-4's. Address: Anaconda American Brass Co., Waterbury 20, Conn. In Canada: Anaconda American Brass Ltd., New Toronto, Ontario.

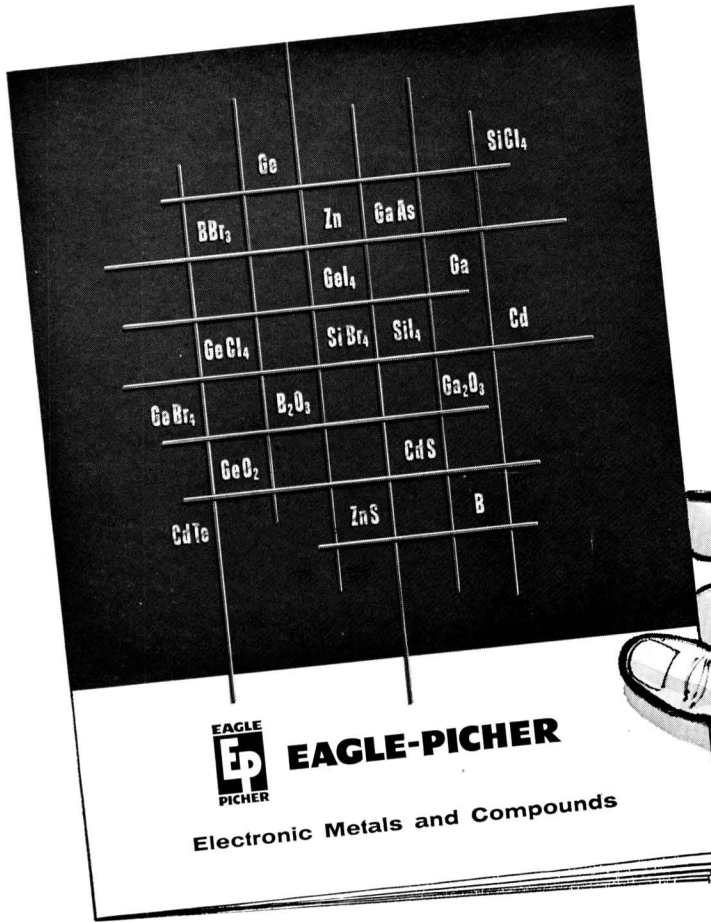
61-950

**New Low price anode**—Electranodes® are pure Anaconda copper anodes a full 1 inch thick. If you need an "economy type" anode, Electranodes are the best for the least.

**ANACONDA**®  
AMERICAN BRASS COMPANY



# Write today *for your copy of this helpful, informative book!*



Our currently most important Electronic Metals and Compounds are described fully, along with complete technical data in this book—it's yours for the asking.



First to perfect a process for recovering Germanium and first to upgrade this metal's resistivity minimum to 40 ohm-cm . . . Eagle-Picher continues to lead in the production and processing of semiconductors. We can (and do) meet the most exacting standards of purity in the manufacture of all these products:

**Germanium**, including Germanium Dioxide, Germanium First Reduction Metal, Germanium Intrinsic Metal and Germanium Single Crystals. **Gallium**, and Gallium Sesquioxide. **Special Electronic Compounds**, including Germanium Tetrachloride, Germanium Tetrabromide, Germanium Tetraiodide, Silicon Tetrachloride, Silicon Tetrabromide, Silicon Tetraiodide, Boron Tribromide and Boron Oxide. **Intermetallics**, including Gallium Arsenide, Cadmium Telluride and Zinc Sulfide. **High Purity Elements**: Boron, Cadmium, Zinc. **Cadmium Sulfide**: High Purity, Ultra High Purity.

## CLIP COUPON AND WRITE FOR YOUR COPY TODAY

The Eagle-Picher Company  
Chemicals & Metals Division  
Dept. JES-1161, Cincinnati 1, Ohio

Please send me a copy of the book,  
"Eagle-Picher Electronic Metals and Compounds."

Name \_\_\_\_\_ Title \_\_\_\_\_

Firm \_\_\_\_\_

Address \_\_\_\_\_



Since 1843

### EAGLE-PICHER

Manufacturer's/Manufacturer  
General Offices, Cincinnati 1, Ohio

# FUTURE MEETINGS OF The Electrochemical Society



**Los Angeles, Calif., May 6, 7, 8, 9, and 10, 1962**

Headquarters at the Statler Hilton Hotel

Sessions probably will be scheduled on

Electric Insulation (including sessions on Ceramics and Integrated Circuits,  
Thin Film Dielectrics and Electrolytic Capacitors, Reliability,  
and Paper), Electronics (including Luminescence,  
Semiconductors, Optical Masers, and Nonconventional Electron Emitters),  
Electrothermics and Metallurgy (including a Symposium on Thermodynamics and  
Kinetics of Gas-Condensed Phase Reactions at High Temperatures),  
Industrial Electrolytics, and Theoretical Electrochemistry

★ ★ ★

**Boston, Mass., September 16, 17, 18, 19, and 20, 1962**

Headquarters at the Statler Hilton Hotel

★ ★ ★

**Pittsburgh, Pa., April 14, 15, 16, 17, and 18, 1963**

Headquarters at the Penn Sheraton Hotel

★ ★ ★

**New York, N. Y., September 29, 30, and October 1, 2, and 3, 1963**

Headquarters at the New Yorker Hotel

★ ★ ★

**Toronto, Ont., Canada, May 3, 4, 5, 6, and 7, 1964**

Headquarters at the Royal York Hotel

Papers are now being solicited for the meeting to be held in Los Angeles, Calif., May 6-10, 1962. Triplicate copies of each abstract (*not exceeding 75 words in length*) are due at Society Headquarters, 1860 Broadway, New York 23, N. Y., *not later than December 15, 1961* in order to be included in the program. *Please indicate on abstract for which Division's symposium the paper is to be scheduled, and underline the name of the author who will present the paper.* No paper will be placed on the program unless one of the authors, or a qualified person designated by the authors, has agreed to present it in person. An author who wishes his paper considered for publication in the JOURNAL should send triplicate copies of the manuscript to the Managing Editor of the JOURNAL, 1860 Broadway, New York 23, N. Y.

Presentation of a paper at a technical meeting of the Society does not guarantee publication in the JOURNAL. However, all papers so presented become the property of The Electrochemical Society, and may not be published elsewhere, either in whole or in part, unless permission for release is requested of and granted by the Editor. Papers already published elsewhere, or submitted for publication elsewhere, are not acceptable for oral presentation except on invitation by a Divisional program Chairman.



# Cathodic Reduction of Oxide Scales on Cr and Fe-25 Cr Alloy

D. Caplan and M. Cohen

Division of Applied Chemistry, National Research Council, Ottawa, Canada

## ABSTRACT

Information on the nature of the scales on oxidized Cr and Fe-25 Cr alloy can be obtained by means of the cathodic reduction technique. At low and intermediate temperatures the oxide films formed on the alloy are two phase, consisting of a high-Fe, reducible oxide and a high-Cr, less readily reducible phase. At the higher temperature of 980° the oxide on the alloy is single phase, at least its outer portion. At 320° the cathodic reduction curve is complex, but can be interpreted with the aid of electron diffraction and microscopy.

Cathodic reduction of thin oxide films on Cr alloys has provided some information as to their characteristics (1). It was proposed that  $\text{Cr}^{6+}$  in nonstoichiometric  $\text{Cr}_2\text{O}_3$  was cathodically reduced to  $\text{Cr}^{3+}$ , that the concentration of  $\text{Cr}^{6+}$  was greater in oxides formed under more strongly oxidizing conditions, and that the hydrogen discharge potential was lower on the reduced oxide. It seemed reasonable, therefore, to use this electrochemical approach to examine the thicker oxide films obtained by oxidation at elevated temperatures. Electron diffraction, electron microscopy, and microchemical analysis assisted in the interpretation.

## Experimental

Specimens were cut from high-purity, vacuum-melted Fe, Cr and Fe-25% Cr sheet and the surfaces prepared by electropolishing in 20:1 acetic-perchloric acid, in some cases followed by a short etch in 5% (1.38N) HF. Composition and preparation details of the specimens were as previously described (1).

Oxidation was carried out in air or oxygen at temperatures from 25° to 980°C. The oxide films so produced were treated in a cathodic reduction cell in borate-HCl buffer at pH 7.6 with an impressed cathodic current of  $17 \mu\text{A}/\text{cm}^2$  (2). In spite of the high electrical resistance of the thicker films formed at higher temperatures, satisfactory results were obtained, although the potential/time curves were displaced by an amount dependent on the IR drop through the film. The thickest film studied was  $4.2 \mu$ .

The surfaces were examined before and after cathodic reduction by reflection electron diffraction and replica electron microscopy.

## Results

Figure 1 shows the cathodic reduction curves of Fe, Fe-25% Cr and Cr oxidized for 60 min at 320°C in 2 cm of oxygen. The approximate thicknesses of the films were 700Å for Fe and 100Å for the others. Previous work has indicated that reduction of  $\alpha\text{-Fe}_2\text{O}_3$  to yield  $\text{Fe}^{2+}$  in solution is responsible for the potential wave in curve 1 (2), and reduction of  $\text{Cr}^{6+}$  to  $\text{Cr}^{3+}$  in cation-deficient  $\text{Cr}_2\text{O}_3$  for the sharp minimum of curve 3 (1).

The cathodic reduction curves of five Fe-25 Cr panels oxidized in  $\text{O}_2$  as above at 320° for 60 min are shown in Fig. 2. Cathodic reduction was stopped at the points evident on the curves and the electro-

lyte analyzed for Fe and Cr. Reproducibility in cathodic reduction behavior is seen to be good. Table I summarizes the examination of the specimens of Fig. 2. The Fe content of the electrolyte is expressed in  $\mu\text{g}/\text{cm}^2$  of specimen area. Cr was never found in

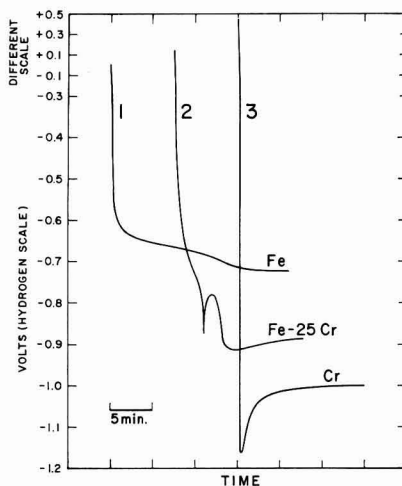


Fig. 1. Cathodic reduction curves of Fe, Fe-25 Cr and Cr oxidized 60 min at 320° in 2 cm oxygen.

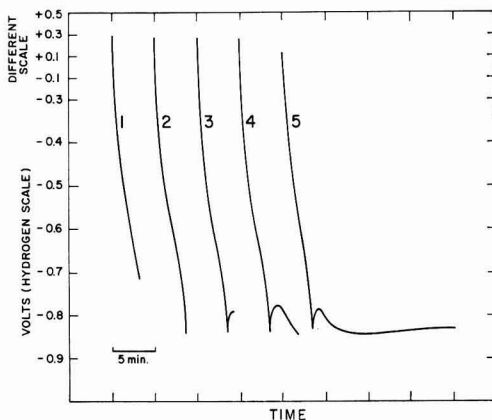


Fig. 2. Cathodic reduction curves of Fe-25 Cr oxidized 60 min at 320°. Five separate specimens; cathodic reduction stopped at different times.

Table I. Change in Fe content of electrolyte and in surface condition during cathodic reduction of Fe-25 Cr alloy oxidized at 320°

Status in Fig. 2	Fe in electrolyte $\mu\text{g}/\text{cm}^2$	Result from electron diffraction	Result from electron microscopy
a. Before C.R.	0	Oxide, random orientation, diffuse, crystallite size $<50\text{\AA}$ ; probably rhomb. $(\text{Fe, Cr})_2\text{O}_3$ .	Matte surface (Fig. 3).
b. After curve 1	1.3	Sharper pattern of cubic oxide, $<50\text{\AA}$ ; $(\text{Fe, Cr})_2\text{O}_3$ spinel or $\gamma$ - $(\text{Fe, Cr})_2\text{O}_3$ .	No apparent change.
c. After curve 2	1.7	1. B.c.c. metal, sharp, random, $>100\text{\AA}$ . 2. Oxide, diffuse, rhomb. or cubic but presumably cubic after preceding pattern.	No apparent change.
d. After curve 3	1.6	1. As in preceding. 2. Two diffuse bands, presumably air-formed oxide on deposited b.c.c. metal.	Surface peppered with bumps up to $3000\text{\AA}$ in size.
e. After curve 4	1.2	No further change.	As in preceding but bumps more numerous (Fig. 4).
f. After curve 5	0.9	No change.	No further change.
g. Etched in $\text{HNO}_3$ (in etchant)	0.7	Diffuse bands.	Matte surface, peppered bumps gone.

the solutions. In the last two columns are the diffraction and microscopy results of the specimens removed at the various stages. Item g in the table refers to etching of the specimen after curve 5 in 1:1  $\text{HNO}_3$  for 5 sec; a control experiment, in which an electropolished and cathodically reduced Fe-25 Cr specimen was etched similarly, yielded no Fe in the

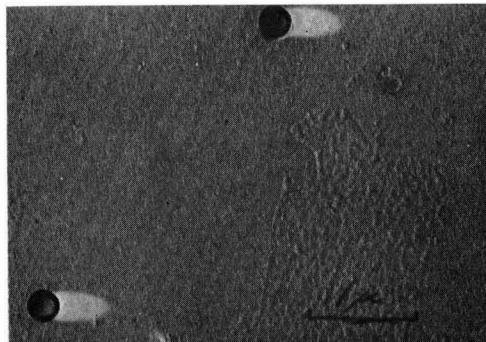


Fig. 3. Electron photomicrograph of surface of Fe-25 Cr oxidized 60 min at 320°. Circles are  $0.264\mu$  polystyrene spheres put on replica to distinguish between pits and bumps. Magnification 18000X.

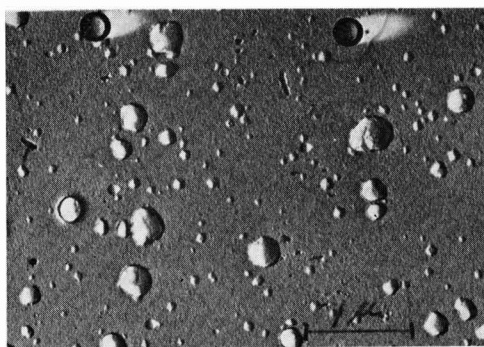


Fig. 4. Electron photomicrograph of surface of oxidized Fe-25 Cr after cathodic reduction. After curve 4 of Fig. 2. Scattered spots are bumps of electrodeposited Fe. Magnification 18000X.

etchant. Figures 3 and 4 are electron photomicrographs illustrating the surface topography before and after cathodic reduction. The circles visible on the photomicrographs are  $0.264\mu$  polystyrene spheres added to the replica before shadowing to identify features as elevations or depressions.

Not unexpectedly, no such sequence was obtained when oxidized Cr was cathodically reduced. Cr was not detected in the electrolyte. Only  $\alpha$ - $\text{Cr}_2\text{O}_3$  was revealed by x-ray or electron diffraction. An interesting feature is the appearance of blister-like protuberances during cathodic reduction. Figure 5 is an electron photomicrograph of the surface of the Cr panel after oxidation at 320° and cathodic reduction for 15 min. It follows from the apparent hydrogen blistering that proton transfer through the  $\text{Cr}_2\text{O}_3$  is a major part of the cathodic process. Hydrogen blisters were observed previously when electropolished Cr was cathodically reduced (1).

Figure 6 illustrates the effect of oxidation temperature on the form of the cathodic reduction curve. The time at the more positive potentials can be taken as a measure of the quantity of readily reducible or high-Fe oxide. For curves 1, 2, and 3 these times are 35, 150, and 3 sec, respectively, from which it is apparent that the 980° specimen has no readily reducible oxide.

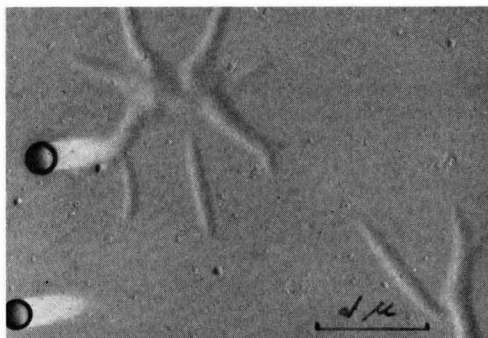


Fig. 5. Electron photomicrograph of surface of Cr oxidized 60 min at 320° and cathodically reduced. The protuberances are hydrogen blisters. Magnification 18000X.

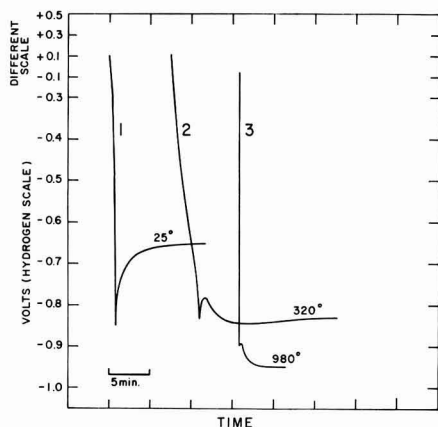


Fig. 6. Cathodic reduction curves of electropolished and oxidized Fe-25 Cr alloy. 1, Oxidized 6 days at 25°; 2, oxidized 60 min at 320°; 3, oxidized 24 hr at 980°C. 2.8 $\mu$  of oxide.

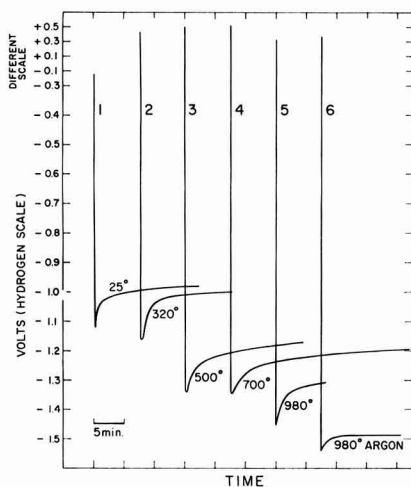


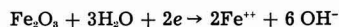
Fig. 7. Cathodic reduction curves of electropolished and oxidized Cr. 1, Oxidized 6 days at 25°; 2, 60 min at 320°; 3, 60 min at 500°; oxide 0.03 $\mu$  thick; 4, 150 min at 700°; oxide 0.35 $\mu$  thick. 5, 70 hr at 980°; oxide 4.2 $\mu$  thick; 6, 60 min at 980° in argon at 1 atm containing 10 ppm oxygen.

For Cr, the temperature of oxidation does not affect the form of the cathodic reduction curve (Fig. 7). The increase in depth of the minimum with increase in temperature merely reflects an increasing electrical resistance of the film, as referred to above. Curve 4 does not quite follow this orderly progression because of cracking of the scale that occurred on cooling.

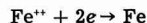
### Discussion

A logical interpretation of the cathodic reduction of the oxide formed on Fe-25 Cr at 320° can be deduced from the data of Table I and the reduction curves for Fe and Cr oxidized at the same temperature. In curve 2 of Fig. 1, the first wave around -0.7 v represents the reduction of an oxide high in Fe, presumably  $\alpha$ -(Fe,Cr) $_2$ O $_3$  by analogy to curve 1. If

Cr in the oxide is neglected, the cathodic reaction may be written



When this is mainly complete, the potential decreases rapidly because of the high reduction potential and large hydrogen overvoltage of the remaining high-Cr oxide (1). At the sharp minimum, the overpotential has become high enough for plating of Fe to occur

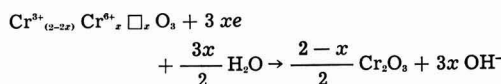


Once sufficient nuclei of Fe have formed on the unreduced Cr oxide the potential rises sharply as the rate of this reaction becomes appreciable and falls again as concentration polarization is established (3). Nevertheless Fe plating continues at a slower rate well past the second minimum, as evident from column 3 of Table I. The final, moderately steady potential is a mixed potential representing a number of cathodic processes including plating of Fe, hydrogen discharge on Cr oxide and on deposited Fe, and perhaps still some reduction of Fe oxide to Fe $^{2+}$  or Cr $^{3+}$  oxide to Cr $^{3+}$  oxide. The observed potential differs from the normal polarized value of the mixed potential by the magnitude of the IR drop through the oxide.

This sequence is consistent with the results of chemical analysis, electron microscopy, and diffraction. As the amount of deposited Fe increases, the Fe content of the electrolyte decreases, and the diffraction pattern of Fe obscures the pattern of the oxide on which it is depositing. Etching after cathodic reduction yields an amount of Fe in the HNO $_3$  etchant consistent with the amount that had been deposited, and electron microscopy shows that the deposited bumps are gone.

The interpretation of the cubic pattern obtained after most of the  $\alpha$ -Fe $_2$ O $_3$  has been reduced (Table I, item b) is not clear, unless it is spinel, as in the case of cathodic reduction of oxidized Fe where an Fe $_3$ O $_4$  pattern appears after the outer Fe $_2$ O $_3$  has been removed (2). Alternatively, the high-Cr oxide left when the Fe oxide has gone may itself be cubic. X-ray and electron diffraction of oxidized Cr in this work has failed to detect such a structure although, on Cr oxidized at low pressure, Shimaoka (4) has reported a cubic oxide in the temperature range 25°-500°.

But regardless of this, the results show that the oxide film formed at 320° on Fe-25 Cr is not a single phase. Furthermore, it may be inferred that the oxide formed at 25° also is two phase since in curve 1 of Fig. 6 a relatively positive cathodic process persists for 35 sec. Analysis after cathodic reduction shows 0.3  $\mu$ g/cm $^2$  of Fe in solution, which is consistent with the time of 35 sec. The sharp minimum is evidence of the high-Cr second oxide. This is not due to Fe plating, as for 320° oxide, but to the decrease in hydrogen discharge potential when the surface of the Cr oxide is cathodically reduced, described previously by





where  $\square$ , is the concentration of cation vacancies (1).

However, the 980° oxide apparently is not two-phase, at least not its outer portion. The short time of 3 sec at relatively positive potential (Curve 3, Fig. 6) shows the absence of readily reducible oxide. X-ray diffraction showed only  $\alpha$ -(Fe,Cr)<sub>2</sub>O<sub>3</sub> containing no more than 2% Fe<sub>2</sub>O<sub>3</sub>, confirmed by chemical analysis as less than 2% Fe. Cathodic reduction after oxidizing for only 5 min at 980°, including the time for the specimen to come to temperature, does show a reducible Fe oxide wave. It follows that two-phase oxide, which forms before the diffusion barrier oxide layer is properly established, becomes incorporated into a single phase  $\alpha$ -(Fe,Cr)<sub>2</sub>O<sub>3</sub> by a solid-state reaction. (The slight minimum at -0.9 v of curve 3, Fig. 6, is believed due to plating out of Fe which entered the electrolyte by autocorrosion at the base of cracks in the oxide before the reducing current was switched on.)

According to the cathodic reduction curves of oxidized Cr, no change in the nature of the oxide takes place with temperature of oxidation. Nor was anything other than  $\alpha$ -Cr<sub>2</sub>O<sub>3</sub> detectable by electron or x-ray diffraction. The blistering in Fig. 5 is evidence of proton transfer through the oxide to the metal substrate and suggests that electronic conductivity is more difficult through the oxide on Cr than on Fe-25 Cr. Curve 6 is included to show that in an atmosphere of lesser oxidizing potential the potential increase from the sharp minimum is smaller (60 mv for curve 6 vs. 120-160 mv for curves 1 to 5). This was interpreted to reflect a decrease in Cr<sup>6+</sup> content

for Cr<sub>2</sub>O<sub>3</sub> formed in lower oxygen partial pressures. In a still weaker oxidizing atmosphere, vacuum at 1100°, the sharp minimum was totally absent, even though electron diffraction demonstrated the presence of a Cr<sub>2</sub>O<sub>3</sub> film.

In summary, the results indicate that the oxide films formed on Fe-Cr alloys at low and high temperatures differ in type as well as thickness. At low and intermediate temperatures, a two-phase film is observed of a readily reducible oxide high in Fe, and a high-Cr oxide in which only a small Cr<sup>6+</sup> content is reducible. The multiple cathodic processes that may occur in the cathodic reduction of a thick alloy scale can be sorted out with the help of diffraction and microscopy and parallel experiments with the pure metals. At higher temperature the scale on Fe-25 Cr is single-phase  $\alpha$ -(Fe,Cr)<sub>2</sub>O<sub>3</sub> containing no more than 2% Fe<sub>2</sub>O<sub>3</sub>.

#### Acknowledgment

The authors wish to thank Mr. E. G. Brewer for preparing the electron photomicrographs.

Manuscript received May 22, 1961; revised manuscript received July 17, 1961.

Any discussion of this paper will appear in a Discussion Section to be published in the June 1962 JOURNAL.

#### REFERENCES

1. D. Caplan, A. Harvey, and M. Cohen, *This Journal*, **108**, 134 (1961).
2. K. H. Buob, A. F. Beck and M. Cohen, *ibid.*, **105**, 74 (1958).
3. D. A. Vermilyea, *ibid.*, **106**, 66 (1959).
4. G. Shimaoka, paper presented at Philadelphia meeting of AIME, October 1960.

## The Kinetics of Oxidation and Nitridation of Lithium, Calcium, Strontium, and Barium

M. S. Chandrasekharaiah and John L. Margrave

*Department of Chemistry, University of Wisconsin, Madison, Wisconsin*

#### ABSTRACT

Reaction rates for lithium, calcium, strontium, and barium during 50-120 min of exposure to O<sub>2</sub> or N<sub>2</sub> were measured as a function of temperature and pressure by a manometric method. Many of the reaction rates were found to be exponential functions of time, but in some cases a linear rate law was found.

Detailed studies of oxidation or nitridation rates for the active metals such as lithium, calcium, strontium, barium, etc., are almost nonexistent. They do not allow the formulation of a consistent viewpoint about either the ease of oxidation or the mechanism of these reactions. As a continuation of the general program for the study of gas-metal interactions (1), studies of the oxidation and nitridation of lithium, calcium, strontium, and barium were undertaken. A special point of interest was to see whether any other element besides magnesium has low-temperature nitridation rates which are higher than the corresponding oxidation rates.

#### Experimental Procedure

*Apparatus.*—The reaction rates were measured by a differential manometric technique suggested by Campbell and Thomas (2). The experimental procedure was similar to the one used previously in this laboratory (1). Details of the construction of the apparatus and experimental procedure are given elsewhere (3).

*Samples.*—All metallic samples were obtained in the form of cast rods of highest purity available from A. D. Mackay and Company, New York, and were cut into required sizes just before each run. Spectro-

scopic analysis indicated only traces of metallic impurities (less than 0.5%).

Before each run, the small samples, approximately  $1 \times 1 \times 0.5$  cm, were abraded successively with silicon carbide papers of grit No. 280, 320, and 400, respectively, polished with a polishing microcloth, and the exact dimensions measured. All these processes were done under purified normal heptane and excess heptane was removed by rinsing with purified, low-boiling petroleum ether (bp  $42^\circ\text{--}46^\circ\text{C}$ ) before introducing into the high vacuum system. All samples were degassed for about 60 min in vacuum ( $<1\mu$ ) at the temperature of the reaction prior to the introduction of the gas into reaction bulbs.

High-purity nitrogen gas (99+%) was further purified by passing over heated copper granules (at  $400^\circ\text{C}$ ) and then through two drying towers of magnesium perchlorate and finally through a trap cooled in liquid air before it was collected in the gas reservoir and used in the nitridation runs.

Linde dry (H.P.) oxygen was further purified by passing over magnesium perchlorate and through a cold trap before it was used in oxidation runs.

### Calibration Runs

Although the manometric method has often been successfully employed for the study of oxidation of metals (1, 4), several calibration runs were made for comparison with other investigators. Tantalum and niobium were used, since the oxidation and nitridation of these metals have been measured quite extensively (5-7), and also the rates appear to follow simple rate laws.

**Calibration results.**—Four nitridation runs with tantalum sheets were measured at a nitrogen gas pressure of  $76 \pm 4$  mm between  $600^\circ\text{--}720^\circ\text{C}$ . All tantalum metal samples used in these calibration runs were cut and abraded under normal heptane with silicon carbide papers of varying fineness and polished with a polishing cloth. The excess heptane was removed by rinsing with petroleum ether, then with absolute alcohol, and the samples were dried in a vacuum desiccator before the nitridation run. The samples were weighed before introducing them into the reaction bulb and weighed again after the nitridation runs. Tantalum samples were obtained in the form of high-purity sheet from Fansteel Metallurgical Corporation.

Two oxidation runs at  $404^\circ$  and  $408^\circ\text{C}$  and an oxygen pressure of  $100 \pm 4$  mm and one nitridation run at  $760^\circ\text{C}$  and a nitrogen pressure of  $76 \pm 4$  mm were made with a very high-purity niobium metal sample, supplied by the Pigments Division of the DuPont Company. The experimental procedure was similar to that for tantalum except that the same metal sample was used in all the runs after reabrasion.

The agreement between the weight gains observed by direct weighing and those calculated from the differential manometer readings was generally good to  $\pm 10\%$ , and the Ta results fitted a parabolic rate equation as reported earlier (5-7). However, rate constants from this study were smaller than the corresponding values of these authors. This discrepancy between the two sets of results may be the result

of different histories of the samples. Similar smaller oxidation rates of tantalum were reported by Vermilyea (7). Such differences in the surface reaction rates may not necessarily be due to differences in the experimental methods, but may arise even when the same experimental technique is employed. For example, recently Gulbransen and Andrew (6) obtained a value for the rate constant for the oxidation of niobium at  $375^\circ\text{C}$ , which is only one-seventh as large as their earlier result (5).

Although the rate constants for these calibration runs were smaller, the activation energy for the nitridation of tantalum was found to be  $41 \pm 2$  kcal/mole as compared to 39 kcal/mole reported by Gulbransen and Andrew (5).

### Experimental Results

**Lithium.**—There is only one report (8) of kinetic data for either oxidation or nitridation of lithium. This note does not give any rates, but makes the statement that the oxidation rate was slow up to the ignition of Li at  $630^\circ\text{C}$ . The oxidation of lithium was too slow for measurement at low temperatures and no container which was oxidation resistant, but nonreactive with lithium at high temperatures, was found. Thus, no oxidation rate measurements were made.

Nitridation rates for lithium were measured as a function of temperature and pressure up to  $310^\circ\text{C}$ . A slight alteration in the experimental procedure was necessitated by the low melting point of lithium ( $186^\circ\text{C}$ ) and the destructive attack of molten lithium on Vycor bulbs. Samples of metal in the form of small cubes were cut from a high-purity metal block under purified petroleum ether and placed in a boat of tantalum foil. Another similar tantalum boat was introduced into the balancing bulb. After the nitridation reaction, the surface of the samples was observed to be covered by a dark-colored film, which was identified as  $\text{Li}_3\text{N}$  by x-ray diffraction. Uncertainty introduced by the reaction of tantalum with nitrogen is small, since the rate of nitridation of tantalum at these temperatures is negligible.

If the empirical relation of Pilling and Bedworth (9) is strictly correct, this nitridation should follow a linear rate law, since the ratio of molar volumes ( $\text{Li}_3\text{N}$  to Li) is 0.7 (10). However, the observed rates are much more complex functions of time. Rate constants were calculated from slopes of  $\log(\Delta m)$ , the weight gain per unit area, vs. time plots which were essentially linear (Fig. 1). The variation of the rate constants with temperature was erratic and the apparent activation energy could lie anywhere between 10 and 45 kcal/mole.

**Calcium.**—Pilling and Bedworth (9) studied the oxidation of calcium over long periods of time and concluded that the oxidation followed a simple linear rate. Recently, however, Cubicciotti (4) has shown that the data for the oxidation of calcium below  $425^\circ\text{C}$  fits a parabolic rate equation better than the linear equation, at least for the first 2 hr of the reaction. At  $425^\circ$  and higher, an induction period was followed by a very rapid reaction and eventually by a linear reaction rate.

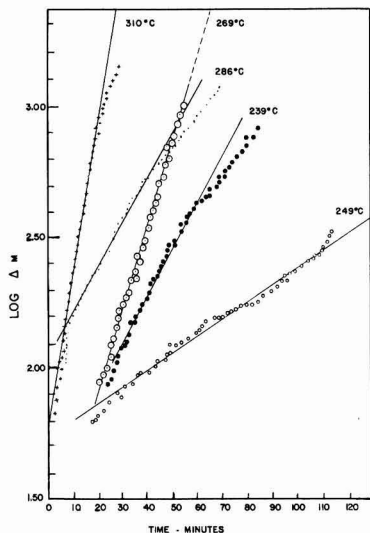


Fig. 1. Nitridation of lithium, logarithmic plot.  $P_{N_2} \approx 110$  mm for 310°, 286°, and 239° runs;  $P_{N_2} \approx 200$  mm for 269° and 249° runs.

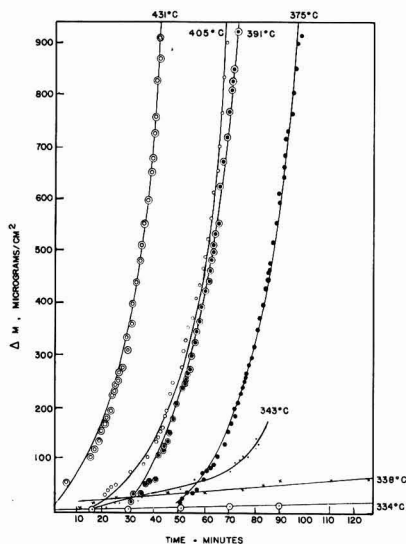


Fig. 2. Oxidation curves for calcium.  $P_{O_2} \approx 110$  mm for all runs except at 343° and 338°C where  $P_{O_2} \approx 160$  mm.

In this work, small pieces of carefully prepared samples of calcium were used in oxidation measurements from 300° to 435°C at oxygen gas pressures of 100-200 mm. None of the oxidation runs followed the simple parabolic rate law during the time of observation. Figure 2 shows some of these oxidation runs on calcium. Below 350°C, the rates were small and nearly linear, but above this temperature, a sudden increase in rates following an induction period was noted. The rates above 350°C were more nearly an exponential function of time. It is likely that if one waited long enough the rates would become linear as Cubicciotti (4) observed for Ca at higher temperatures.

Plots of  $\log(\Delta m)$  vs. time were linear where  $\Delta m$  is the weight gain of the sample per unit area. An x-ray diffraction analysis of the surface product yielded CaO as the only product. Rates were calculated from the slopes of such logarithmic plots, and an activation energy of 6.3 kcal/mole was obtained from the temperature variation of these rate constants.

According to Shushnov and Baryshnikov (11), a film of freshly distilled calcium combines readily with nitrogen gas to form  $Ca_3N_2$  even at 300°C, and they suggest a reaction catalyzed by the product. By contrast at 300°C a piece of calcium metal oxidizes very slowly. Hence, the nitridation rates of a solid piece of metal, rather than a film, were measured to see whether any difference is observed.

Unlike the rapid reaction rates for nitrogen gas with a freshly distilled film, the reaction rates with large pieces of calcium were very slow even up to a temperature of 550°C. Except for one run at 595°, when a highly reactive film of the metal was condensed on the cooler parts of the bulb, the uptake of nitrogen was slow and points were generally scattered. Moreover, in a number of runs, an increase of pressure rather than a decrease was noted in early periods of the runs, followed by the normal decrease. This was probably due to vaporization of calcium on sudden heating and accumulation of calcium vapors during the induction period, after which the reaction became fast enough to overcome this small pressure change. The reaction of calcium is further complicated by the existence of a phase transition in this temperature range (12).

No detailed analysis of nitridation rates was possible.

*Strontium.*—Strontium, when heated with oxygen or nitrogen, combines readily, forming the oxide SrO and the nitride  $Sr_3N_2$ , respectively, but no quantitative rate measurements have been reported. In this work, oxidation rates from 100° to 200°C at an oxygen pressure of 210 mm and nitridation rates from 300° to 400°C at a nitrogen gas pressure of 100-200 mm were measured using the experimental

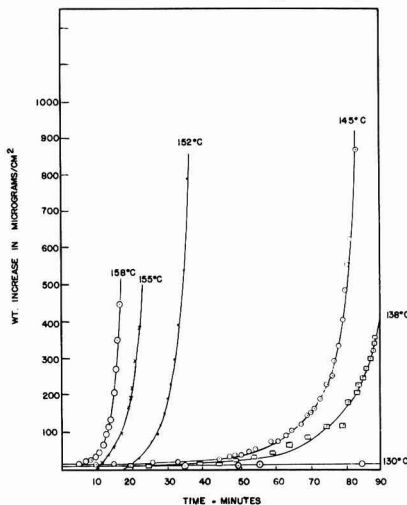
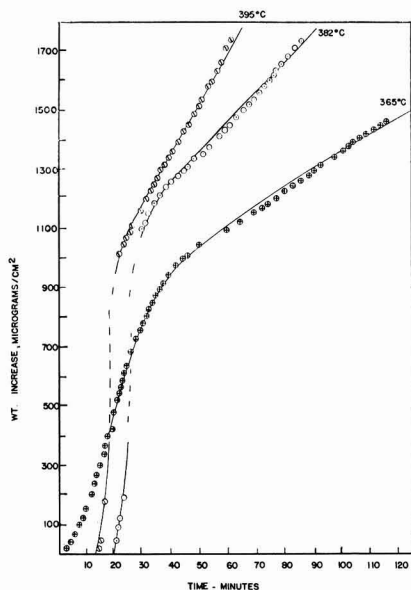


Fig. 3. Kinetics of oxidation of strontium.  $P_{O_2} \approx 210$  mm



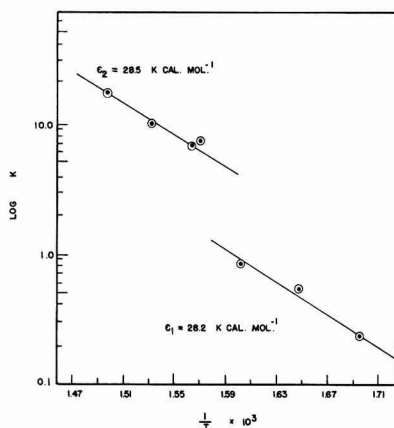
Fig. 4. Nitridation of strontium.  $P_{N_2} \approx 110$  mm

procedure described. X-ray diffraction analysis of the surface films of reaction indicated  $SrO$  and  $Sr_3N_2$  as the only reaction products.

Figure 3 illustrates some typical oxidation runs for strontium while Fig. 4 shows some nitridation runs at 110 mm pressure. Oxidation of strontium followed a similar pattern to that of calcium oxidation discussed earlier. Plots of  $\log \Delta m$  vs. time were linear and slopes gave the rate constants for the oxidation of strontium. From an Arrhenius-type plot of these rate constants an activation energy of  $29 \pm 2$  kcal/mole was obtained for this rapid-rise process. It is not known, but seems likely, that the rate of oxidation will level off and become linear at longer times.

The rates for strontium nitridation were quite different from the oxidation rates in a number of ways. Nitridation rates were small and linear up to  $360^\circ C$ . At higher temperatures, the rates were slow in the beginning, but suddenly became very rapid. This induction period decreased with the increase of temperature. The increase in the rates persisted for about 10 to 20 min and then changed gradually to a linear rate once again. The time interval during which this rapid growth of film existed was of the same order of magnitude for all runs and was independent of temperature. In all such runs, it was observed that the samples were coated with a number of dark spots in addition to the uniform nitride film. These spots were also  $Sr_3N_2$ , as determined by x-ray diffraction. These sudden increases of rate might be due to spot nitridation on surface strains, or they might indicate a nonisothermal reaction.

The rate constants for the nitridation of strontium were calculated from the linear parts of the weight increase of the sample vs. time plots and may be divided into two groups. One group consists of the reactions up to  $360^\circ$ , where no dark spots were ob-

Fig. 5. Nitridation of strontium,  $\log K$  vs.  $1/T$ 

served, and the other group consists of the rates above this temperature in which there were always dark spots on the surface of the sample after the nitridation runs. Rate constants from both groups gave the same value for the activation energy (Fig. 5). This suggests that the mechanism for the linear rates of nitridation is the same for both cases, and that the sudden rise in the higher temperature measurements is merely due to surface heating as the initial film is rapidly formed.

**Barium.**—As the most reactive element of the alkaline earth series, excluding radium, barium combines readily with oxygen and nitrogen forming  $BaO$  and  $Ba_3N_2$ , respectively. From the relative molar volume consideration as defined by Pilling and Bedworth (9), both of these processes should follow a linear rate equation, and the oxidation rate at room temperature is reported to obey a linear law (13). The rapidity of oxygen uptake by a piece of barium above  $100^\circ C$  was such as to preclude any investigation of oxidation of barium with the presently available equipment. The rates of nitrogen uptake by a piece of barium metal were measured as a function of time between  $300^\circ$  and  $420^\circ C$ . Figure 6 represents some of these runs with  $P_{N_2} \approx 240$  mm.

It was observed that rates were approximately linear in the beginning and then became almost ex-

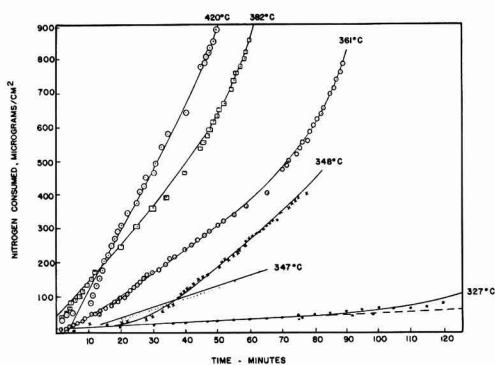


Fig. 6. Nitridation of barium, 245 mm of nitrogen pressure

Table I. Results of oxidation and nitridation studies of Ca, Sr, Ba, and Li

Metal	Gas	Pressure, mm	Temp, °C	$E_{act.}$ , kcal/mole	Rate law
Ba	N <sub>2</sub>	245 ± 5	(i) 320-425	17.2	linear for film thickness ≤ 100 μg/cm <sup>2</sup> exponential after an induction period*
			(ii) 346-425	5.9	
Sr	O <sub>2</sub>	not studied; too fast		—	—
	N <sub>2</sub>	110 ± 1	317-395	28	nearly linear**
Ca	O <sub>2</sub>	210 ± 1	138-158	29	exponential*
	N <sub>2</sub>	200	300-595	—	inconclusive; too slow
Li	O <sub>2</sub>	110-160	334-430	6.3	exponential*
	N <sub>2</sub>	110-200	150-310	10-45 (erratic)	exponential*

\* Exponential rates are possibly indication of a nonisothermal reaction.

\*\* A sudden increase followed by a linear rate was observed in some cases.

ponential after some time had elapsed. This transition from a linear rate into an exponential rate did not take place until a certain minimum film thickness was first formed (approximately 100 μg/cm<sup>2</sup> in this case). Plots of log Δ*m* vs. time were linear after this film of 100 μg/cm<sup>2</sup> was reached. Rate constants calculated from the linear plots and from the logarithmic plots and plotted vs. 1/*T* yielded activation energies of 17.2 kcal/mole and 5.9 kcal/mole, respectively.

### Conclusions

Rates of oxidation and nitridation for the active metals studied were not observed to be simple functions of time during the first 50-120 min of reaction. Rate constants for the early rapid reactions may be obtained from log Δ*m* vs. time plots, and Table I summarizes the activation energies obtained from the temperature dependence of the rates.

A linear rate law should be observed in all the systems of this study if one waits long enough, since they all form a noncovering, macroscopically defective reaction film and the rates should be independent of the film thickness.

The small activation energies for those systems which show the exponential time relation after an induction period suggest either a nonisothermal reaction or a catalytic process. From the heats of formation of the various oxides and nitrides, one can show that temperature rises of 6-10°C/min are possible for systems undergoing very rapid surface reaction. Although the entire reaction system was under careful temperature control, it is conceivable that surface heating could have occurred and caused the exponential rates. The same qualitative arguments for surface heating can be made for the oxidation and nitridation reactions of other metals although the highest heat evolution per gram-atom of oxygen or nitrogen reacted is expected for Ca, Sr, Ba, and Li. Such surface heating might also explain the exponential rate for nitridation of a thin calcium film reported by Shushnov and Baryschnikov (11).

Studies of clean metal films with precise temperature control and for long periods of time are needed before conclusive reaction mechanisms can be proposed.

### Acknowledgment

One of the authors (M.S.C.) wishes to thank the Minnesota Mining and Manufacturing Corporation and the Wright Air Development Center of the United States Air Force for financial support during the period of this investigation and the Ministry of Education, Government of India, for a travel grant.

Manuscript received May 3, 1961; revised manuscript received July 21, 1961. This paper was abstracted in part from the thesis presented by one of the authors (M.S.C.) in partial fulfillment of the requirements for the Ph.D. degree, University of Wisconsin, October 1958, and was presented in part before the 134th Meeting of the American Chemical Society, Chicago, in September 1958.

Any discussion of this paper will appear in a Discussion Section to be published in the June 1962 JOURNAL.

### REFERENCES

1. P. Sthapitanonda and J. L. Margrave, *J. Phys. Chem.*, **60**, 1628 (1956).
2. W. E. Campbell and U. B. Thomas, *Trans. Electrochem. Soc.*, **91**, 623 (1947).
3. M. S. Chandrasekharaiah, Ph.D. Thesis, University of Wisconsin (1959).
4. D. Cubicciotti, *J. Am. Chem. Soc.*, **74**, 557 (1952).
5. E. Gulbransen and K. F. Andrew, *J. Metals*, **2**, 586 (1950).
6. E. Gulbransen and K. F. Andrew, *This Journal*, **105**, 4 (1958).
7. D. A. Vermilyea, *Acta Met.*, **6**, 166 (1958).
8. C. Tyzack and P. B. Longton, United Kingdom Atomic Authority, Tech. Note No. 131 (1955).
9. N. B. Pilling and R. E. Bedworth, *J. Inst. Metals*, **29**, 529 (1923).
10. O. E. Kubaschewski and B. E. Hopkins, "Oxidation of Metals and Alloys, p. 15, Butterworth Scientific Publication, London (1952).
11. V. A. Shushnov and Yu. Baryschnikov, *Zhur. fiz. Khim.*, **27**, 703 (1953).
12. Gmelins Handbuch, **28A**, 397 (1957).
13. O. E. Kubaschewski and B. E. Hopkins, *op. cit.*, p. 39.

# Impedance Phenomena in Molten Salts

G. J. Hills and K. E. Johnson<sup>1</sup>

Department of Chemistry, Imperial College, London, England

## ABSTRACT

Impedances have been measured of polarized platinum micro-electrodes in the molten salt systems, LiCl-KCl at 400°C, NaNO<sub>3</sub>-KNO<sub>3</sub> at 270°C, NaBr-AlBr<sub>3</sub> at 225°C, and PbCl<sub>2</sub> at 530°C. Frequency dispersion of both the observed resistance and capacitance was evident in all cases, but apparent double layer capacities obtained by extrapolation to infinite frequency are in reasonable accord with some previously reported data. They are of magnitudes consistent with a simple Helmholtz model although the anodic values tend to be high, perhaps because of specific adsorption. Some measurements of faradaic impedance have also been made, but these were less successful and the exchange current for the Pt/Pt<sup>2+</sup> system is high.

Metal-melt interfaces are met with in four connections:

(i) undergoing steady cathodic electrolysis either as part of an electroanalytical study or as part of an electrowinning process;

(ii) at equilibrium in a melt which may or may not contain a significant concentration of the metal ions, e.g., at the internal surface of a metal vessel containing molten salts;

(iii) approximately at equilibrium but subject to a small applied voltage changing periodically with time; and

(iv) undergoing steady anodic electrolysis where in many cases the metal dissolves smoothly to form ions of its lowest stable valence state.

In each case, the composition of the metal-melt interface and the degree of reactivity of the metal should be explicable in terms of the kinetic parameters (particularly exchange currents) of the various feasible electrode reactions. The structure of the melt in contact with the metal is an important related property of such systems, and some conclusions with regard to this may be drawn from values of double layer capacities at metal-melt interfaces.

Until recently, only the a-c impedance method has been applied to the measurement of exchange currents and double layer capacities in melts. Double layer capacities of 15-20  $\mu\text{F cm}^{-2}$  were observed at carbon electrodes in cryolite-alumina melts (1), and impedance measurements at carbon electrodes in halide melts were interpreted in terms of a slow heterogeneous anode reaction such as  $\text{Cl} + \text{Cl} \rightarrow \text{Cl}_2$  (2).

Randles and White (3) found that the capacity-potential curves for mercury in molten alkali nitrates, perchlorates, and bisulfates were shallow parabolas with minimum values of  $\sim 20 \mu\text{F cm}^{-2}$ . In the case of nitrates, a very high concentration of water increased the capacity and produced some semblance of the "hump" found in the curves for aqueous solutions. The rate constant for the discharge of Ni<sup>2+</sup> from nitrates was obtained by a straightforward application of the faradaic impedance theory.

Hill (4) measured the impedance of Ag in dilute solutions of AgNO<sub>3</sub> in molten LiNO<sub>3</sub>-NaNO<sub>3</sub>-KNO<sub>3</sub>, of Ag in solutions of AgCl in LiCl-KCl, of W in LiCl-KCl and W in solutions of TiCl<sub>2</sub> and TiCl<sub>3</sub> in LiCl-KCl. In all cases the residual capacity and resistance of the solvent were markedly frequency dependent, the double layer capacities obtained by extrapolation to infinite frequency being 300, 500, 112, and 88  $\mu\text{F cm}^{-2}$ , respectively. Some of the faradaic impedance plots behaved ideally, but many had a phase angle,  $\phi$ , exceeding  $\pi/4$ , where  $\tan \phi = \omega C_p R_p$ , and  $C_p$  and  $R_p$  are the capacitive and resistive components of the faradaic impedance. Laitinen and Osteryoung (5) and Laitinen and Gaur (6) also found a frequency dispersion and impedance at platinum in molten LiCl-KCl and the latter workers, using a purer solvent, were able to make empirical corrections to bring  $\phi$ , in the presence of the depolarizers Pb<sup>2+</sup>, Co<sup>2+</sup>, Ni<sup>2+</sup>, Zn<sup>2+</sup>, and Cd<sup>2+</sup>, to values less than  $\pi/4$  and thus to calculate rate constants for the discharge of these ions. The corrections consisted of inserting a frequency-independent impedance in parallel with the double layer capacity and faradaic impedance and were interpreted in terms of the adsorption of heavy metal ions and subsequent surface electron exchange without diffusion. Extrapolated values of double layer capacity in the pure solvent were 77 to 38  $\mu\text{F cm}^{-2}$  over the potential range -0.5 to -1.5 v (*vs.* Pt/0.1M PtCl<sub>2</sub>). Stein (7) found the capacity at Pt in NaCl-KCl at 980 cps to be symmetric about a potential of +0.03 v *vs.* Ag/AgCl with a maximum value of  $\sim 380 \mu\text{F cm}^{-2}$ , the values at -0.33 v and +0.40 v being  $\sim 2.90 \mu\text{F cm}^{-2}$ ; the magnitude of these quantities and their potential dependence suggests that the pseudocapacity of Ag<sup>+</sup> discharge may have been included.

Recently, exchange currents and transfer factors for a number of electrode couples in LiCl-KCl have been measured by the double-impulse and voltage-step methods (8) and double layer capacities at Pt, Bi, and Zn in LiCl-KCl have been recorded.

In the work described here, impedances at platinum electrodes in LiCl-KCl have been analyzed in some detail and the results considered together with those of a brief study of molten PbCl<sub>2</sub>, NaBr-AlBr<sub>3</sub>, and alkali nitrates.

<sup>1</sup> Present address: Department of Chemistry, University of Illinois, Urbana, Illinois.

### Experimental

The preparation and purification of molten LiCl-KCl eutectic was performed in a manner similar to that used by Laitinen *et al.* (9) and by Janz *et al.* (10). Briefly, the solids were dried by heating them slowly to 300°C *in vacuo*. Then, in an atmosphere of dry HCl gas, they were melted rapidly and filtered through sintered glass, the excess HCl being pumped off until the residual polarographic current at a planar Pt electrode (area  $8 \times 10^{-6}$  cm<sup>2</sup>) was less than  $\sim 2 \mu\text{a}$  at  $-2.0$  v *vs.* the Pt/PtCl<sub>2</sub> reference electrode and until the apparent decomposition voltage was  $\sim -2.65$  v.

NaBr-AlBr<sub>3</sub> eutectic was prepared similarly, HBr being substituted for HCl. The residual polarographic current of the pure solvent was zero up to  $-1.6$  v (*vs.* Pt/0.05M PtBr<sub>2</sub> in NaBr-AlBr<sub>3</sub>), increased gradually up to  $-1.8$  v, and then rose sharply at this potential.

PbCl<sub>2</sub> was either filtered molten in air or used directly (its degree of hydrolysis in air is much less than that of LiCl-KCl and its volatility and melting point [501°C] much greater). The residual polarographic current of the melt was zero to  $-0.75$  v (*vs.* Pt) where a small wave varying in shape, but not in mean current, from one polarogram to another appeared, up to the solvent decomposition at  $-0.9$  v.

Hydrolyzable substances were handled in a dry box, and measurements were made in an atmosphere of dry oxygen-free argon.

The furnace consisted of a quartz tube closed at one end and wound with nichrome wire. It was suspended from pulleys attached to a rigid frame and exactly counterbalanced so that it could be lowered at will to expose all or part of the cell envelope. The temperature of the furnace was controlled by a Roberts Temperature Controller (11). Temperatures were measured with a chromel-alumel thermocouple enclosed in a sheath of Pyrex glass or alumina.

A melt was contained in a Pyrex lipless beaker or liner in a Pyrex envelope suspended in the furnace.

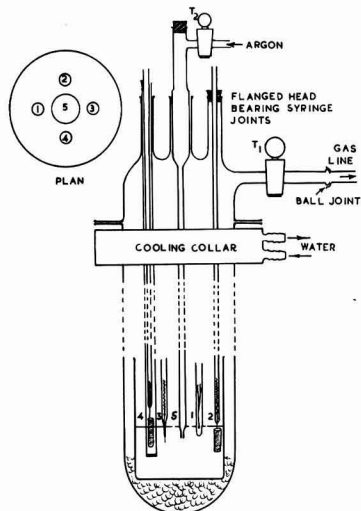


Fig. 1. High-temperature cell

The envelope was sealed with picein wax to a cell head bearing a number of parallel ground glass joints through which electrodes were inserted, and connections made to vacuum and argon lines as illustrated in Fig 1 in which 1 represents a thermocouple, 2 a cylindrical platinum foil macro-electrode, 3 a platinum micro-electrode, 4 a reference electrode, and 5 a gas delivery tube. The melt in the reference electrode was separated from the bulk by a sintered glass disc, and platinous ions were generated coulometrically in it from the platinum foil and an auxiliary cathode.

Two types of electrode were used, thin wires (0.1 mm diameter) sealed into Pyrex tubing and somewhat thicker wires (0.35 mm) also sealed into Pyrex, but ground off to expose the circular cross section of the wire. The latter electrodes were buffed smooth, but always showed a greater frequency dispersion of impedance and higher absolute values of its component admittances than the thin wire electrodes. The more satisfactory performance of the wire electrodes is ascribed to the fact that the smooth surface of the metal produced in the drawing of the wire is not disturbed in preparing the electrodes. Unfortunately, their greater area gave rise to high admittances and lower precision of measurement.

Micro-electrode impedances were measured as a series combination of resistance,  $R_x$ , and capacitance,  $C_x$ , using a high sensitivity Wheatstone bridge across which a signal of 2 mv amplitude or less was applied from an "Advance" oscillator.

The measurements were made at constant temperatures  $\pm 2^\circ\text{C}$ , (as indicated by the sheathed thermocouple in the melt and close to the electrode system). The effect of small temperature fluctuations was, in any case, negligible as can be seen from the over-all temperature dependence of the measurements shown in Fig. 2.

### Results and Discussion

The principal limitation to reproducibility in the present work was the durability of the Pyrex-plati-

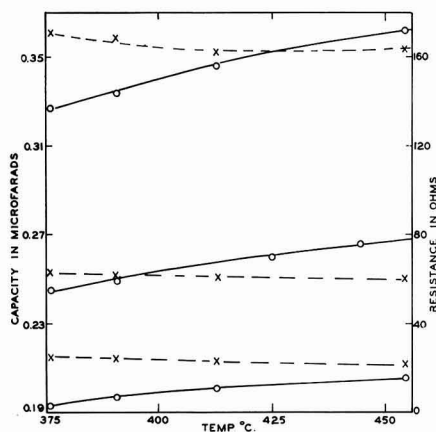


Fig. 2. Variation with temperature of the series equivalent capacity,  $C_x$  (solid lines) and series equivalent resistance (broken lines) of a platinum micro-electrode in the LiCl-KCl eutectic.

num seal. Almost a third of the hundred or so electrodes used were found to be irretrievably defective and were discarded. The remainder were satisfactory and often remained so after many hours continuous use. Only if they were polarized to  $-2$  v and beyond did they become erratic in behavior. Then, alkali metal-platinum alloys were formed, followed by cathodic reduction of the glass around the metal wire. Provided the system was free from oxidizing impurities, the results from any one electrode were not significantly time-dependent and were reproducible to 1%. From electrode to electrode, the reproducibility was only 3-5% and mainly reflects the difficulty of determining the surface areas of individual electrodes.

The observed impedances were always frequency dependent. A number of reasons may be advanced for this, but none of them is wholly convincing. Small concentrations of impurities could give rise to faradaic admittances, but over the whole potential span there is remarkable continuity of the effect. Then, a faradaic contribution from the  $\text{Li}^+/\text{Li}$  equilibrium at large underpotentials may be postulated, but this does not seem realistic. Finally the type of relaxation process described by Bockris and Conway (12) and the space-charge theory of Macdonald (13) are worth considering. The last three approaches view the frequency dispersion as an intrinsic property of molten salts. There is some prospect that Macdonald's equations can be tested by conductance experiments although they are not readily applicable to the type of measurement described here.

Nevertheless, if the frequency dependence is taken to be of faradaic origin, most of the impedances can be broken down into a frequency-independent capacity in parallel with a "faradaic-type" admittance.

#### Interfacial Capacities

The equivalent circuit of the micro-electrode is assumed to be that of two parallel admittances, (a) the interfacial or double layer capacity,  $C_L$ , and (b) the series combination of  $R_s$  and  $C_s$ , the usual components of the faradaic admittance. The electrolyte resistance and the leads capacitance are very small in molten salt systems and can be neglected safely. Even so, the resolution of  $C_L$ ,  $R_s$ , and  $C_s$  from  $R_s$  and  $C_s$  remains difficult, especially if they are of similar magnitude.

If the charge-transfer reaction(s) are relatively fast, the faradaic admittance is close to the inverse of the corresponding Warburg impedance, and  $R_s$  and  $C_s$  can be expressed (14) in terms of the Warburg coefficient  $\sigma$ , defined as

$$\sigma = \frac{2^{1/2} RT}{n^2 F^2 A C D^{1/2}} \quad [1]$$

where the terms have their usual significance. It can be shown that

$$R_s = \frac{\sigma}{\omega^{1/2} (1 + 2C_L \sigma \omega^{1/2} + 2C_s \sigma^2 \omega)} \quad [2]$$

and

$$C_s = C_L + \frac{1}{\sigma \omega^{1/2}} \left[ \frac{1 + C_L \sigma \omega^{1/2}}{1 + 2C_L \sigma \omega^{1/2}} \right] = C_L + \frac{\beta}{\sigma \omega^{1/2}} \quad [3]$$

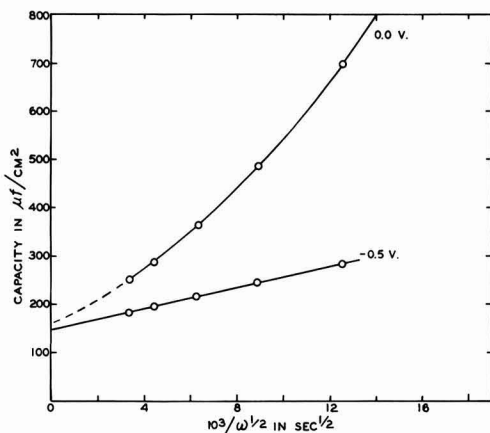


Fig. 3. Variation of series capacity,  $C_s$  with  $\omega^{1/2}$  for pure LiCl-KCl.

It follows that at low frequencies  $C_s$  varies as  $C_L + 1/\sigma\omega^{1/2}$ , at intermediate frequencies as  $C_L + \beta/\sigma\omega^{1/2}$ , and at high frequencies as  $C_L + 1/\sigma\omega^{1/2}$ . At infinite frequency  $C_s = C_L$  for all values of  $C_L$  and  $\sigma$ . Thus, if  $C_s$  is plotted against  $\omega^{-1/2}$ ,  $C_L$  may be obtained by extrapolation to infinite frequency of either very high-frequency data or of data for which approximately  $C_L \sigma \omega^{1/2} < 10^{-2}$  or  $> 10^2$ . In the latter case the value of  $C_L$  would be expected to be a little low. This has been confirmed in the case of molten nitrates where  $C_L$  values of 29 and  $9 \mu\text{F cm}^{-2}$  were obtained for anodic and cathodic capacities compared with values of 30 and  $12 \mu\text{F cm}^{-2}$  calculated by solving simultaneous equations (the behavior of the remaining admittance was unusually simple in this system).

The series capacitance,  $C_s$ , for each pure melt was a linear function of  $\omega^{-1/2}$  (cf. Fig. 3), and approximate values of  $C_L$  were obtained for various degrees of polarization. An exception to this generalization was noted in the case of Pt electrodes in the LiCl-KCl eutectic polarized at 0 v vs. the Pt/PtCl<sub>2</sub> (0.01M) reference electrode. Here, the  $C_s - \omega^{-1/2}$  relation was curved, presumably because of the enhanced faradaic admittance resulting from spontaneous dissolution of the platinum or from leakage of PtCl<sub>2</sub> through the reference electrode diaphragm. This is consistent with Eq. [3].

In Fig. 4, the variation of  $C_L$  with polarizing voltage is shown for the 4 molten salt systems.

The  $C_L$  values for the LiCl-KCl eutectic are in reasonable accord with the recent results of Laitinen, Tischer, and Roe (8), and there is no reason to doubt the general validity of the first three figures. The size and shape of the PbCl<sub>2</sub> data are, however, anomalous. It is likely that the marked reactivity of lead toward platinum and the appreciable solubility of Pb in PbCl<sub>2</sub> will add to the experimental uncertainties, and these results must be regarded with reserve.

The capacity data for the other three systems are interesting in that they each show two shoulders, reminiscent of the idealized anodic and cathodic branches of electrocapillary curves for electrolyte



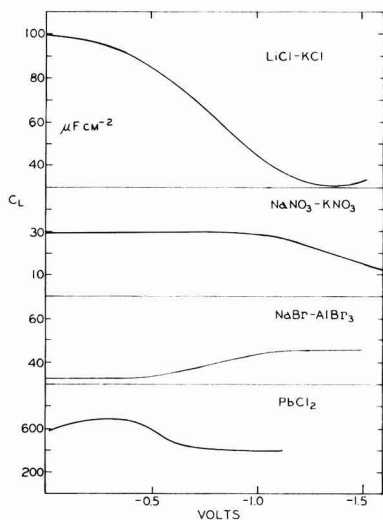


Fig. 4. Variation of double layer capacity,  $C_L$ , with polarizing potential for (a) LiCl-KCl at 400°C; (b) NaNO<sub>3</sub>-KNO<sub>3</sub> at 270°C; (c) NaBr-AlBr<sub>3</sub> at 225°C; and (d) PbCl<sub>2</sub> at 530°C.

solutions. Here, however, the voltage scale is an arbitrary one, and the zero-charge potential is not known. Nevertheless, each diagram is bounded on the left-hand side by the voltage at which anodic attack on the platinum takes place, *i.e.*, where the electrode surface has a significant coverage of specifically adsorbed anions, and it is reasonable to suppose that the inflections in Fig. 4(a), (b), and (c) represent the change from this state to one with a relative surface excess of cations.

There is no sign of the steeply rising capacities which characterize the extremes of polarization of a mercury surface in electrolyte solutions, both in water and in other solvents. There is also no evidence of an anodic "hump." The absence of these two phenomena in molten salt systems could be regarded as evidence that they are properties of the solvent liquid and result from its electrostriction and re-orientation in the surface. It also does not support the thesis of the importance of "ad-atoms" in interfacial capacities.

The extreme values of  $C_L$  from each of the systems studied here can be compared with values calculated from a simple Helmholtz model of a parallel plate condenser, *i.e.*,  $C_L = \epsilon/4\pi d$ , the total separation in each case,  $d$ , being equated to the diameter of the ion predominating in the surface (15).

The problem here is the assignment of a reasonable value for the dielectric constant. At first sight the value for the appropriate solid (16) might be

used, and this does lead to fair agreement between experimental and calculated capacities, but does not allow for the freer motion of ions in melts compared with solids. It seems more likely that the metal atoms of the electrode and the melt ions will be close-packed at the interface in which case a composite electronic and ionic dielectric constant of 3, based on a value of the refractive index of a gaseous ion of 1.0 to 1.5 (17) should be used for all the systems. Calculations with both values of  $\epsilon$  are summarized in Table I.

The anodic capacity observed in the LiCl-KCl eutectic is considerably higher than that given in Table I, and we conclude, as do Laitinen, Tischer, and Roe (8) that there is some close and extracoulombic interaction between platinum and chloride ions. The shape of the capacity-potential curve for the sodium aluminum bromide is in better accord with the relative ionic radii. Specific adsorption is less likely in the nitrates system, but the planar nitrate ion could be oriented parallel to the electrode surface, *i.e.*, with the axis of its dipole normal to the surface; then  $d$  will be 1.0Å and the calculated ( $\epsilon = 3$ ) and the experimental values of  $C_L$  become remarkably close.

It is clear that further measurements, involving other metals, would be useful, and since this work was completed there have been further reports (18, 19) of the successful use of liquid electrodes in melts. It is hoped that these electrodes will be used to extend the range of capacity data in molten salt systems and to confirm the tentative values shown in Fig. 4.

#### Faradaic Admittances

Since the total micro-electrode impedance was observed in each case, the evaluation of  $C_L$  also enabled the faradaic component at each voltage and frequency to be found, *i.e.*, from the relation

$$\text{faradaic admittance} = \left[ \frac{1}{R_s^2 + \frac{1}{\omega^2 C_s^2}} \right]^{1/2} - \omega C_L \quad [4]$$

the electrolyte resistance being negligibly small. In Fig. 5 an analysis of the total admittance as a function of potential at an arbitrary frequency of 1000 cps is given for LiCl-KCl containing some Pt<sup>+</sup> and with and without traces of water present. In most cases, the origin of the faradaic process was not clear, and certainly the concentration of electro-active species was not known. In two cases, both involving the LiCl-KCl melt, a definite concentration of metal ion was added, and here the evaluation of the exchange current for the metal  $\rightleftharpoons$  metal ion equilibrium was possible, in principle at least, from the

Table I. Calculated (Helmholtz) capacities in molten salt systems

Melt	Mean dielectric constant of solid	Anionic diameter $d \times 10^8$ cm	Cationic diameter	Anodic capacity based on $\epsilon$ of solid	Cathodic capacity based on $\epsilon$ of solid	Anodic capacity based on $\epsilon = 3$	Cathodic capacity based on $\epsilon = 3$
LiCl-KCl	8.3	3.6	1.2 (Li <sup>+</sup> )	20	61	7	22
NaBr-AlBr <sub>3</sub>	6.1 (NaBr)	3.9 (Br <sup>-</sup> ) ~9 (AlBr <sub>4</sub> <sup>-</sup> )	2.0 (Na <sup>+</sup> )	14	27	7	13
NaNO <sub>3</sub> -KNO <sub>3</sub>	5.5	1.0 (min) 2.5 (max)	2.0 (Na <sup>+</sup> )	49 20	24	27 11	13

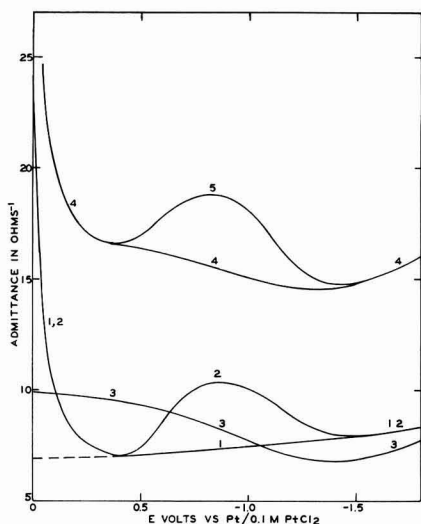


Fig. 5. Analysis of the admittance at planar platinum electrodes in LiCl-KCl at 400°C for a frequency of 1000 cps,  $\text{Pt}^{2+}$  present. 1 is faradaic admittance, 3 is double layer admittance, 4 is total admittance. The presence of small quantities of water changes 1 to 2 and 4 to 5.

usual theoretical expressions for the individual components of the faradaic impedance (20),

$$R_r = \frac{RT}{n^2 F^2 AC} \left[ \left( \frac{1}{2\omega D} \right)^{1/2} + \frac{1}{C^{(1-a)k}} \right] \quad [5]$$

and

$$C_r = \frac{n^2 F^2 AC}{RT} \left( \frac{2D}{\omega} \right)^{1/2} \quad [6]$$

where the terms have their usual significance. The two systems examined were  $\text{Pt} \rightleftharpoons \text{PtCl}_2$  (0.01M in LiCl-KCl) and  $\text{Ni} \rightleftharpoons \text{NiCl}_2$  (0.006M in LiCl-KCl) each at their equilibrium potentials. The frequency

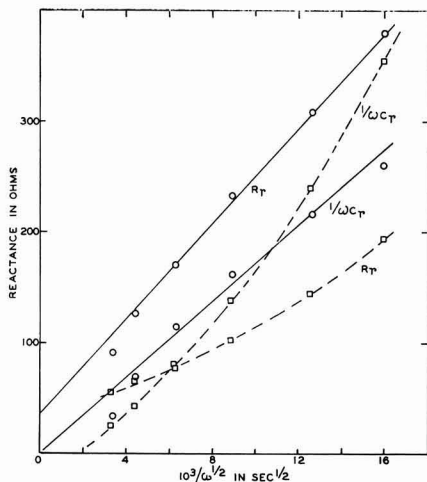


Fig. 6. Variation with frequency of the components  $R_r$  and  $C_r$  of the faradaic impedance for the systems  $\text{Pt}/\text{PtCl}_2$ -LiCl-KCl (solid lines) and  $\text{Ni}/\text{NiCl}_2$ -LiCl-KCl (broken lines), at 400°C.

dependence of  $R_r$  and  $C_r$  in each case is shown in Fig. 6. The nickel data are inverted, and no correction of the type used by Laitinen and Gaur (6) could be found to produce an uninverted form. The platinum data, on the other hand, showed normal behavior and enabled the appropriate exchange current to be estimated, i.e.,  $i_0 = 37 \text{ amp cm}^{-2}$  which is higher than the molar value of  $40 \pm 10 \text{ amp cm}^{-2}$  obtained by Laitinen, Tischer, and Roe (8). Further experiments would be required to establish that this difference is a real one.

It can be shown that the faradaic impedance  $Z_R$  is given approximately by

$$Z_R = \frac{a}{\omega^{1/2}} + \frac{RT}{nFi_0}$$

and it was interesting to note that the impedances due to  $\text{Pt}^{2+}$ ,  $\text{Ni}^{2+}$ , and water in LiCl-KCl gave positive, negative, and zero intercepts on the  $Z_R$  axis of linear  $Z_R$  vs.  $\omega^{-1/2}$  plots. The zero intercept in the case of water implies a very high value of  $i_0$ , i.e., that  $\text{H}^+$  or  $\text{OH}^-$  undergoes fast discharge at the electrode.

It may be remarked that a principal failing of the existing a-c method is that it seeks to provide certain intensive properties of the electrode system, such as  $i_0$  and  $\alpha$ , from measurements of the extensive properties,  $C_r$  and  $R_r$ , both of which depend on the effective area of the electrode. This is not easy to define in molten salt systems where the sheathing material is appreciably conducting. Methods involving only intensive properties, such as the measurement of faradaic rectification (20, 21), suffer these uncertainties to a smaller degree and may therefore be used advantageously in molten salt systems.

#### Acknowledgment

The authors are grateful to the A.E.R.E. (Harwell) for financial support of this work and to the Department of Scientific and Industrial Research for a maintenance grant held by one of them (K.E.J.).

Manuscript received Nov. 16, 1960; revised manuscript received June 28, 1961. This paper was prepared for delivery before the Houston Meeting, Oct. 9-13, 1960.

Any discussion of this paper will appear in a Discussion Section to be published in the June 1962 JOURNAL.

#### REFERENCES

1. S. I. Rempel and L. P. Khodak, *Zhur. Priklad. Khim.*, **26**, 857 (1953).
2. P. Drossbach, *Z. Elektrochem.*, **60**, 387 (1956).
3. J. E. B. Randles and W. White, *ibid.*, **59**, 666 (1955).
4. D. L. Hill, G. J. Hills, J. O'M. Bockris, and L. Young, *J. Electroanalytic Chem.*, **1**, 79 (1959).
5. H. A. Laitinen and R. A. Osteryoung, *This Journal*, **102**, 598 (1955).
6. H. A. Laitinen and H. C. Gaur, *ibid.*, **104**, 730 (1957).
7. R. Stein, *Compt. rend.*, **246**, 2611 (1958).
8. H. A. Laitinen, R. P. Tischer, and D. K. Roe, *This Journal*, **107**, 546 (1960); H. A. Laitinen and D. K. Roe, *Coll. Czech. Chem. Commun.*, in press.
9. H. A. Laitinen, W. S. Ferguson, and R. A. Osteryoung, *This Journal*, **104**, 516 (1957).
10. C. Solomons, J. Goodkin, H. J. Gardner, and G. J. Janz, *J. Phys. Chem.*, **62**, 248 (1958).
11. M. H. Roberts, *Electronic Engineering*, **23**, [276], 51 (1951).
12. J. O'M. Bockris and B. E. Conway, *J. Chem. Phys.*, **28**, 707 (1958).

13. J. R. Macdonald, *Phys. Rev.*, **92**, 4 (1953).
14. P. Delahay, "New Instrumental Methods in Electrochemistry," p. 154, Interscience, New York (1954).
15. L. Pauling, *Proc. Roy. Soc.*, **A114**, 181 (1927); L. Pauling and J. Sherman, *Z. Krist.*, **81**, 1 (1932).
16. Landolt-Bornstein Tabellen, Bd II, part 6, section 274 (1959).
17. J. R. Macdonald, Private communication; J. R. Macdonald and C. A. Barlow, Jr., To be published.
18. R. J. Heus and J. J. Egan, *This Journal*, **107**, 824 (1960).
19. A. Ramanamurthy, Private communication.
20. K. B. Oldham, *Trans. Faraday Soc.*, **53**, 80 (1957).
21. Yn. A. Vdovin, *Doklad. Akad. Nauk.*, **120**, 264 (1958).

## Measurement of Stress In Very Thin Electrodeposits

H. Watkins and A. Kolk

*Electronics Division, The National Cash Register Company, Hawthorne, California*

### ABSTRACT

A modified form of the Brenner-Senderoff contractometer is described. Greater sensitivity is achieved by using jeweled bearings and optical read-out. The instrument is sensitive enough to yield quantitative stress data in films as thin as 40Å average thickness. This instrument has been used to study the initial growth of the plating in thin electrodeposited films of nickel and iron-nickel alloys. Electron micrographs of the films were made to help in interpreting the stress data.

In 1949, Brenner and Senderoff (1) described a spiral contractometer for measuring stress in electrodeposits. This instrument was an extension of the "bent strip" principle which had been used in one form or another since the first quantitative determinations of stress in electrodeposits were made by Stoney (2) in 1909. The spiral contractometer has gained wide acceptance in both research and production control activities.

Since Brenner and Senderoff's paper, three other references to electroplate stress instrumentation have appeared in the literature. In 1954, Kushner (3) described a sensitive instrument which used a flexible metal diaphragm as the plating surface and a differential hydraulic piston system to magnify the stress effect to readable proportions. Hoar and Arrowsmith (4), in 1957, described a "bent strip" instrument which used a solenoid-armature system to apply a counterforce to the strip. The current in the solenoid necessary to prevent the strip from bending was measured and related to the stress in the electrodeposit. In 1959, Fry and Morris (5) described a Brenner-Senderoff Contractometer which was constructed using miniature ball bearings, but otherwise followed the original design.

This paper describes a sensitive modification of the Brenner-Senderoff Contractometer. The object in constructing a more sensitive variation of the contractometer was to study the stress during the very early stages of growth of the electrodeposit. Other instruments described in the literature, with the possible exception of Kushner's "Stresometer" (3), do not have the sensitivity required for observation of stress in films in the 1000Å thickness region and below.

Experimental means for observing the physical structure of very thin electrodeposits are limited. The electron microscope, which has been used extensively for research on evaporated films, is of somewhat limited utility because of difficulties in

specimen preparation and the fact that dynamic measurements cannot be made. It is hoped that combining stress measurements with electron micrographs may permit better inferences to be drawn regarding structural detail in the very thin film region. One of the possible uses of the stress data is to indicate beginning of film continuity and to indicate structural change as the electroplate increases in thickness.

### Modified Brenner-Senderoff Contractometer

Two requirements for an increase in sensitivity were considered in the new instrument. These were a very low friction bearing system and a large "amplification" in the read-out system.

To achieve low friction, synthetic sapphire jeweled cap bearings were used.<sup>1</sup> The effectiveness of this type of bearing is determined by the degree of polish on the journal shaft and the general alignment and machining tolerances of the various parts. Because of the highly polished shaft and close tolerance, it was decided to have all the bearings outside the corrosive and thermal conditions of the plating solution. This was accomplished as shown in Fig. 1 by

<sup>1</sup> Supplied by R. P. Gallien and Son, 220 West Fifth Street, Los Angeles 13, California.

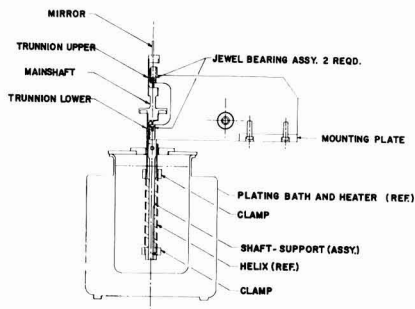


Fig. 1. Modified Brenner-Senderoff contractometer

using a special trunnion arrangement which restricts the rotation of the instrument to approximately  $270^\circ$ . However, this is more than adequate for the optical read-out system.

A wheel, 1 in. in radius, was incorporated in the bearing shaft to allow simple calibration of the spirals. It also allows the shaft to be clamped out of contact with the thrust bearings when the instrument is not in use.

Even with the jewel bearings, it was still found necessary to mount a small vibrator on the apparatus to relieve static friction. It was also found advantageous to lubricate the bearing with a small drop of fine oil. Any dust in the bearings caused a considerable loss in sensitivity due to increased friction.

To amplify the rotation of the spiral, the optical system from a ballistic galvanometer was used as an optical lever arm. A mirror was mounted on the axis of the instrument. The mirror is adjustable to allow the reticle to be set at "zero" at the beginning of a run. Displacement of the reticle was visually noted.

All the components are mounted on a standard optical bench to maintain the proper positioning of the optical system.

To enhance the sensitivity further, the spirals used with this instrument were approximately 0.005 in. in thickness. The other dimensions of the spirals were essentially the same as described by Brenner and Senderoff (1).

A Du-Nouy tensiometer was calibrated in grams of force and mounted on a ring stand in such a way as to exert this force in a horizontal direction by means of a fine thread which was attached to the calibration wheel. This was used to calibrate every spiral just prior to starting a stress determination, following the method given by Brenner and Senderoff.

The plating cell was a standard 2-liter beaker, and a heating mantle was used to maintain any desired temperature. The anode was a helix of pure nickel wire. A filtered rectifier power supply was used.

The sensitivity of the instrument is dependent on the spiral used and the length of the optical lever arm. The apparatus was set up with a 10-ft lever arm and a brass spiral. Calibration of the instrument under these conditions indicated that a stress of 10  $\text{ksi}^2$  in a 200Å film would cause a deflection of the light beam of 1 cm; the reticle position can be determined to  $\pm 1$  mm (or  $\pm 10\%$ ) or better. At this sensitivity the readings were steady and reproducible. The starting torque of the bearing system was calculated to be of the order of  $1 \times 10^{-6}$  in.-lb or less.

Before every run, the reproducibility of the "zero point" was checked and, if found to be less than  $\pm 1$  mm, the bearings were cleaned and re-oiled. Cleaning always resulted in a zero point reproducibility of  $\pm 1$  mm, or better.

**Automatic recording feature.**—For obtaining stress data on films of 200Å and thinner, an automatic recording system was necessary. Under usual plating conditions, films this thin are formed in a matter of seconds and visual recording of the data is out of the question. The light reticle was replaced by a high intensity "point source" arc lamp. The point source

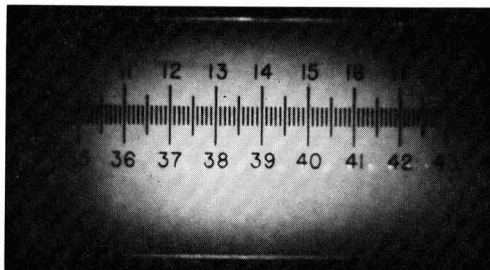


Fig. 2. Photographically recorded spiral deflections

was focused on the galvanometer scale to give a small bright spot.

A small aperture in a rotating disk, driven by a synchronous motor, was placed in the light path. This caused the light to be chopped into short pulses at 1-sec intervals. To record the light pulses, a standard "Polaroid" oscilloscope camera was focused on the translucent scale. A time exposure was made while the light pulses swept across the scale during a plating run (see Fig. 2). By switching on the plating current and chopper motor at the same time, and placing the aperture so that a light pulse would be transmitted as soon as the chopper was started, a "zero" time mark was recorded. The displacement of the light pulses on the Polaroid print was measured with a vernier microscopic eyepiece. The instrument was calibrated as previously described, and the light beam deflection was recorded photographically.

### Experimental

The modified contractometer was used to study the stress in nickel plated from a sulfamate bath and the stress in high-iron, low-nickel alloy prepared from a variation of the ferrous chloride-calcium chloride bath with the slight additions of nickel chloride.

#### Substrate Preparation and Plating

Spirals were formed from 5 mil beryllium copper sheet, alloy 25, and heat treated in an inert atmosphere to 160,000 psi tensile strength. The light surface oxide, which was formed, was removed by a 10-sec dip in 8N  $\text{HNO}_3$ , followed by brief dip in 2N HCl. The spirals were then thoroughly rinsed and dried.

After weighing to 0.1 mg the spirals were dipped in Glyptal. The Glyptal was wiped from the outside surface of the spiral with paper tissues wetted with acetone, leaving the inside "stopped off." The spiral was mounted on the instrument, taking care not to touch the surface to be plated, and then the spiral was calibrated. The spiral was briefly dipped in 2N HCl, rinsed, and immersed in the plating bath.

The spirals were normally in the bath about 15 sec before the plating current was started. No deflection of the contractometer was detectable prior to plating. Readings were taken every 5 sec for the first minute and every 10 sec until the run was discontinued. The plated spiral was quickly removed from the plating solution and rinsed.

The stop-off lacquer was removed with acetone, the spiral was dried in a vacuum dessicator and re-

<sup>2</sup>  $\text{ksi} = 1000$  pounds per square inch.

weighed. The appropriate physical dimensions of the spiral were measured.

The final thickness of the plate was calculated by dividing the weight of the plate by the bulk density of the plated metal and by the area plated. The plate thicknesses throughout the run were calculated by assuming a constant cathode efficiency and multiplying the final thickness by the fraction of the total time plated for each point. The method gives an average thickness and does not necessarily imply a continuous, uniform film. The average and instantaneous<sup>3</sup> stresses were calculated as outlined by Brenner and Senderoff (1) without the thickness or modulus of elasticity corrections. This is valid because of the very thin plates involved.

#### Stress in Nickel Plated From a Sulfamate Bath

**Plating conditions.**—The sulfamate nickel bath was prepared from reagent grade nickelous carbonate, 99+ % sulfamic acid, and reagent grade boric acid. The bath composition and plating conditions were:

Nickel sulfamate	1M
Boric acid	0.5M
pH	3.6 to 3.7
Temperature	23 ± 1°C
Current density	10 amp/ft <sup>2</sup>

The pH was adjusted with nickelous carbonate and/or sulfamic acid. The bath was filtered as necessary.

**Results and discussion.**—Figure 3 shows the stress-thickness curves for two sulfamate nickel plating runs. The average and instantaneous stress for each run are shown on the graph.

The runs have several characteristics in common. The initial stress values are high, above 50 ksi. The stress rapidly decreases with the instantaneous stress passing through a minimum. The stress tends to approach a common value as the thickness increases. However, the position and shape of the minima and the rate of decrease in stress are not reproducible.

Similar minima have been noted in the literature (1, 6) in instantaneous stress curves for much thicker deposits, but they seem to be reproducible in that

<sup>3</sup> Average stress,  $S_a = 1/t \int_0^t S_i dt$ ; where  $t$  is the thickness of electrodeposit and  $S_i$  the instantaneous stress. The average stress is calculated directly from the experimental data. The instantaneous stress is calculated from the average stress curves by a graphical technique and is therefore more uncertain than the average stress.

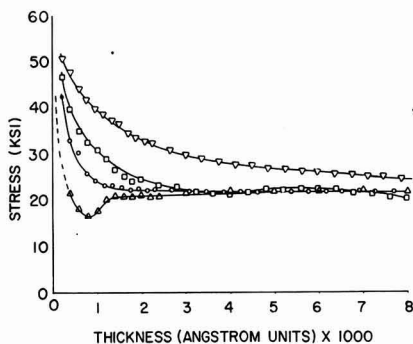


Fig. 3. Stress vs. thickness curve for sulfamate nickel electroplates. Run 1, O, average stress;  $\Delta$ , instantaneous stress. Run 2,  $\nabla$ , average stress;  $\square$ , instantaneous stress.

case. They are interpreted in the thick deposits to be an indication of structural changes in the deposit due to an unknown cause. The origin of the minimum in the stress curves in the very thin films is probably also a structural change and not an experimental artifact.

The stress value found at 8000Å agrees with an extrapolation of the stress data on a deposit from a nickel sulfamate bath made under comparable conditions<sup>4</sup> by Kushner (6). For much thicker deposits (25,000Å and thicker), Kushner found that the stress continued to decrease to a value of about 10 ksi.

#### Prepolarization

The initial high stress found in nickel deposits on copper has been postulated to be due to a pseudomorphic effect. The copper lattice constants are larger than those of nickel so that the copper substrate was presumed to increase the normal lattice constants of nickel at and near to the boundary.

Recent work by Pashley *et al.* (7) has indicated that the pseudomorphism theory is invalid in the case of vacuum evaporated films. No evidence is found for change in lattice constants at the boundary of two materials unless a solid solution alloy is possible. In this case, the change in lattice constants cannot be considered to be true pseudomorphism.

It was felt that the results found in vacuum evaporation are also valid in the case of electrodeposited films. In order to determine if alloy formation might explain the initial high stress found in the nickel electrodeposits investigated, the following experiments were performed. A microammeter was connected between the nickel "anode" and the beryllium copper spiral in the plating cell with no external power supply. A corrosion current amounting to a current density of 200  $\mu\text{a}/\text{ft}^2$  was noted with the beryllium copper spiral anodic, *i.e.*, dissolving in the solution. To suppress (in part, at least) the dissolving of the spiral prior to the start of plating a 1  $\mu\text{a}$  cathode current (current density of 10  $\mu\text{a}/\text{ft}^2$ ) was placed on the spiral simultaneously with immersion in the plating bath. This was accomplished with a 45 v battery and a 45 megohm series resistor connected in parallel with the plating power supply. This caused the spiral to be "prepolarized" with no appreciable plating taking place. No deflection of the contractometer was noted as a result of this prepolarization. The prepolarization current was maintained for 5 min, after which the plating current was turned on and the stress data taken as outlined above. The initial form of the average stress curve was different from the nonprepolarized runs in that it started at about 30 ksi at 200Å and rose to a maximum of about 40 ksi at 500Å. The stress after 1000Å was similar to the nonprepolarized runs. The instantaneous stress, however, was nearly the same as before, indicating that the change in the average stress values was due to an effect operating at thicknesses less than 200Å.

To investigate the stress in the thickness range of 200Å and thinner, the contractometer was set up for automatic recording as previously described. Stress

<sup>4</sup> In Kushner's work the pH was 4.0 rather than 3.6 and the current density was 30 amp/ft<sup>2</sup> rather than 10 amp/ft<sup>2</sup>.



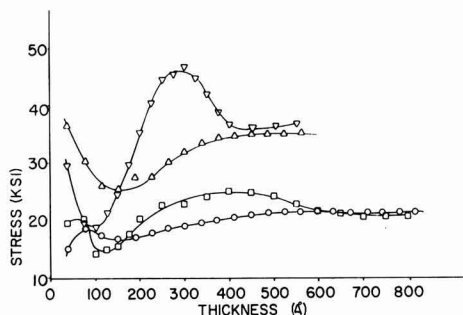


Fig. 4. Stress vs. thickness curve for very thin sulfamate nickel electroplates.  $\Delta$ , not prepolarized average stress;  $O$ , prepolarized average stress;  $\nabla$ , not prepolarized instantaneous stress;  $\square$ , prepolarized instantaneous stress.

data was taken for the nonprepolarized and prepolarized cases as mentioned above. The curves of average and instantaneous stress are shown in Fig. 4. The thinnest films measured had an average thickness of about 40Å. In this case, the thicknesses were assumed to be a linear function of plating time, based on the measured thicknesses of the previous runs. This assumption was checked by plating small beryllium copper coupons (approximately 2 in.<sup>2</sup> surface area) for 3, 30, and 300 sec. The weight change due to the electrodeposited nickel was measured on a microbalance. Within experimental error, the weight of nickel plated was a linear function of plating time.

For these thinner films the stress in the nonprepolarized case is again higher than for the prepolarized case. However, the correlation between these runs and the previous runs (Fig. 3) is not very good. The peculiar oscillatory form of the instantaneous stress for the nonprepolarized run (Fig. 4) cannot be explained at this time. It is not due to mechanical resonance in the contractometer.

The lack of correlation is felt to be due to a difference in surface condition of the spirals even though they all received the same chemical treatment (except for prepolarization) prior to plating.

*Electron micrographs.*—In a further attempt to elucidate the initial mechanism of plating, electron micrographs were prepared from spirals plated with prepolarization. Two of these micrographs are shown in Fig. 5 and 6. The plating thicknesses investigated were approximately 120, 600, and 4800Å. These correspond to the areas before, at, and after the maximum in the average stress curves of the prepolarized runs.

For the 120Å film (Fig. 5) it can be noted that there appears to be preferential plating at and near the substrate grain boundaries. There is also plated metal on the interior of the substrate grain, but it is not uniform or continuous. For the 600Å film (not shown) the plating seemed to be fairly uniform and continuous. The general structure of the deposit was apparently still controlled by the substrate. At 4800Å (Fig. 6) the plated film has assumed a different surface structure which is probably now controlled by the plating bath and conditions. The position of the substrate grain boundaries is again evident, but now the plating seems to be inhibited at the boundaries.



Fig. 5. Electron micrograph of 120Å thick nickel film. Magnification 7200X before reproduction.

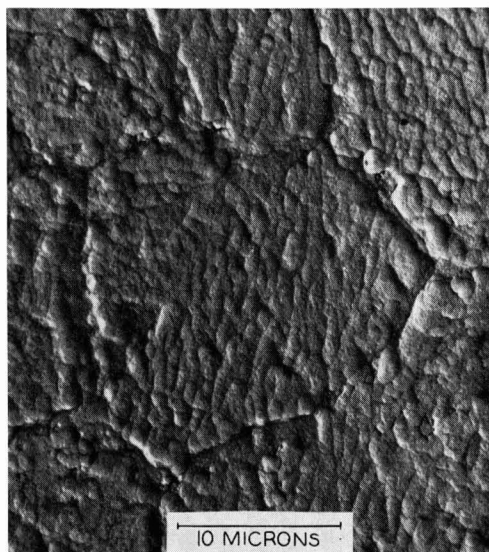


Fig. 6. Electron micrograph of 4800Å thick nickel film. Magnification 6800X before reproduction.

This is opposite to the situation in the 120Å film case. A detailed correlation between the stress data and the electron micrographs cannot be made, but it appears significant that changes in the stress effect are paralleled by changes in the surface structure of the electrodeposit.

#### *Stress in High-Iron, Low-Nickel Alloy Plates*

*Substrate effect.*—Stress data for high-iron, low-nickel alloy plates were taken on three different substrates: copper-plated stainless steel, beryllium copper, and chemically reduced silver on stainless steel.

*Experimental procedure.*—The copper-plated stainless steel spirals (0.005 in. thick) were pre-

pared essentially as described by Brenner and Senderoff. The copper plate was deposited from a cyanide copper strike solution and was, therefore, extremely thin although the spirals had a uniform copper color. The beryllium-copper spirals were prepared exactly as mentioned before.

The chemically reduced silver was applied to previously stopped-off stainless steel spirals by simultaneously spraying commercially available silvering and reducing solutions. The spiral was rotated during the spraying operation and, when silvered, thoroughly rinsed with distilled water. The silvered spirals were not weighed but were mounted immediately on the contractometer, calibrated, and plated.

In all runs, readings were taken every 5 sec until a total time of 50 sec, at which time, the run was terminated. In the case of the silver substrate the amount of metal plated was determined by chemical analysis. Otherwise the stress values were calculated as previously described.

The plating bath was prepared from reagent grade chemicals with the following composition and plating conditions:

$\text{FeCl}_2 \cdot 4\text{H}_2\text{O}$	= 285 g/l
$\text{NiCl}_2 \cdot 6\text{H}_2\text{O}$	= 10 g/l
$\text{CaCl}_2 \cdot 2\text{H}_2\text{O}$	= 238 g/l
pH	$1.0 \pm 0.1$
Temperature	$80^\circ \pm 2^\circ\text{C}$
Current density	50 amp/ft <sup>2</sup>

Prior to use a slight excess of hydrochloric acid and iron powder were added to the bath and it was heated to about  $80^\circ\text{C}$  for half an hour. The solution was cooled, activated charcoal and Celite Filter-Aid added, and the solution filtered.

The average and instantaneous stress curves for the various substrates are shown in Fig. 7 and 8. These are curves averaged from several runs on each substrate. The dashed curves in Fig. 7 indicate the standard deviation for the solid curves. Two things can be noted from these curves: (A) there is

<sup>2</sup> The solutions were obtained from Peacock Laboratories, Philadelphia, Pa.

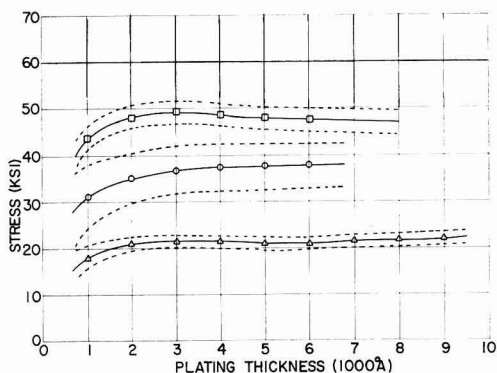


Fig. 7. Effect of substrate on average stress in thin electroplates.  $\square$ , Copper plated stainless steel substrate;  $\circ$ , beryllium copper substrate;  $\triangle$ , silver coated stainless steel substrate.

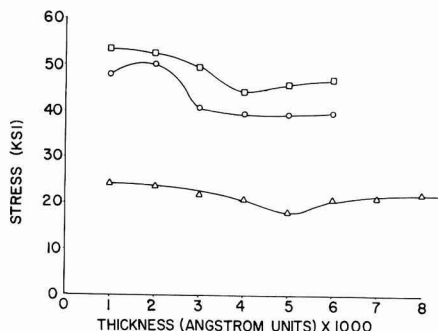


Fig. 8. Effect of substrate on instantaneous stress in thin electroplates.  $\square$ , Copper plated stainless steel;  $\circ$ , beryllium copper;  $\triangle$ , silver coated stainless steel.

a considerable difference in stress on the different substrates, and (B) there is a difference in reproducibility of the stress curves on the different substrates. This points up the necessity for well-standardized substrates for this work.

*Effect of bath pH on stress.*—Stress data for the high-iron, low-nickel alloy were taken on beryllium copper spirals for several bath pH values. The experimental procedures were exactly as earlier stated except for the change in bath pH.

The results are shown in Fig. 9 which is a plot of the average stress at 2000Å and 5000Å of plate thicknesses for various bath pH values. The stress at both thicknesses decreases with increasing pH, and the two curves tend to merge at the higher pH values. It seems that the stress at 5000Å is more dependent on the bath pH than that at 2000Å. This is consistent with the hypothesis that the properties of the initial plating depend to a large extent on the substrate, while the properties of thicker plates are principally determined by the bath and the physical properties of the plated metal.

## Conclusions

The experimental work reported in this paper is admittedly incomplete and does not lead to firm conclusions. It is included mainly to demonstrate the capabilities of the modified contractometer as herein described. Certain general statements can be made, however:

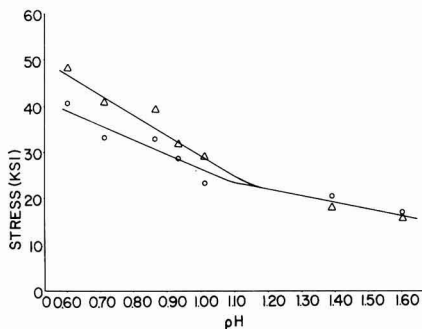


Fig. 9 Effect of pH average stress in thin electroplates.  $\circ$ , stress at 2000Å;  $\triangle$ , stress at 5000Å.

1. The instrumentation as described is sensitive enough to yield quantitative stress data in films that are the minimum thickness for which such data would be considered meaningful.

2. The surface condition of the substrate prior to plating is probably the most important factor in obtaining reproducible stress data in the very thin film region. Great pains must be taken to standardize the substrate surface if any correlation of data is to be hoped for.

3. Electron microscopy used in conjunction with stress determinations may be helpful in investigating the mechanism of the nucleation and growth of very thin electrodeposits.

#### Acknowledgments

The authors wish to acknowledge the services of Dr. Robert D. Sloan of Sloan Research Industries, Inc., Santa Barbara, California, for preparing the electron micrographs presented in this paper.

Manuscript received April 17, 1961; revised manuscript received July 10, 1961. This paper was prepared for delivery before the Houston Meeting, Oct. 9-13, 1961.

Any discussion of this paper will appear in a Discussion Section to be published in the June 1962 JOURNAL.

#### REFERENCES

1. A. Brenner and Senderoff, *J. Research Nat. Bur. Standards*, **42**, 89 (1949).
2. G. G. Stoney, *Proc. Roy. Soc. (London)*, **A82**, 172 (1909).
3. J. B. Kushner, *Proc. Am. Electroplaters' Soc.*, **41**, 188 (1954).
4. T. P. Hoar and D. J. Arrowsmith, *Trans. Inst. Metal Finishing*, **34**, 354 (1956-57).
5. H. Fry and F. G. Morris, *Electroplating and Metal Finishing*, **12**, [6], 207 (1959).
6. J. B. Kushner, *Metal Finishing*, **56**, [5], 82 (1958).
7. G. A. Bassett, J. W. Menter, and D. W. Pashley, *Proc. International Conf. on Structure and Properties of Thin Films*, Bolton Landing, New York, Sept. 9-11, p. 11 (1959).

## Electrical Characteristics of Anodized Niobium Foil and Sintered Pellets

Robert B. Hand,<sup>1</sup> Harry W. Ling, and Thaddeus L. Kolski

Pigments Department, E. I. du Pont de Nemours & Company, Wilmington, Delaware

#### ABSTRACT

Anodized niobium foil and sintered pellets were evaluated in terms of capacitance, leakage, and dissipation factor. Calculated film thickness was shown to be proportional to forming voltage. Field strength in the oxide after anodization was an exponential function of reciprocal absolute temperature for films formed at 25 ma/in.<sup>2</sup>, but not at 2.5 ma/in.<sup>2</sup>. An average charge value of 82  $\mu\text{f v/in.}^2$  was found for foils anodized over a forming potential range of 50-250 v, and between temperatures of 25° and 100°C. Sintering pellets at 2100°C and using 0.01% H<sub>3</sub>PO<sub>4</sub> electrolyte permits anodization to 200 v. Several solid electrolyte capacitors were prepared which had low leakage levels at 35 working volts.

The use of tantalum for electrolytic capacitor anodes is well established. The following report is a description of work which has been undertaken in an effort to demonstrate that niobium may be useful also for this purpose.

#### Experimental Procedure

##### Foil Specimens

*Preparation of samples.*—Samples measuring 1/2 x 1 in. were cut from 0.001 in. niobium foil. The samples were cleaned by washing in trichloroethylene, reagent grade acetone, and distilled deionized water. After cleaning, the specimens were heated 2 hr at 2200°C in a vacuum maintained at less than 5 x 10<sup>-5</sup> mm Hg pressure (Brew furnace<sup>2</sup>), and were cooled to below 50°C in vacuum before being removed from the furnace.

*Anodization.*—Specimens were centered between

two flat, parallel platinum cathodes (2 x 2 in.) which were spaced 2 in. apart. The anodizing electrolyte consisted of 43% ethylene glycol, 43% diethylene glycol, 10% ammonium pentaborate octahydrate and 4% deionized water (by weight). The electrolyte was filtered before being used.

A Sorenson 300B Nobatron was used for power supply. Simpson Model 260 meters were used for current and voltage measurements; the latter were taken across ammeter and anodizing cell. Total quantity of charge passed during anodization was determined by feeding the appropriate meter signal to a Minneapolis-Honeywell Elektronik 2 mv strip recorder. This was accomplished by disconnecting the meter movement and adjusting the signal with shunts so that the full range of each meter setting corresponded linearly to full scale deflection on the strip recorder.

Anodic films were formed to various potentials up to 250 v and at several temperatures up to 100°C. Two current densities were used; based on total sur-

<sup>1</sup> Present address: Flight Propulsion Laboratory Department, General Electric Company, Evendale, Ohio.

<sup>2</sup> Richard D. Brew and Company, Inc., Concord, N. H., Model 424B.

face area of the specimen, these were 2.5 and 25 ma/in.<sup>2</sup>. Samples were held at forming potential for 1 hr to "heal" the anodic film; during this period, current flow usually decayed to 0.02-0.3 ma. After removal from the cell, specimens were washed in deionized distilled water at 90°C and air dried.

**Testing.**—The test cell was identical to the anodizing cell except that platinized platinum cathodes were used. Testing was done at 25° ± 1°C in an electrolyte consisting of 7% ammonium pentaborate octahydrate, 56% ethylene glycol, and 37% deionized water (by weight).

An RCA WV-48B ultrasensitive d-c microammeter was used to measure leakage current; values were noted 5 min after the test potential (80% of forming potential) was applied across the cell.

Capacitance and dissipation factor were measured at 10 v d-c bias using a 120 cps, 1 v a-c signal. A General Radio Type 1611-B Capacitance Bridge in conjunction with a General Radio Type 1204-B Unit Variable Power Supply and a General Radio Type 1214-D, 120 cps oscillator were used for these measurements. The oscillator signal was reduced to the desired value by means of a potentiometer.

#### Sintered Pellet Specimens

**Preparation of samples.**—Powders containing particles of several size ranges were formed into ¼ in. diameter x ½ in. thick pellets by pressing 0.5 to 0.6 g of powder around 0.018 in. diameter niobium wires. Satisfactory green compactions were made using pressures of 10-15 tsi without the use of a binder. For less dense pellets compression as low as 1 tsi yielded compactions of good green strength when stearic acid binder was used. The binder was applied by pouring the powder into an ether solution containing the correct amount of stearic acid (1% of powder weight) and stirring until the ether had volatilized completely.

Sintering of green compactions was accomplished in a Brew furnace using temperatures of 1700°-2100°C. During heat-up, temperature was carefully controlled so that vaporization of the binder and other outgassing did not cause pressure to rise above 10<sup>-4</sup> mm Hg. Pressure was never greater than 5 x 10<sup>-6</sup> mm Hg during a 2-hr sintering period after sintering temperature was reached.

**Anodization.**—The cell was that used for foil anodization. Each of the following aqueous solutions was used as forming electrolyte: 0.01% H<sub>3</sub>PO<sub>4</sub>, 10% H<sub>2</sub>PO<sub>4</sub>, 1% KH<sub>2</sub>PO<sub>4</sub>, and 60% acetic acid.

For maximum pore penetration, sintered pellets were immersed in electrolyte at reduced pressure (about 20 mm). Anodic films were formed to 100 or 200 v at 25°C and a current density of 50 ma/g, and the forming potential was maintained for 2 hr to permit film healing. After removal from the cell, pellets were drained of excess electrolyte, washed in deionized distilled water at 90°C, and air dried.

**Testing.**—Using the same test equipment described above, anodized pellets were tested in 10% H<sub>2</sub>PO<sub>4</sub> at room temperature. Leakage current was measured after 5 min at 70% of forming potential. Capacitance and dissipation were measured as described above.

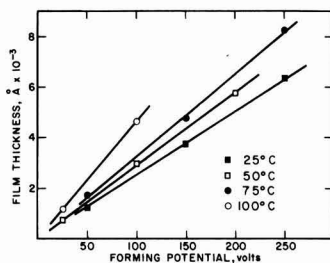


Fig. 1. Final film thickness vs. forming potential on Nb foil anodized at 2.5 ma/in.<sup>2</sup>.

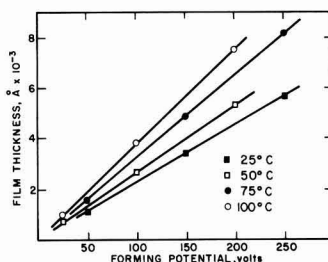


Fig. 2. Final film thickness vs. forming potential on Nb foil anodized at 25 ma/in.<sup>2</sup>.

## Results and Discussion

### Anodized Foils

**Final field and forming field.**—Figures 1 and 2 show anodic film thickness (calculated from total charge transferred) plotted against forming potential. Total charge transferred was determined from continuous plots of current against time obtained with the Simpson meter-Electronik recorder combination. The film was assumed to be Nb<sub>2</sub>O<sub>5</sub> with a density of 4.55 g/cm<sup>3</sup> and current efficiency was taken as 100%.

Reciprocal slopes of the plots in Fig. 1 and 2 have dimensions of field intensity and may be considered to be the field intensities in the oxide after film growth has virtually ceased. These have been designated the final field intensities and are plotted on a logarithmic scale against reciprocal absolute temperature in Fig. 3. A linear relationship is observed

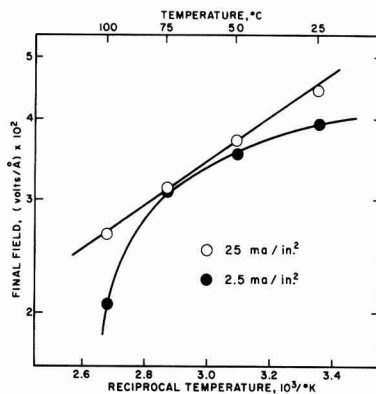


Fig. 3. Final field vs. reciprocal absolute temperature on anodized Nb foil.

for the 25 ma/in.<sup>2</sup> data, but strong deviations from linearity occur at low current density and high temperature, conditions which lead to crystal growth (1, 2) and low current efficiency (3).

Field strengths in the oxide during film formation but prior to reaching final forming potential, i.e., the forming fields, were determined by anodizing specimens at constant current density and making continuous plots of voltage against time using the Simpson meter-Electronik recorder combination. Figures 4 and 5 show charge transferred per unit area plotted against forming potential at several temperatures. Since, for a given current efficiency, oxide thickness is directly proportional to charge transferred per unit area, reciprocals of the slopes of these lines are proportional to forming fields. Assuming 100% current efficiency, these slopes are equal to the forming fields; they are plotted against reciprocal absolute temperature in Fig. 6. Since current flow through the film is an exponential function of reciprocal temperature, the linear relationships found confirm Young's (3) demonstration that the Tafel slope is independent of both temperature and current density, within the limits indicated. The forming fields were determined by averaging incremental slopes of the plots in Fig. 4 and 5 between 50 and 200 v, excepting the 100°C field at 2.5 ma/in.<sup>2</sup> which was determined from the slope at 50 v.

Resistance due to electrolyte was measured and the IR drop across the cell was found to decrease by

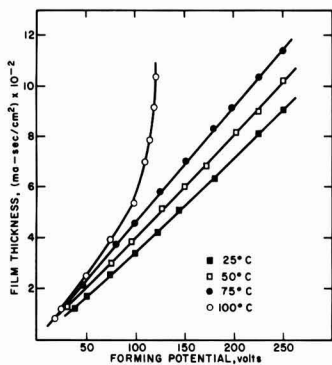


Fig. 4. Film thickness vs. forming potential prior to current decay on Nb foil anodized at 2.5 ma/in.<sup>2</sup>.

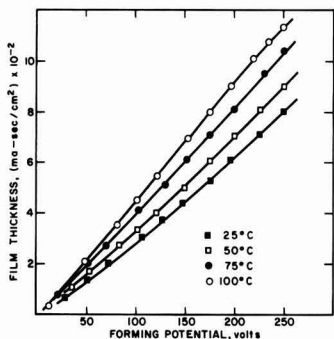


Fig. 5. Film thickness vs. forming potential prior to current decay on Nb foil anodized at 25 ma/in.<sup>2</sup>.

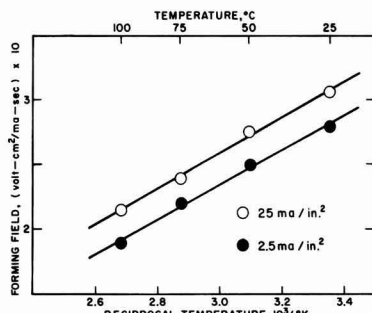


Fig. 6. Forming field vs. reciprocal absolute temperature on anodized Nb foil.

5 v at 25 ma/in.<sup>2</sup> when temperature was increased from 25° to 100°C, indicating that at 100°C during formation at 25 ma/in.<sup>2</sup> voltage across the oxide layer was about 5 v higher than at 25°C. This has the effect of shifting the plots shown in Fig. 5 along the abscissa, but does not change the slopes and hence does not alter the relationships indicated in Fig. 6.

At the end of the current decay period, voltage drop due to the electrolyte was negligible with respect to total voltage drop across the cell since current at that time was less than 300  $\mu$ a.

**Capacitance.**—Capacitance per unit area shown by niobium foils anodized under different conditions is presented in Table I. To obtain these values, the measured capacitance was divided by the total surface area of the specimen. Figures 7 and 8 show reciprocals of the 25° and 100°C values plotted against forming potential. The data for intermediate temperatures, omitted for simplicity, generally fall

Table I. Electrical characteristics of anodized niobium foil

Anodizing temp, °C	Forming potential, v	Capacitance, $\mu$ f/in. <sup>2</sup>	Leakage current, $\mu$ a/ $\mu$ f v	Dissipation factor, %
Anodized at 2.5 ma/in. <sup>2</sup> :				
25	50	1.72	0.0069	7.00
25	150	0.61	0.0113	2.76
25	250	0.36	0.0379	2.36
50	25	3.18	0.0049	10.80
50	100	0.89	0.0076	3.60
50	200	0.46	0.0081	2.80
75	50	1.62	0.0059	5.20
75	150	0.56	0.0064	2.26
75	250	0.32	0.0147	1.38
100	25	2.75	0.0050	9.16
100	100	0.74	0.0232	3.44
Anodized at 25 ma/in. <sup>2</sup> :				
25	50	1.66	0.0064	5.92
25	150	0.58	0.0160	2.70
25	250	0.32	0.0221	2.18
50	25	3.04	0.0067	10.00
50	100	0.84	0.0114	3.44
50	200	0.40	0.0132	2.86
75	50	1.58	0.0088	5.16
75	150	0.56	0.0081	2.62
75	250	0.34	0.0081	1.34
100	25	2.84	0.0050	9.62
100	100	0.77	0.0072	3.32
100	200	0.39	0.0094	2.20



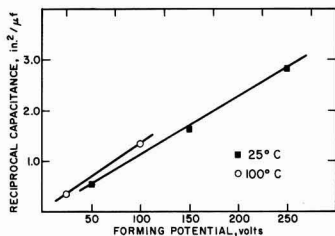


Fig. 7. Reciprocal capacitance vs. forming potential on Nb foil anodized at 2.5 ma/in.<sup>2</sup>.

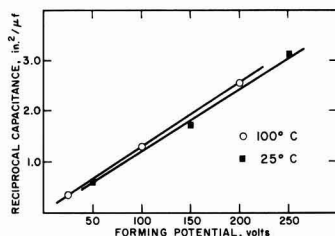


Fig. 8. Reciprocal capacitance vs. forming potential on Nb foil anodized at 25 ma/in.<sup>2</sup>.

between these limiting plots in the expected manner. The average value of charge per unit area for anodized niobium foil, as determined from reciprocal slopes of these plots, is 82  $\mu\text{f v/in.}^2$ . This is about 10% higher than the value of 75  $\mu\text{f v/in.}^2$  reported for tantalum (4). While this may be due partially to comparison of the two values under unlike conditions of anodization, particularly with respect to temperature, it has been demonstrated in this laboratory that anodization of niobium and tantalum foils under identical conditions in both glycol-ammonium pentaborate and 0.01%  $\text{H}_3\text{PO}_4$  electrolytes results in higher capacitance per area values for niobium. The higher value of charge is due to the higher dielectric constant of niobium anodic films, the apparent value of which is estimated to be nearly twice that of tantalum anodic films. However, full advantage of higher dielectric constant is not realized because the anodic films on niobium are 75% thicker than those on an-

odized tantalum formed under the same conditions, as calculated from charge transfer measurements.

**Leakage current.**—Typical values for leakage current are presented in Table I. An attempt to correlate leakage current with anodizing conditions was unsuccessful. While leakage current generally increases with forming (and consequently testing) potential, no clearly defined relationship was evident. Leakage current is about the same for specimens anodized at 25 ma/in.<sup>2</sup> as for those formed at 2.5 ma/in.<sup>2</sup>. The data show no discernible relationship when room temperature leakage currents are compared with the anodizing temperature. While the leakage currents measured on these niobium foils are about twice those observed on tantalum foils formed under the same conditions, the sensitivity of leakage current to factors such as sample purity, sample surface preparation, nature of forming electrolyte, and conditions of anodization is so great that any statements about lowest practicably attainable leakage levels on anodized niobium would be premature. Recently, it has been demonstrated in this laboratory that anodization of niobium foils to 200 v in 0.01%  $\text{H}_3\text{PO}_4$  at 25°C and 25 ma/in.<sup>2</sup> yields anodic films which display leakage currents about 50% lower when tested in 10%  $\text{H}_3\text{PO}_4$ , as compared to those formed and tested in glycol-ammonium pentaborate solutions. The anodic layers formed on foil specimens using dilute phosphoric acid electrolyte are being investigated further.

**Dissipation factor.**—Dissipation factors of the anodized niobium foils, shown in Table I, decrease with increasing forming voltage as expected and are well below 5% for foils anodized to potentials above 50 v.

#### Anodized Pellets

The data presented in Table II are typical for sintered pellets anodized to 200 v in 0.01%  $\text{H}_3\text{PO}_4$ .

**Powder characterization.**—Contrary to expectations, it is not axiomatic that a high surface area niobium powder produces high capacitance anodized pellets. Presence of fines induces excessive sintering during heat treatment at temperatures which range up to a few hundred degrees below the melting

Table II. Properties of anodized porous pellets from niobium powder

Powder designation:	A	B	C	D		
Mesh size, U.S. stand.	−140 +200	−200 +325	−200	−325		
Powder surface area, m <sup>2</sup> /g	0.036	0.046	0.101	0.258		
Compaction pressure, tsi	15	15	15	10	5	
Sintered 2 hr at 2100°C:						
Capacitance, $\mu\text{f/g}$ (200 v formation)	6.6	8.5	10.9	13.7	5.0	5.6
Leakage current, $\mu\text{a}/\mu\text{f v}$	0.004	0.008	0.007	0.007	0.022	0.022
Dissipation factor, %	4.7	4.7	8.7	8.8	85	81
Equivalent series resistance, ohm/pellet	13.3	13.5	20.4	15.2	425	333
Sintered density, % theoretical	66	65	72	61	81	83
Sintered 2 hr at 1700°C:						
Capacitance, $\mu\text{f/g}$ (200 v formation)	9.1	12.7	17.9	20.8	18.5	20.0
Leakage current, $\mu\text{a}/\mu\text{f v}$	0.022	0.024	0.020	0.020	0.025	0.025
Dissipation factor, %	5.0	7.0	11.5	9.6	26	24
Equivalent series resistance, ohm/pellet	12.2	13.3	14.4	10.8	33	26
Sintered density, % theoretical	62	57	64	53	72	71

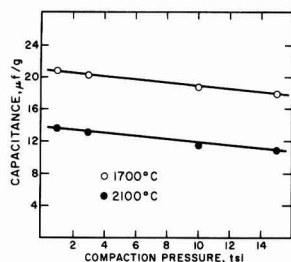


Fig. 9. Effect of compaction pressure on final capacitance of pellets made from Nb powder "C" after sintering at two temperatures and anodizing to 200 v.

point of niobium, and leads to anodized pellets characterized by decreased capacitance, increased leakage current and high dissipation factor.

Based on the results of this research, it would appear that the most desirable niobium powder has a rather narrow particle size range with a peak concentration of  $44\mu$  particles and upper and lower limits of about  $74\mu$  and  $25\mu$ , respectively. The specific surface of such a powder, as measured by the BET krypton adsorption method, is in the range 0.06-0.09  $\text{m}^2/\text{g}$ .

**Compaction pressure.**—High compaction pressures during formation of the green pellets result in sintered bodies with high density and hence low capacitance. Therefore, it is advantageous to compact the powder at as low a pressure as feasible. Variation of final observed capacitance with compaction pressure is linear between 1 and 15 tsi as shown in Fig. 9, although the slopes are generally dependent on particle size and sintering temperature. Use of stearic acid binder to impart sufficient green strength to pellets pressed at 5 tsi or less was found to have no adverse effect on leakage current of the anodized body.

**Sintering temperature.**—High sintering temperatures yield pellets with high density and consequently low capacitance. This is shown in Table III, which tabulates results on bodies sintered for 2 hr and anodized in 0.01%  $\text{H}_3\text{PO}_4$ . However, sintering temperatures near  $2100^\circ\text{C}$  are necessary in order to attain low levels of leakage current for porous bodies anodized to 200 v. Sintering at  $1900^\circ\text{C}$  appears to produce as low a leakage level as sintering at  $2100^\circ\text{C}$  on pellets anodized to only 100 v. Sintering

Table III. Effect of sintering temperature and forming potential on electrical properties of anodized porous pellets made from niobium powder "A"

Sintering temp., $^\circ\text{C}$	Capacitance, $\mu\text{f/g}$	Leakage current, $\mu\text{a}/\mu\text{f v}$	Dissipation factor, %	Equivalent series resistance, ohm/pellet
Formed to 200 v:				
2100	6.58	0.0039	4.66	13.3
1900	8.25	0.0069	5.04	13.9
1700	9.09	0.0222	5.04	12.2
Formed to 100 v:				
2100	14.03	0.0018	8.00	13.1
1900	16.83	0.0013	9.04	12.0
1700	18.69	0.0087	10.54	12.1

at  $1700^\circ\text{C}$  results in markedly higher leakage currents when pellets are anodized to 100 v, and when such pellets are anodized to 200 v, leakage currents are so high as to be generally unsatisfactory.

**Forming electrolytes.**—Among the forming electrolytes tested, both 0.01%  $\text{H}_3\text{PO}_4$  and 10%  $\text{H}_3\text{PO}_4$  were found to give anodic films having low leakage current when formed to 200 v. Although 1%  $\text{KH}_2\text{PO}_4$  produced some anodized bodies with low leakage currents, this result was not obtained as consistently as when the dilute phosphoric acid solutions were used. Pellets sintered at  $1900^\circ$  and  $2100^\circ\text{C}$  gave good leakage tests when formed to only 100 v in 60% acetic acid, but when formed to 200 v in this electrolyte leakage values were very high. Much higher leakage values were obtained using pellets sintered at  $1700^\circ\text{C}$  when formed in 60% acetic acid than in the other three electrolytes mentioned here.

Capacitance and dissipation factor appear to be independent of forming electrolyte.

**Reproducibility of test results.**—In general, capacitance and dissipation factor were reproducible to within a few per cent. Using constant forming conditions, these properties were clearly a function of particle size of the starting powder and sintering conditions. Leakage current was much less reproducible. Even under the best of conditions, i.e., sintering at  $2100^\circ\text{C}$  and forming in 0.01%  $\text{H}_3\text{PO}_4$ , leakage levels varied by a factor of 2 or 3. Pellets sintered at lower temperatures and/or formed in the electrolytes other than dilute phosphoric acid showed a much larger range of leakage currents with variations of a factor of 10 or more being observed. Even under the best conditions, an occasional "wild" result was obtained; this leakage might be as high as 500 times the average value shown by other pellets anodized under exactly similar conditions. The occurrence of wild results increased with lower sintering temperatures. Reasons for the occurrence of wild results and variability of leakage currents almost certainly are connected with defects or regions of incipient crystallization in the anodic oxide film, these inhomogeneities resulting from surface impurities and unknown electrolyte effects. These phenomena have been investigated in the case of tantalum anodization and are discussed at length by Vermilyea (1, 2).

The test electrolyte was found to have an important effect on final properties of anodized pellets. A given pellet tested in the glycol-ammonium pentaborate electrolyte used for foil testing (and probably in any other relatively high viscosity, low conductivity electrolyte) exhibits lower leakage current, lower capacitance, and higher dissipation factor than in 10%  $\text{H}_3\text{PO}_4$  (or probably in any other low viscosity, relatively high conductivity electrolyte).

**Solid electrolyte capacitors.**—Several niobium solid electrolyte capacitors were prepared successfully using known art for applying the counter electrode (5, 6). For example, after anodizing to 200 v in 0.01%  $\text{H}_3\text{PO}_4$  and coating with  $\text{MnO}_2$ , the finished device showed a capacitance of  $4.80\mu\text{f}$  and dissipation factor of 2.4% at a frequency of 120 cps. The d-c leakage under 35 v potential was about  $0.75\mu\text{a}$  or  $0.0045\mu\text{a}/\mu\text{f v}$ . Life tests are in progress; preliminary

results show that some of these devices exhibit life in excess of two weeks.

Recent work (7) has shown that solid electrolyte niobium capacitors have poor life characteristics above 20 working volts; this has been related to the previously observed difficulty of forming niobium pellets to potentials greater than about 100 v. The demonstrated ability to anodize porous bodies to 200 v, which probably was a result of forming in dilute  $H_3PO_4$ , rather than 60% acetic acid as well as availability of a higher purity niobium powder, suggests that it may be possible to fabricate niobium solid electrolyte capacitors which exhibit good life under loads greater than 20 v.

### Conclusions

It is concluded from the data presented above that niobium is an excellent candidate for further development as an anode material in electrolytic capacitors. It should be pointed out that the metal used in this investigation was not prepared especially for use in capacitors. Improvement of niobium quality, particularly with regard to reduction of impurity levels, and in the case of foils, better rolling techniques, should lead to improved capacitor char-

acteristics for anodized niobium substrates. A search for better anodization electrolytes should also be continued.

### Acknowledgment

The authors wish to express their grateful appreciation to Mr. Charles E. Perry for technical assistance in carrying out a major portion of the experimental work.

Manuscript received April 4, 1961; revised manuscript received July 21, 1961.

Any discussion of this paper will appear in a Discussion Section to be published in the June 1962 JOURNAL.

### REFERENCES

1. D. A. Vermilyea, *This Journal*, **102**, 207 (1955).
2. D. A. Vermilyea, *ibid.*, **104**, 542 (1957).
3. L. Young, *Trans. Faraday Soc.*, **52**, 502 (1956).
4. L. H. Belz, *This Journal*, **108**, 229 (1961).
5. D. A. McLean and F. S. Power, *Proc. Inst. Radio Engrs.*, **44**, 872 (1956).
6. R. L. Taylor and H. E. Haring, *This Journal*, **103**, 611 (1956).
7. D. A. McLean, N. Schwartz, J. K. Werner, and M. Gresh, "Improved Electrolytic Capacitors," Final Report No. 25309-E, Contract DA 36-039 sc-74996, Bell Telephone Laboratories, Inc., Jan. 15, 1960.

## Effects of Interaction among Particles in Electroluminescent Layers

A. T. Halpin and P. Goldberg

*General Telephone & Electronics Laboratories Inc., Bayside, New York*

### ABSTRACT

The optical and electrical behavior of electroluminescent layers are discussed in terms of experimentally determined properties of individual phosphor grains modified by interactions with neighboring particles. Pronounced interaction effects were found and were studied by determining the dependence of cell brightness and electrical dissipation on variables that alter the degree of particle-particle interaction, *i.e.*, phosphor volume fraction and fluidity of embedment medium. One result of interaction between particles is to increase the average luminous flux per unit volume of phosphor as volume fraction increases. A statistical analysis is given which correctly describes this effect in terms of the number of particles in contact in the layer.

The role of particle interaction in determining the dielectric properties of the phosphor is evaluated for two purposes: (a) To test the validity for electroluminescent layers of theoretical formulas that give the dielectric constant of mixtures in terms of component properties and volume fractions, and (b) to evaluate intrinsic phosphor efficiency at infinite dilution (zero interaction). It was found that the dielectric mixture formulas apply only at very low volume fractions and that phosphor efficiency falls with decreasing volume fraction.

This paper is directed toward an understanding of optical and electrical behavior of electroluminescent layers in terms of the average properties of the individual constituent particles. Of prime concern is how single particle behavior is modified by interaction with neighbors. Experimentally the single-particle data required for this problem are the luminous flux and electrical dissipation, both as functions of applied field and phosphor volume fraction. With these quantities the performance of a cell made up

of many particles may be compared with that predicted from the experimental properties of isolated particles and the differences expressed in terms of interaction.

Interaction between grains is likely to be important for at least two reasons. First, several investigators have reported changes in the luminous flux from particles on establishing contact with electrodes and with neighbors (1, 2). Second, high fields, when applied to semiconducting particles in close prox-

imity, can be expected to cause local breakdown with attendant high in-phase current which may dominate the over-all electrical behavior of the cell.

The experimental approach in this work was to study the dependence of cell brightness (emittance) and electrical losses as functions of phosphor volume fraction and applied voltage. The resulting data, when put in appropriate form, can be extrapolated to infinite phosphor dilution. The phosphor properties at infinite dilution will be (except for certain electrode effects) those of isolated non-interacting randomly oriented grains and will be used in interpreting cell data at practically useful volume fractions.

The experimental results that are presented in the following sections are interpreted in terms of interparticle and particle-electrode contacts. Results will be given of a statistical calculation that relates the number of contacts occurring to the phosphor volume fraction and to the observed variation in average particle emission.

The effects of interaction are also to be found in the dielectric properties of the electroluminescent condensers. It will be shown that the usual formulas specifying the dielectric constant of mixtures in terms of the properties of its constituents cannot be applied to electroluminescent layers without regard to interaction effects.

### Experimental Technique

The experimental method was to study phosphor-dielectric mixtures over a wide range of phosphor volume fraction,  $f$ . The range of  $f$  extended from 0.2 down to 0.01 and in some cases to 0.005.

Several phosphor samples of the type ZnS:Cu, Cl were employed. These phosphors were dispersed in dielectrics of varying degrees of viscosity to allow some control over phosphor mobility under applied fields. The embedment dielectrics were castor oil (fluid), "DC-4," solidified castor oil (both semi-rigid), and epoxy resin (rigid). With the exception of the plastic, the dielectrics have very low electrical losses, e.g., for DC-4, the dissipation factor  $D = 0.006$ .

Mixtures of varying volume fraction were incorporated into a demountable, fixed gap sandwich cell. The surface brightness,  $L$ , was viewed through a transparent conductivity coated glass electrode ( $\sim 500\Omega/\text{square}$ ). The demountable sample holder was of Bakelite plus Teflon for optimum insulation. Reproducible measurements on one such cell set its leakage resistance at  $2.2 \times 10^8$  ohms ( $\pm 10\%$ ). Reliable assessment of electrical performance of layers with very small dissipation is possible only if the sample holder contribution to electrical loss is held down at least to the same magnitude as that of the dielectric.

The plastic-embedded cells were prepared by a technique that involved the refrigeration of the phosphor-epoxy mixture before and after forming the layers on glass by the blade method. In this way, a nearly random dispersion of particles in the epoxy resin was maintained. Following 24 hr under refrigeration, the curing of the plastic was completed by a heat treatment.

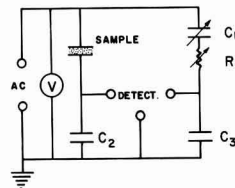


Fig. 1. Electrical circuit of bridge

Before any measurements were taken, all layers were aged for a period of 5 min at 600 v and 1 kc. During this period, a steady state was approached by all cells except those using fluid castor oil. Here a drift in the emission and the electrical characteristics of the layers continued at a slow but noticeable rate.

Cell capacitance and dissipation data were measured with a Wien-type bridge circuit employing a Tektronix Type 53-54D plug-in differential amplifier and Type 535 oscilloscope as a null detector. The bridge was specially constructed to allow operation at high voltages (to 700 v rms) and to yield dissipation factors of the order of  $10^{-3}$  with an error of  $\pm 10\%$ . The measurement circuit is shown in Fig. 1.

Brightness and electrical measurements were taken simultaneously, as a function of voltage. Cell brightness was monitored with a Photovolt Model 520-M photometer employing a 1P21 photomultiplier corrected to the eye response with a Wratten Filter No. 106. A Spectra regulated source (Photo Research Corporation) was used for brightness calibration. The photomultiplier response was found to be linear with incident light over the range of brightness encountered in this investigation, i.e.,  $10^{-2}$  to 100 ft-L.

### Results of Brightness Studies— "The Specific Luminous Flux"

The emittance of an electroluminescent layer will increase with  $f$  simply because mixtures with more particles will emit more light. The exact functionality of this increase may be controlled by factors that are themselves functions of volume fraction. For example, the degree of optical absorption within the layers and the average field in the phosphor will vary with  $f$ , as will other factors which will be discussed later. The cumulative result of these effects may be seen by plotting the emittance data in terms of the ratio  $L/fl$ . We shall define this ratio as the *specific luminous flux*,  $S$ . It will be shown in the following section that  $S$  is equal to the total luminous flux per unit volume of phosphor material. It is a quantity which is suitable for expressing intensive changes in light emission as volume fraction increases. Experimental values of  $S$  may be considered as proportional to the luminous flux from an average individual particle in the layer.

The dependence of  $S$  on  $f$  is shown in Fig. 2 for a system employing an epoxy resin dielectric. The curve shows a sharp rise as  $f$  varies from 0.01 to 0.2 so that  $S(f = 0.2)/S(f = 0) = 3.5$ . It may be argued from a simple consideration of the layers as two phase dielectric mixtures without interactions that

<sup>1</sup> Dow-Corning-4 Compound, a silicone composition,  $k_2 = 2.6$ .

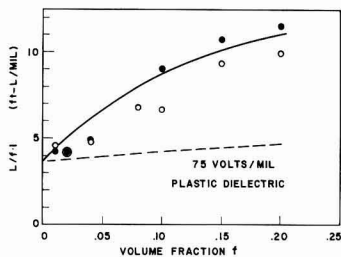


Fig. 2. Specific luminous flux  $S$  vs.  $f$ , 75 v/mil, 1 kc, epoxy resin dielectric. Dotted line shows dependence of  $S$  vs.  $f$  from considerations of dielectric constant change alone. Open and closed circles represent measurements on duplicate layers.

the course of  $S$  vs.  $f$  should be as shown by the experimental points in Fig. 2. For example, an increase in  $f$  raises the average dielectric constant of the medium  $k_2$ . As shown by Roberts (3) an increase in  $k_2$  serves to augment the working field within the phosphor and consequently to increase the luminous flux from the phosphor particles. The contribution of this dielectric effect, however, is small. The dotted line in Fig. 2 shows the dependence of  $S$  on  $f$ , calculated by applying the above argument. It can be seen that the effect amounts to only 15% of the overall increases in  $S$ . Any contribution of self-absorption would tend to decelerate the rise of  $S$  with  $f$ .

A more likely explanation for the shape of the curve in Fig. 2 lies in the occurrence of interparticle contacts. In a mixture in which the crystallites are dispersed and randomly oriented, a certain fraction of particles will be in contact with each other. Higher volume fractions increase this number. The establishment of contacts of this type in electroluminescent layers has been reported by Kremheller (1) as resulting in higher luminous flux from the contacting particles. Our own microscopic studies have verified his findings. We suggest that the enhancement of the average luminous flux from a phosphor particle, as shown by the increase in  $S$ , is due primarily to an increasing percentage of particles that engage in contacts as one goes to higher values of  $f$ . This behavior has been observed as well in mixtures employing other embedments. Figure 3 shows the  $S$  vs.  $f$  characteristics of two phosphors in two semi-rigid dielectrics, DC-4 and solidified castor oil. The same sharp rise in  $S$  with  $f$  is found in both cases.

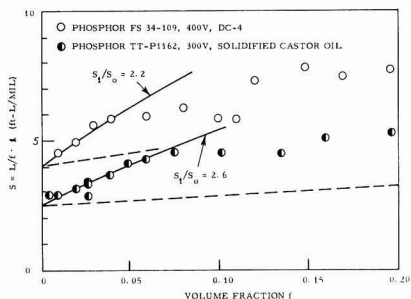


Fig. 3.  $S$  vs.  $f$ ; 1 kc, DC-4 and solidified castor oil dielectrics.

In the following section we give a statistical analysis of the number of contacts that occur in mixtures containing randomly distributed particles. The number of contacts and its dependence on  $f$  will be important in understanding the shape of the  $S$  vs.  $f$  characteristics.

### Statistical Analysis of Occurrence of Contacts

The following calculation gives the number of interparticle and particle-electrode contacts occurring in a phosphor-dielectric mixture. To each particle in contact there will be assigned an average luminous flux which is greater than the luminous flux from an uncontacted particle (1, 2). An expression will then be obtained for the relation between specific luminous flux  $S$  and volume fraction, and this will be compared with the experimental data.

As the statistical model we view the electroluminescent layer as composed of a monodisperse system of  $n$  phosphor spheres, each with a radius  $r_0$ , randomly distributed in a dielectric occupying volume  $V$ . For the purposes of the calculation we replace each of the spheres by a point at its center. A particle is considered to be in contact with an electrode when its center lies at a distance  $\leq r_0$  from the electrode. Two particles are considered to be in contact with each other when the distance between their centers is  $\leq 2r_0$ . The number of interparticle contacts will be derived first.

Consider one test particle of  $n$  particles in a cell. We wish to know the probability,  $p(r)$ , of finding the nearest neighbor of the test particle at a distance  $r$  from it. To obtain  $p(r)$  two simultaneous probabilities must be evaluated: (a)  $p_1$ , the probability of finding a particle at a distance  $r$  from the test particle, and (b)  $p_2$ , the probability that this particle is the nearest neighbor of the test particle. The probability that a particle will be found in the spherical volume element between  $r$  and  $r + dr$  about the test particles is  $p_1 dr$ , and

$$p_1 dr = N4\pi r^2 dr; \quad N = n/V$$

The condition that the particle at a distance  $r$  from the test particle is the nearest neighbor requires that none of the points representing the other  $(n-2)$  particles in the cell shall fall within the volume  $v(r) = 4\pi r^3/3$  around the test particle. The probability for this is

$$p_2 = (1 - v(r)/V)^{n-2}$$

Now for  $v(r) \ll V$  and replacing  $n-2$  by  $n$ , we have<sup>2</sup>

$$p_2 = \exp(-nv(r)/V) = \exp(-Nv(r))$$

Thus

$$p(r) dr = p_1 p_2 dr = N4\pi r^2 \exp(-Nv(r)) dr \quad [1]$$

It can be shown that  $N = 3f/4\pi r_0^3$ . Therefore, from [1]

$$p(r) dr = \frac{3f}{r_0} \left(\frac{r}{r_0}\right)^2 \exp\left[-f\left(\frac{r}{r_0}\right)^3\right] dr \quad [2]$$

The quantity  $p(r)$  is already normalized since the integral of this expression from  $r = 0$  to  $r = \infty$  is

$$\int_0^\infty p(r) dr = \int_0^\infty \frac{3f}{r_0} \left(\frac{r}{r_0}\right)^2 \exp\left[-f\left(\frac{r}{r_0}\right)^3\right] dr = 1$$

<sup>2</sup>  $(1-y)^n = 1 - ny + \frac{n(n-1)}{2!} y^2 - \dots \approx e^{-ny}$  for  $y \ll 1$ ,  $n > 0.1$ .



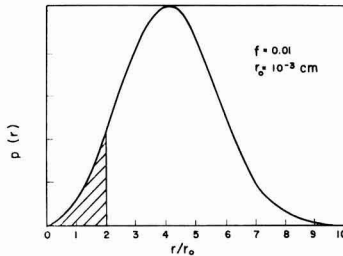


Fig. 4.  $p(r)$  vs.  $r/r_0$ .

unity. Thus if we set  $dv(r) = 4\pi r^2 dr$ , from Eq. [1] we obtain

$$\int_0^\infty p(r) dr = \int_0^\infty \exp[-Nv(r)] N dv(r) = [-\exp(-Nv(r))]_0^\infty = 1$$

The value of  $r$  for which  $p(r)$  is a maximum,  $r_{max}$ , is found by setting  $dp(r)/dr = 0$ . This leads to  $r_{max} = (2\pi N)^{-1/3}$ . Figure 4 shows the function  $p(r)$  vs.  $r/r_0$  for the case of  $f = 0.01$  and  $r_0 = 10^{-3}$  cm, from Eq. [2].

To get the number of particles per unit volume that are in contact, we note that  $p(r)$  is equivalent to the distribution of nearest neighbor distances in the cell. The number of particles in contact per unit volume,  $N_c$ , is therefore

$$N_c = N \int_0^{2r_0} p(r) dr = N \int_0^{v(2r_0)} \exp[-Nv(r)] N dv(r) \quad [3]$$

where  $v(2r_0) = 4\pi(2r_0)^3/3$ , i.e.,  $v(2r_0)$  is an excluded volume around each particle such that if  $v(2r_0)$  includes the center of another particle in the system the two are considered in contact. The shaded area in Fig. 4 represents the fraction of particles "in contact" with neighbors in accordance with the definition of contact.

Then from integration of Eq. [3], and noting that  $Nv(r)_{r=2r_0} = 8f$ , we have

$$N_c/N = 1 - \exp(-8f) \quad [4]$$

This expression gives the fraction of spheres in contact with neighbors and depends only on the volume fraction  $f$ .

The number of particles per unit area in contact with an electrode,  $N_s$ , will now be evaluated. Let  $p_s$  be the probability that a particle placed in a cell will be in contact with either of the two planar electrodes which are a distance  $l$  apart. Particles are defined as "in contact" with electrodes if their centers are located in a slab of thickness  $r_0$  adjoining each electrode. The number of particles per unit area of electrode in contact with electrodes is  $n_s = np_s$  where  $p_s$  is the probability that any of the particles makes an electrode contact.  $p_s$  is determined by the ratio of the volume which constitutes electrode contact to the total volume of the cell. Thus  $p_s = 2r_0/l$ . For a cell of unit area  $V = l$  and  $n = Nl$ ; consequently

$$n_s = np_s = 2Nr_0 \quad [5]$$

Let the total luminous flux from an uncontacted particle be  $F_u$  and that from a particle in contact with a neighbor be  $F_c$ ;  $F_c > F_u$ . The number of uncontacted

particles in the cell of volume  $V$  is  $n_o = n - n_c - n_s$ , (assuming that no particles make contacts to both neighbors and electrodes). Therefore from Eq. [4] and [5] we have

$$n_o = Nl - Nl [1 - \exp(-8f)] - 2Nr_0 \quad [6]$$

The total luminous flux from the cell is then:

$$L = n_o F_u + n_c F_c + n_s F_e$$

and from Eq. [4], [5], and [6] we have

$$L = F_u Nl [\exp(-8f) - 2r_0/l] + F_c Nl [1 - \exp(-8f)] + 2F_e N r_0$$

$$L = Nl [F_c + (F_u - F_c) \exp(-8f) + 2(F_e - F_u) r_0/l]$$

Recalling that  $N = 3f/4\pi r_0^3$  we have

$$S \equiv \frac{L}{fl} = \frac{3F_u}{4\pi r_0^3} \left[ \frac{F_c}{F_u} + 2 \left\{ \frac{F_e}{F_u} - 1 \right\} \frac{r_0}{l} + \left\{ 1 - \frac{F_c}{F_u} \right\} \exp(-8f) \right] \quad [7]$$

Equation [7] is the defining relationship for the specific luminous flux,  $S$ . The quantity  $S$  is equal to the luminous flux per unit volume of phosphor and is therefore a quantity related to intrinsic phosphor performance. It depends on voltage, frequency, and phosphor composition and volume fraction.

At infinite dilution ( $f = 0$ ),  $S = S_o$ , where

$$S_o = \frac{3F_u}{4\pi r_0^3} \left\{ 1 + 2 \left( \frac{F_e}{F_u} - 1 \right) \frac{r_0}{l} \right\} \quad [8]$$

$S_o$  therefore depends on  $F_u$ , on cell and particle dimensions and consequently on the number of electrode contacts and the luminous flux from particles so contacted. For cells of large gap width for which  $l \gg r_0$ ,  $S_o = 3F_u/4\pi r_0^3$  which is a function only of isolated particle properties.

As  $f$  increases above 0.3-0.4,  $S \rightarrow S_i$ , where

$$S_i = \frac{3F_u}{4\pi r_0^3} \left\{ \frac{F_c}{F_u} + 2 \left( \frac{F_e}{F_u} - 1 \right) \frac{r_0}{l} \right\} \quad [9]$$

Eq. [7] can be rewritten using Eq. [8] and [9] as

$$S = S_i + (S_o - S_i) \exp(-8f)$$

or

$$S = S_o [ (S_i/S_o) + (1 - S_i/S_o) \exp(-8f) ] \quad [10]$$

By curve fitting the data of Fig. 2 with Eq. [10] a value of  $S_i/S_o$  may be obtained. The line in Fig. 2 through the experimental points is drawn from Eq. [10] with  $S_i/S_o = 3.5$ .  $S_i/S_o$ , the only parameter requiring adjustment, is a combination of several factors including the fluxes from particles in contact (with either electrodes or neighbors) and both cell and particle geometry. No absolute values can be given to  $F_u$ ,  $F_c$ , or  $F_e$ , although from the data of Fig. 2 something may be said about certain limiting values. Self-consistency of the data requires that

$$S_i/S_o \geq 3.5^3 \text{ otherwise } 2 \left( \frac{F_e}{F_u} - 1 \right) \frac{r_0}{l} \text{ will be negative and } F_e/F_u \text{ will be } < 1, \text{ which is counter to ex-}$$

<sup>3</sup> This value of  $S_i/S_o$  is reasonable since Krehmeller estimates from experiment that a value of  $m = 4$  is common (1), where  $m = F_c/F_u \approx S_i/S_o$ .

perience. This further requires that  $3F/4\pi r_s^3 \leq 3.7$  ft-L/mil which sets an upper limit on the specific luminous flux from an uncontacted particle. This limit provides information on the maximum number of photons which are emitted under the given excitation condition. Thus if  $S = 3.7$  ft-L/mil = 1.56 lumens/cm<sup>3</sup> =  $3.3 \times 10^{-8}$  watts/cm<sup>3</sup> =  $2 \times 10^{18}$  photons/cm<sup>3</sup> sec, then for a frequency of 1000 cps we have  $2 \times 10^{18}$  photons/cm<sup>3</sup>-cycle emitted from the phosphor. The activator content ( $10^{-3}$  g at./mole) is  $2.4 \times 10^{10}$  at./cm<sup>3</sup>. Therefore from these data no more than one in  $10^6$  activator atoms emit radiatively at 75 v/mil and 1000 cps in the interval of one cycle from an uncontacted particle.

It should be noted finally that the treatment of phosphor data in this way should facilitate comparison with measurements of the total luminous flux from macroscopic single crystal experiments where the measurement of  $S$  can be accomplished readily.

This analysis, while giving reasonable agreement with the experimental data, is only an approximation to the actual phosphor-dielectric system. Factors that have not been included in the derivation are:

- (i) consideration of particle shape to allow for deviation from sphericity
- (ii) consideration that the particle sizes are not monodisperse but probably follow log normal distribution of size.
- (iii) consideration that the average dielectric constant (and, hence, the effective electric field strength in a particle) may vary throughout the cell volume depending upon local variations of  $f$ .
- (iv) consideration of interactions among three or more particles.

These factors may in part explain the departure of the theoretical line from the experimental data in Fig. 3 and 6 for  $f > 0.08$ .

The following section will trace the consequences of interaction effects on the electrical properties of the electroluminescent layers.

### Electrical Behavior of Electroluminescent Layers

Roberts (3) was the first to apply to electroluminescent layers the classical formulas of two-phase dielectric systems. These formulas, used by him for the case of spheres immersed in a continuous dielectric medium, provide the dielectric properties of the phosphor phase from the known properties of the embedment dielectric and the experimental data of the mixture. Later, Lehmann (4) employed two-phase dielectric calculations based on a geometrical model other than spheres. Goffaux (5) devised semi-empirical formulas for the electrical characteristics of the layers based on the data of Luyckx, Vandewauwer, and Ries (6). In these reports only Lehmann considered volume fraction as a working variable. His data, however, are obscured by the use of a fluid dielectric. Thus even at very low volume fractions large interactions prevail owing to interparticle attractions, migration, and phosphor settling.

The electrical data reported here will serve two ends. The first is to ascertain the conditions under which Roberts' methods of calculation are valid for evaluating phosphor properties. The second is to determine the effects of interactions on electrical power consumption in the phosphor phase and their attendant contribution to phosphor efficiency.

### Electroluminescent Layer As A Two-Phase Dielectric System

The formula applied by Roberts for the field in the phosphor is

$$\frac{E_1}{E} = \frac{3k_2}{2k_2 + k_1 - f(k_1 - k_2)} \quad [11]$$

and the relationship for the complex dielectric constant of the phosphor phase is

$$k_1 = \frac{k_m k_2 (2 - 3f) - 2k_m}{k_m (1 - 3f) - k_2} \quad [12]$$

where  $k_m$ ,  $k_1$ , and  $k_2$  are the complex dielectric constants of the mixture, the phosphor, and medium, respectively.  $E$  is the applied field and  $E_1$  the electric field in the phosphor.

These equations and other similar ones, recently summarized by Reynolds and Hough (7), are all based upon the Clausius-Mossotti relation which does not consider interactions. Our experience has been that these formulas are invalid for electroluminescent layers except for extremely dilute mixtures. That is, the layers behave like ideal two-phase systems when particle concentration is low enough so that most of the particles are isolated from each other.

The layers begin to depart from the idealized behavior as more particles begin to interact when  $f$  is increased. This behavior may be illustrated with the following example. Two layers were prepared, using the same phosphor, and were identical except for the suspending media which had dissimilar dielectric constants. The  $\log L$  vs.  $V^{-1/2}$  characteristics for two such layers are shown in Fig. 5. Here semi-rigid dielectrics were employed: DC-4 and solidified castor oil. In order for the two mixtures to produce the same brightness, the electric field in the phosphor phase of each mixture must be the same. The voltages that must be applied to the two mixtures, to give the same field in the phosphor, will of course be different due to the dissimilar dielectric constants of the embedments.

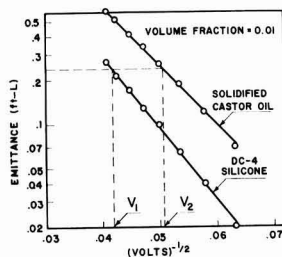


Fig. 5.  $\log L$  vs.  $V^{-1/2}$ , DC-4 and solidified castor oil dielectrics, 1 kc.

\* Using the lumen equivalent for green emission of 475 lpw.

Assuming the mixtures to be ideal systems, one can calculate the ratio of the applied voltages required for the pair of mixtures to give the same brightness. This is done by applying Eq. [11] and by using experimentally determined values of the phosphor dielectric constant,<sup>5</sup> at 75 v/mil,  $k_1 = 20$ . In Table I these voltage ratios, derived theoretically and based on no interactions, are compared with corresponding experimental values, *i.e.*,  $V_1/V_2$  in Figure 5, for three values of volume fractions.

Table I. Test of Eq. [11] using L to monitor phosphor field

$f$	L (ft-L)	$V_1/V_2$ (exper.)	$V_1/V_2$ (Theor.)
0.01	0.2	1.45	1.34
0.058	1.0	1.72	1.33
0.10	2.0	2.01	1.32

For  $f = 0.01$  there is reasonable agreement. At higher volume fractions, for which interactions are likely to be large, the ratios grow further apart, signifying a departure from the physical state of noninteraction represented by Eq. [11] and [12].

Power Dissipation in the Phosphor Phase

The phosphor efficiency may be written as

$$\eta = \frac{S}{P_1} \text{ lpw}$$

where  $P_1$  is electrical power dissipation per unit volume of the phosphor phase. It is our aim in this section to show the dependence of  $P_1$  on  $f$  and, together with the data for  $S(f)$ , to evaluate  $\eta(f)$ . The power dissipation per unit volume of the two-phase mixture,  $P$ , is

$$P = fP_1 + (1 - f) P_2$$

from which

$$P_1 = [P - (1 - f) P_2]/f \quad [13]$$

It can be seen from Eq. [13] that experiments designed to trace the change in  $P_1$  vs.  $f$  at very low  $f$  must be performed with a dielectric for which  $P_2$  is low. DC-4 is satisfactory and when used together with a cell with  $D \approx 0.001$ , the phosphor dissipation can readily be obtained from Eq. [13].

Figure 6 shows the dependence of  $S$ ,  $P_1$ , and  $\eta$  on  $f$  for volume fractions up to 0.12. It should be noted

<sup>5</sup> Determined by applying Eq. [12] to mixtures with  $f$  in the range 0.03-0.20 and extrapolating the plot of the calculated  $k_1$  values vs.  $f$  to  $f = 0$ .

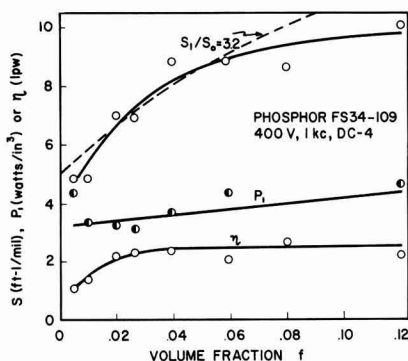


Fig. 6.  $S$ ,  $P_1$ , and  $\eta$  vs.  $f$  for DC-4 dielectric, 400 v, 1 kc

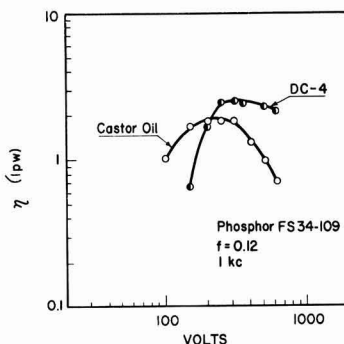


Fig. 7.  $\eta$  vs.  $V$  for fluid (castor oil) and semi-rigid (DC-4) media, 1 kc,  $f = 0.12$ .

that, in the range 0.005 to 0.04,  $P_1$  increases very slowly with  $f$  and almost the total change in  $\eta$  is due to changes in  $S$ . Apparently the physical processes that are responsible for increasing  $S$  as interactions become more frequent do not bring about any appreciable increased power dissipation in this range of  $f$ . The rise in  $\eta$  with  $f$  is in agreement with Thornton's results (8).<sup>6</sup> The specific luminous flux data of Fig. 6 are effectively a check on the reproducibility of the data in Fig. 3. The  $S_1/S_0$  values in the two cases are comparable (2.2 vs. 3.2).

With a fluid dielectric the system can be quite complex. A demonstration of this is seen in Fig. 7 which shows the  $\eta$  vs.  $V$  curves for one phosphor under conditions of strong interaction (fluid dielectric) and less strong interaction (semi-rigid dielectrics) at  $f = 0.19$ . It is clear from Fig. 7 that the sharply peaked curve of  $\eta$  vs.  $V$  under the conditions of measurement (high  $f$ ) is not a true indication of intrinsic phosphor properties but rather of the way in which many particles interact. The over-all result is that (a) intrinsic phosphor efficiencies can only be evaluated at low  $f$ , and (b) efficiencies measured at higher  $f$  represent collective effects of many particles.

Discussion

Two possible explanations will be offered to explain why  $F_c/F_0 > 1$  and therefore to explain the rise of  $S$  with  $f$ .

The first of these is based on the concentration of voltage in one of the two contacting particles. For example, if the line between the geometrical centers of two particles roughly parallels the field direction, then the voltage across the two when they have joined will be approximately the sum of their separate voltage drops before contact. Following contact there may be a redistribution of the total voltage drop available to the pair of particles, resulting in an increase in the voltage drop across one and a decrease across the other. Under favorable conditions this can lead to a net increase in total luminous flux from the pair.

Other explanations may be offered in terms of contacts between grains serving as (i) additional

<sup>6</sup> The experimental error in determining efficiencies at very low  $f$  is due to uncertainties in determining  $P_1$ . It is estimated that the error in  $P_1$  at  $f = 0.005$  is 50%; at  $f = 0.01$  it is about 30%. For  $f > 0.04$  it is about 10%. The rise of  $\eta$  with  $f$  appears to be real.

barriers for excitation or (ii) sources of electrons from one particle for recombination with centers in the other. This requires the ultimate return of electrons to maintain charge neutrality. No choice can as yet be made among the possibilities. Particles in contact with electrodes may be brighter owing to processes described by the Hahn and Seeman (2) which involve injection of electrons from electrodes.

With respect to the electrical properties it is possible to describe the phosphor-dielectric system with the model of noninteracting spheres immersed in an isotropic homogeneous dielectric provided the volume fraction is low. This approach may appear incompatible with the view that electroluminescent phosphor particles possess local regions of high field (9) and, therefore, electrical inhomogeneities. The most that can be said here is that one may evaluate the average field in the phosphor from Eq. [11] and then distribute this field in the particle as demanded by the theory.

We cannot specify an appropriate dielectric mixing formula that will describe the dielectric behavior of the system as  $f$  increases into the range of strong interaction. This is due chiefly to the inability to describe in quantitative terms the dielectric behavior of two semiconducting particles in contact.

#### Acknowledgment

It is a pleasure to acknowledge many helpful discussions with Dr. D. H. Baird and Dr. R. N. Sumnergrad on all aspects of this work and also their aid in deriving Eq. [2]. The authors greatly appreciate the help of Dr. J. J. Dyman in preparing the layers with plastic dielectric.

Manuscript received May 19, 1961; revised manuscript received July 14, 1961. This paper was prepared for delivery before the Chicago Meeting, May 1-5, 1960.

Any discussion of this paper will appear in a Discussion Section to be published in the June 1962 JOURNAL.

#### REFERENCES

1. A. Krehmeller, *This Journal*, **107**, 8 (1960).

2. D. Hahn and F. W. Seeman, *Z. Physik*, **146**, 644 (1956).
3. S. Roberts, *J. Opt. Soc. Am.*, **42**, 850 (1952).
4. W. Lehmann, *This Journal*, **103**, 24 (1956).
5. R. Goffaux, *J. Phys. Rad.*, **20**, (suppl. to No. 4), 18A (1959).
6. A. Luyckx, J. Vandewauwer, and S. Ries, *Ann. Soc. Scientifique de Bruxelles*, **72**, 58 (1958).
7. J. A. Reynolds and J. M. Hough, *Proc. Phys. Soc.*, **B70**, 769 (1957).
8. W. A. Thornton, *J. Appl. Phys.*, In press.
9. P. Zalm, *Philips Research Repts.*, **11**, 353, 417 (1956).

#### DEFINITIONS OF SYMBOLS

- $E$ , Applied electric field.  
 $E_1$ , Electric field in the phosphor phase.  
 $f$ , Volume fraction of phosphor.  
 $F_u$ , Total luminous flux from uncontacted particle.  
 $F_c$ , Total luminous flux from particle in contact with a neighbor.  
 $F_e$ , Total luminous flux from particle in contact with an electrode.  
 $k_1$ , Complex dielectric constant of phosphor.  
 $k_2$ , Complex dielectric constant of embedding medium.  
 $k_m$ , Complex dielectric constant of phosphor-dielectric mixture.  
 $l$ , Cell thickness.  
 $L$ , Surface brightness or emittance.  
 $n$ , Total number of particles in cell.  
 $n_u$ , Number of particles in cell without contacts.  
 $n_c$ , Number of particles in the cell making contact with neighbors.  
 $n_e$ , Number of particles in the cell making contact with electrodes.  
 $N$ , Total number of particles per unit volume =  $n/V$   
 $N_e$ , Number of particles per unit volume making contact with neighbors.  
 $p_1, p_2, p_3$ , Probabilities entering into calculations of contact occurrences.  
 $p(r)$ , Distribution of nearest neighbor distances; probability of finding the nearest neighbor of a test particle at a distance  $r$ .  
 $P$ , Power dissipated per unit volume of phosphor—dielectric mixture.  
 $P_1$ , Power dissipated per unit volume of phosphor.  
 $P_2$ , Power dissipated per unit volume of dielectric.  
 $r$ , Radial distance from the center of a test particle.  
 $r_p$ , Particle radius.  
 $S$ ,  $L/4\pi r^2$  = "Specific Luminous Flux."  
 $S_0$ , Value of  $S$  at  $f = 0$ .  
 $S_1$ , Limiting value of  $S$  as  $f$  increases toward unity.  
 $v(r)$ ,  $4\pi r^2/3$ .  
 $V$ , Total cell volume;  $V = l$  for cell of unit area.  
 $V$ , Voltage (rms).  
 $\eta$ , Phosphor efficiency.

## A Photosensitive Single Crystal p-n Junction in Lead Selenide

M. F. Kimmitt and A. C. Prior

Royal Radar Establishment, Malvern, England

#### ABSTRACT

A single crystal with a thin surface p-n junction has been grown from the vapor and its photovoltaic properties measured at various temperatures. The detector has high quantum efficiency but low electrical resistance, which is discussed. With the detector cooled to 77°K the experimentally achieved value of  $D^*$  was  $3 \times 10^8$  cm cps<sup>1/2</sup> watt<sup>-1</sup> at 4 $\mu$ . Analysis indicates that with a quieter amplifier and a more suitable contact arrangement a  $D^*$  of  $7 \times 10^9$  cm cps<sup>1/2</sup> watt<sup>-1</sup> should have been achieved with the same junction. With development substantially better performance seems probable.

Evaporated or chemically deposited photoconductive layers of lead selenide are well known. In principle, better performance would be expected from single crystal detectors if these could be made with the appropriate geometries, carrier concentrations,

and recombination properties. For photoconductive detectors, particularly those cooled below room temperature, low extrinsic carrier concentrations are necessary, and the achievement of concentrations in single crystals as low as have been attained in

layer devices would be a formidable task. However, for a p-n junction photovoltaic detector very low carrier concentrations should not be necessary and, furthermore, the theoretical performance of such a detector should increase rapidly as the temperature is reduced. Consequently, when single crystals of PbSe grown from the melt by Lawson (1) became available in this laboratory, several attempts were made by one of the authors (A.C.P.) and his colleagues to prepare suitable junctions. Methods tried included epitaxial deposition of an opposite type layer *in vacuo*, diffusion of selenium into n-type crystals, and the diffusion of a surface layer of copper into p-type crystals. Although surface junctions were produced, none showed marked electrical non-linearity or significant photosensitivity. This was attributed to a combination of low carrier lifetime, the difficulty of obtaining junctions sufficiently sharp and close to the surface, and to mechanical irregularities of the surface resulting in the contacts short circuiting the junctions. A method of growing single crystals of PbSe from the vapor has since been developed by Prior (2), and the object of this paper is to describe the properties of a junction prepared with the aid of this new technique.

#### Junction Preparation and Measurement

The crystal was grown by sublimation in a controlled atmosphere of selenium by the method described (2). Initial growth conditions were chosen to give a crystal with an extrinsic electron concentration of about  $1.5 \times 10^{17} \text{ cm}^{-3}$ , but for the last 10 min of growth the selenium pressure was increased to give a predicted extrinsic hole concentration of about the same magnitude. The oven was finally cooled rapidly within a few minutes under conditions tending to maintain the p-type surface layer. The product was, as indicated by thermoelectric probe measurements, a single n-type crystal with a p-type surface layer.

Figure 1 indicates the way in which the specimen was prepared and mounted. The silver contacts

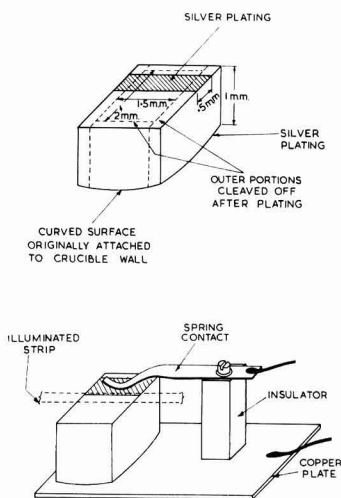


Fig. 1. Method of preparing and mounting specimen

were applied by vacuum deposition. For measurement of the photoeffects the mounted specimen was placed in an optical absorption cell for use at low temperatures, as described by Roberts (3). A Leiss double monochromator, also described by Roberts (4), was used. An image of the output slit of the monochromator was focused onto the specimen parallel to the silvered strip. The width of this image could be varied by adjustment of the slit, and it could be traversed perpendicular to itself by a tilting screw on the focusing mirror. The radiation was chopped at 800 cps, and the resulting signal passed through an amplifier and phase sensitive detector. Account was taken of the specimen resistance, and results are expressed in terms of the open-circuit photovoltage developed. The radiation intensity falling on the specimen was measured over the wavelength range by means of a calibrated thermocouple, and the measured signals were scaled to a constant energy flux.

Measurements were made at 290°, 249° (bp methyl chloride), 77°, and 20°K. Results are plotted in Fig. 2, 3, 4, and 5.

A rough determination of the effective area of the junction was made at 77°K and at room temperature. At 77°K little reduction in signal occurred until the width of the illuminated strip was reduced below 0.2 mm, and for this width a total movement of 0.32 mm changed the signal from 50% to 50% through the maximum; the effective width can thus be taken as about 0.2 mm. At room temperature the width was considerably less and more difficult to determine reliably, but appeared to be about 0.05 mm.

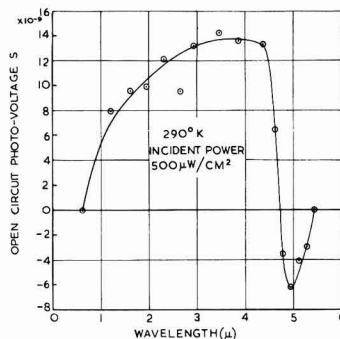


Fig. 2. Photovoltage response at 290°K

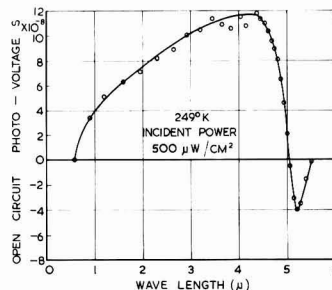


Fig. 3. Photovoltage response at 249°K



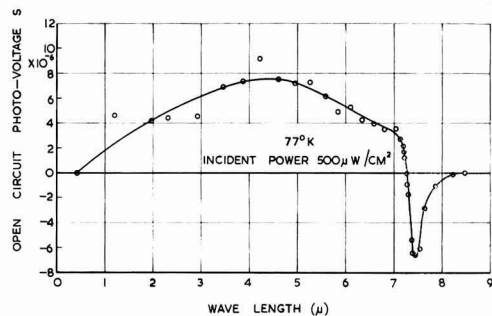


Fig. 4. Photovoltaic response at 77°K

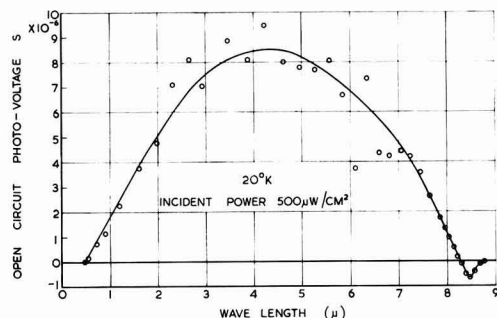


Fig. 5. Photovoltaic response at 20°K

The approximate resistance of the specimen between the contacts was 0.6, 0.7, 3.0, and 2.8 ohms at 290°, 249°, 77°, and 20°K, respectively.

### Discussion

The arrangement can be represented by the equivalent circuit shown in Fig. 6, where  $R_s$  is the surface resistance of a square of the p-type layer,  $R_j$  the resistance of a unit area of the junction,  $\phi$  the open-circuit photovoltage that would be developed by each element of the illuminated strip, and  $S$  the observed open-circuit signal. The neglect of possible shunting effects due to surface leakage across the junction at the edges will be justified later. The application of transmission line theory shows that

$$S = \phi \left[ 1 - \exp(-l \sqrt{R_s/R_j}) \right] \left[ (R_s/a) / (R_s/a + \sqrt{R_s R_j}) \right] \quad [1]$$

where the meaning of the symbols is indicated on Fig. 6. The assumption made that  $b \rightarrow \infty$  is justified by the relation between the experimentally observed effective area and the specimen dimensions.

For an assessment of the basic properties of the junction produced, the quantities of principal interest are  $\phi$ ,  $R_j$  and  $R_s$ .

For the junction cooled to 77°K the experimental data are adequate for a reasonable evaluation of these quantities. Since the bulk resistance should be negligible compared with the measured resistance of the specimen between the contacts, this can be taken as due entirely to the junction resistance. From the way in which  $S$  varies with  $l$  or from the variation of  $S$  as the illuminated strip of fixed width

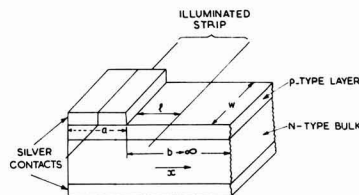


Fig. 6. Equivalent circuit of specimen

is moved, the quantity  $R_s/R_j$  can be deduced. From this and the resistance between the contacts,  $R_s$  and  $R_j$  can be found, and  $\phi$  can then be obtained from [1]. Values so deduced from the 77°K data are  $R_s = 0.034 \text{ ohm cm}^2$ ,  $R_j \sim 200 \text{ ohm}$ , and hence  $\phi = 5S$ . With a flux of  $500 \mu\text{W cm}^{-2}$  the peak signal, occurring at a wave length of  $4\mu$ , was  $8\mu\text{V}$ , corresponding to  $\phi = 4 \times 10^{-5} \text{ v}$ .

The quantum efficiency of the process can be estimated by comparing the number of photons absorbed with the current flow across the junction, due to  $\phi$ ; this current exactly cancels that due to the separation by the junction field of the photo-generated electron-hole pairs. The current density across the junction is

$$\begin{aligned} \phi/R_j &= 4 \times 10^{-5} / 0.034 \text{ amp cm}^{-2} \\ &\equiv 7.4 \times 10^{15} \text{ electrons sec}^{-1} \text{ cm}^{-2} \end{aligned}$$

Some 40% of the incident radiation flux of  $500 \mu\text{W cm}^{-2}$  would be reflected, leaving  $300 \mu\text{W cm}^{-2}$  which is equivalent to  $6.3 \times 10^{15} \text{ photons sec}^{-1} \text{ cm}^{-2}$  at  $4\mu$ . The apparent quantum efficiency is thus 1.2.

While the fact that this value exceeds unity is simply an indication of the approximate nature of the measurements, it does imply that the efficiency of the junction in separating photogenerated electron-hole pairs is high.

To estimate the ideal detectivity of the junction,  $\phi$  must be compared with the junction noise. Experimentally it was found that the current that had to be passed through the specimen to produce a significant increase in the observed noise was several orders higher than the calculated current that would be produced by 300°K background radiation. Johnson noise is therefore the only source of noise from the device which need be considered. Comparing Johnson noise with the  $\phi$  produced by the signal radiation gives a value for the detectivity  $D^*$  of  $7 \times 10^9 \text{ cm cps}^{1/2} \text{ watt}^{-1}$  at  $4\mu$ , the wavelength for peak response. Because of amplifier noise and electrical losses due to the nonideal arrangement of electrodes

(i.e.,  $S < \phi$ ) the value of  $D^*$  actually achieved was  $3 \times 10^8$  cm cps<sup>1/2</sup> watt<sup>-1</sup>.

To obtain an estimate of the thickness of the p-type surface layer a knowledge of its bulk resistivity is required. Growth conditions were designed to give a layer with a carrier concentration of about  $10^{17}$  cm<sup>-3</sup>. Using this together with a value for  $R_s$  of 200 ohm and a typical value of  $2 \times 10^4$  cm<sup>2</sup> sec<sup>-1</sup> volt<sup>-1</sup> for the mobility, the thickness is found to be  $\sim 0.2 \mu$ . If a uniform rate of deposition for the whole period of growth of the crystal is assumed, a thickness about ten times greater than this would be expected for the layer formed during the last 10 min of growth, under the increased selenium pressure; however, the rate of deposition is likely to have fallen as the crystal size increased. Further, any diffusion of selenium from the selenium rich surface layer into the bulk could reduce the thickness. Another possibility is that the layer was in fact formed by diffusion during the initial rapid cooling of the crystal before the selenium pressure had dropped significantly. Such p-type surface layers have been found on normally grown n-type crystals with bulk carrier concentrations not exceeding about  $10^{17}$  cm<sup>-3</sup>. Thus, even if the p-type layer were formed during the cooling period, a carrier concentration of about  $10^{17}$  cm<sup>-3</sup> in the layer, as assumed above, seems reasonable.

The performance of a junction detector with a given quantum efficiency depends on the junction resistance  $R_j$ ; the signal increases as  $R_j$  and the Johnson noise as  $R_j^{1/2}$ , so that the performance will improve as  $R_j^{1/2}$  until background radiation noise effects become important. Comparison of the observed value of  $R_j$  with the theoretical expectation is therefore of interest. To make any theoretical estimates the value of the intrinsic concentration,  $n_i$ , is required, and a rough value can be deduced from the energy of the optical absorption edge. Taking the energy gap as 0.182 eV at 77°K (5) a value for  $n_i \sim 10^{18}$  cm<sup>-3</sup> is obtained. A knowledge of the carrier life time is also required; no measurements of this are available, but indirect deductions from photoconductive measurements on other crystals suggests that it is unlikely to be less than  $10^{-9}$  sec, corresponding to a diffusion length of about  $10 \mu$ . With these values and with mobilities of  $2 \times 10^4$  cm<sup>2</sup> volt<sup>-1</sup> sec<sup>-1</sup> and carrier concentrations of  $10^{17}$  cm<sup>-3</sup> on both sides, the simple Shockley theory (6) gives a zero bias resistance  $R_j \sim 1.5 \times 10^4$  ohm cm<sup>2</sup>.

This treatment has neglected the effect of the surface very close to the junction. If the surface recombination velocity were infinite, the effective diffusion length would be reduced to about the distance between the junction and the surface, say  $10^{-5}$  cm; this would reduce  $R_j$  to  $\sim 300$  ohm cm<sup>2</sup>, still  $10^4$  times greater than the experimental value. The simple theory also neglects the effect of generation and recombination within the junction region. Sah, Noyce, and Shockley (7) have developed a theory taking this into account and give an expression for the zero bias junction resistance. However, even with the insertion of rather extreme values into their expression a junction resistance of

10 ohm cm<sup>2</sup> is obtained, and with more likely values a much higher resistance would result.

Another possible cause of the low apparent junction resistance is surface leakage at the specimen edges. This can however be ruled out from consideration of the effective sensitive area. If the true junction resistance were much higher than the apparent value, the attenuation of the equivalent transmission line (Fig. 6) would be much reduced, and in the center of the specimen away from the edges the useful sensitive area would extend much further away from the contact than was observed.

From the foregoing considerations it seems that the properties of the structure cannot be explained on the basis of a uniform p-type surface layer, and the system behaves as though the junction were being short circuited by some form of distributed defects, possibly associated with dislocations or impurity aggregates, and perhaps aggravated by the thinness of the layer.

The room temperature data on the junction are inadequate for a detailed analysis, but a rough calculation suggests that the quantum efficiency is close to unity, and the junction resistance is not more than ten times lower than the value of  $\sim 2 \times 10^3$  ohm cm<sup>2</sup> calculated from the simple Shockley theory.

For a quantum detector the energy sensitivity should increase linearly with wavelength up to the absorption edge. The 290° and 249°K spectra are roughly of this form, but at 77° and 20°K the sensitivity falls off beyond about  $4\mu$ . This fall off seems likely to be connected with the relation between the absorption coefficient  $K$  and the thickness  $t$  of the p-type layer. From the room temperature measurements of Avery (8),  $K = 2.4 \times 10^4$  cm<sup>-1</sup> at a wavelength of  $4\mu$ , and varies approximately inversely with the wavelength.  $K$  was not measured below room temperature; however at a given wavelength, within the region of heavy absorption, only small variations of its value with temperature are to be expected theoretically. It seems reasonable therefore to assume the room temperature values of  $K$  to apply throughout. With  $t \sim 2 \times 10^{-5}$  cm the product  $Kt$  is then  $\sim 0.5$ , and approximately 40% of the radiation will be absorbed on the surface side of the junction. On the other hand at  $7\mu$  with  $K \sim 1.3 \times 10^4$  the proportion absorbed on the surface side would be only about 25%. Almost all the carrier pairs generated on the surface side of the junction should reach the latter and be separated by it, since no reasonable value of surface recombination velocity would be adequate to cause significant loss. However some of the carriers generated on the interior side of the junction could diffuse away from it and be lost by recombination. To account for the fall off in response at long wavelengths on this basis alone would require an unrealistically short bulk diffusion length of less than  $1\mu$ . On the other hand quite small variations of impurity concentration within the bulk would be sufficient to set up local fields which, if acting in a direction opposite to the main junction field, could draw the carriers away from the junction.

The negative signal in the region of the absorption edge could be due either to inhomogeneities in the crystal or to effects at the other electrode of the specimen.

### Conclusions

The main characteristics of a surface p-n junction on a PbSe crystal grown from the vapor have been revealed by an analysis of its photovoltaic properties at 77°K. The experimentally achieved value of  $D^*$  was  $3 \times 10^8$  cm cps<sup>1/2</sup> watt<sup>-1</sup>, but analysis of the results shows that with a quieter amplifier and a more suitable arrangement of evaporated contacts on the specimen a value approaching  $7 \times 10^9$  cm cps<sup>1/2</sup> watt<sup>-1</sup> should have been obtained with the same junction, the latter figure being within about an order of the limiting value for room temperature background radiation.

The quantum efficiency appears to be close to unity, but the junction resistance is several orders lower than can be explained by normal junction theory, including carrier generation within the transition region, or by surface leakage. The reason for the low resistance is not understood, but seems likely to be associated with some distributed defects in the junction. If junctions with higher resistance can be produced, these should have higher inherent sensitivity, a simpler electrode system would be adequate to make full use of the junction area, and the amplifier noise problem would be less severe.

The analysis indicates that the surface p-type layer has a thickness of only a few tenths of a micron. A substantially greater thickness should be possible without reducing the quantum efficiency significantly and would probably increase it at the longer wavelengths. A thicker layer would also have lower surface resistance, which would ease

the contact problem, and might also, by a general improvement in junction perfection, result in increased junction resistance and hence performance.

This paper has described the results obtained from the single attempt which has been made to prepare a p-n junction in PbSe by the vapor growth technique. Since this work was done, Coates (9) has developed in this laboratory a chemical etch for PbSe which yields surfaces of high quality, and diffusion into a crystal with such a surface may be an alternative approach.

In view of the fact that a detectivity has been achieved not greatly inferior to that of other relatively intensively developed detectors (10), it seems not unreasonable to hope that development could lead to detectors approaching the background radiation limit, although the resistance may always be rather inconveniently low.

Manuscript received April 28, 1961. This paper was prepared for delivery before the Indianapolis Meeting, April 30-May 3, 1961 and is published by permission of the Controller, H. M. Stationery Office.

Any discussion of this paper will appear in a Discussion Section to be published in the June 1962 JOURNAL.

### REFERENCES

1. W. D. Lawson, *J. Appl. Phys.*, **22**, 1444 (1951); *ibid.*, **23**, 495 (1952).
2. A. C. Prior, *This Journal*, **108**, 82 (1961).
3. V. Roberts, *J. Sci. Instrum.*, **32**, 294 (1955).
4. V. Roberts, *ibid.*, **29**, 134 (1952).
5. A. F. Gibson, *Proc. Phys. Soc. B*, **65**, 378 (1952).
6. W. Shockley, *Bell Syst. Tech. J.*, **28**, 435 (1949).
7. C. T. Sah, R. N. Noyce, and W. Shockley, *Proc. I.R.E.*, **45**, 1228 (1957).
8. D. G. Avery, *Proc. Phys. Soc. B.*, **66**, 133 (1953); *ibid.*, **67**, 2, (1954).
9. D. G. Coates, W. D. Lawson, and A. C. Prior, *This Journal*, **108**, 1038 (1961).
10. F. F. Rieke, L. H. DeVaux, and A. J. Tuzzolino, *Proc. I.R.E.*, **47**, 1475 (1959).

## Single Crystal Photoconductive Detectors in Lead Selenide

D. G. Coates, W. D. Lawson, and A. C. Prior

Royal Radar Establishment, Malvern, England

### ABSTRACT

Near intrinsic single crystals of PbSe grown from the vapor have been used to construct photoconductive detectors for operation at room temperature. Fabrication of the detectors depends on the use of a newly developed chemical etch to reduce the specimens to thicknesses of a few microns, and to provide surfaces with low carrier recombination velocity. The highest detectivity,  $D^*$ , achieved was  $3.7 \times 10^8$  cm cps<sup>1/2</sup> watt<sup>-1</sup> at 4.4 $\mu$ . Various methods of estimating bulk carrier lifetimes have been used; the value for the best crystal measured was in excess of 4  $\mu$ sec. The surface recombination velocity of the best etched surface was below 80 cm sec<sup>-1</sup>. Similar etches can be used for PbS and PbTe.

PbSe photoconductive detectors made in the form of evaporated or chemically deposited layers are well known. These devices exhibit considerable current noise, believed to be associated with their polycrystalline nature. Detectors made from single crystals would be expected to be relatively free from such noise and should therefore have higher detec-

tivities, provided that the necessary requirements of crystal quality and geometry can be met. To compete with layer detectors, the single crystals must have extrinsic carrier concentrations at least as low as the intrinsic concentration at the temperature of operation. In addition, some means of preparing very thin specimens with high quality surfaces is essential.

Prior (1) has developed a method of crystal growth from the vapor whereby crystals can be produced with approximately intrinsic properties at room temperature. The present paper reports the use of such crystals, together with a fabrication technique based on a chemical etching process, for the preparation of single crystal photoconductive detectors operating at room temperature.

### Specimen Preparation and Etching

The crystals are sawed and ground with 4F carborundum to produce parallel sided specimens about 0.2 mm in thickness, and typically 5 mm x 1 mm in area. One side of the specimen is polished with Linde A fine abrasive, and thin wire contacts are fixed to this surface near the ends with pure indium. After mounting in a holder, the contact areas and leads are covered with a masking varnish in preparation for etching.

The etching mixture comprises 5 volumes of a solution of potassium hydroxide in water, saturated at 20°C, 1 volume of hydrogen peroxide (100 volume strength), and 5 volumes of ethylene glycol. During etching the specimen is moved slowly backwards and forwards through the solution. The reaction leads to the formation of soluble products, so that no deposit is left on the surface being etched. The specimen is finally rinsed in distilled water.

The etching rate of a freshly prepared solution at 35°C is about 1-3  $\mu$  a minute on each surface, depending on the degree of agitation. The rate diminishes with time, and after about 15 min a fresh solution is made up, or alternatively a few drops of H<sub>2</sub>O<sub>2</sub> are added.

Small bubbles of oxygen are released in the solution, and the etching rate is roughly proportional to the degree of bubbling, which decreases with time after mixing the reagents. The effervescence increases with agitation and temperature. If the crystal surface becomes dull gray during etching, insufficient oxygen is being released, and this can be remedied by increasing the agitation, whereupon the surface becomes bright again. If the oxygen is released too rapidly, either because the temperature is too high, or from an excess of H<sub>2</sub>O<sub>2</sub>, the surfaces become pitted or reddish brown in color, probably due to the presence of free selenium. In this event the crystal is removed until the solution is cooler and less vigorous. With the etch at 35°C surfaces with a good polished appearance are produced, but a rather lower temperature favors the production of surfaces of still higher quality.

The etching is very uniform, and specimens can be reduced readily in thickness to a few microns, with retention of regular shape and parallel sides. Provided that the initial specimen is sufficiently accurately parallel, reduction to a thickness of 1  $\mu$  can be accomplished without much difficulty. PbSe crystals can be cleaved into thin slices which are normally very fragile and readily broken. Etched specimens a few microns in thickness are, however, relatively easily handled, since they can be bent easily without fracture. Some have been successfully straightened after being bent quite sharply through a right angle.

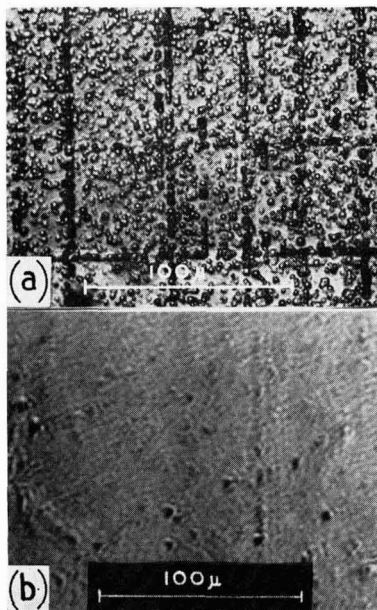


Fig. 1(a). Pitted surface produced by an abnormally vigorous etch. Fig. 1(b). A surface etched to a high polish.

In Fig. 1(a) is shown a surface produced by an abnormally vigorous etch. Pits can be clearly seen, largely arranged in parallel and perpendicular lines. This pattern may be compared with that obtained by Brebrick and Scanlon (2) using an HCl-thiourea etch on natural PbS. These workers found that synthetic crystals grown from the melt did not show this regular pattern, but that such alignment of pits as was found was along irregular curves. By analogy the observed pattern of Fig. 1(a) may be indicative of a degree of crystalline perfection similar to that of natural PbS and superior to that of crystals grown from the melt.

Figure 1(b) shows a crystal which has been etched under more normal conditions to produce a highly polished surface. Few etch pits can be seen, but the faint traces of a straight line of pits are still just visible.

Mixtures of the same reagents have been found effective for etching PbS and PbTe. Relatively little work has been done to find the optimum conditions, but the best proportions so far tried are as follows: for lead sulphide KOH—1 volume, H<sub>2</sub>O<sub>2</sub>—1 volume, glycol—1 volume; and for lead telluride 10, 1, and 10 volumes of the same reagents, respectively.

*Measurements of photoconductivity.*—For the bulk of the measurements the specimens were illuminated by radiation, chopped at 800 cps, from a tungsten filament lamp. The specimen was supplied with a constant current from a high impedance, and the signal was passed through a matching transformer into a calibrated 800 cps amplifier having a band width of 50 cps. For absolute measurements a line source of known wavelength and intensity was substituted for the tungsten lamp. A Leiss-type

double monochromator (3) was employed for the determination of spectral response.

The general procedure was to measure the signal and noise after the initial preparation of the specimen and then after successive stages of etching, each usually of about 15 min in duration. The electrical resistance and dimensions were noted at each stage. The object was to optimize the signal to noise ratio, and the process was normally discontinued at the stage at which, from experience, the optimum seemed likely to have been reached. Some of these measurements have been analyzed with a view to obtaining information on bulk lifetime and surface recombination velocity; this is discussed in a later section.

Most specimens showed only Johnson noise even with currents sufficient to cause substantial heating; thus the signal to noise ratio normally increases with current until the heating effect causes the signal to fall. Mounting the specimens on a backing plate to increase the thermal dissipation would therefore be expected to increase the signal to noise ratio. This was tried with a few specimens by sticking them to glass plates with cellulose cement. This increased the current that could be passed without overheating, and usually increased the signal to noise ratio (see Fig. 3, discussed later). The process was, however, difficult and did tend to increase the noise, probably as a result of the introduction of strains. No work has been done to develop these techniques or to reduce strain effects by the use of other adhesives or backing materials, but such techniques probably could be worked out to produce substantial improvements in performance.

Detailed analysis was unnecessary to show that the etching of a mechanically polished specimen resulted in a great reduction in surface recombination velocity. This was apparent both from the large increase in signal after etching and from the shapes of the spectral response. Figures 2(a) and (b) show the typical response of a mechanically polished and etched crystal, respectively. The peak near the absorption edge in the response of the former shows that carriers generated well within the interior of the crystal have a substantially longer lifetime than those generated close to the surface. For an etched crystal the position of generation of the carriers appears not to affect their lifetime, and the response shows the linear rise up to the absorption edge, characteristic of an ideal quantum detector. For comparison Fig. 2(c) shows the response of a typical evaporated layer cell; this exhibits marked irregularities, and the sensitivity does not extend to as long a wavelength as the single crystal detector. The shape of this response curve is probably a result of the crystallite size distribution in the layer (4).

A total of about forty detectors have been made and the detectivities  $D^*$  of some of these are plotted against the conductivity of the crystals in Fig. 3. The detectors ranged in thickness from 2 to 80  $\mu$ , most lying between 5 and 30  $\mu$ , and this accounts in part for the spread in  $D^*$ . Most of the spread, however, seems to be a function of the initial crystal, since the variation from one detector to another

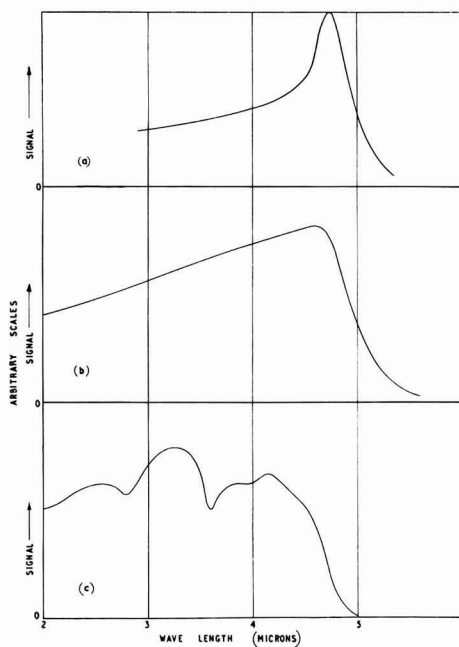


Fig. 2. PbSe photoconductive spectral response at room temperature. (a) Single crystal with a mechanically polished surface; (b) single crystal with an etched surface; (c) evaporated layer cell.

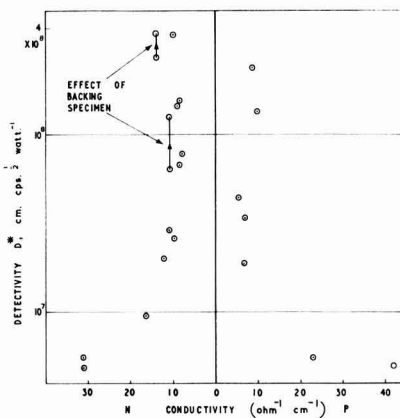


Fig. 3. Observed detectivities at 4.4  $\mu$  at room temperature

made from the same crystal was normally a factor of 2 or less.

The improvement produced in two specimens by cementing them to glass backing plates is shown.

#### Bulk Lifetime and Surface Recombination Velocity

During the course of this work a variety of methods have been tried in attempts to estimate carrier lifetime  $\tau$ , but none are free from objections. The traveling light spot method for measuring diffusion length was used first on natural, cleaved, and mechanically polished surfaces, the etching technique not yet having been developed at the time. Considerable scatter and dependence on surface



conditions was apparent, so that much reliance could not be placed on the interpretation of the results. However, a dependence on the purity of the initial material used for the preparation of the crystals did appear to be statistically significant; carrier lifetimes deduced from these measurements on early crystals were typically  $\sim 10^{-7}$  sec, whereas when a substantially purer grade of selenium was used the values obtained were typically  $\sim 10^{-8}$  sec. The relatively less pure material of the early crystals was not used subsequently, but various different grades of high-purity lead and selenium were tried. However, no subsequent measurements showed any apparent statistically significant dependence on the particular high-grade material used.

On one near intrinsic crystal four different methods of measuring lifetime were compared, again before the etching technique was available. In one method the photoconductive spectrum was analyzed in relation to the absorption spectrum; the value of  $0.5 \mu$  sec deduced for  $\tau$  should have been independent of surface conditions. The most likely source of error here was the uncertainty in the absorption spectrum under the conditions for which the photoconductive spectrum was obtained; the current necessary to obtain adequate photoconductive signals caused a significant, and probably nonuniform, rise in crystal temperature. The absolute value of the peak photoconductive signal in the same experiment gave  $\tau = 0.5 \mu$ sec, but this would be a low estimate due to the neglect of surface recombination. A determination of the ratio of a photoconductive signal to a photoelectromagnetic signal gave a value of  $\tau = 1.8 \mu$ sec, which ideally should be independent of surface recombination velocity. The traveling light spot method gave  $\tau = 3 \mu$ sec.

Some rather more comprehensive data were obtained from an analysis of the photoconductive signals from etched specimens. The relative importance of surface and bulk recombination will vary from specimen to specimen, and, for any particular specimen, an effective lifetime,  $\tau_{eff}$ , can be defined as the average lifetime of the photogenerated carriers within it. It can be shown that  $\tau_{eff}$  is related to the bulk lifetime,  $\tau$ , by the expressions

$$\frac{\tau_{eff}}{\tau} = \frac{(1 + \alpha) \exp(t/L) - (1 - \alpha) \exp(-t/L) - 2\alpha}{(1 + \alpha)^2 \exp(t/L) - (1 - \alpha)^2 \exp(-t/L)} \quad [1]$$

$$\alpha = \frac{Ls}{D} \quad [2]$$

where  $t$  is the thickness of the specimen,  $L$  the diffusion length,  $D$  the ambipolar diffusion coefficient, and  $s$  the surface recombination velocity, assumed the same for both surfaces. The width of the specimen is assumed large compared with  $t$ , and recombination at the edges is neglected. In deriving this expression photogeneration is assumed to occur on the surface, the absorption coefficient being taken as infinite; consideration shows that this will not lead to significant error for etched specimens, which have a spectral response as Fig. 2 (b). Some error will result with mechanically polished specimens with spectral response as Fig. 2(a), but the values for such specimens are not of primary interest.

If  $s$  remains constant as the thickness of the specimen is reduced by etching, then  $\tau_{eff}$  should fall as  $t$  decreases, the surface recombination becoming of increasing importance. By a process of curve fitting the relation between  $\tau_{eff}$  and  $t$  should then enable both  $\tau$  and  $s$  to be determined. In fact this could not be done since  $s$  was found not to be the same after each etch. However, some information can still be obtained from the results.  $\tau_{eff}$  was calculated by relating the flux of photons absorbed to the increase in carrier concentration, as indicated by the fractional change in specimen resistance. A constant mobility of  $1000 \text{ cm}^2 \text{ volt}^{-1} \text{ sec}^{-1}$  was assumed for both holes and electrons throughout. Table I shows  $\tau_{eff}$  as a function of  $t$  for three specimens.

As would be expected the initial etching greatly increases  $\tau_{eff}$ , but the anticipated decrease in  $\tau_{eff}$  as the specimen is further reduced in thickness does not occur until the thickness has been reduced to about  $10 \mu$ . An analysis based on the assumption of a constant  $s$  for an etched surface clearly can not be used; instead a value of  $\tau$  has been assumed and  $s$  calculated from Eq. [1] and [2]. The least possible value of  $\tau$  is the maximum value of  $\tau_{eff}$ , and for column (a)  $\tau$  has been taken equal to this maximum

Table I.  $\tau_{eff}$  as a function of  $t$

Type Conductivity	N 14 ohm <sup>-1</sup> cm <sup>-1</sup>						P 8.6 ohm <sup>-1</sup> cm <sup>-1</sup>						N 8.8 ohm <sup>-1</sup> cm <sup>-1</sup>					
	$t, \mu$		$s, \text{ cm sec}^{-1}$			$t, \mu$		$s, \text{ cm sec}^{-1}$			$t, \mu$		$s, \text{ cm sec}^{-1}$					
			(a)	(b)	(c)			(a)	(b)	(c)			(a)	(b)	(c)			
Before etching	270	0.040	220,000	270,000	340,000	190	0.080	78,000	93,000	120,000	255	0.066	87,000	120,000	190,000			
	190	1.08	5,100	6,900	8,800	100	0.76	3,400	5,200	6,600	85	1.01	1,200	2,600	4,200			
	124	4.1	0	740	1,500	85	1.49	960	1,700	2,900	40	1.09	510	1,200	1,800			
After successive periods of etching	5	3.0	23	56	84	70	2.15	150	870	1,600	20	1.53	0	330	660			
						50	1.98	200	710	1,300	10	1.37	37	220	360			
						37	1.77	260	640	1,000								
						32	1.50	390	730	1,100								
						25	1.65	230	480	760								
						20	2.37	0	200	420								
						10	2.1	28	140	240								

Underlined values are ( $\tau_{eff}$ ) max.

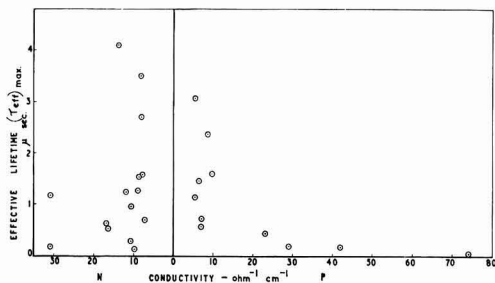


Fig. 4. Effective lifetimes at room temperature

value. For column (b)  $\tau$  has been taken twice as great, and for column (c) it has been assumed infinite.

The truth must be somewhere between (a) and (c), but the figures do not in fact show any obvious characteristic from which the correct values of  $\tau$  could be deduced. Apart from the final rise in  $s$  for the extreme assumption (a), the lowest value of  $s$  is achieved in each case for the final value of  $t$ . The successive stages of etching were not carried out with this particular analysis in view, and perhaps the most likely explanation for the final low value of  $s$  is that, as a specimen became very thin, the etching process was carried out slightly differently; a fresh etch was usually employed, but allowed to stand before use until its activity had fallen substantially. From the figures extreme values of  $s$  can be deduced; for the best etched surface  $s$  could not exceed  $84 \text{ cm sec}^{-1}$ , and was more probably under  $50 \text{ cm sec}^{-1}$ , while for the worst polished surface  $s$  could not be less than  $220,000 \text{ cm sec}^{-1}$ .

A calculation of  $\tau_{\text{eff}}$  as a function of thickness has been done for 26 specimens; results are shown in Fig. 4. On this the maximum value of  $\tau_{\text{eff}}$  has been plotted against specimen conductivity. The main scatter seems most likely to be due to variation in  $\tau$  rather than in  $s$ , since, in general, different specimens from the same crystal gave maximum values of  $\tau_{\text{eff}}$  agreeing within a factor of 2.

The variation from crystal to crystal has not been correlated with apparent crystal perfection or any other observed property. Figure 4 tends to indicate a decrease in  $\tau$  as the carrier concentration increases, particularly on the p side but the data seem hardly sufficient to attach much significance to this. The etched surfaces of about ten specimens, covering the extreme range of values of  $\tau_{\text{eff}}$  examined microscopically to see whether any obvious correlation existed between etch pit density and  $\tau_{\text{eff}}$ . Although the etch pit density differed considerably from one specimen to another no correlation with  $\tau_{\text{eff}}$  was apparent. However the surfaces used were not of controlled orientation, and the etching procedure was not optimized for the production of etch pits, so that these observations cannot be regarded as very conclusive.

Three specimens were cooled to liquid oxygen temperature; results are summarized in Table II.

Table II. Three specimens cooled to liquid oxygen temperature

Type	(i) P	(ii) P	(iii) ?
Conductivity, $\text{ohm}^{-1} \text{cm}^{-1}$	23	29	5.3
$\tau_{\text{eff}}$ at $290^\circ \text{K}$ , $\mu\text{sec}$	0.42	0.18	1.13
$\tau_{\text{eff}}$ at $90^\circ \text{K}$	2.17	0.065	1.45

Unlike their behavior at room temperature specimens (i) and (iii) showed considerable current noise when cooled. The lifetimes do not seem to vary systematically with temperature and are within the same range as the room temperature values.

### Summary and Conclusions

PbSe single crystal photoconductive detectors have been made with detectivities at room temperature comparable with those of layer devices. This has been made possible by the availability of near intrinsic single crystals grown from the vapor, and by the development of a chemical etch which enables thin specimens to be prepared with surfaces having low recombination velocities. The bulk carrier lifetimes show considerable variation from one crystal to another, but this has not been correlated with other observed properties. The highest value of lifetime for the crystals examined was in excess of  $4 \mu\text{sec}$  and may have considerably exceeded this figure. The surface recombination velocity of the best etched surface was below  $80 \text{ cm sec}^{-1}$  and was more probably about half this value.

By the etching technique specimens can be reduced to about  $1\mu$  in thickness, but the surface recombination velocity achieved is still too high to enable full advantage to be taken of this facility in terms of detectivity; the optimum thickness is usually about  $10\text{--}20\mu$ .

Substantial further improvements in detectivity seem quite possible, but would probably depend mainly on an understanding of the factors governing the bulk lifetime and on still better control of the surface properties. Development of a satisfactory technique for increasing the thermal dissipation by mounting the detectors on a suitable backing should produce a worthwhile improvement.

Manuscript received April 28, 1961. This paper was prepared for delivery before the Indianapolis Meeting, April 30–May 3, 1961 and is published by permission of the Controller, H. M. Stationery Office.

Any discussion of this paper will appear in a Discussion Section to be published in the June 1962 JOURNAL.

### REFERENCES

1. A. C. Prior, *This Journal*, **108**, 82 (1961).
2. R. F. Brebrick and W. W. Scanlon, *J. Chem. Phys.*, **27**, 607 (1957); W. W. Scanlon, *Phys. Rev.*, **106**, 718 (1957).
3. V. Roberts, *J. Sci. Instrum.*, **29**, 134 (1952).
4. W. D. Lawson, F. A. Smith, and A. S. Young, *This Journal*, **107**, 206 (1960).

# A Metallographic Investigation of the Damaged Layer in Abraded Germanium Surfaces

E. N. Pugh and L. E. Samuels

*Defence Standards Laboratories, Australian Defence Scientific Service, Sydney, Australia*

## ABSTRACT

The structure of the damaged layer produced on {111} surfaces of germanium by several abrasion processes has been studied by a metallographic taper-sectioning technique. The study confirms that the abrasion process involves both cleavage and noncrystallographic fracture and establishes that the surface layers contain many cracks initiated by these fracture processes. Dislocations are not introduced into the surface layers. Measurements of the depth of the layers containing the damage cracks are in sufficiently good agreement with estimates of the depth of damage made by established methods to indicate that the cracked layer is the classical damaged layer.

Slices of germanium for use in semiconductor devices are usually cut mechanically from large single crystals and lapped to size. These operations produce surface "damage" which, because it has undesirable effects on the electrical properties, has to be removed at each lapping stage and finally by etching. While the depths of the damaged layers produced by a number of processes have been determined by various indirect methods, the exact nature of the damage is not understood (1). Two suggestions have been made. The first is that the damage is due to deep cleavage cracks (1), and the second is that, although some superficial cracking may be present, the damage is due essentially to high densities of dislocations (2-5). The origin of these dislocations has been ascribed to plastic deformation of the surface layers (2) analogous to that found in metals (6) or, alternatively, to the formation of "dislocation crack" arrays (5). The presence of either cracks or dislocations could account for the deterioration in the electrical properties, but as yet no direct evidence has been obtained for the presence of either in the damaged layer.

The purpose of the present work was to apply modern metallographic techniques to the study of the damaged layer. A major obstacle to such an approach is the fact that the layer is extremely shallow. This was overcome by means of a taper-sectioning technique which, in effect, provides a geometrical magnification of X 10 perpendicular to the section line, thus allowing the details of the surface layers to be resolved.

## Experimental Methods

Specimens were cut parallel to a {111} plane in single-crystal bars of transistor quality germanium. Most were of n-type although some experiments were carried out on p-type crystals. Previous work indicates that no differences are to be expected between the two types, and this was confirmed in the present experiments. Before abrasion, the surfaces to be examined were polished by standard metallographic methods (7), and it was confirmed that they were free from any of the features to be discussed

later. Unless stated otherwise, all abrasion was carried out unidirectionally along an approximately  $\langle 110 \rangle$  direction by the method under investigation.

Hand abrasion processes using silicon carbide and alumina abrasives as a water slurry on a glass plate were investigated. In the case of silicon carbide abrasives, lapping on abrasive papers using flowing water as a lubricant was also studied. The grades of silicon carbide then used in the two abrasion methods were identical, that used in the slurry being grains extracted from the corresponding grade of abrasive paper by chemical treatment.

The abraded surfaces were taper sectioned at a nominal angle of  $5^\circ 43'$  (taper ratio 10:1) by a method which enables the taper ratio of the final section to be measured with accuracy (8). Surface protection for the sectioning operation was achieved by means of an electrodeposited nickel coating. The section line was made approximately perpendicular to the abrasion direction. The taper-sectioned surfaces were polished metallographically (7), examined microscopically in the as-polished condition and then after etching in a reagent which is known to reveal dislocations in germanium. The etchant selected was the ferricyanide reagent developed by Billig (9);<sup>1</sup> this reagent removes very little material, produces small etch pits, and will satisfactorily develop dislocation etch pits in surfaces which are as much as  $10^\circ$  from true {111} faces (10). It was found that, under the particular conditions used, etching times of 3-5 min were required to produce well-defined etch pits at low-angle boundaries.

For reliance on this technique, it is important to establish that the taper-sectioning procedure does not introduce any damage features which might be confused with those due to the abrasion process under investigation. It was established by many trials that the procedure reliably produces surfaces in germanium which are completely free from damage artifacts of the type to be discussed. Moreover, it is to be noted that this can be checked in the taper

<sup>1</sup> 6 g: KOH; 4 g:  $K_3Fe(CN)_6$ ; 50 ml:  $H_2O$ .

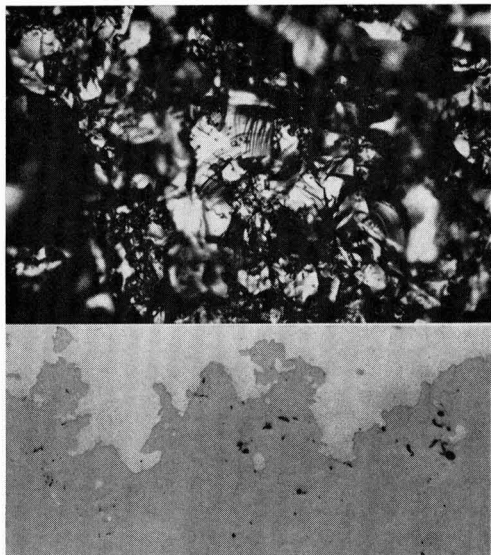


Fig. 1a. (top) Surface abraded on 220-grade silicon carbide slurry. Magnification 500X. Fig. 1b (bottom). Taper section of surface abraded as for Fig. 1a; unetched; taper ratio: 12. Magnification 250X. Abrasion direction vertical in both cases.

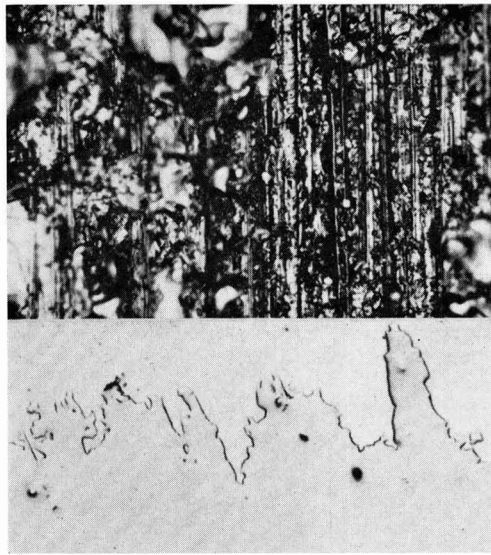


Fig. 2a (top). Surface abraded on 220-grade silicon carbide paper. Magnification 500X. Fig. 2b (bottom). Taper section of surface abraded as for Fig. 2a; unetched; taper ratio: 10.0. Magnification 250X. Abrasion direction vertical in both cases.

section itself. The features due to the abrasion process under investigation must be confined to a zone adjacent to the section line, whereas artifacts introduced during the taper-sectioning procedure would be more or less uniformly distributed over the section surface. A section was accepted for further examination only if it was completely free from features of the latter type.

### Metallographic Observations

**Surface topography.**—Direct examination of surfaces lapped on slurries of either type of abrasive indicated that they consisted entirely of irregular arrangements of pits (Fig. 1a), the faces of which often showed well-defined "river patterns" characteristic of cleavage fracture. The surface contours, as shown by taper sectioning, contained the traces of numerous small facets (Fig. 1b) which were aligned at angles consistent with their being  $\{111\}$  traces. These observations confirm the results of Wolff *et al.* (11), who showed by optical means that a large proportion of  $\{111\}$  cleavage facets are developed in lapped germanium surfaces. The curved segments in the surface contours presumably correspond to noncrystallographic fracture.

Surfaces prepared with silicon carbide papers also contained numerous pits, but a feature of the surface texture in this case was the existence of parallel grooves (Fig. 2a), generally similar in appearance to those cut in ductile materials. The taper sections (Fig. 2b) showed, however, that each groove contained many small cleavage facets. The development of cleavage cracks is undoubtedly still a major feature of this abrasion process.

**Structure of the surface layers.**—More detailed examination of the taper-sectioned specimens revealed extremely fine cracks extending for con-

siderable depths below the surface irregularities. An example is shown in Fig. 3a<sup>2</sup> for a specimen abraded with 220-grade silicon carbide papers. The cracks could only be resolved using high-aperture objec-

<sup>2</sup> The cracks located at some distance from the section line must be interpreted as having been connected with the original surface at some point above its trace in the section.

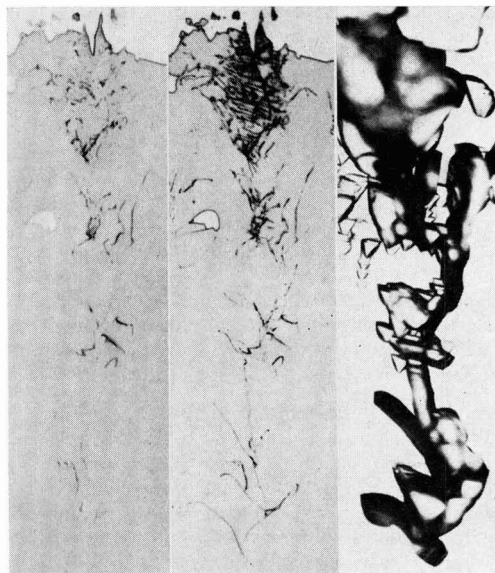


Fig. 3. Taper section of surface abraded on 220-grade silicon carbide paper; abrasion direction vertical; taper ratio: 10.5. Fig. 3a (left), unetched; Fig. 3b (center), etched in ferricyanide reagent for 2 sec; Fig. 3c (right), etched in ferricyanide reagent for 5 min. Magnification 1000X before reduction for publication.



tives, but they were made readily visible by a short etching treatment (2-3 sec) with the ferricyanide reagent (Fig. 3b). By this means, the shape and distribution of the cracks could be studied at lower magnifications. For example, Fig. 4 and 5 illustrate the structures in specimens abraded with papers and slurries, respectively.

The cracks contained many segments which were straight and aligned in directions consistent with their being {111} traces, and which result from cleavage. Segments were also present which were

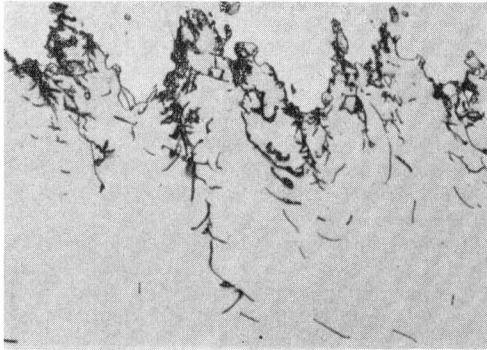


Fig. 4. Taper section of surface abraded on 220-grade silicon carbide paper; etched for 10 sec in ferricyanide reagent; abrasion direction vertical; taper ratio: 10.0. Magnification 250X.

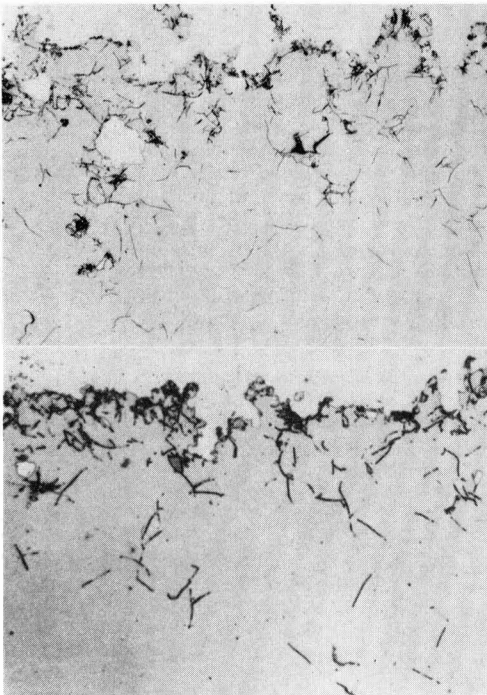


Fig. 5. Taper sections of surfaces abraded on silicon carbide slurries; abrasion direction vertical; etched for 10 sec in ferricyanide reagent. Fig. 5a (top). 220-grade abrasive; taper ratio: 10.0. Magnification 100X. Fig. 5b (bottom). 600-grade abrasive; taper ratio: 9.0. Magnification 500X.

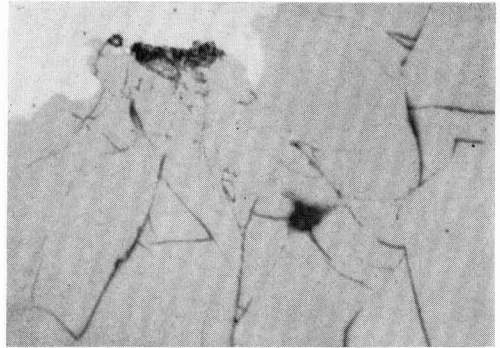


Fig. 6. Taper section of surface abraded on 220-grade silicon carbide slurry; unetched; taper ratio: 9.5. Magnification 2000X.

curved and which appeared to be noncrystallographic. The ratio between crystallographic and noncrystallographic segments was similar to this ratio for surface facets, and it seems clear that the subsurface cracks are extensions of some of those cracks responsible for the formation of the surface. The distribution of the cracks was also consistent with this conclusion; the cracks in surfaces abraded on slurries were randomly arranged (Fig. 5) even though the abrasion had been unidirectional, whereas those abraded on papers tended to be grouped in rays extending beneath the surface grooves (Fig. 4).

In both cases, the immediate subsurface layer was severely shattered (Fig. 3b and 6). A characteristic of this region in surfaces abraded on papers was the presence of groups of closely spaced, parallel cracks (Fig. 3b).

Allen (5) has described features on abraded indium antimonide surfaces which appear to be identical with those illustrated in Fig. 4 and 5 and which he identifies as "dislocation cracks." He describes a dislocation crack as being a wall of dislocations whose macroscopic features resemble an ordinary crack. However, it is emphasized that, in the present instance, cracks could always be detected at the sites of the features illustrated if the unetched surfaces were examined carefully enough. They are real cracks and not arrays of dislocations, and have been illustrated after etching only to improve their visibility. In any event, the etching times used were considerably less than those normally required to develop dislocation etch pits.

To determine whether the surface layers did contain dislocations in addition to the cracks, the taper sections were etched for long periods (5-10 min) in the ferricyanide reagent. While the etchant progressively attacked the pre-existing cracks, no new etch pits were developed (cf. Fig. 3a, 3b, and 3c). Since it is widely accepted that this method of revealing dislocations is reliable, it is concluded that no dislocations are introduced by the abrasion process.

A further experiment was carried out based on the observation made by Faust (12) that the strain introduced by a scratch on germanium was relieved



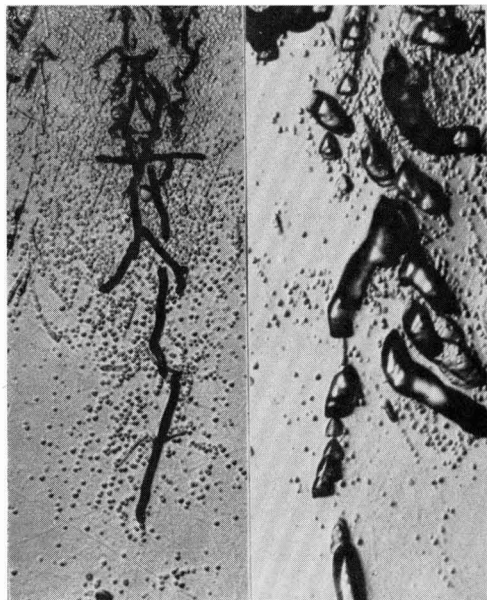


Fig. 7. Taper sections of a surface abraded on 220-grade silicon carbide paper and annealed at 500°C; abrasion direction vertical; taper ratio: 10.5 Fig. 7a (left). Etched in ferricyanide reagent for 10 min. Fig. 7b (right). Etched in ferricyanide reagent for 25 min. Magnification 500X.

by the formation of dislocation arrays during heating at 500°C. A specimen was abraded with 220-grade silicon carbide paper, annealed at 500°C for 15 min and then taper sectioned and etched as before. Arrays of etch pits now developed which had the correct etching characteristics for dislocation etch pits and which were strictly confined to traces of {111} planes (Fig. 7a). These clearly are true dislocation etch pits and are easily distinguishable from the larger etch pits developed at the sites of the damage cracks (Fig. 7b).

These observations, apart from confirming that any dislocations present in the as-abraded surfaces would have been detected in the earlier experiments, support theoretical predictions (13) that

edges in the surface should be preferred sites for the nucleation of etch pits. Indeed, under these particular circumstances, the edges of the cracks are more highly preferred sites than dislocations. The generation of the dislocations during annealing can be attributed to the relief of elastic stresses in the damaged layer, which are known to be high (14), since it is well established that the tip of a crack is a potent generating source of dislocations (15).

#### Depth of the Cracked Layer

The metallographic examination indicates that the electrical "damage" is not due to dislocations but suggests that it is due to subsurface cracking. However, it is still necessary to determine whether or not the crack-containing layer corresponds fully with the electrically damaged layer. To do this, it is necessary to measure the depths of crack-containing layers and to compare these measurements with those determined by established methods which are more closely related to the electrical properties of the material.

Both the surface irregularities and the crack-containing layers were extremely irregular in depth. Consequently, to facilitate the estimation of the maximum depths of these features from taper sections, composite micrographs representing the full width of each specimen were assembled. On each, a line was drawn parallel to the estimated mean surface at a position locating the outermost crest of the surface irregularities, and this was used as a datum. Parallel lines were then drawn to locate the innermost root of the surface irregularities and the maximum depth of the cracks. From these, true depths were calculated, knowing the calibrated microscope magnification and the true taper ratio of the section. The results for the range of abrasion processes investigated are given in Table I.

Buck (1) has collated previous determinations of the depth of the damaged layer, the only results which can be compared with those in Table I being those for abrasion on a slurry of 600-grade silicon carbide abrasive. The damage depths so determined by a variety of methods all lie in the range 15-18 $\mu$ , i.e., they are consistently higher than the value ob-

Table I. Depths of surface irregularities and cracked layer measured by metallographic method

Type	Abrasive Grade	Method of use	Depth of surface irregularities, $\mu$	Depth of cracked layer, $\mu$	Depth of damage determined by PME method, $\mu$
Silicon carbide	220	Abrasive paper. Unidirectional abrasion.	7	22	20
	400		2.5	10	—
	600		1.5	6.5	—
	220	Water slurry on glass plate. Unidirectional abrasion.	23	85	60
	400		6	22	—
	600		3.5	11.5	10
	850		3	10	—
	220		Water slurry on glass plate. Random motion abrasion.	16	66
	400	6		25	—
	600	2.2		8.7	—
Alumina	320	Water slurry on glass plate. Unidirectional abrasion.	6	24	—
	600		2.5	9	—
	900		2	8.5	—
	1200		1.5	5.5	—

tained in the present work. This could be due to differences in abrasion conditions, the most obvious one being that unidirectional abrasion was used here whereas previous workers most probably used a more random motion. However, further tests indicated that this produced an even shallower damaged layer (Table I). To obtain a more direct comparison, the depth of damage in surfaces prepared by some of the particular abrasion conditions used in the metallographic experiments was determined by the photomagnetolectric (PME) method developed by Buck and McKim (16). The values were generally less than those determined by the metallographic taper-sectioning method (Table I).

The reason for the discrepancy between the depth determination made by the two methods requires further investigation. However, the discrepancy is in a direction which leaves little doubt that the crack-containing layer detected by the metallographic taper-sectioning method does correspond fully with the classical damaged layer.

### Conclusions

The metallographic observations confirm the view advanced by Buck (1) that the abrasion process involves "chipping, cracking and conchoidal fracture." During abrasion, both cleavage and noncrystallographic fracture occurs, the resulting cracks meeting and thus removing chips from the surface. Many of these cracks extend below the surface so produced, and it is these subsurface cracks which are responsible for at least the bulk of the electrical "damage." While the observations strongly suggest that the surface layers do not contain dislocations, it is not possible to rule out the existence of other defects (e.g., vacancies) which cannot be detected by metallographic methods. Such defects may contribute to the damage but, if so, it appears unlikely that they extend for any significant distance beneath the crack-containing layer.

Several results of a more empirical nature emerge from the depth measurements (Table I). A notable feature is the considerable influence of the method by which the abrasive is supported on the depth of damage. Such factors should be taken into consideration in any attempt to deduce general relationships between the size of abrasive particle and depth of damage (1). The measurements also confirm those made by Faust (2) on silicon that the depth of damage produced by alumina abrasives is less than for corresponding commercial grades of silicon carbide,

although the effect is a rather small one in the case of germanium. It was also found that the depth of damage is slightly less for random motion than unidirectional abrasion. It is of interest that the ratio of depth of damage to depth of surface irregularities is about the same (approx. 4) for all the abrasion conditions investigated. Too little is known about abrasion processes in general to attempt explanations for empirical observations of this nature.

### Acknowledgments

The authors gratefully acknowledge the assistance received from Dr. T. M. Buck, Bell Telephone Laboratories Inc., and Mr. I. R. Stevenson, Standard Telephone and Cables Pty. Ltd., for helpful discussions and supply of the specimen material. They also acknowledge the assistance received from Mr. M. B. McGirr and Mr. D. K. Sewell in the PME determinations. The paper is published by permission of the Chief Scientist, Department of Supply, Australian Defence Scientific Service, Australia.

Manuscript received May 26, 1961.

Any discussion of this paper will appear in a Discussion Section to be published in the June 1962 JOURNAL.

### REFERENCES

1. T. M. Buck in "The Surface Chemistry of Metals and Semiconductors," H. C. Gatos, Editor, p. 107, John Wiley & Sons, Inc., New York (1960).
2. J. W. Faust, Jr., Paper presented before the Buffalo Meeting of the Society, Oct. 1957.
3. R. L. Hopkins, *Phys. Rev.*, **98**, 1567 (1955).
4. D. Baker and H. Yemm, *Brit. J. Appl. Phys.*, **8**, 302 (1957).
5. J. W. Allen, *Phil. Mag.*, **4**, 1046 (1959).
6. L. E. Samuels in "The Surface Chemistry of Metals and Semiconductors," H. C. Gatos, Editor, p. 82, John Wiley & Sons, Inc., New York (1960).
7. L. E. Samuels, *J. Inst. Metals*, **81**, 471, (1952).
8. L. E. Samuels, *Metallurgia*, **51**, 161 (1955).
9. E. Billig, *Proc. Roy. Soc., A*, **235**, 37 (1956).
10. P. J. Holmes, *Acta Met.*, **7**, 283 (1959).
11. G. A. Wolff, J. M. Wilbur, Jr., and J. C. Clark, *Z. Elektrochem.*, **61**, 101 (1957).
12. J. W. Faust, Jr., A.S.T.M. Symposium on Cleaning of Electronic Device Components and Materials, *Special Tech. Publ. No. 246*.
13. N. Cabrera in "Semiconductor Surface Physics," R. H. Kingston, Editor, p. 327, University of Pennsylvania Press (1956).
14. W. C. Dash, *J. Appl. Phys.*, **29**, 228 (1958).
15. J. J. Gilman, *Trans. Am. Inst. Mining Met. Engrs.*, **209**, 449 (1957).
16. T. M. Buck and F. S. McKim, *This Journal*, **103**, 593 (1956).

# The Semiconducting Properties of CdSb

F. Ermanis

*Bell Telephone Laboratories, Incorporated, Murray Hill, New Jersey*

and E. Miller

*College of Engineering, New York University, New York, New York*

## ABSTRACT

Infrared absorption in the  $\langle 100 \rangle$  direction of single crystal samples of CdSb gave a value for the energy gap at room temperature for indirect transitions of 0.45 eV with a temperature variation of  $-6 \times 10^{-4}$  eV/°K. From resistivity, Hall coefficient and Seebeck coefficient data the energy gap at 0°K was calculated to be 0.57 eV, the mobility ratio 0.9, and the hole effective mass was found to increase with temperature from 0.2 to 0.38 between 100° and 300°K. The conductivity was found to be anisotropic, the three principal conductivities being in the ratio  $\sigma_{010} : \sigma_{100} : \sigma_{001} = 1.45 : 1.09 : 1.00$ .

The semiconducting intermetallic compound CdSb may be of interest for application in thermoelectric cooling or power generation either as the base material or as an alloying material with other compounds such as ZnSb. The compound crystallizes in the orthorhombic Be structure, and therefore the electronic properties should be anisotropic.

The original work by Justi and Lautz (1) on polycrystalline material prepared by melting in air under a flux showed that the compound has an energy gap of about 0.5 eV. They observed several different impurity ionization energies ranging from 0.47 to 0.0008 eV. Later studies (2) showed that all samples of CdSb are p-type regardless of whether excess Cd or Sb was present. However, samples with n-type conductivity can be prepared by the addition of suitable impurities, such as Pb or Pd (2).

More recently, the electronic properties of single crystal samples have been studied (3, 4), giving the value of 0.57 eV for the energy gap at 0°K. Turner *et al.* (5) determined the energy gap to be 0.5 eV at 0°K from resistivity measurements and from optical measurements to be 0.465 at 300°K and 0.585°K at 78°K. The data of Andronik and Kot (4) shows that the electrical properties of CdSb are indeed anisotropic. However they did not determine the true directions of anisotropy in the crystal, but rather the anisotropy in relation to the cleavage planes.

The purpose of the present investigation, therefore, was to determine the crystallographic directions corresponding to the anisotropic variation of properties in CdSb, and to study carefully the electronic and optical properties in one crystal direction as a function of temperature.

## Experimental Procedures

*Single crystal growing.*—Preparation of single crystal samples of CdSb is complicated by the fact that a metastable system exists as well as the stable one (5). If liquid of the composition corresponding to CdSb is permitted to solidify, the stable compound does not generally solidify at the freezing point (456°C), but rather the liquid supercools to

402°C at which temperature a hypoeutectic mixture of a metastable compound, Cd<sub>3</sub>Sb<sub>2</sub>, and Sb begins to solidify instead. If the solid is cooled further, at about 320°C the metastable compound reacts exothermally with the Sb present to yield the stable compound CdSb. The large atom movements occurring during this transformation result in large cracks and voids developing in the ingot.

Therefore, to obtain sound ingots of CdSb, formation of the metastable phase must be avoided. This was done in the present investigation by melting 100-g samples in evacuated Pyrex capsules at 500°C, cooling the capsules to room temperature, and then annealing at 200°C for 48 hr in order to complete the transformation to the stable phase. Since metastable Cd<sub>3</sub>Sb<sub>2</sub> had formed during solidification and then transformed, the resultant ingots were polycrystalline and cracked. The ingots were remelted at various temperatures, and then passed at a rate of 0.5 cm/hr through a vertical furnace held at the melting temperature. The stable phase nucleated and a sound single crystal of CdSb resulted if the furnace temperature was less than 15°C above the melting point of CdSb. If the melt were heated more than 15°C above the melting point, the resultant ingot was cracked, indicating that metastable Cd<sub>3</sub>Sb<sub>2</sub> had been nucleated instead of stable CdSb.

This dependence of the phase solidifying on the amount of superheating may be due to nucleation by unmelted particles of solid which are stabilized by surface energy in cavities in the crucible walls or on insoluble impurities and therefore melt at a higher temperature than the bulk material. These small particles then act as nucleation sites for crystal growth (6). If the liquid is superheated more than about 15°C above the melting point, then the CdSb nuclei disappear and the metastable phase Cd<sub>3</sub>Sb<sub>2</sub> appears on cooling.

*Measurement techniques.*—Single crystals of CdSb have a tendency to cleave perpendicular to the  $\langle 100 \rangle$  direction, and difficulty was found in taking measurements along this direction due to the

tendency of small cracks to form during measurement, giving erroneous readings.

The electronic properties were determined using standard d-c techniques. Resistivity measurements at elevated temperatures were determined with the specimen sealed in an evacuated Pyrex capsule, the tungsten lead wires passing through Pyrex-metal seals. The capsule prevented vaporization of the specimen and oxygen contamination at elevated temperatures, as can be seen by the reproducibility of the resistivity data in Fig. 5 on heating and cooling. In determining the Hall coefficient, the galvanothermoelectric effects were quite severe, and the Hall coefficient could not be determined to better than 15%.

The infrared absorption measurements were performed with a Beckman IR-2A spectrophotometer with resolution of 0.007 eV in the region of the absorption edge. A special Dewar flask with NaCl windows was used for the low-temperature measurements, the specimen being cooled by conduction from a copper bar which in turn was cooled by a regulated flow of liquid nitrogen. The specimens were ground to desired thickness on a low speed polishing wheel with 600X alundum powder, a final polish with alpha alumina No. 2 being used to eliminate surface scratches.

#### Optical Data

All absorption measurements were performed on p-type specimens with the photon beam along the  $\langle 100 \rangle$  direction. No measurements could be made in other directions due to the tendency of the specimen to cleave along the (100) planes during polishing. The per cent transmission obtained as a function of thickness for several different wavelengths is shown in Fig. 1 for room temperature. The extrapolation of these lines to zero thickness yields the reflectivity of the material. The reflectivity is essentially constant in the 5-13 $\mu$  wavelength range and was calculated to be 21%, corresponding to a refractive index of 2.7.

The absorption coefficient vs. wavelength is plotted for the temperature range from 77° to 360°K in Fig. 2. The absorption coefficients were calculated taking into account the fact that multiple reflections occur in the highly transmitting samples. The free carrier absorption was found to increase smoothly with increasing wavelength, and this component of the ab-

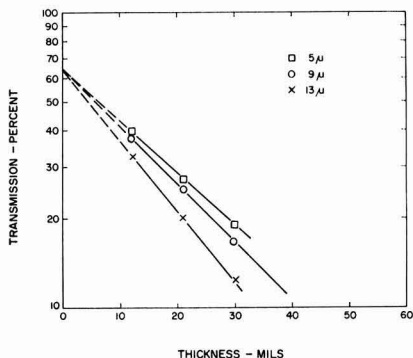


Fig. 1. Determination of reflectivity of CdSb

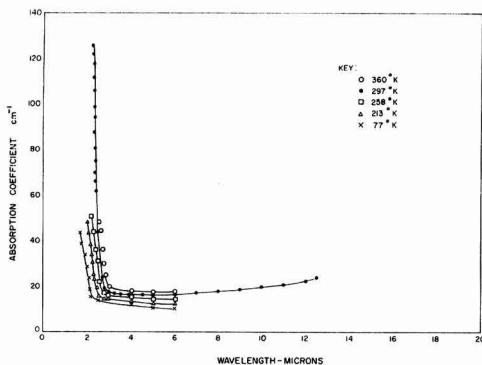


Fig. 2. Absorption coefficient vs. wavelength in the temperature range 360°-77°K.

sorption coefficient was extrapolated back beyond the absorption edge and subtracted when calculating the threshold energy for electron transitions.

On cooling to liquid nitrogen temperatures there was a steady decrease in the free carrier absorption. This decrease is presumably due to the observed increase in carrier mobility, since the carrier concentration is constant from 77° to 300°K. Measurements on several different samples showed no variation of the position of the absorption edge as a function of hole concentration. This is as expected due to the fairly high effective mass of the carriers ( $0.3 m_0$ , as determined from electrical measurements) and since the specimen did not become degenerate in the temperature range investigated.

The theory of the shape of the absorption edge in semiconductors as a function of photon energy has been studied by a number of authors (7). The general theoretical relationship between the absorption coefficient  $\alpha$  and the frequency  $\nu$  is:

$$\alpha = K(\nu - \nu_r)^n \quad [1]$$

where  $\nu_r$  is the threshold frequency, and the exponent  $n$  is equal to 1/2 for permitted transitions, 3/2 for forbidden transitions, and 2 for indirect transitions.

The threshold energy for the beginning of transitions is difficult to determine accurately. Scanlon (8) has proposed that for indirect transitions the square root of the absorption coefficient be plotted vs. the photon energy, and the extrapolated intercept at  $\alpha = 0$  be taken as the energy gap for indirect transitions. Such a plot for the room temperature data of Fig. 2 is shown in Fig. 3. A good straight line is obtained, with an extrapolated value of the energy gap corresponding to 0.45 eV.

The indirect energy gap determined as a function of temperature is shown in Fig. 4. The variation obtained with temperature was found to be linear, the temperature coefficient being  $-6 \times 10^{-4}$  eV/°K. No tendency for a deviation from the linear relationship was observed at the lower end of the temperature range as has been found in Ge and Si (9).

#### Electronic Data

The resistivity determined for the  $\langle 010 \rangle$ ,  $\langle 001 \rangle$ , and  $\langle 100 \rangle$  directions, and Seebeck coefficient and

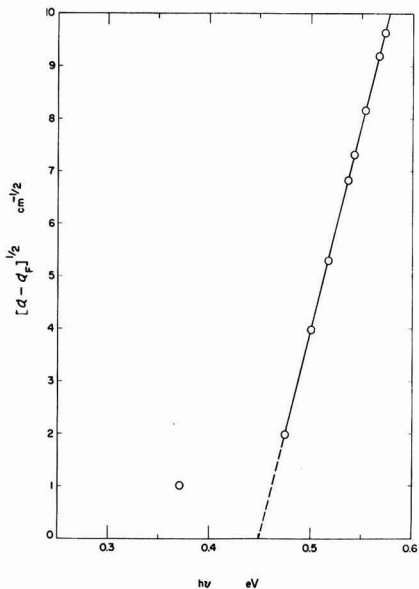


Fig. 3. Extrapolation of square root of the absorption coefficient vs. photon energy to yield absorption edge.

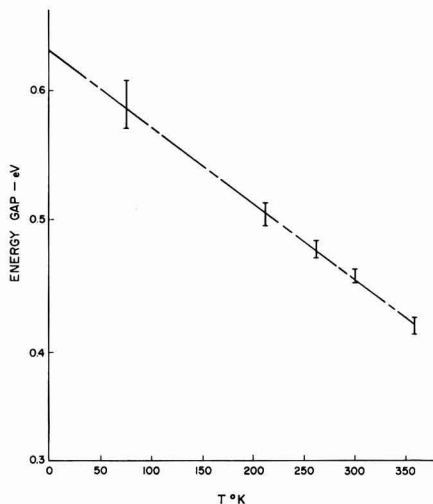


Fig. 4. Energy gap vs. temperature for CdSb

Hall coefficient data for a single crystal of CdSb, determined in the  $\langle 010 \rangle$  direction are shown in Fig. 5, 6, and 7. This specimen had a carrier concentration of  $3 \times 10^{18}$  holes/cm<sup>3</sup>, the carrier concentration remaining constant from 77° to 300°K. In these highly doped samples, no evidence for any levels having appreciable activation energy was observed, as had been reported by Justi and Lautz (1) in samples having lower carrier concentrations. The specimen investigated became intrinsic at about 600°K.

The energy gap at 0°K can be determined from the resistivity data by means of the relationship:

$$\sigma = \frac{2(2\pi kT)^{3/2}}{h_s} (m_h m_e)^{3/4} \exp - [E/2kT] (\mu_n + \mu_p) \quad [2]$$

Assuming that  $m^*$  is independent of temperature and that  $\mu = cT^{-3/2}$  at elevated temperatures, then Eq. [2] simplifies to:

$$\sigma = A \exp - (E_0/2kT) \quad [3]$$

and  $E_0$  can be obtained from the slope of the intrinsic resistivity curve. The value calculated in this man-

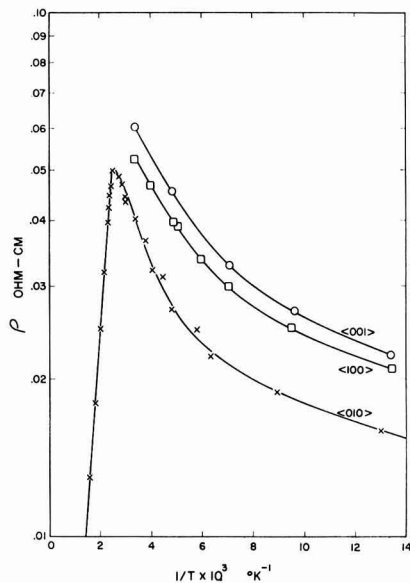


Fig. 5. Resistivity vs. temperature

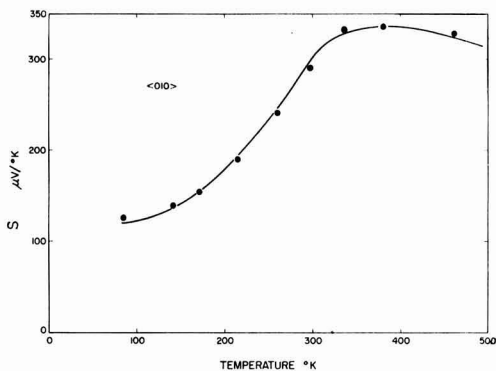


Fig. 6. Seebeck coefficient vs. temperature,  $\langle 010 \rangle$  direction.

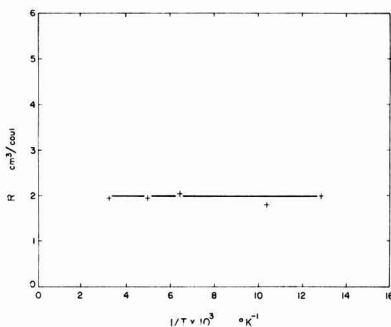


Fig. 7. Hall coefficient vs. temperature,  $\langle 010 \rangle$  direction



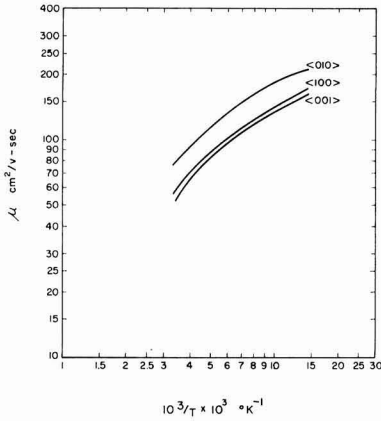


Fig. 8. Hole mobility vs. temperature

ner is 0.57 eV, in good agreement with the values of Andronik and Kot, but lower than the value of 0.63 eV at 0°K extrapolated from the absorption data.

Mobility values calculated in the exhaustion range are shown in Fig. 8. The mobility of the charge carriers is quite low, the room temperature hole mobility being about 80 cm<sup>2</sup>/v-sec. The mobility between 77° and 300°K does not follow a simple power law, but rather, if  $\mu = cT^{-m}$ , then  $m$  is found to increase from 0.6 at liquid nitrogen temperature to 0.95 at room temperature. The smaller dependence of  $\mu$  on  $T$  at lower temperatures is probably due to significant impurity scattering in this highly doped sample. The decrease in the exponent with decreasing temperature indicates that the impurity scattering contributes to a greater extent as the temperature is decreased.

From the sign of the Seebeck and Hall coefficient data, the carriers in the extrinsic range must be holes, and since the Seebeck coefficient does not change sign with temperature, the ratio  $b$  of the electron to hole mobility must be less than unity. The mobility ratio cannot be determined by the usual procedure from the Hall coefficient maximum (10) since when  $b < 1$  the Hall coefficient will decrease continuously to zero. The mobility ratio can be determined in this case from the resistivity data by the method derived by Hunter (11). The mobility ratio can be given in p-type material by:

$$b = \frac{1}{\tau - 1} - \tau \quad [4]$$

where  $\tau$  is the ratio  $\rho_e/\rho_o$ , where  $\rho_e$  is the resistivity of the extrinsic line extrapolated to its intersection with the intrinsic line, and  $\rho_o$  is the actual resistivity at the same temperature. However, since the ratio of the two resistivities is used, the resistivity in the transition region must be determined very accurately. Another difficulty associated with this procedure is the determination of a satisfactory method of extrapolation. Hunter (11) suggests extrapolation of the extrinsic line assuming the mobility is a simple power function of temperature. However, this is not the case for the sample investigated (Fig. 9),

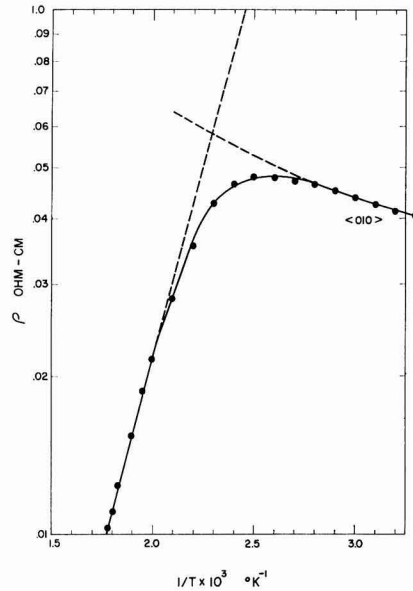


Fig. 9. Determination of mobility ratio

and the extrinsic resistivity curve was extrapolated by extension as a smooth curve approaching a slope of  $-1.5$  at 600°K. This extrapolation and the determination of the mobility ratio are shown in Fig. 9. The mobility ratio found by this method was 0.9, verifying the Seebeck coefficient data that electrons have a smaller mobility than holes in CdSb. The inaccuracies in this extrapolation are so great however, that essentially all that can be said is that the mobility ratio calculated by this method agrees with the Seebeck coefficient data, in that the ratio  $b$  is close to unity.

The effective mass of the charge carrier can be calculated from the Seebeck coefficient data plotted in Fig. 6. For ellipsoidal energy surfaces the effective mass can be calculated from the equation (12)

$$S = -\frac{k}{e} \left[ \left( \frac{5}{2} - s \right) + \ln \frac{2(2\pi m^* kT)^{3/2}}{n h^3} \right] \quad [5]$$

where  $s$  is the parameter determined by the dependence of the relaxation time  $\tau$  on the energy of the charge carriers:

$$\tau = aE^{-s} \quad [6]$$

The value of  $m^*$  calculated from Eq. [5] depends on the value  $s$  chosen. If  $s = 1/2$  choosing the simplified case of lattice scattering in a covalently bonded material, then  $m^*$  varies from 0.2 at 100°K to 0.38 at 300°K. These data are in agreement with the cyclotron resonance data of Stevenson (13) who obtained a value of 0.15  $m_o$  (at liquid helium temperatures). A temperature variation of the effective mass in the homologous compound ZnSb has also been reported (14).

It is appropriate also to consider combined imperfection and lattice scattering. This also has been studied by Johnson and Lark-Horovitz (15) who

have derived an expression for the Seebeck coefficient in this more general case. The equation is:

$$s = \pm \frac{k}{e} \left[ \ln \frac{RT^{3/2}}{r} - 7.16 + 1.5 \ln \frac{m^*}{m_0} + q \right] \quad [7]$$

where  $r$  and  $q$  are numerical factors which depend on the ratio of impurity to lattice scattering. If the Seebeck coefficient data is substituted into Eq. [7], then the data can be fitted for  $m^* = 0.35 m_0$  with a ratio of impurity to total resistivities of 0.6 from liquid nitrogen to room temperature. However, this is not very satisfactory, since impurity scattering as indicated by the mobility data should become increasingly more important as the temperature is lowered.

### Anisotropy

The resistivity was determined in the exhaustion region for the three principal axes of the orthorhombic unit cell (Fig. 5).

Although random impurity differences between the three sections studied may introduce scatter in the data, it appears as if there is a definite anisotropy in the resistivity. The quite small variation in resistivity between the  $\langle 100 \rangle$  and  $\langle 001 \rangle$  directions and the large difference between these values and the resistivity in the  $\langle 010 \rangle$  direction agrees well with the data of Stevenson, who observed anisotropy of the effective mass in the plane containing the  $b$  crystal direction.

The values also agree well with the data of Andronik and Kot (4), and from the magnitude of the values we can assign the correlation that the conductivities  $\sigma_{11}$ ,  $\sigma_{22}$ ,  $\sigma_{33}$  given by Andronik and Kot are the conductivities in the  $\langle 100 \rangle$ ,  $\langle 010 \rangle$ , and  $\langle 001 \rangle$  directions, respectively. The three principal conductivities are in the ratio  $\sigma_{010} : \sigma_{100} : \sigma_{001} = 1.45 : 1.09 : 1.00$  over the entire temperature range studied.

### Acknowledgment

The work in this paper is based on research sponsored by Air Force Cambridge Research Center, Air Research and Development Command, Bedford, Massachusetts on Contract AF19(604)-3902, Dr. N. Rosenberg, project engineer. Permission to publish the results is gratefully acknowledged.

Manuscript received March 23, 1961; revised manuscript received July 17, 1961.

Any discussion of this paper will appear in a Discussion Section to be published in the June 1962 JOURNAL.

### REFERENCES

1. E. Justi and G. Lautz, *Z. Naturforsch.*, **7a**, 191, 602 (1952); E. Justi and G. Lautz, *Abh Braunsch Wiss. Gess.*, **4**, 107 (1952).
2. I. M. Pilat, *Zhur. Tekh. Fiz.*, **27**, 119 (1957); I. M. Pilat, *Fiz. Metal. i Metalloved.*, **4**, 232 (1957); G. Kretschmar, R. F. Potter, and P. R. Bradshaw, *Bull. Am. Phys. Soc.*, Ser. II, **4**, 134 (1958); J. Yahia and R. Overstreet, *Bull. Am. Phys. Soc.*, Ser. II, **4**, 134 (1958); M. V. Kot and I. K. Andronik, *Uchenye Zapiski Kishinev Univ.*, **29**, 147, 209 (1957); I. K. Andronik, *Uchenye Zapiski Kishinev Univ.*, **29**, 215 (1957).
3. A. J. Strauss, *This Journal*, **106**, 206C (1959).
4. I. K. Andronik and M. V. Kot, *Fiz. Tverdogo Tela*, **2**, 1128 (1960).
5. M. Hansen, "Constitution of Binary Alloys," 2nd ed., McGraw-Hill Book Co., New York (1958).
6. D. Turnbull, *J. Chem. Phys.*, **18**, 198 (1950).
7. H. Y. Fan, *1956 Rep. Prog. Phys.*, **19**, 107 (London: Physical Society).
8. W. W. Scanlon, *J. Phys. Chem. Solids*, **8**, 423 (1958).
9. G. G. MacFarlane, T. P. McLean, J. E. Quarrington, and V. Roberts, *Phys. Rev.*, **108**, 1377 (1957).
10. R. A. Breckenridge, et al., *Phys. Rev.*, **96**, 573 (1954).
11. L. P. Hunter, *ibid.*, **91**, 579 (1953).
12. V. A. Johnson and K. Lark-Horovitz, *ibid.*, **92**, 226 (1953).
13. M. J. Stevenson, *Bull. Am. Phys. Soc.*, Ser. II, **5**, 177 (1960).
14. K. C. Bourke, R. Simon, and E. H. Lougher, Paper presented at Electrochemical Society Meeting, Chicago, May 1960.

## Molten Carbonate Electrolytes: Physical Properties, Structure, and Mechanism of Electrical Conductance

George J. Janz and Max R. Lorenz

Department of Chemistry, Rensselaer Polytechnic Institute, Troy, New York

### ABSTRACT

The present communication reports the results of an investigation of the properties of surface tension, density, and electrical conductance for molten  $\text{Li}_2\text{CO}_3$ ,  $\text{Na}_2\text{CO}_3$ , and  $\text{K}_2\text{CO}_3$  and some mixtures in the temperature range of 750°-1000°C. The surface tensions are approximately twice the values for the corresponding chlorides; the densities and electrical conductance are quite comparable to those of the chlorides. The ionic nature of the molten carbonates is examined from the physicochemical criteria based on these properties; and the mechanism of electrical transport is considered in the light of current theoretical concepts. Relative to  $\text{Na}_2\text{CO}_3$ - $\text{K}_2\text{CO}_3$  mixtures, the surface tensions and partial molal volumes indicate but little deviation from the predictions for thermodynamically ideal mixtures.

Knowledge of a broad cross section of physical and electrochemical properties for molten salts is important to advance the understanding of this important class of electrolytes. Recent surveys of the literature (1-3) show that, whereas very accurate

values for the physicochemical properties and electrical conductance are now known for the halides of the Group I and Group IIA elements, data for molten salts in which the anionic species are polyatomic are extremely limited. With the exception of the data for

a few selected nitrates, there are no values for this class of electrolytes of sufficient precision and for a sufficient temperature range to be used in calculation or formulation of molten salt theories. The present communication reports the results of an investigation of the properties of surface tension, density, and electrical conductance for  $\text{Li}_2\text{CO}_3$ ,  $\text{Na}_2\text{CO}_3$ , and  $\text{K}_2\text{CO}_3$ . Preliminary to these measurements, exploratory studies on the  $\text{CO}_2$  dissociation pressures were essential for the design of the experimental conditions. The results of these experiments are briefly described as well.

### Experimental

The apparatus and furnace, designed in this laboratory for the simultaneous measurement of density and surface tension for molten salt up to  $1000^\circ\text{C}$ , have been described elsewhere in detail (4). The furnace was capable of a uniform temperature zone at  $900^\circ\text{C}$  of  $\pm 0.2^\circ\text{C}$  in a 10 cm sample zone. In all the measurements, *i.e.*, densities, surface tensions, conductances, thermal stabilities, all metal components of the apparatus contacting the molten carbonates were made from a noble metal alloy, 80% Au-20% Pd. It was found, in preliminary measurements, that this alloy withstood corrosion after being exposed in such melts at  $900^\circ\text{C}$  for periods as long as 30-60 hr.

**Thermal Stability.**—The dissociation pressures were determined by a dynamic method in which the weight of a sample was continuously observed while  $\text{CO}_2$  at controlled pressures was streamed through the furnace tube. An analytical balance with an optical scale (100 mm range) was used to monitor the weight changes as follows. With the sample exposed in an atmosphere of a fixed partial pressure of  $\text{CO}_2$  the temperature of the specimen was changed gradually. As the equilibrium temperature for the selected partial pressure of  $\text{CO}_2$  was passed in the heating cycle, a weight loss was noted; on cooling the specimen, a weight increase was noted as the temperature passed through the equilibrium value for this partial pressure. The thermal cycle was repeated at various arbitrarily selected  $\text{CO}_2$  pressures for each specimen. The method was checked using  $\text{CaCO}_3$  as standard (5); it was found that at each partial pressure the equilibrium dissociation temperature was readily determined within  $1^\circ\text{C}$ . For  $\text{Li}_2\text{CO}_3$  (m.  $726^\circ\text{C}$ ) the following equilibrium temperatures and  $\text{CO}_2$  dissociation pressures were thus found:  $735^\circ\text{C}$ , 11.6 mm;  $776^\circ$ , 53.2;  $797^\circ$ , 111;  $821^\circ$ , 247;  $843^\circ$ , 501; for  $\text{Na}_2\text{CO}_3$  (m.  $858^\circ\text{C}$ ):  $840^\circ$ , 0.0 mm;  $858^\circ$ , 8 mm;  $885^\circ$ , 15 mm. No measurements were made with  $\text{K}_2\text{CO}_3$  (m.  $899^\circ\text{C}$ ); its thermal stability is known to be equal to or better than that of  $\text{Na}_2\text{CO}_3$ . Comparison with the earlier results for  $\text{Li}_2\text{CO}_3$  (6-8) shows that the earlier data can be brought into accord with the present results if a correction for 0.004, 0.02, and 0.1 mole  $\text{Li}_2\text{O}/\text{mole Li}_2\text{CO}_3$ , respectively, in the samples of the earlier investigators is taken into consideration. Repeated evacuations of the specimens in the static method (6-8) would contribute to the formation of such impurities.

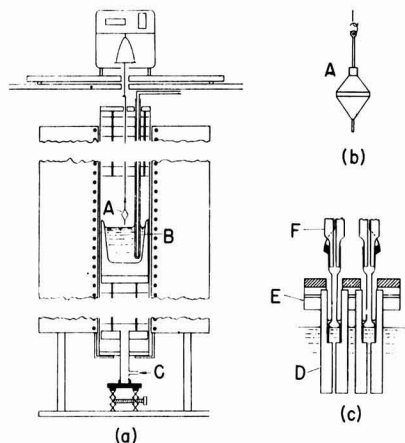


Fig. 1. Assembly for surface tension, density, and electrical conductance measurements for molten electrolytes. (a) Surface tension—density apparatus showing arrangement of the bob (A), crucible with molten salt (B), variable height mount with  $\text{CO}_2$  gas inlet (C), and analytical balance relative to the furnace; (b) detail of surface-tension density bob design; (c) detail of conductance cell design showing the single crystal  $\text{MgO}$  capillaries (D) suspended from the Au-20% Pd block (E), and insulated electrode leads (F).

**Surface tensions and densities.**—The method and experimental assembly were the same as previously described (4) and is illustrated schematically in Fig. 1a and b. Densities were measured by the Archimedian principle, but the special design of the bob and the continuously variable height crucible containing the melt made it possible to apply, in principle, the method of the du Nouy Tensiometer for the simultaneous surface tension determinations. The design of the bob (Fig. 1b) was a double cone, base to base, with a pin of accurately known dimensions (0.0899 cm diameter  $\times$  0.60 cm) extending from the lower cone. It was possible, thus, to gain the surface tensions from the "make" and "break" weight data as the melt was initially raised to the point of contact with the pin in the density measurements. All density results were corrected for surface tension effects on the suspension. The entire bob was machined from one solid piece of Au-20% Pd alloy to eliminate tapped threads or crevices. For calibration, trimethylpentane, benzene, toluene, and  $\text{CCl}_4$  (all at  $25^\circ\text{C}$ ) and molten  $\text{KNO}_3$  (at  $350^\circ\text{--}465^\circ\text{C}$ ) were used as reference standards. The apparatus and procedure were capable of results precise to  $\pm 0.1$  dyne  $\text{cm}^{-1}$  and  $\pm 0.001$  g  $\text{cm}^{-3}$  at elevated temperatures for surface tensions and densities, respectively.

**Electrical conductance.**—A capillary-type conductance cell, as illustrated in Fig. 1c, was used for the measurements with the molten carbonates. The capillaries were machined from single crystal quality  $\text{MgO}$  and were mounted firmly and securely in a metal suspension block made of Au-20% Pd alloy. The cell constant was  $197.9$   $\text{cm}^{-1}$  and was determined in the conventional manner (9) using the data for molten  $\text{KCl}$  (10) and  $\text{KNO}_3$  (11). All measurements were at 1000, 2000, 5000, and 20,000

cps; by extrapolation, the polarization-free value at infinite frequency was gained. With the present assembly this correction was found to be 0.2% of the value at 1000 cps. A conductance bridge, designed (12) in this laboratory for high precision performance comparable to the Jones Bridge, was used in these measurements.

**Materials.**— $\text{Li}_2\text{CO}_3$ ,  $\text{Na}_2\text{CO}_3$ , and  $\text{K}_2\text{CO}_3$ , reagent grade quality, were dried to constant weight under  $\text{CO}_2$  at 600°C, and stored in  $\text{P}_2\text{O}_5$  desiccators until required.

All measurements were made with an atmosphere of  $\text{CO}_2$  at pressures in large excess to the dissociation partial pressures of the carbonates. As an additional check, since dissociation to oxide would lead to irreproducibility, the measurements were made in thermal cycles at temperatures randomly selected, first higher, then lower, then higher and so on, to detect possible changes in the values of the physical property being determined. A complete set of conductance measurements for any one given salt or mixture required some 30 hr. The reproducibility of the measurements was excellent. Little or no scatter was observed for the data thus obtained in the graphical analyses of the results.

### Results and Discussion

The surface tension,  $\gamma$ , the density,  $\rho$ , and the specific and equivalent conductance,  $\kappa$  and  $\Lambda$ , re-

**Table I. Surface tensions, densities, and specific conductances of molten carbonates**

Temp, °C	$\gamma$ , dynes cm <sup>-1</sup>	Temp, °C	$\rho$ , g cc <sup>-1</sup>	Temp, °C	$\kappa^*$ ohm <sup>-1</sup> cm <sup>-1</sup>
<b><math>\text{Li}_2\text{CO}_3</math> (mp 726°C)</b>					
737.1	243.4	739.0	1.8246	744.7	4.162
753.9	243.2	754.2	1.8189	755.4	4.240
777.0	241.5	756.5	1.8190	764.9	4.304
808.0	240.3	778.9	1.8119	744.2	4.373
794.9	241.9	796.5	1.8036	782.8	4.463
828.9	240.1	809.5	1.7987	804.2	4.617
845.0	239.0	831.9	1.7910	826.5	4.803
		846.9	1.7843	844.5	4.954
<b><math>\text{Na}_2\text{CO}_3</math> (mp 858°C)</b>					
870.7	211.0	864.7	1.9685	864.8	2.887
888.0	210.4	873.0	1.9666	878.7	2.945
901.1	209.4	892.3	1.9576	885.2	2.973
907.4	209.3	905.6	1.9508	893.0	3.004
910.0	209.0	911.5	1.9477	909.6	3.070
927.3	208.1	950.1	1.9288	918.9	3.112
945.7	207.2	960.0	1.9264	926.9	3.138
957.2	206.5	971.6	1.9211	942.3	3.191
968.8	206.2	987.1	1.9142	952.9	3.232
1006.3	204.3	1003.8	1.9080	966.5	3.283
<b><math>\text{K}_2\text{CO}_3</math> (mp 899°C)</b>					
904.7	169.0	907.6	1.8922	910.5	2.062
910.0	168.8	912.1	1.8904	922.5	2.098
916.7	168.0	920.7	1.8864	926.6	2.111
919.2	168.2	922.7	1.8848	938.0	2.143
919.9	167.2	929.4	1.8824	942.6	2.157
926.6	167.5	940.3	1.8778	954.4	2.195
939.5	166.5	946.8	1.8749	955.7	2.196
946.0	166.4	950.4	1.8735	961.3	2.209
948.7	166.3	960.9	1.8684	964.8	2.222
959.1	165.3	963.1	1.8670	976.3	2.255
960.9	165.2	972.1	1.8640	984.4	2.278
969.3	164.7	984.2	1.8584	996.2	2.312
980.9	163.9	996.8	1.8527	1001.5	2.324
993.3	163.2	1010.1	1.8467	1005.9	2.336
1005.3	162.6				

**Table II. Equations for surface tensions, densities, and electrical conductance**

	Surface tension: $\gamma = \gamma_0 - a$ (dynes cm <sup>-1</sup> )			
	$\gamma_0$	$a$ (10 <sup>3</sup> )	max. dev.	$t$ , °C, range
$\text{Li}_2\text{CO}_3$	273.6	40.7	0.67	750-850
$\text{Na}_2\text{CO}_3$	255.8	51.4	0.36	870-1005
$\text{K}_2\text{CO}_3$	226.9	64.2	0.23	905-1010
	Density: $\rho = \rho_0 e^{-\alpha T}$ (g cm <sup>-3</sup> )			
	$\rho_0$	$\alpha$ (10 <sup>4</sup> )	max. dev.	$t$ , °C, range
$\text{Li}_2\text{CO}_3$	2.2496	2.0649	0.0016	750-850
$\text{Na}_2\text{CO}_3$	2.5608	2.309	0.0021	870-1005
$\text{K}_2\text{CO}_3$	2.4992	2.3568	0.0006	905-1010
	Specific conductance: $\kappa = A'k e^{-\Delta E_k/kRT}$			
	$A'k$	$\Delta E_k$ (kcal)	max. dev.	$t$ , °C, range
$\text{Li}_2\text{CO}_3$	29.138	3.94 <sub>2</sub>	0.080	740-850
$\text{Na}_2\text{CO}_3$	13.757	3.5 <sub>2</sub>	0.002	865-970
$\text{K}_2\text{CO}_3$	11.014	3.9 <sub>3</sub>	0.004	910-1010
	Equivalent conductance: $\Lambda = \Lambda_0 e^{-\Delta E_\Lambda/kRT}$ (ohms <sup>-1</sup> cm <sup>-2</sup> equiv. <sup>-1</sup> )			
	$\Lambda_0$	$\Delta E_\Lambda$ (kcal)	max. dev.	$t$ , °C, range
$\text{Li}_2\text{CO}_3$	755.3	4.40 <sub>0</sub>	0.3	740-850
$\text{Na}_2\text{CO}_3$	493.4	4.17 <sub>0</sub>	0.2	865-970
$\text{K}_2\text{CO}_3$	544.8	4.65 <sub>1</sub>	0.1	910-1010

**Table III. Surface tensions and densities for  $\text{Na}_2\text{CO}_3$ - $\text{K}_2\text{CO}_3$  mixtures**

$t$ , °C	Mole % $\text{K}_2\text{CO}_3$ : 25.00					
	$\gamma$ , dynes cm <sup>-1</sup>	$\rho$ , g cm <sup>-3</sup>	$t$ , °C	$\gamma$ , dynes cm <sup>-1</sup>	$\rho$ , g cm <sup>-3</sup>	$t$ , °C
772.9	810.6	847.5	880.0	902.2	924.8	
198.7	196.1	194.4	192.2	191.0	189.8	
774.8	811.8	849.7	881.7	904.6	926.5	
1.9924	1.9734	1.9566	1.9420	1.9302	1.9206	
$t$	Mole % $\text{K}_2\text{CO}_3$ : 50.00					
	$\gamma$	$\rho$	$t$	$\gamma$	$\rho$	$t$
725.0	747.2	782.6	840.8	854.8	897.2	
191.3	190.0	187.7	184.1	183.1	180.7	
727.2	748.9	783.8	842.5	856.5	899.7	
2.0013	1.9906	1.9741	1.9453	1.9390	1.9192	
$t$	Mole % $\text{K}_2\text{CO}_3$ : 75.00					
	$\gamma$	$\rho$	$t$	$\gamma$	$\rho$	$t$
810.1	838.4	886.8	920.3	958.3	964.2	
179.1	177.6	174.2	172.7	169.7	176.2	
810.5	841.5	865.1	888.6	922.4	961.2	
1.9221	1.9333	1.9221	1.9116	1.8949	1.8785	

spectively, for molten lithium, sodium, and potassium carbonates were measured in the temperature range 750°-1000°C. The data are listed in Table I, and the parameters found for the equations by which these may be expressed, together with the maximum deviations from the experimental results, are summarized in Table II. In Table III, the surface tensions and densities for three  $\text{Na}_2\text{CO}_3$ - $\text{K}_2\text{CO}_3$  mixtures over a similar temperature range above the melting points are reported. The particular considerations given to features contributing to reproducibility and accuracy of the results have already been noted. Thus, relative to the conductance measurements, the uncertainty is, at a maximum,  $\pm 0.5\%$ ; for the measurements of surface tensions and densities, the uncertainty in the values is even less. The discussion and evaluation of these results is developed relative to each of the properties investigated.

**Thermal stability.**—The importance of the atmosphere is shown by the following results gained for  $\text{Na}_2\text{CO}_3$ . A 5-g sample under 1 atm  $\text{CO}_2$  showed no weight loss up to 840°C (mp 858°C). At 1000°C, and after 7 hr when the sample weight was constant, the total weight loss was 25.1 mg. The atmosphere was changed to  $\text{N}_2$  at 1 atm; a weight loss (4.8 mg  $\text{hr}^{-1}$ ) was again noted. On changing the atmosphere to  $\text{CO}_2$  (1 atm), the weight increased to the original value of 1000°C. The sample was then exposed to  $\text{N}_2$  gas (1 atm) saturated at 25°C with water vapor; an enhanced rate of weight loss (36.2 mg  $\text{hr}^{-1}$ ) was now evident. On changing this atmosphere to water-saturated (25°C)  $\text{CO}_2$  (1 atm), a weight increase (36.7 mg  $\text{hr}^{-1}$ ) was observed until the original weight at 1000°C had been regained. Finally this sample, still at 1000°C, was exposed to an atmosphere of dry air (1 atm); the weight loss thus initiated was about 1 mg  $\text{hr}^{-1}$ . It is readily apparent that the dynamic method is well suited for facile and rapid evaluation of the thermal stability of such compounds under various atmospheres.

That the molten carbonates were found to show the first appreciable dissociation just above their respective melting points may be attributed in part to the smaller interatomic distances for the nearest neighbors in the first coordination shell, i.e., for the alkali halides this distance is significantly less in the molten salts than in the solid states (13), and it would be predicted that similar conditions prevail for molten carbonates. Cationic polarization effects may be recognized in the resulting decomposition of the  $\text{CO}_3^{2-}$  species to  $\text{CO}_2$  and oxide ion. In the present measurements of the properties of surface tensions, densities, and electrical conductances, the samples were investigated under dry  $\text{CO}_2$  at pressures well above the dissociation partial pressures.

**Surface tension.**—The only surface tensions published previously are the three values of Quincke (14) in 1857-69 (i.e., 152.5, 179.0, and 160.2 for  $\text{Li}_2\text{CO}_3$ ,  $\text{Na}_2\text{CO}_3$ , and  $\text{K}_2\text{CO}_3$ ), and two values by Traube (15) in 1891, (i.e., 210 and 167 for  $\text{Na}_2\text{CO}_3$  and  $\text{K}_2\text{CO}_3$ ) both for temperatures "just at the melting points." Comparison with the present results shows that the Traube data correspond almost exactly to values some 30°C above the respective melting points, i.e.,  $\text{Na}_2\text{CO}_3$ , 210.4 at 888°C;  $\text{K}_2\text{CO}_3$ , 167.5 at 927°C, but that the Quincke values are lower than any of the present results. The surface tension data, Table I, may be reproduced within experimental error over the complete temperature range by simple linear type equations. The latter are summarized in Table II. The surface tensions of the molten carbonates are very nearly twice the values for the corresponding chlorides.

The surface heat, defined by the relation:

$$H_A^s = \gamma - T \frac{d\gamma}{dT}$$

is said to provide a measure of the molecular character of the liquid (16); thus for the three liquids,  $\text{C}_6\text{H}_6$ ,  $\text{MgCl}_2$ , and  $\text{NaCl}$ , the values for this parameter are 59.2, 76.7, and 216.7 erg  $\text{cm}^{-2}$ , respectively. The surface heats for  $\text{Li}_2\text{CO}_3$ ,  $\text{Na}_2\text{CO}_3$ , and  $\text{K}_2\text{CO}_3$  are

Table IV. Values of the parachor for various molten salts

$\text{Li}_2\text{CO}_3$		$\text{Na}_2\text{CO}_3$		$\text{K}_2\text{CO}_3$		KCl		$\text{KNO}_3$	
$t, ^\circ\text{C}$	$P$	$t, ^\circ\text{C}$	$P$	$t, ^\circ\text{C}$	$P$	$t, ^\circ\text{C}$	$P$	$t, ^\circ\text{C}$	$P$
760	160.5	870	205.4	920	263.6	800	154.9	350	176.0
780	161.0	890	206.1	940	264.4	850	156.4	400	178.1
800	161.5	930	207.5	960	265.1	900	157.9	450	180.3
820	162.1	950	208.2	980	265.9				
840	162.6	970	208.9	1000	266.6				

Table V. Comparison of molecular volumes (at  $\theta = 1.10$ )

Salt	Molecular volume ( $\text{\AA}^3/\text{molecule}$ )		From parachor data
	From density data	From ionic volumes	
$\text{Li}_2\text{CO}_3$	68.4	37.9	66.5
$\text{Na}_2\text{CO}_3$	91.6	43.2	85.6
$\text{K}_2\text{CO}_3$	124.4	55.8	109.5
$\text{KNO}_3$	91.8	34.8	72.3
KCl	84.4	34.7	64.5

found to be 284.7, 269.8, and 241.5 erg  $\text{cm}^{-2}$ . The concept of a reference temperature,  $\theta$ , equal to  $T/T_m$ , where  $T$  and the melting point,  $T_m$ , are in  $^\circ\text{K}$ , has been advanced (10) for the comparison of molten salt properties. The surface tensions of  $\text{Li}_2\text{CO}_3$ ,  $\text{Na}_2\text{CO}_3$ , and  $\text{K}_2\text{CO}_3$ , accordingly at  $\theta = 1.10$ , are thus 240.0, 205.9, and 161.7 dynes  $\text{cm}^{-1}$ , respectively. It is clear that as the number of ions per unit length and the polarizing power of the cations decrease, the surface tensions of the carbonate melts decrease.

The Parachor,  $P = M\gamma^{1/4}/(\rho - d)$ , has been calculated from the present results; the values are found in Table IV. A small but definite increase in  $P$  with temperature (approx. 2%/100°) is noted. Values of the surface tension exponent ranging between 0.7 and 1.2 make the parachor temperature-independent for the salts in Table IV. "Ionic" parachor values vary markedly; this difficulty has been noted (16) in a similar analysis for other molten salts. An empirical relation, 1 parachor unit =  $0.41\text{\AA}^3$ , has been demonstrated by Edward (17) from an analysis of a large number of covalent liquids at room temperature. In Table V are compared the molecular volumes from (i) densities, (ii) crystallographic radii, and (iii) the Edward empirical relation (above). Inspection shows that for molten salts either the volume, of which the parachor provides a measure, includes a variable proportion of the "unoccupied volume" of the liquid, or that the empirical relation that applies for ionic liquids such as molten salts is, 1 parachor unit =  $0.52\text{\AA}^3$ .

Relative to mixtures of molten carbonates, the value of the surface tension for an equimolar  $\text{Na}_2\text{CO}_3$ - $\text{K}_2\text{CO}_3$  mixture (950°C) may be found as 183 dyne  $\text{cm}^{-1}$  from the Guggenheim (18) equation:

$$\gamma = \frac{1}{2} (\gamma_A + \gamma_B) - \frac{(\gamma_A - \gamma_B)^2 a}{8 k T}$$

for thermodynamically ideal systems. Comparison with the observed value, 178 dyne  $\text{cm}^{-1}$  (Table III) shows a small negative deviation (approx. 3%) from



thermodynamic ideality in this property for the  $\text{Na}_2\text{CO}_3\text{-K}_2\text{CO}_3$  mixture.

*Density.*—Relative to the densities, the only literature values are a limited series for the three carbonates by Brunner (19) (1904). Comparison with the present results shows that the Brunner data differ only by 0.3–0.5% in the range where comparison is possible. As shown in Table II, the density-temperature relation may be expressed by

$$\rho = \rho_0 e^{-\alpha T}$$

The expansivity  $\alpha$ , defined as  $-\frac{1}{\rho} \frac{d\rho}{dT}$ , was found to be constant within experimental error over the range of temperature for each of the three molten carbonates.

The results for the density measurements for molten carbonate mixtures are summarized in Table III. Relative to the  $\text{Na}_2\text{CO}_3\text{-K}_2\text{CO}_3$  system, the liquidus-solidus phase diagram shows (20) a continuous series of solid solutions (minimum, 55–58%  $\text{Na}_2\text{CO}_3$ , m.  $710^\circ\text{C}$ ). It is of interest to note that the molar volume-composition isotherms for these mixtures, calculated from Table III, deviated less than 1% from the values predicted for thermodynamically ideal mixtures by the principle of additivity.

*Electrical conductance.*—Values of the specific conductances for the three carbonates are found in Table I. Limited data for  $\text{Na}_2\text{CO}_3$  and  $\text{K}_2\text{CO}_3$  have been reported previously (21, 22) comparison at  $900^\circ\text{C}$  shows an agreement with the present results within the limits 2–12%. No prior conductances for  $\text{Li}_2\text{CO}_3$  have been reported. Values for the equivalent conductances for the carbonates can be calculated from the data in Table I and the fundamental definition of equivalent conductance for molten salts:

$$\Lambda = M\kappa\rho^{-1}$$

where  $M$  is the equivalent weight, and  $\kappa$  and  $\rho$  have their conventional significance. The parameters for the temperature dependence of  $\Lambda$  and  $\kappa$  expressed by exponential type equations

$$\Lambda = A_\Lambda e^{-\Delta E_\Lambda^\ddagger/RT} \quad \text{and} \quad \kappa = A_\kappa e^{-\Delta E_\kappa^\ddagger/RT}$$

are given in Table II. These should be recognized as average values, since the  $\ln(\Lambda, \kappa)$  vs.  $1/T$  graphs had a small but definite curvature. The temperature dependence of  $\Delta E^\ddagger$  for sodium carbonate calculated from the more precise analysis of the results is illustrated in Table VI for both the limiting and equivalent conductances. A possible explanation for the decrease in heat of activation,  $\Delta E^\ddagger$ , with increasing temperature is discussed later. The relation between the expansivity of the molten salt,  $\alpha$ , and  $\Delta E_\Lambda^\ddagger$  and  $\Delta E_\kappa^\ddagger$  given by

$$\Delta E_\Lambda^\ddagger = \Delta E_\kappa^\ddagger + \alpha RT^2$$

has been derived elsewhere by Martin (23) from the fundamental definitions of these concepts for molten salts. The internal consistency of the present results (Table I) and a striking confirmation of the

above relation is seen in the close agreement between the observed differences ( $\Delta E_\Lambda^\ddagger - \Delta E_\kappa^\ddagger$ ) and the values of  $\alpha RT^2$  also listed in Table VI.

*Structure of molten carbonate and mechanism of electrical conductance.*—A review of the nature of melts formed by the fusion of ionic salts has been recently given by Ubbelohde (24), and it is sufficient to note that experimental evidence, from thermodynamic and nonthermodynamic methods, supports the concept that ionic melts consist of a highly disordered but quasicrystalline arrangement whose defects include holes, interstitial ions, paired holes and paired ions, as well as cooperative defects similar to dislocations extending over more than two ions. Support for the view that the strong electrostatic ion core potentials effectively force the ions into local close-packed lattice-like arrangements, and that these "pair-interactions" rapidly drop to zero is found in the theoretical treatment by Stillinger, Kirkwood, and Wojtowicz (25) for fused salts. The nearest neighbor anionic-cationic distances being less in the molten alkali halides than in the crystalline state (13) is thus understood in the light of these interactions. It is of interest to evaluate the properties of the molten carbonates in the light of current theories for two limiting cases (i) that the molten carbonates are completely ionized, with the species  $M^+$  and  $\text{CO}_3^{2-}$  as the main kinetic entities contributing to conductance, and (ii) that whereas the molten carbonates are completely ionized, the main kinetic entities are  $M^+$  and the "contact ion pair" ( $M^+\text{CO}_3^{2-}$ ), and that the latter is the important species in the mechanism of conductance. The properties of surface tension, densities for the pure salts, and the thermodynamic properties of the mixtures are in accord with both models so that these properties cannot discern between these two models.

Limited tests of the first model, i.e.,  $M^+$  and  $\text{CO}_3^{2-}$ , are possible for sodium carbonate for which additional data are available. In a recent contribution, a theoretical equation for conductance of the form

$$\Lambda = \sum_{\pm} A_i T^{-1} e^{-\Delta H_i^\ddagger/RT}$$

has been developed by Bockris and co-workers (26) which seems satisfactory for simple molten electrolytes. From this theory, in which the mechanism is according to a hole model for molten salts, it follows that the experimental heat of activation for conductance,  $\Delta H_{\text{expt}}^\ddagger$ , is identified with the enthalpy of hole formation, and ionic jump,  $\Delta H_h^\ddagger$  and  $\Delta H_j^\ddagger$ , respectively, by the equation

$$\Delta H_j^\ddagger + \Delta H_h^\ddagger = \Delta H_{\text{expt}}^\ddagger + RT$$

for any particular ionic species. The free energy for hole formation, and the enthalpy for hole formation in a liquid (27), given by:

$$\Delta F_{h,i} = 4\pi r^2 \gamma$$

$$\Delta H_{h,i} = 4\pi r^2 \left( \gamma - T \frac{d\gamma}{dt} \right)$$

where  $\gamma$  is the surface tension, were calculated for sodium carbonate and the values thus found are:

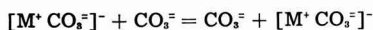
Ion	$r$ , A	$\Delta F_i$ , kcal/eq	$\Delta H_{H^+}^{\ddagger} + \Delta H_{CO_3^{2-}}^{\ddagger}$ , kcal/eq	$\Delta H_{CO_3^{2-}}^{\ddagger}$ , kcal/eq
Na <sup>+</sup>	0.95	3.42	4.84	6.4
CO <sub>3</sub> <sup>2-</sup>	2.05	15.9	22.6	
	2.44	22.6	32.1	

In the preceding, since the carbonate is a planar or disk-shaped anionic species of D<sub>3h</sub> point group symmetry, values were calculated for the smallest hole (to accommodate the disk) and the largest (for the sphere evolved by three-dimensional rotation), and it was assumed, as elsewhere (26), that  $\Delta H_{CO_3^{2-}}^{\ddagger}$  was approximately 0.1  $\Delta H_{H^+}^{\ddagger}$ . It would appear that in the molten carbonates the cationic species, viz., Na<sup>+</sup>, are predominant in the process of conduction, much as for the alkali halides (28, 29). A comparison of the equivalent conductances for the series Li, Na, K/X where X is Cl, Br, I, and CO<sub>3</sub>, viz:

at $\theta = 1.0$ , ohm <sup>-1</sup> cm <sup>2</sup> equiv <sup>-1</sup>	Cl	Br	I	CO <sub>3</sub>
Li	183	177	(170)	95
Na	150	148	150	90
K	120	109	104	87
$\Delta$	63	68	(66)	8

shows that the conductances for the molten carbonates differ from the trend predicted from a series of salts treated satisfactorily by this model (27).

An explanation for the limited variation in equivalent conductance (above) is seen in the second alternate. Paired ion species, such as (M<sup>+</sup>CO<sub>3</sub><sup>2-</sup>), are predicted as statistically more probable since relatively much smaller distances of closest approach are found in melts in which the anions are planar disk-shaped species rather than spheres. The importance of such species to migration is seen, in part, by the cooperative effect:



in which the rate-determining step is the jump of M<sup>+</sup> from one anionic species to the other, followed by rotation of the "anionic pair" much in the manner of the Grotthuss chain for proton transport in aqueous solutions. The entropy change, including rotation, is predicted zero for the over-all process. By reference to absolute reaction rate theory, the following equation can be derived, as for proton transference elsewhere (30), for this mechanism:

$$\Lambda_1 = d_1 (5.185 \times 10^{18}) (D + 2) (zd_2) e^{-\Delta F^{\ddagger}/RT}$$

where  $d_1$  and  $d_2$  are the half-migration and half-jump distances,  $D$  the dielectric constant, and the other symbols have their conventional significance.

Similar equations have been used (31) for molten silicates and alkali chlorides. The migration distance

(for jump-rotation scheme) is seen to be ( $d_{CO_3^{2-}} + 2.8 r_+$ ) where  $d_{CO_3^{2-}}$  is the short distance through the planar CO<sub>3</sub><sup>2-</sup> and the rotation is about the C<sub>2</sub> axis in the D<sub>3h</sub> point group symmetry of this species. The jump distance was taken as 0.8  $r_+$ , the assumption being in line with the view that the two anionic species must be in a favored configuration for this act. The values for  $d_1$  and  $d_2$  and the values for  $\Delta F^{\ddagger}$  and  $\Delta S^{\ddagger}$  thus found for the three molten carbonates at the reference temperature  $\theta = 1.10$ , are:

Cationic species	$r_+$	$2d_1$	$2d_2$	$\Delta F^{\ddagger}$	$\Delta H_{CO_3^{2-}}^{\ddagger}$	$\Delta S^{\ddagger}$
	cm $\times 10^8$			kcal		eu
Li <sup>+</sup>	0.60	4.26	0.48	3.8 <sub>2</sub>	3.8	0.0
Na <sup>+</sup>	0.95	6.24	0.76	4.7 <sub>8</sub>	4.0	-0.6
K <sup>+</sup>	1.33	7.30	1.06	5.1 <sub>7</sub>	4.4	-0.5

The dielectric constants for molten salts are unknown, and the estimated value of  $D = 3$  was used as elsewhere for the molten chlorides (33). The values

for  $\Delta H_{CO_3^{2-}}^{\ddagger}$  above and the values of the equivalent conductances for the three molten carbonates were the experimental values at  $\theta = 1.10$ , calculated from

Table I. The entropy of activation,  $\Delta S^{\ddagger}$ , is apparently very nearly zero and may be understood if the activated complex differs but little from the species in the ground state, viz., [M<sup>+</sup>CO<sub>3</sub><sup>2-</sup>]<sup>-</sup> and CO<sub>3</sub><sup>2-</sup>, and indicates a similar conduction mechanism in the three molten carbonates. Support for the cooperative jump-rotation mechanism in molten carbonates is seen in the temperature dependence of  $\Delta H^{\ddagger}$  (Table VI); the increased kinetic energy of the species at the higher temperatures should be realized in a more facile jump-rotation process although this factor may well be a viscosity effect much as in aqueous electrolytes. This migration mechanism, in the first approximation, would be largely independent of the nature of the cationic species. Support for this is seen in the limited variation of equivalent conductance for the molten carbonates for the series Li, Na, K/CO<sub>3</sub>, as already noted.

Re-examination of the criterion of the interionic friction coefficients (32) for molten carbonates (33) in the light of the present precise conduction results is possible, and provides a further evaluation of the above models.

The equations relating the interionic friction coefficients to the measured properties of conduction and diffusion for binary molten salts are:

Table VI. Variation of  $\Delta E_A$  and  $\Delta E_s$  with temperature for Na<sub>2</sub>CO<sub>3</sub> ( $10^4 \alpha = 2.309/^\circ K$ )

$t$ , °C	$\Delta E_A$ , kcal equiv <sup>-1</sup>	$\Delta E_s$ , kcal equiv <sup>-1</sup>	$\Delta E_A - \Delta E_s$ , kcal equiv <sup>-1</sup>	$\alpha RT^2$ , kcal equiv <sup>-1</sup>
880	4.24 <sub>2</sub>	3.66 <sub>5</sub>	0.57 <sub>7</sub>	0.60 <sub>6</sub>
900	4.22 <sub>6</sub>	3.56 <sub>5</sub>	0.66 <sub>5</sub>	0.63 <sub>2</sub>
920	4.15 <sub>7</sub>	3.49 <sub>6</sub>	0.65 <sub>7</sub>	0.65 <sub>3</sub>
940	4.13 <sub>7</sub>	3.46 <sub>1</sub>	0.67 <sub>5</sub>	0.67 <sub>5</sub>
960	4.02 <sub>2</sub>	3.32 <sub>7</sub>	0.69 <sub>5</sub>	0.69 <sub>3</sub>

$$r_{+-} = \frac{(z_+ + z_-)F^2}{\Lambda}$$

$$r_{++} = \frac{1}{z_-} \left[ \frac{(z_+ + z_-)RT}{D_{++}} - z_+ r_{+-} \right]$$

and

$$r_{--} = \frac{1}{z_+} \left[ \frac{(z_+ + z_-)RT}{D_{--}} - z_- r_{+-} \right]$$

While the results are limited, the recent analysis of a series of molten salts has shown that the like-ion friction coefficients,  $r_{++}$ , and  $r_{--}$ , both have negative values only for highly associated liquids (*viz.*,  $\text{ZnBr}_2$ ,  $\text{H}_2\text{O}$ ). Using the self-diffusion coefficients (33) for molten  $\text{Na}_2\text{CO}_3$ ,

$$D_{\text{Na}^+} = 1.92 \times 10^{-4} \quad \text{and} \quad D_{\text{CO}_3^{2-}} = 2.79 \times 10^{-4}$$

and the equivalent conductance at 1170°K (Table I), the following values for the interionic friction coefficients (watt sec<sup>2</sup> cm<sup>-2</sup> equiv<sup>-1</sup>) are found:<sup>1</sup>

$$r_{--} = 3.42 \times 10^6; \quad r_{++} = -0.95 \times 10^6; \quad r_{+-} = -5.79 \times 10^6$$

Further, the ratio of self-diffusion coefficients,  $D_{\text{CO}_3^{2-}}/D_{\text{Na}^+}$ , is 1.45 in molten  $\text{Na}_2\text{CO}_3$ . It appears, from these criteria, that  $\text{Na}_2\text{CO}_3$  is less than completely "dissociated." This is an unexpected result. The physical properties and electrical conductances are understood if the molten carbonates are completely ionic melts, with species such as  $\text{Na}^+$ ,  $\text{CO}_3^{2-}$ ,  $[\text{M}'\text{CO}_3]^-$  . . . contributing to the migration processes. The failure of the criterion of the interionic friction coefficients is seen in the apparently high value of  $D_{\text{CO}_3^{2-}}$ . An extra mode of diffusion for  $\text{C}^{14}$  in these melts is seen (33) in the diffusion of  $\text{CO}_2$  molecules. In molten carbonates the dissociation:



is finite at all temperatures above the melting point. The equilibrium pressure of 10 mm Hg at 900°C for molten  $\text{Na}_2\text{CO}_3$  implies a significant activity of  $\text{CO}_2$  molecules in the liquid phase. The exchange of  $\text{C}^{14}\text{O}_3^{2-}$  with  $\text{CO}_2$ , with a more rapid diffusion of the linear un-ionized species,  $\text{C}^{14}\text{O}_2$ , before suffering further exchange, seems not improbable and would account, in large part, for the relatively high  $D_{\text{CO}_3^{2-}}$  values found for molten  $\text{Na}_2\text{CO}_3$ .

It is apparent from the preceding that the properties of such complex salts as the carbonates in which the anions are disk-shaped polyatomic species rather than simple spheres are understood in part, at least, if "contact ion pairs" for gegen-ion species and cooperative jump-rotation interactions are recognized as important features of the model. Additional data, especially in the areas of transport, dielectric constants, viscosities, and thermodynamic properties, are needed to further knowledge in this area.

#### Acknowledgments

This work was made possible in large part, by support received from the Office of Naval Research,

<sup>1</sup> The difference in values for  $r_{+-}$ ,  $r_{++}$ , and  $r_{--}$  from those reported by Djordjevic and Hills elsewhere (33) is attributed to much less precise conductance data in the earlier calculations (34).

Division of Chemistry, Washington, D. C. The authors wish to thank Dr. F. J. Kelly of this laboratory for assistance in the calculations and stimulating discussions.

Manuscript received March 21, 1961; revised manuscript received July 26, 1961. This paper was prepared for delivery before the Indianapolis Meeting April 30-May 3, 1961 and is abstracted in part from a thesis by one of the authors (M.R.L.) submitted in partial fulfillment of the requirement for the Ph.D. degree, to Rensselaer Polytechnic Institute, June 1960.

Any discussion of this paper will appear in a Discussion Section to be published in the June 1962 JOURNAL.

#### REFERENCES

- G. J. Janz, C. Solomons, and H. J. Gardner, *Chem. Rev.*, **58**, 461 (1958).
- H. Bloom and J. O'M. Bockris, "Modern Aspects of Electrochemistry," 2, Academic Press, New York (1959).
- H. Bloom, *Rev. Pure Appl. Chem.*, **9**, 139 (1959).
- G. J. Janz and M. R. Lorenz, *Rev. Sci. Instr.*, **31**, 18 (1960).
- H. Mauras, *Bull. Soc. Chim. France*, **1959**, 16.
- P. Lebeau, *Ann. Chem. Phys.*, **6**, 422 (1905).
- J. Johnston, *Z. Phys. Chem.*, **62**, 330 (1908).
- J. T. Howarth and W. E. S. Turner, *J. Soc. Glass Tech.*, **14**, 394 (1934); **15**, 360 (1931).
- G. J. Janz and M. R. Lorenz, *Rev. Sci. Instr.*, submitted (1960).
- I. S. Yaffe and E. R. Van Artsdalen, *J. Phys. Chem.*, **60**, 1125 (1956).
- H. Bloom, W. I. Knaggs, J. J. Molloy, and D. Welch, *Trans. Faraday Soc.*, **49**, 1458 (1953).
- G. J. Janz and J. D. E. McIntyre, *This Journal*, **108**, 272 (1961).
- H. A. Levy, P. A. Agron, M. A. Bredig, and M. D. Danford, *Ann. N. Y. Acad. Sci.*, **79**, 762 (1960).
- G. Quincke, *Ann.*, **99**, 443 (1857); **135**, 624 (1868); **138**, 141 (1869).
- J. Traube, *Ber.*, **24**, 3074 (1891).
- H. Bloom, F. G. Davis, and D. W. James, *Trans. Faraday Soc.*, **56**, 1179 (1960).
- J. T. Edward, *Chem. & Ind.*, **1954**, 774.
- E. A. Guggenheim, *Trans. Faraday Soc.*, **41**, 180 (1945).
- E. Brunner, *Z. anorg. Chem.*, **38**, 350 (1904).
- A. Reisman, *J. Am. Chem. Soc.*, **81**, 807 (1959).
- K. Arndt, *Z. Elektrochem.*, **12**, 337 (1906).
- E. Ryskevitch, *ibid.*, **39**, 531 (1931).
- R. L. Martin, *J. Chem. Soc.*, **1954**, 3246.
- A. R. Ubbelohde, *Proc. Chem. Soc. London*, **1960**, 332.
- E. H. Stillinger, J. Kirkwood, and P. J. Wojtowicz, *J. Chem. Phys.*, **32**, 1837 (1960).
- J. O'M. Bockris, E. H. Crook, H. Bloom, and R. E. Richards, *Proc. Roy. Soc.*, **A255**, 558 (1960).
- R. Fürth, *Proc. Roy. Soc. Camb. Phil. Soc.*, **27**, 252 (1941).
- H. Bloom, B. S. Harrap, and E. Heymann, *Proc. Roy. Soc. London*, **A194**, 237 (1953).
- E. R. Van Artsdalen and I. S. Yaffe, *J. Am. Chem. Soc.*, **59**, 118 (1955).
- S. Glasstone, K. V. Laidler, and H. Eyring, "The Theory of Rate Processes," McGraw Hill Book Co., Inc., New York (1943).
- J. O'M. Bockris, J. A. Kitchener, S. Ignatowicz, and J. W. Tomlinson, *Trans. Faraday Soc.*, **48**, 75 (1952).
- R. W. Laity, *Ann. N. Y. Acad. Sci.*, **79**, 997 (1960).
- S. Djordjevic and G. J. Hills, *Trans. Faraday Soc.*, **56**, 269 (1960).
- G. J. Hills, Private communication.

# Electronic Commutator Method for Determining $E^\circ$ of Formation of Fused Halides

Anthony F. Wilde<sup>1</sup> and Ralph L. Seifert

Department of Chemistry, Indiana University, Bloomington, Indiana

## ABSTRACT

Previous experimental determinations of the  $E^\circ$  of formation of fused metal halides have depended largely on the equilibrium cell method rather than the simpler, but less precise, decomposition potential method. This report describes a modification of the latter method, the electronic commutator method, which provides some improvements. This technique, with its simple cell and electrodes, was used to evaluate  $E^\circ$  of formation for fused AgCl in the temperature range 500°-907°C in direct comparison with the equilibrium cell method. The results agree well with equilibrium cell values obtained both in this study and by other investigators.

Thermodynamic data for the formation of a fused, binary salt are most conveniently derived from electrochemical measurements if a reversible cell can be formed in which the voltaic cell reaction is the formation of the fused salt. In the past, most electrochemical determinations of this type have been made by the equilibrium cell method (1-6). The equilibrium cell containing the fused salt has an anode consisting of the reduced cation and a cathode containing the oxidized anion, which are usually the elements in their standard states. If the salt is a metal halide, the halogen is supplied from an external source and is bubbled over an inert, porous, electronic conductor as cathode. Practical problems arise in the construction and operation of such cells. A relatively large quantity of halogen is required to maintain unit activity at the cathode surface. The halogen may chemically attack the cell container and the metal electrode if considerable time is required for the saturation of the inert electrode material and attainment of cell equilibrium. At temperatures of interest the metal may be liquid or gas, introducing problems of handling and greater danger of chemical attack on the cell container. As a result, relatively few salts have been studied by this method, although a number of them have been studied by several different investigators. That this method, although simple in principle, presents difficulties in application is shown by the lack of agreement between many of these investigations [Fig. 1 and 2 in (7)].

In the decomposition potential method small inert electrodes are placed in the body of the fused salt, and the potential difference is determined at which electrolysis produces the reduced cation and oxidized anion. If all substances involved are present at unit activity during electrolysis, the potential drop through the cell equals  $E^\circ$  for the cell plus the  $IR$  drop within the cell and the overvoltage that may be present at one or both electrodes. The usual empirical method to correct for the  $IR$  drop

and overvoltage has been to extrapolate the potential required for decomposition to zero current (8) or to electrolyze the fused salt with pulsed current and measure the emf between pulses. The latter is the commutator method. Mechanical commutators have been used (9), but have not furnished a convenient way for following the emf decrease that occurs between pulses. This decrease is due to decay of electrode overvoltage and decrease in activity of electrolysis products at the electrodes by diffusion and possibly reaction with electrolyte. The emf may therefore drop from a value above  $E^\circ$  to a value below  $E^\circ$  if the time between pulses is long enough; and a single measurement at an arbitrary time or an average measurement gives only an approximate value for  $E^\circ$ . However, cell construction and maintenance are greatly simplified. Thus in the case of a metal halide, the small amounts of metal and halogen produced in the body of the melt reach the cell container only by diffusion. Liquid or vapor metal may be formed as easily as solid. If either electrode product has appreciable solubility in the fused salt, larger pulses are required to maintain unit activity at the electrode, but useful measurements can still be made. This investigation was therefore undertaken to develop an electronic commutator technique that both permits accurate measurement of the emf throughout its decay between electrolysis pulses and provides a means for evaluating  $E^\circ$  accurately in spite of the effects of electrode overvoltage and decrease in activity of electrolysis products.

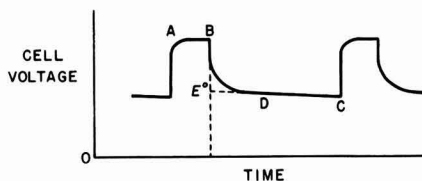


Fig. 1. Typical emf curve for a pulsed electrolysis cell. Dashed lines indicate extrapolation giving  $E^\circ$  by the electronic commutator method.

<sup>1</sup> Present address: Monsanto Research Corporation, Everett Station, Boston, Massachusetts.

Figure 1 shows the periodic behavior of cell potential when current in the form of square pulses is passed through a fused halide. During interval *AB* the cell emf is high because of the cell overvoltage produced by the applied current pulse, but the emf decreases between pulses, where the cell is functioning as a voltaic cell. The overvoltage continues to be present when current ceases, but it decreases rapidly as the cell adjusts to equilibrium conditions at the electrode surfaces. During and after this adjustment the cell emf also decreases due to diffusion of the halogen away from the cathode and possibly to interaction of the electrolyte with the halogen or metal at their respective electrodes. If the rate of decrease due to overvoltage decay is far greater than that due to diffusion and reaction, the experimental curve can be resolved into two component curves since the overvoltage drops to a negligible value at some point such as *D* in Fig. 1. If sufficient time remains before the succeeding pulse, the second component curve is well defined and can be extrapolated back to the end of the preceding pulse to give  $E^{\circ}$ , as shown in Fig. 1.

For measurements made with silver chloride the experimental curves could be resolved into a rapidly decaying exponential curve and a straight line. In this case, where silver crystals remained on the anode, the linear decay is consistent with the concept of loss of chlorine at the cathode by a net first order process. Thus if *a* is its activity at the cathode surface,

$$\frac{da}{d\tau} = -ka \quad \text{and} \quad \log_e a = \log_e a_0 - k\tau \quad [1]$$

where *k* is the constant for the process removing chlorine from the cathode,  $\tau$  is the time after the end of the current pulse, and  $a_0$  is the activity when  $\tau$  is zero. The value of *k* in the silver chloride experiments was found to have a minimum near 700°C. Therefore, although the net change in chlorine concentration in this case decreased in accordance with a first order rate law, at least two processes are involved in the change of *a* with time, e.g., diffusion of chlorine in the electrolyte and release of adsorbed chlorine from the electrode. Since silver accumulates on the anode it is always in its standard state. Therefore, substitution of the above in the Nernst equation for the emf of the cell gives

$$E = E^{\circ} + \frac{RT}{2F} \log_e a_0 - \frac{RT}{2F} k\tau \quad [2]$$

In the region following the decay of electrode overvoltages the cell emf in this case will decrease linearly with time. If each current pulse is sufficiently large to re-establish saturation of the inert cathode at 1 atm halogen pressure,  $a_0$  equals unity and extrapolation of the linearly decaying cell emf back to the end of the pulse ( $\tau = 0$ ) will give  $E^{\circ}$ .

### Apparatus

The electronic commutator for this investigation is similar in some respects to that used by Staicopoulos, Yeager, and Hovorka (10) to measure the overvoltage occurring when the current through an aqueous solution of electrolyte was in-

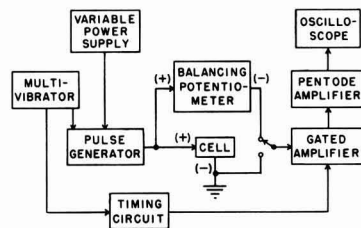


Fig. 2. Block diagram of electronic commutator and associated equipment.

terrupted at repetition rates of 1000 cps. Their circuit, however, will not provide sufficient time between pulses for the overvoltage to become negligible and the nature of the slowly decaying component to become well defined. Figure 2 shows a block diagram of the apparatus comprising the electronic commutator used in the present investigation.<sup>2</sup> The multivibrator output governs the frequency and duration of the square-wave current pulses supplied by the pulse generator to the cell. The duration of these square current pulses and the period between pulses could be varied in steps between 4 and 60 milliseconds (msec). The magnitude of the current pulses is controlled by the variable power supply. With the cell and the L&N K-2 balancing potentiometer connected in series, but with opposed polarities, the signal which reaches the gated amplifier is the difference between these two sources of emf.

The gated amplifier responds to the signal at its input only during a short interval when the amplifier is triggered by a gate signal from the timing circuit, which in turn derives its timing triggers from the multivibrator. The duration of the gate signal (gate width) and its time of arrival at the gated amplifier with respect to the end of the preceding cell current pulse (gate delay time) are determined by the settings of two univibrators in the timing circuit and are both measured by means of the oscilloscope. The gate delay time could be varied from 0 to 58 msec. The gate width used throughout this investigation was  $0.5 \pm 0.1$  msec. The output of the gated amplifier is further amplified and observed on the oscilloscope.

To determine the cell potential at a particular value of gate delay time, the balancing potentiometer is adjusted until the oscilloscope indicates that the net input signal to the gated amplifier is zero. At this point the cell emf equals that supplied by the balancing potentiometer. This circuit therefore sends current through the cell in the form of square pulses of adjustable amplitude, frequency, and duration, and provides means for measuring the resultant cell emf at any time between these pulses by means of a gated balancing circuit.

To make a direct comparison between the equilibrium cell method and the electronic commutator method, the 3-armed cell shown in Fig. 3 was constructed from quartz tubing for the simultaneous employment of both techniques, utilizing the same

<sup>2</sup> For a discussion in greater detail see "Electrochemical Study of Fused Salts," thesis by A. F. Wilde, Indiana University, Bloomington, Ind., June 1959; available as microfilm from University Microfilms, Ann Arbor, Michigan.



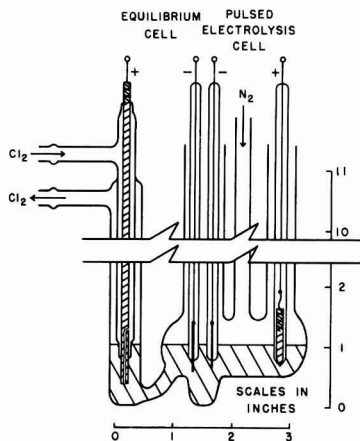


Fig. 3. Silver chloride cell and electrodes

fused silver chloride electrolyte. The positive electrode of the equilibrium cell was a 0.32 cm diameter graphite rod (National Carbon Company, grade AGR, maximum impurity 0.5%) with a hole drilled in from the bottom end and out the side. Chlorine, entering the upper side arm (Fig. 3), passed inside the electrode portion of the graphite and possibly diffused through it in addition to bubbling over the outside surface. Chlorine diffusion into the rest of the cell was reduced by the constriction between the two electrolyte chambers. Each of the negative electrodes was a short length of B&S 22 platinum wire, sealed in the end of a quartz tube. That for the equilibrium cell was electroplated with silver in a fused silver chloride bath. The positive electrode of the pulsed electrolysis cell consisted of a 2.5 cm length of 0.3 cm graphite rod (National Carbon Company, grade AGR), tapered at one end and encircled by a platinum wire lead at the other end. One end of a quartz tube was shrunk on to the entire length of the graphite and then ground down enough to expose about 1 mm<sup>2</sup> of the graphite tip. All of the electrodes were connected to platinum wire leads (B&S 28). To avoid introduction of thermal emf, the positive electrode of the equilibrium cell was connected in series with a 0.3 cm graphite rod placed in the furnace parallel to the first arm of the cell. An insulated platinum wire lead was connected to the rod at the level of the electrodes. A side arm leading to the right-hand chamber permitted sweeping out chlorine from the second and third arms of the cell with a stream of nitrogen. A thermocouple well dipped into the fused salt in the right-hand chamber. The thermocouple was calibrated at the melting points of zinc, aluminum, and copper samples furnished by the U.S. National Bureau of Standards. Throughout each series of measurements the cell temperatures remained constant within  $\pm 1^\circ\text{C}$ .

#### Procedure

Eighty-five grams of Fisher Certified Reagent silver chloride were fused in the cell, the open arms were loosely plugged with Pyrex wool around the removable electrodes, and nitrogen flow was started

before each run. Square current pulses of 40 and then 50 ma were put through the pulsed electrolysis cell. Results, both from preliminary work and with this cell, indicated that the emf at a given time in the linear region between pulses was practically independent of the magnitude of the current pulse above 30 ma, indicating that silver and chlorine were both being produced at unit activity. For both 40 and 50 ma, pulsed current was sent through the cell for about 10 min, after which the emf between current pulses was measured as a function of gate delay time. Reproducibility was frequently verified by repetition of the emf measurements after an additional pulsing period of approximately 10 min. For this work the current pulses were  $8.5 \pm 0.5$  msec in duration and were separated by periods of  $29.5 \pm 0.5$  msec, resulting in a frequency of 26.3 pulses per second. The cell emf was measured at each of eight values of gate delay time: 0.3, 0.6, 1.5, 3.0, and 8.8 msec (all  $\pm 0.1$  msec); and 14.7, 21.3, and 26.8 msec (all  $\pm 0.5$  msec). Noise and instability in the electronic circuits and in the cell limited the precision of the cell emf measurements to  $\pm 1$  mv.

Chlorine flow to the chlorine electrode was then started and the emf of the equilibrium cell was measured directly with the same K-2 potentiometer used for the above measurements. Constant emf was attained within a few minutes except at the higher temperatures where some unsteadiness was noted.

Since only one run was made each day due to slow attainment of the desired thermal equilibrium in the furnace, this series of runs lasted 19 days. The silver chloride was kept in the fused state this entire time to avoid danger of fracturing the quartz cell. The reproducibility of emf values over this period indicates that there was no detrimental reaction with the quartz cell.

#### Results and Discussion

With pulsed electrolysis at temperatures of 797°C and less, the cell emf obtained with current pulses of 40 ma agreed with those obtained with 50 ma to within 2 mv at gate delay times of 8.8 msec and greater. In a majority of cases this spread was

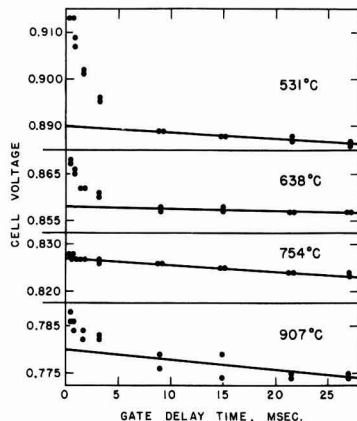


Fig. 4. Typical emf decay curves for pulsed electrolysis of fused silver chloride.

Table I.  $E^\circ$  values for fused salt cell: Ag/AgCl/Cl<sub>2</sub>

Cell temp, °C	Number of gate positions used for extrapolation	Maximum deviation from line, mv	$E^\circ$ by electronic commutator method		$E^\circ$ by equilibrium cell method, v
			Expt'l., v	Eq. (3), v	
562	4	1	0.882	0.882	0.879
531	4	½	0.890	0.891	0.888
500	3	1	0.900	0.900	0.897
583	3	1	0.874	0.876	0.873
638	4	½	0.858	0.860	0.858
699	4	½	0.839	0.842	0.841
754	4	1	0.827	0.827	0.827
797	4	1	0.814	0.814	0.811
846	4	1	0.802	0.800	0.796
907	4	2½	0.780	0.783	0.776
729	5	½	0.835	0.834	0.815
612	4	½	0.867	0.867	0.842

random. At higher temperatures the spread was greater, due principally to the greater instability of the cell with consequently poorer reproducibility of cell emf measurements. Figure 4 shows typical emf decay curves for the cell between current pulses of 40 ma. At each temperature two series of measurements were made at the same gate delay times and plotted as a function of gate delay time. Where the emf values were identical the points are plotted beside each other in Fig. 4, equidistant from the gate delay time. The linear emf decay was defined in each case by the last three to five gate positions. The best straight line through these points was extrapolated to zero gate delay time to obtain  $E^\circ$  for the cell. The resulting values of  $E^\circ$  are given in Table I along with the maximum deviation of any experimental value in the linear region from the line used to obtain  $E^\circ$ . The equilibrium cell emf values obtained practically simultaneously with the above are also tabulated in Table I. Values appear in chronological order.

The value of  $E^\circ$  obtained by the electronic commutator method is equal to or slightly higher than that for the equilibrium cell except in three cases. In one case it is 2 mv lower. In the remaining two cases the equilibrium cell values are obviously out of line. Since these occurred at the very end of the series of measurements and immediately after the runs performed at the highest temperatures, it is suspected that the discrepancies result from deterioration of the electrode(s) of the equilibrium cell. The corresponding emf values obtained by the electronic commutator method agree with earlier measurements.

The  $E^\circ$  values were linear with temperature, within the experimental error of the measurements.

The constants for the best straight line were calculated by the method of least squares, yielding the linear equation

$$E^\circ = 1.043 - 2.87 \times 10^{-4}t \quad [3]$$

where  $E^\circ$  is in volts and  $t$  is in °C. Agreement with the experimental values is indicated in Table I. This equation was used to calculate  $E^\circ$  values at temperatures permitting the comparison in Table II with corresponding values from other sources.

The values in Table II attributed to Senderoff and Mellors (5) were taken from their graph of  $E^\circ$  vs.  $t$ , based on equilibrium cell measurements. The values by Hamer, Malmberg, and Rubin (7) are computed from thermochemical data. The values obtained by the electronic commutator method are in best agreement with those obtained with an equilibrium cell by Panish, Newton, Grimes, and Blankenship (6). At the higher temperatures the emf values computed from thermochemical data become increasingly greater than those obtained electrochemically.

Based on the data obtained by the electronic commutator method, the standard free energy of formation,  $\Delta F^\circ$ , of liquid silver chloride at 1000°K is  $-19.24$  kcal mole<sup>-1</sup> and the corresponding values of  $\Delta H^\circ$  and  $\Delta S^\circ$  of formation are  $-25.85$  kcal mole<sup>-1</sup> and  $-6.62$  e.u., respectively. The corresponding values calculated from the recent compilation of thermochemical data by Kelley (11) are  $-20.37$  kcal mole<sup>-1</sup>,  $-25.49$  kcal mole<sup>-1</sup>, and  $-5.12$  e.u., respectively. Such variation between electrochemical and thermochemical data has been observed with a number of other salts, as pointed out by Hamer, Malmberg, and Rubin (7). The excellent agreement between the electrochemical values obtained by several investigators, and now by two different methods, indicates that for silver chloride the extrapolated thermochemical data must be in error.

Since the commutator method requires such simple cells, it may provide a means to study electrochemically many fused salts heretofore avoided because of the experimental difficulties involved. The accuracy of  $E^\circ$  values may in some cases be limited due to electrolytic side effects or other factors giving rise to nonlinearity in the second part of the emf decay curve. However, as the precision of measurement is increased this method can provide data that may help elucidate such effects as well as the relative effects on the decaying emf due to diffusion of electrolysis products in the fused salt and their release from the electrode. As supplementary information the method can also provide

Table II.  $E^\circ$  values for the fused salt cell: Ag/AgCl/Cl<sub>2</sub>

Source	Temperature in °C				
	500	600	700	800	900
Electronic commutator method of this investigation	0.900	0.871	0.842	0.813	0.785
Senderoff and Mellors (5)	0.893	0.867	0.841	0.815	0.789
Panish, Newton, Grimes, and Blankenship (6)	(0.8982)	0.8700	0.8419	0.8138	0.7859
Hamer, Malmberg, and Rubin (7)	0.896	0.870	(0.847)	0.826	(0.805)

Values in parentheses are interpolations from published values.

accurate overvoltage data which are related to the kinetics of the electrode processes.

Manuscript received Jan. 16, 1961. This research was supported in part by the Directorate of Chemical Sciences, Air Force Office of Scientific Research.

Any discussion of this paper will appear in a Discussion Section to be published in the June 1962 JOURNAL.

#### REFERENCES

1. V. Czepinski, *Z. anorg. u. allgem. Chem.*, **19**, 208 (1899).
2. R. Lorenz and H. Velde, *ibid.*, **183**, 81 (1929).
3. J. H. Hildebrand and E. J. Salstrom, *J. Am. Chem. Soc.*, **54**, 4257 (1932).
4. K. H. Stern, *J. Phys. Chem.*, **60**, 679 (1956).
5. S. Senderoff and G. W. Mellors, *Rev. Sci. Instr.*, **29**, 151 (1958).
6. M. B. Panish, R. F. Newton, W. R. Grimes, and F. F. Blankenship, *J. Phys. Chem.*, **62**, 1325 (1958); *ibid.*, **63**, 668 (1959).
7. W. J. Hamer, M. S. Malmberg, and B. Rubin, *This Journal*, **103**, 8 (1956).
8. R. C. Kirk and W. E. Bradt, *Trans. Electrochem. Soc.*, **70**, 239 (1936).
9. L. Cambi and G. Devoto, *Giorn. chim. ind. applicata*, **8**, 303 (1927); *Gazz. chim. ital.*, **57**, 836 (1927).
10. D. Staicopoulos, E. Yeager, and F. Hovorka, *This Journal*, **98**, 68 (1951).
11. K. K. Kelley, Bulletin 584, U. S. Bureau of Mines (1960) together with "Selected Values of Chemical Thermodynamic Properties," U. S. National Bureau of Standards Circular 500 (1952).

## Simultaneous Solution of Voltage and Mass Balances in Electrolytic Cells

Edward A. Grens, II, and Charles W. Tobias

*Lawrence Radiation Laboratory and*

*Department of Chemical Engineering, University of California, Berkeley, California*

#### ABSTRACT

A method for the prediction of performance of electrolytic cells by simultaneous solution of differential voltage and material balances is presented. The method is illustrated by the example of a simplified model based on the Krebs type amalgam caustic-chlorine cell. In this example numerical solutions are obtained for a variety of combinations of design and operating parameters by use of a digital computer. Average current density and current distribution are presented as functions of certain of these parameters. The method outlined should lead to the development of more accurate design and operating procedures.

Rational design and operation of electrolytic cells require the ability to predict the performance of the cell from a knowledge of parameters characterizing cell operation. These operating parameters are independent variables whose levels are established by the cell operator or fixed by cell environment. Frequently conditions of electrolysis vary from point to point within the cell due to the effect of electrode reactions on the properties of the electrolyte and on the electrodes themselves. In situations of this nature the performance of the cell is related to operating parameters by a group of interacting phenomena described mathematically by a set of simultaneous differential expressions, which in general are nonlinear. Usually no explicit relationships for variables describing cell performance in terms of cell operating parameters can be obtained.

For many electrolytic processes, theoretical or empirical relationships are available expressing various aspects of performance at some point in the cell in terms of the conditions existing at that point. These relations, together with a description of the effects of local performance throughout the cell on conditions existing at various points in the cell, permit over-all cell performance to be determined for any given values of the operating parameters.

All too frequently, because of the complexity of the calculational procedures involved, analyses of this sort have not been attempted even when suitable expressions for local functioning of the cell were available. With increasing amounts of basic data available, numerical techniques implemented by modern digital computing machinery often can be used to carry through the type of calculations outlined above with relative ease. Thus, decisions regarding the design and operation of electrolytic cells may, in many cases, be made on a more rational basis by use of this method than has been possible previously by the use of purely empirical techniques.

#### *Example*

*Description of model.*—To illustrate the application of this technique an idealized electrolytic cell based on a Krebs-type caustic-chlorine cell with flowing mercury cathode will be considered.

The model chosen for analysis at steady state is an electrolytic cell in the form of a trough, 1000 cm long and of unit width. The sides are nonconducting and of such a configuration as to give rise to no edge effects. The bottom of the trough is covered by a 0.5 cm thick layer of dilute sodium amalgam, the cathode, flowing from one end of the trough (the inlet end) to the other (the outlet

end). Above the amalgam, in a plane parallel to its surface, is a graphite anode which is considered continuous except for gaps which serve only to permit the escape of gas. An electrolyte brine (sodium chloride in water) flows cocurrent with the amalgam in the uniform space between the anode and the cathode. The brine is electrolyzed as it passes through the cell, the sodium dissolving in the amalgam cathode and the chlorine evolving at the anode, where it saturates the brine with dissolved  $\text{Cl}_2$ . This model is described in greater detail in ref. (1).

The following basic assumptions are incorporated in the definition of this model:

1. The amalgam flow is turbulent with complete cross mixing and a negligible diffusion boundary layer [see ref. (1), pg. 14].
2. The brine flow is turbulent with a diffusion boundary layer at the cathode [see Ref. (1), pg. 16].
3. The cell is isothermal at  $65^\circ\text{C}$ .
4. Evolved gas distribution is independent of flow rates.
5. No appreciable  $\text{ClO}_3^-$  is formed.
6. Current loss is 4% due to recombination of dissolved  $\text{Cl}_2$  with sodium amalgam at the cathode.<sup>1</sup>
7. There is no significant overvoltage for the primary cathode reaction.
8. Electrolyte pH is 4.
9. Current flow is independent of position in the direction normal to the electrode surfaces.

Although this model does not represent any actual cell, it incorporates certain salient features of industrial mercury cells.

In the model described, moving from the inlet end to the outlet end, the brine becomes depleted in sodium chloride and the amalgam becomes enriched in sodium. This causes current density to change with position in the direction of flow. Thus, although the model represents a cell of simple geometry, the variables describing cell performance cannot be given as explicit relations involving cell operating parameters. In this case the conditions at an electrode and in the brine vary with position in one dimension (the direction of flow) only.

In the analysis of this model the operating parameters are: (a) anode type; (b) applied cell potential; (c) brine flow rate; (d) amalgam velocity; (e) inlet concentration of NaCl in brine; (f) inlet concentration of Na in amalgam; and (g) distance between the electrodes. These variables may be established arbitrarily by the designer or operator of the cell.

The variables describing cell performance which are determined by the values of the operating parameters are: (a) current density (local and average); (b) concentration of NaCl in brine at any point; (c) concentration of Na in amalgam at any

point; (d) anode potential, cathode potential, and ohmic potential drop in brine (local and average.)

**Voltage balance.**—The total potential of the cell is composed of the anode potential ( $-E_A$ ), the cathode potential ( $E_C$ ) and the ohmic potential drop in the electrolyte ( $E_R$ ).

$$E_T = -E_A + E_R + E_C \quad [1]$$

Based on theoretical and empirical relationships described in the appendix to this article, values of these component potentials are expressed in terms of local conditions at any point along the length of the cell. Empirical data are represented in the form of second order power series expansions by regression analysis. Thus for anode potential:

$$\begin{aligned} -E_A &= -E_A^0 + \frac{RT}{F} \ln \frac{a_{\text{Cl}_2}}{a_z} + \omega \\ &= -\frac{RT}{F} \ln \frac{a_z}{a_{\text{NaCl}}} + \alpha + \beta I + \gamma I^2 \end{aligned} \quad [2]$$

for cathode potential

$$E_C = E_C^0 - \frac{RT}{F} \ln \frac{a_z}{a_{\text{NaHg}}} \quad [3]$$

and for the ohmic potential drop in the electrolyte

$$E_R = \frac{Id}{k_m} = \frac{Id}{k_c[\lambda + \mu (\ln I) + \xi (\ln I)^2]} \quad [4]$$

The activities are represented in terms of concentration as

$$a_z = 1.84 - 0.28 \ln m + 0.152 m^2 \quad [5]$$

[see ref. (1), App. I]

and

$$\ln a_{\text{NaHg}} = 1.26 \ln N - 1.31 \quad 0 \leq N \leq 0.25\% \quad [6]$$

[see ref. 1, App. II]

and the pure brine conductivity is related to concentration by

$$k_c = -0.093 + 0.161m - 0.0114m^2 \quad 4.5 \leq m \leq 6.43 \quad [7]$$

Combining Eq. [1], [2], [3], and [4], the voltage balance for the cell becomes (with values of  $a_{z(\text{NaCl})}$ )

$$\begin{aligned} \gamma I^2 + \left\{ \beta + \frac{d}{k_c[\lambda + \mu (\ln I) + \xi (\ln I)^2]} \right\} I \\ + 0.0537 + \alpha + E_C^0 - E_T + \frac{RT}{F} \ln \frac{a_{\text{NaHg}}}{a_z^2} = 0 \end{aligned} \quad [8]$$

For given concentrations of brine and amalgam, current density may thus be found.

**Material balances.**—In order to determine concentrations at any point in the cell consider an increment of length of cell  $\Delta x$  in the direction of brine and amalgam flow. If we take this as small enough so that current density changes but slightly over its length, then the changes in brine and amalgam concentration over  $\Delta x$  are:

$$-\Delta m = \frac{1000\eta I}{QF} \Delta x \quad [9]$$

$$\Delta N = \frac{100M_{\text{Na}}\eta I}{U\delta\rho_{\text{Na}}F} \Delta x \quad [10]$$

<sup>1</sup> In this case, the current efficiency is governed essentially by the character of the mass transfer boundary layer at the brine-amalgam interface. Thus in order to evaluate the dependence of current efficiency on the parameters involved, a more profound understanding of the hydrodynamics at liquid-liquid interfaces (with relative flow, potential gradient, and composition changes) would be required than has been reached to this time.

Given concentrations at the upstream end of such an increment of cell length, the corresponding concentrations at the downstream end can be computed.

*Numerical solution.*—By use of Eq. [5] through [10], the variables describing cell performance at all points of the cell can be determined for any desired operating condition as specified by the values of the operating parameters. This is accomplished numerically in the following manner:

1. Using given inlet concentrations (and other operating parameters) calculate  $I$  at  $x = 0$  by trial and error numerical solution of Eq. [8].
2. Assuming value of  $I$  calculated in step 1 or 4 to be valid over  $\Delta x$ , calculate changes in concentrations  $-\Delta m$  and  $\Delta N$  by Eq. [9] and [10].
3. Use increments of concentrations found in step 2 to calculate concentrations at downstream end of increment  $\Delta x$ .
4. Using concentrations calculated in step 3, find  $I$  at upstream end of next increment (by calculation similar to step 1).
5. Repeat step 2.

In this manner local cell performance is determined at intervals  $\Delta x$  along the length of the cell ( $\Delta x$  chosen sufficiently short). When the outlet end of the cell is reached, outlet concentrations are known, and average current density for the entire cell may be determined. Because of the extremely laborious nature of these calculations, they were conducted using a digital computer.<sup>3</sup>

In order to utilize calculations of this type to examine the effects of variations in the operating parameters upon cell performance, a base example, analogous for the model to normal operation in an industrial cell, was selected. The values used in this base example, although not necessarily representative of typical industrial practice, are of reasonable magnitude and certainly can serve to illustrate the calculational method. They are shown in Table I. Other examples were then chosen in order to investigate the effects of varying each of

<sup>3</sup> IBM 650.

the operating parameters individually. These examples are also listed in Table I. It should be noted that in each case the values of all the parameters except the one being investigated are maintained at the level used in the base example.

*Representation of cell performance.*—From these calculations, the effect of individual variations of the operating parameters on variables representing cell performance can be expressed graphically. Thus, in Fig. 1, 2, 3, and 4 the effects on average current density due, respectively, to changes in brine flow rate, initial NaCl concentration, initial sodium concentration in amalgam, and electrode spacing are shown.<sup>3</sup> In Fig. 5 the effect of initial sodium concentration in the amalgam upon current distribution is represented. It can be seen that, for this model, for example, brine flow rate and initial amalgam concentration have little effect on cell current. However, the current distribution is affected markedly by the initial amalgam concentration. The electrode spacing significantly affects cell current. The effect on cell current for each of the operating parameters may be evaluated similarly.

It should be noted that for this case the complete set of numerical results for any given operat-

<sup>3</sup> In industrial practice, cell potential for a given total cell current is frequently of more interest. These data can be obtained from the type of calculations outlined in this paper by adjusting applied cell potential, in each case considered, to give the desired cell current (or average current density). A computer program can be formulated easily to perform this operation automatically.

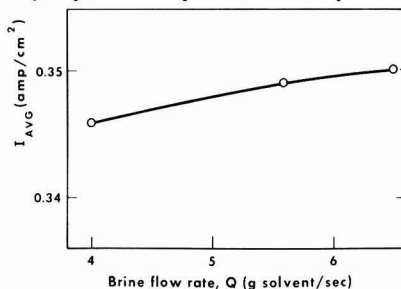


Fig. 1. Effect of brine flow rate on average current density. (All other operating parameters are at base example values.)

Table I. Values of operating parameters for examples considered

Example No.	Anode type	$E_T$ , v	$Q$ , g Hg/sec	$U$ , cm/sec	$m_0$ , molality	$N_0$ , wt %	$d$ , cm
1 (base example)	drilled	3.80	5.60	6.25	6.00	0.010	0.500
2	grooved	3.80	5.60	6.25	6.00	0.010	0.500
3	plane	3.80	5.60	6.25	6.00	0.010	0.500
4	drilled	3.40	5.60	6.25	6.00	0.010	0.500
5	drilled	3.60	5.60	6.25	6.00	0.010	0.500
6	drilled	4.00	5.60	6.25	6.00	0.010	0.500
7	drilled	4.10	5.60	6.25	6.00	0.010	0.500
8	drilled	3.80	4.00	6.25	6.00	0.010	0.500
9	drilled	3.80	6.50	6.25	6.00	0.010	0.500
10	drilled	3.80	5.60	4.00	6.00	0.010	0.500
11	drilled	3.80	5.60	10.00	6.00	0.010	0.500
12	drilled	3.80	5.60	6.25	5.00	0.010	0.500
13	drilled	3.80	5.60	6.25	6.40	0.010	0.500
14	drilled	3.80	5.60	6.25	6.00	0.005	0.500
15	drilled	3.80	5.60	6.25	6.00	0.020	0.500
16	drilled	3.80	5.60	6.25	6.00	0.050	0.500
17	drilled	3.80	5.60	6.25	6.00	0.010	1.00
18	drilled	3.80	5.60	6.25	6.00	0.010	3.00



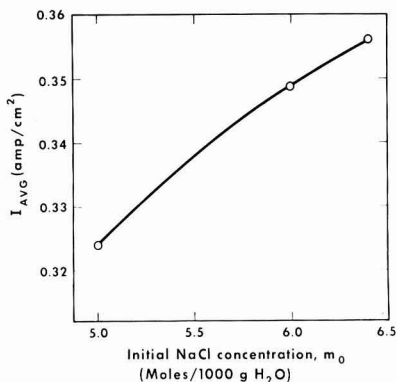


Fig. 2. Effect of inlet sodium chloride concentration in electrolyte on average current density. (All other operating parameters are at base example values.)

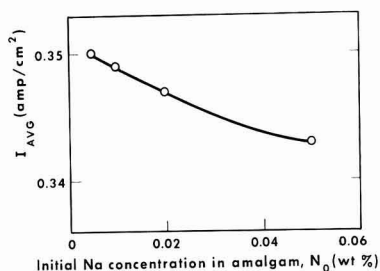


Fig. 3. Effect of inlet sodium concentration in amalgam on average current density. (All other operating parameters are at base example values.)

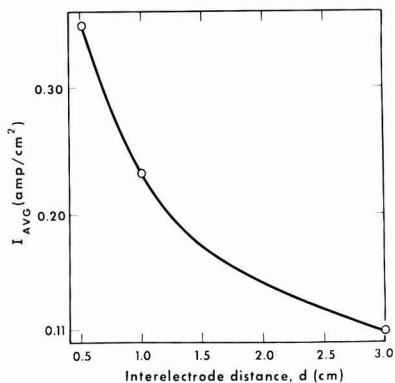


Fig. 4. Effect of distance between electrodes on average current density. (All other operating parameters are at base example values.)

ing condition can be obtained in a matter of seconds on high-speed digital computing machinery. More results for this model are given in Ref. (1).

### Conclusions

The example presented illustrates an elementary application of a rational approach to prediction of cell performance. In more complex situations, numerical solutions of much greater refinement may be required. In particular, simultaneous consideration of a differential heat balance, along with

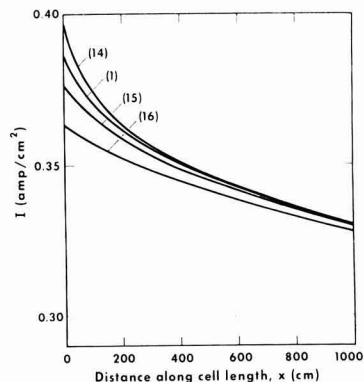


Fig. 5. Effect of inlet sodium concentration in amalgam on current distribution: (1) Base example ( $N_0 = 0.010$  wt %); (14)  $N_0 = 0.005$  wt %; (15)  $N_0 = 0.020$  wt %; (16)  $N_0 = 0.050$  wt %.

potential and material balances, usually will be necessary for realistic representation of actual cell operation. However, with high-speed computing machinery available numerical solutions usually will not present a serious problem. As long as theoretical or empirical relationships for the local, detail processes involved are available, this approach can yield valuable information. Of course, the accuracy of the results derived will be dependent on the closeness with which the expressions concerning local cell behavior represent the actual phenomena in question.

If industrial electrolytic cells are to be designed and operated efficiently, effective use must be made of available data and relationships concerning processes occurring within the cell. The approach described here utilizes these data to predict cell performance.

Manuscript received March 6, 1961; revised manuscript received June 30, 1961.

Any discussion of this paper will appear in a Discussion Section to be published in the June 1962 JOURNAL.

### REFERENCES

1. E. A. Grens, Analysis of Current Distribution in Electrolytic Cells with Flowing Mercury Cathodes, UCRL-9187, (AEC report) (1960).
2. C. W. Tobias, M. Eisenberg, and C. R. Wilke, *This Journal*, **99**, 359 (1952).
3. S. Okada, S. Yoshiyawa, F. Hine, and Z. Takehara, *J. Electrochem. Soc. Japan (O.E)*, **26**, [4-6], E 66 (1958).
4. S. Okada, So. Yoshiyawa, F. Hine, and Z. Takehara, *ibid.*, **26**, [4-6], E 66 (1958).

### APPENDIX

*Cathode potential.*—The cathode potential for the model concerned can be given in the assumed absence of overvoltages as:

$$E_c = E_c^\circ - \frac{RT}{F} \ln \frac{a_{z(wa11)}}{a_{NaHg(wa11)}} \quad (a)$$

where the activities are at the mercury surface. Since the amalgam is completely cross mixed we have

$$a_{NaHg(wa11)} = a_{NaHg} \quad (b)$$

and thus

$$E_c = E_c^\circ - \frac{RT}{F} \ln \frac{a_z}{a_{NaHg}} - \frac{RT}{F} \ln \frac{a_{z(wa11)}}{a_z} \quad (c)$$

where the last term on the right side constitutes the mass transfer polarization. The diffusion relationship governing this phenomenon is [as developed in ref. (2)]:

$$a_z - a_{z(w_{n1})} = \frac{Ib}{FD} (1 - t_+)$$

To investigate the significance of the term take typical values of  $I = 0.35$  amp/cm<sup>2</sup>,  $D = 4.3 \times 10^{-5}$  cm<sup>2</sup>/sec,  $t_+ = 0.5$ , and a value for  $b = 3.4 \times 10^{-3}$  cm, derived in ref. (1), p. 16 from consideration of the recombination reaction. Then

$$a_z - a_{z(w_{n1})} = 0.143$$

and at a typical activity of 5.6 this will cause a potential component of only

$$E = -\frac{RT}{F} \ln \frac{5.60 - 0.14}{5.60} = 0.00072 \text{ v}$$

which is considered negligible and is ignored in what follows.

Thus cathode potential can be represented as

$$E_c = E_c^\circ - \frac{RT}{F} \ln \frac{a_z}{a_{\text{NaHg}}}$$

**Anode potential.**—The anode potential cannot be represented in a simple theoretical relation such as that for the cathode potential. This is because of the appreciable overvoltages for chlorine evolution at graphite electrodes and the masking effect of the evolved chlorine on the surface area of the anode.

The overvoltage phenomena are not covered by any adequate theory. The magnitude of overvoltage varies with anode construction as well as current density. Therefore the empirical relations of Okada *et al.* for electrode potentials at horizontal graphite anodes with chlorine evolution are utilized (3, 4). These data apply to saturated pure sodium brine, and thus a correction must be made for brine concentration. Assuming polarization is an insensitive function of brine concentration

$$-E_A = -E_A^\circ + \frac{RT}{F} \ln \frac{a_{\text{Cl}}}{a_z} + \omega \quad (d)$$

and for saturated brine

$$-E_{A(\text{sat})} = -E_A^\circ + \frac{RT}{F} \ln \frac{a_{\text{Cl}}}{a_{z(\text{sat})}} + \omega \quad (e)$$

combining

$$-E_A = -E_{A(\text{sat})} - \frac{RT}{F} \ln \frac{a_z}{a_{z(\text{sat})}}$$

The term  $-E_{A(\text{sat})}$  is represented as a second order power series expansion in  $I$ , by means of regression analysis, from the data of Okada *et al.* for 65°C (or adjusted to that temperature) for plane anodes, drilled anodes, and grooved anodes [see Fig. 2, ref. (1)]. Thus

$$-E_{A(\text{sat})65^\circ\text{C}} = \alpha + \beta I + \gamma I^2 \quad 0.10 \leq I \leq 0.50 \quad (f)$$

where  $\alpha$ ,  $\beta$ , and  $\gamma$  are as given in Table I, Ref. (1), and we have for  $-E_A$

$$-E_A = -\frac{RT}{F} \ln \frac{a_z}{a_{z(\text{sat})}} + \alpha + \beta I + \gamma I^2$$

**Ohmic potential drop in electrolyte.**—The potential drop in the electrolyte between the anode and the cathode is determined not only by the conductivity of the electrolyte solution itself ( $k_m$ ) but also by the presence of nonconducting gas bubbles from the evolution of chlorine at the anode. The effective conductivity of

the electrolyte ( $k_m$ ) can be stated in terms of solution conductivity at the temperature and concentration in question, and a relative conductivity factor ( $K_m$ ) which accounts for the effect of the dispersed phase

$$k_m = K_m k_e \quad (g)$$

The distribution of gas bubbles cannot be predicted by any known theoretical means. It is a function of anode configuration and current density but, because of the uniformity of the flow channel, it is assumed not to be a function of brine velocity. In order to derive a quantitative expression for  $K_m$ , the empirical data of Okada *et al.* for relative resistivities of electrolytes in cells evolving chlorine at horizontal (downward-facing) graphite anodes in saturated sodium chloride brines are used (3, 4). It is assumed that relative resistivity is not affected by changes in brine concentration. Converting relative resistivity to relative conductivity and scaling data to 65°C, the relative conductivity is represented by regression analysis as a second order power series expansion in  $\ln I$  for the three types of anodes previously mentioned:

$$K_m = \lambda + \mu (\ln I) + \xi (\ln I)^2$$

where  $\lambda$ ,  $\mu$ , and  $\xi$  are as given in Table II, ref. (1).

Then

$$E_R = \frac{Id}{k_m} = \frac{Id}{K_m k_e} = \frac{Id}{k_e [\lambda + \mu (\ln I) + \xi (\ln I)^2]} \quad (h)$$

## NOMENCLATURE

### English Letters

- a*, Activity (refers to bulk of solution unless otherwise indicated)
- b*, Thickness of cathode diffusion layer, cm
- D*, Diffusion coefficient, cm<sup>2</sup>/sec
- d*, Distance between electrodes, cm
- $-E_A$ , Anode potential, v
- $E_c^\circ$ , Cathode potential, v
- $E_R$ , Ohmic potential drop in electrolyte, v
- $E_T$ , Total applied cell potential, v
- F*, Faraday constant
- I*, Current density, amp/cm<sup>2</sup>
- K*, Relative conductivity
- k*, Conductivity, ohm<sup>-1</sup>cm<sup>-1</sup>
- M*, Molecular weight
- m*, NaCl concentration in brine, mole/1000 g H<sub>2</sub>O
- N*, Na concentration in amalgam, wt %
- Q*, Brine flow rate, g H<sub>2</sub>O/sec
- R*, Gas constant
- T*, Temperature, °C or °K
- t*<sub>+</sub>, Transference number of positive ion
- U*, Velocity of flowing mercury cathode, cm/sec
- x*, Distance along length of cell from inlet, cm

### Greek Letters

- $\alpha$ ,  $\beta$ ,  $\gamma$ ,  $\lambda$ ,  $\mu$ ,  $\xi$ , regression constants
- $\delta$ , Mercury layer thickness, cm
- $\eta$ , Current efficiency
- $\rho_{\text{Hg}}$ , Density of amalgam, g/cm<sup>3</sup>
- $\omega$ , Total electrode overvoltage, v

### Subscripts

- avg, Average over cell
- Cl, Pertaining to chlorine
- e*, Pure electrolyte
- m*, Electrolyte with entrained gas
- o*, Conditions at inlet end of cell
- NaHg, Pertaining to sodium in amalgam
- sat, Saturated
- wall, Pertaining to conditions at electrode surface
- $\pm$ , Mean ionic value

### Superscripts

- o*, Standard electrode potential



## Rhenium-Tungsten-Carbon Interactions

R. F. Havell and Y. Baskin

Armour Research Foundation of Illinois Institute of Technology, Chicago, Illinois

Graphite nozzles coated with plasma-sprayed tungsten were examined as part of a program on analysis of failure mechanisms of rocket materials. One of the nozzles had a thin (0.005-in.) layer of metallic rhenium between the tungsten and graphite. The purpose of the layer was to prevent formation of tungsten carbides and/or eutectics in the W-C system which, because of their lower melting points (2475°-2730°C), would reduce the usefulness of the tungsten coating. Rhenium was chosen because of its refractoriness and the fact that it is not known to form any high-temperature stable carbides. Interactions between rhenium and carbon are limited to absorption of about 1% carbon in the rhenium lattice producing slight changes in the lattice constants and a reduction of the c/a ratio from 1.615 to 1.600 (1). Rhenium and tungsten form a sigma phase (Re<sub>3</sub>W<sub>2</sub>) below the peritectoid temperature of 3000°C which is stable between 43.5 to 66 w/o rhenium. Solubility of rhenium in tungsten ranges from 28 w/o at 1600°C to 37 w/o at 3000°C; tungsten solubility in rhenium varies from 11 w/o at 1600°C to 20 w/o at 2800°C. One eutectic (74 w/o Re) melts at 2825°C (2).

Examination of the fired nozzle disclosed that melting had occurred at the rhenium-graphite interface in the diverging section of the nozzle. X-ray analysis of the melted material revealed that it has a close-packed hexagonal structure with lattice constants intermediate between rhenium and W<sub>2</sub>C; spectrographic analysis showed the presence of both tungsten and rhenium. Since the temperature attained by the nozzle surfaces was not known with any accuracy, the question of whether rhenium had beneficial or deleterious effects could not be answered unequivocally.

The present study was undertaken to determine the high-temperature behavior of rhenium in the presence of tungsten and carbon. Rhenium powder in amounts ranging from 18.2 to 82.4 mole % was mixed with tungsten and carbon powders (tungsten to carbon molecular ratio of 1:1) and pressed into small pellets. The specimens were placed on graphite boats and fired in a graphite resistance furnace under argon atmosphere. The quasi-binary system Re-W<sub>2</sub>C was not investigated at this time because contact of such samples with the graphite boat would

result in absorption of additional carbon, thus shifting the compositions toward those of the Re-WC systems.

All compositions between 46.2 and 75.0% rhenium had fused into shiny balls at 2310° ± 20°C, considerably below the melting point of WC (2600°C) or rhenium (3180°C). Specimen 7 did not melt, retaining the dull appearance characteristic of WC. Although specimen 1 did not fuse, it showed much localized melting.

The results of x-ray diffraction analysis are given in Table I and show a single solid solution phase down to a composition of about 67 mole % rhenium. Patterns for WC and an unknown phase or phases make their appearance in compositions containing less than 67 mole % of rhenium. Thus it appears that rhenium absorbs considerable amounts of tungsten and carbon with a concomitant sharp

Table I. Summary of x-ray analysis

Specimen No.	Starting composition, mole %		Phases present
	Re	WC	
1	82.4	17.6	(Re, WC)ss
2	75.0	25.0	(Re, WC)ss
3	66.7	33.3	(Re, WC)ss*
4	62.2	37.8	(Re, WC)ss* + WC + unknown phase(s)
5	57.2	42.8	(Re, WC)ss* + WC + unknown phase(s)
6	46.2	53.8	WC + unknown phase(s)
7	18.2	81.8	WC + unknown phase(s)

\* Solubility limit of (Re, WC) solid solution.

Table II. Lattice constants of Re-W-C solid solutions

Specimen composition, mole %	Lattice constants			
	Re	WC	a, a.u.	c/a
100	0		2.760*	4.458*
82.4	17.6		2.830	4.512
75.0	25.0		2.852	4.532
66.7	33.3		2.877	4.561
62.2	37.8		2.882	4.564
				1.615
				1.594
				1.589
				1.585
				1.584

\* Swanson and Fuyat, NBS Circular 539, Vol. II, p. 13.

Table III. X-ray powder data

A. Re solid solution saturated with WC			
d, a.u.		I/I <sub>1</sub>	hkl
2.484		27	100
2.272		30	002
2.183	100	101	101
1.678		22	102
1.437		27	110
1.295		36	103
1.247		3	200
1.215		28	112
1.200		16	201
1.137		3	004
1.092		7	202
1.035		5	104
0.962			203
0.941			210
0.927			211
0.893			114
0.870			212
0.856			105
0.840			204
0.830			300
0.800			123
0.780			302

B. Extraneous unknown phase (s)							
Specimen 4		Specimen 5		Specimen 6		Specimen 7	
d	I	d	I	d	I	d	I
2.15	W	2.15	W	2.28	M	2.26	S
2.05	VW	2.05	VW	2.19	S	2.20	VVW
1.95	VW	1.82	VW	1.58	W	2.15	M
		1.36	VW	1.36	VW	2.12	VVW
		1.27	VVW	1.30	VVW	2.05	VVW
						1.82	VVW
						1.60	VVW
						1.53	VVW
						1.36	W
						1.26	M

reduction in melting point. In fact, the melting point is lower than those of any of the compounds or eutectics in the tungsten-carbon system, the formation of which the rhenium coating was designed to prevent.

The variation of lattice constants with tungsten carbide content is shown in Table II. The compositions given are the starting ones; however, the very slight weight losses that occurred on firing suggest that compositional changes occurring as a result of firing would be minor. The slight decrease of the c/a ratio with rising tungsten carbide content might be attributed to distortion of the close-packed hexagonal structure as a result of the presence of carbon atoms in the interstitial positions. The solubility limit at 2310°C of the rhenium-WC solid solution appears to be at approximately 33 mole % WC. X-ray pattern intensity values for this composition (specimen No. 4) tabulated in Table III, were measured as peak areas above background in a diffractometer chart. The lattice constants and d-values shown in Table II and III were obtained by measuring additional patterns made on photographic film in 114.59 mm cameras.

#### Acknowledgment

This study was supported in part by the Materials Laboratory at Wright Air Development Division, Wright-Patterson Air Force Base, Ohio.

Manuscript received March 1, 1961; revised manuscript received Aug. 11, 1961.

Any discussion of this paper will appear in a Discussion Section to be published in the June 1962 JOURNAL.

#### REFERENCES

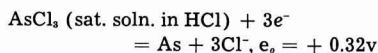
1. W. Trzebiatowski, *Z. anorg. Chem.*, **233**, 376 (1937).
2. J. M. Dickinson and L. S. Richardson, *Trans. A.S.M.*, **51**, 758 (1959).

## On the Electrodeposition of Arsenic and Its Role in Corrosion Prevention

Gösta Wranglén

*Division of Applied Electrochemistry and Corrosion, Royal Institute of Technology, Stockholm, Sweden*

Arsenic can be deposited electrolytically according to the reactions



and



From the electrode potentials, calculated from thermodynamic data, it follows that arsenic is considerably (0.15 – 0.32 v) more noble than hydrogen. A good current efficiency in the deposition would therefore be expected.

A series of electrolysis experiments were carried out by the author with both the electrolytes referred to above, at temperatures of 20°, 50°, and 60°C and current densities of 0.5 – 5 amp/dm<sup>2</sup>, using various cathode materials and cells both with and without a

diaphragm. It was found that in short experiments, lasting one day, the current efficiency was around 50%. In longer experiments, lasting up to a week, the current efficiency was just about 10%. The current efficiency appeared to fall steadily, and finally only hydrogen seemed to be evolved at the cathode. If the current was kept constant, the cell voltage increased continuously, e.g., from 2 to 20 v. Furthermore it was found that metallic impurities in the raw material, arsenic trioxide, were actually enriched in the cathode product. The arsenic obtained usually consisted of dark-gray flakes which adhered very badly to the cathode. In the hydrochloric acid bath, however, coherent, light-gray deposits of good metallic appearance were obtained.

The explanation of these somewhat puzzling features was found when the physical properties of the

deposited arsenic were investigated. The cathode product, even from the hydrochloric acid bath, was found to be amorphous, as revealed by x-rays, and practically a nonconductor. This clearly explains the increasing cell voltage and the decreasing current efficiency in the course of experiments.

The very low conductivity of electrodeposited arsenic does not seem to have been observed earlier. In particular, it has been overlooked in investigations of the overvoltage in the electrodeposition of arsenic. Very high values, obtained by the direct method, have been reported, reaching 1.2 v at as low a c.d. as 2 ma/cm<sup>2</sup> (1,2). The measurement of polarization in the deposition of a virtually nonconducting matter is obviously not possible by the direct method, since the measured potential differences will then contain a large ohmic drop, increasing with time and c.d. The same thing applies to hydrogen overvoltage, if it is measured on an electrodeposited arsenic surface. This explains why Grube (3), using the direct method, obtained much higher values than Salzberg and Goldschmidt, using a current interrupter technique in a recent investigation (4) of the overvoltage of hydrogen and arsine evolution on electrodeposited arsenic. The unusual physical properties of electrodeposited arsenic may also explain the "dishearteningly irreproducible" results, referred to by the latter authors. Probably, electrolysis occurred mainly at the bottom of pores in the arsenic layer, the underlying cathode support being brass, silver, or lead. Since the porosity must have changed from cathode to cathode, erratic results seem natural. The real current density in the pores was obviously very high. This seems to explain why the authors found evidence of concentration polarization and a limiting current density of hydrogen ion discharge at a very low apparent c.d.

It is also evident that the physical nature of electrodeposited arsenic renders its electrowinning or electrorefining from aqueous solutions impossible.

The fact that electrodeposited arsenic is practically an insulator seems to explain the use of arsenic and arsenic compounds in corrosion prevention. Hence, it has long been known that compounds of trivalent arsenic act as inhibitors of the corrosion of steel in acids (5). Evidently, elementary arsenic will be electrodeposited at cathodic sites and, having a very low conductivity, will prevent corrosion.

The well-known inhibiting effect of small amounts of arsenic on the dezincification of  $\alpha$ -brass might be explained in a similar way if it is assumed that arsenic, initially dissolved, is subsequently redeposited in a nonconducting form, preventing the further flow of corrosion currents. Theories in terms of high or low hydrogen overvoltage of arsenic (6) seem difficult to accept.

#### Acknowledgment

Thanks are due to the Boliden Mining Company, Sweden, for permission to publish these results.

Manuscript received June 14, 1961.

Any discussion of this paper will appear in a Discussion Section to be published in the June 1962 JOURNAL.

#### REFERENCES

1. W. Schopper, in Engelhardt, *Handb. der techn. Elektrochemie*, Vol. I, 1st Part, p. 492.
2. R. Piontelli and G. Poli, *Gazz. chim. Ital.*, **79**, 214 (1949).
3. G. Grube, *Z. Elektroch.*, **30**, 517 (1924).
4. H. W. Salzberg and B. Goldschmidt, *This Journal*, **107**, 348 (1960).
5. U. Bertocci, *Metallurgia Ital.*, **46**, (1954), Suppl. to No. 5, p. 64.
6. P. Lombardi, *ibid.*, **46**, 91 (1954).

## A Method for the Deposition of SiO<sub>2</sub> at Low Temperatures

J. Klerer<sup>1</sup>

*Semiconductor and Materials Division, Radio Corporation of America, Somerville, New Jersey*

One possible means of protecting a semiconductor surface is to deposit an insulating inorganic coating, such as an oxide, on it. If a thick film could be used, the influence of ambient atmospheres on the substrate would be eliminated or attenuated simply because of their separation from the semiconductor-oxide interface.

Although organic polymeric resins serve the function of separating the surface from the atmosphere, they generally absorb water, and eventual migration of the water to the surface leads to deleterious effects. Other ambient gases probably also diffuse through resin coatings at rates which are orders of magnitude above their diffusion rates through inorganic coatings.

The deposition of inorganic coatings on devices

containing low-melting constituents requires that the substrate temperature not exceed 150°C for alloyed p-n-p germanium devices and 300°C for n-p-n or diffused structure devices. Evaporation or sputtering of oxides onto a device is possible, but generally requires the use of vacuum systems and high source temperatures.

One possible solution to the problem is the thermal decomposition of organo-oxy-metallic compound of the formula (RO)<sub>x</sub>M<sub>y</sub>, where R denotes the organic radical and M the central metal atom (1). Because the cracking temperature is usually higher than the limitation set for coating devices, the compound can be decomposed in a furnace at high temperature and the resultant oxide and gaseous organic radicals forced out through a jet. The sample to be coated can be placed at a suitable distance so that the jet stream impinging on it has reduced in temperature.

<sup>1</sup> Present address: Bell Telephone Laboratories, Incorporated, Murray Hill, New Jersey.



Table I. Silanes investigated

Name of silane	Optimum temperature, °C	Decomposition temperature, °C
Ethyl-triethoxy-silane	700	650-750
Vinyl-triethoxy-silane	650	600-700
Phenyl-triethoxy-silane	730	610-750
Amyl-triethoxy-silane	650	600-740
Diphenyl-diethoxy-silane	No coatings	
Dimethyl-diethoxy-silane	800	760-900
Tetraethoxy-silane	740	728-840

Accordingly, an investigation into the deposition of SiO<sub>2</sub> by decomposition of its organic compounds was initiated and a successful method was defined.

### Experimental

An organo-oxy-silane, namely ethyl-triethoxy-silane, was placed in a gas bubbler, and dry oxygen-free Ar or N<sub>2</sub> was passed through to function as a carrier gas. The gas stream then entered a furnace, previously purged of oxygen and preheated to the desired temperature, and emerged through a jet opening approximately 5-7 mm in diameter. The exit temperature was calibrated by use of a thermocouple located about 2 mm from the jet exit (approximately at the position where the samples would be placed). Variation of the gas flow and/or furnace temperature made it possible to obtain suitable exit gas temperatures in the range from 150° to 250°C. Table I lists the various silanes investigated together with their optimum temperature of deposition. The temperature ranges shown in the table indicate the temperatures at which coating of SiO<sub>2</sub> actually occurred.

Ethyl-triethoxy-silane was chosen as the test material because it produced the best coating and could be deposited on alloyed p-n-p germanium devices without harming them. Coatings up to and greater than 20,000Å could be obtained easily; cracking and spalling of the film from the substrate occurred above 20,000Å because of the thickness of the film and the mismatch of thermal coefficients of expansion between the film and the substrate.

For identification of the films, infrared spectra of films deposited on silicon and germanium were taken. In addition, the refractive index of the films was measured (2). These data were then compared with similar data for oxides produced by heating silicon in O<sub>2</sub> at elevated temperatures, as shown in Table II.

The data shown in Table II indicate that an amorphous SiO<sub>2</sub> film is formed by the process reported.

Continuity and uniformity of the films were checked by measurement of dielectric strength. The film was deposited on a germanium wafer, a voltage

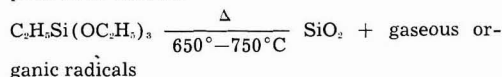
Table II. Comparison of data

	SiO <sub>2</sub> produced by thermal decomposition of ethyl-triethoxy-silane on silicon	Thermally grown SiO <sub>2</sub> on silicon
Infrared absorption maxima, $\mu$	9.3 Very strong 12.3 Medium	9.3 Very strong 12.4 Medium
Refractive index	1.430	1.450

was applied to mercury pool contacts placed on both sides of the wafer, and the breakthrough voltage was observed. Dielectric strengths from 10<sup>6</sup> to 10<sup>7</sup> v/cm were obtained. Reproducible values of 5x10<sup>6</sup> v/cm were obtained for films which had been baked at 125°C for a minimum of 15 min (for example, a 2000Å coating could sustain a voltage of 300 v). These values are of the same order of magnitude as the dielectric strength of amorphous silica. The film has also been successfully deposited on other materials, such as stainless steel, tantalum, and quartz.

### Discussion

The general reaction for the process can be expressed as follows:



At temperatures below 650°C, the coating is spotty in appearance and "oily" to the touch; a polymerized silane possibly was obtained. Above 750°C, white particles of SiO<sub>2</sub> appear which are nonadherent to any surface. This result suggests that, at the point where good continuous coatings are obtained, the silicon is in a radical form in which it can link with others of its kind to form the desired film. The determination of this radical form and the detailed mechanism for the reaction are now under study.

This coating has many possible uses, particularly in the semiconductor industry. Some of these uses include (a) surface protection for semiconductor devices; (b) alloying mask; (c) means to restrict spreading during alloying; (d) thin-film dielectric for use in the construction of capacitors or voltage-variable devices.

Manuscript received June 12, 1961.

Any discussion of this paper will appear in a Discussion Section to be published in the June 1962 JOURNAL.

### REFERENCES

1. E. Jordan, Paper presented at Chicago Meeting of the Society, May 1960.
2. R. Archer, Private communication.

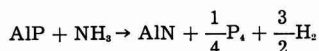
# On the Preparation of the Nitrides of Aluminum and Gallium

Arrigo Addamiano

Lamp Research Laboratory, General Electric Company, Nela Park, Cleveland, Ohio

The nitrides of aluminum and gallium have been the object of recent investigations dealing with their electrical, optical, and other properties (1-6). Some simple methods of preparation of these compounds are described here.

**Aluminum nitride.**—If a fine powder of aluminum phosphide is fired for 1-2 hr at 1000°-1100°C in a slow stream of dry ammonia phosphorus evolves which condenses downstream and the theoretical weight of aluminum nitride is obtained:



The white to light gray powder so prepared is not, however, well crystallized and only after overnight firing at 1100° gives sharp x-ray diffraction patterns and shows the stability<sup>1</sup> and properties already reported in the literature (4-6) for AlN. X-ray powder photographs taken at room temperature (22°C) with a camera of 14.32 cm diameter and nickel filtered copper radiation gave lattice constants in excellent agreement with those reported by Ott (8). High-temperature powder photographs taken with a 19 cm diameter Unicam camera did not show the occurrence of any phase transformation up to 1170°C. Only extremely small shifts of the lines were observed to occur over the whole range of temperatures investigated. Thus the reported good resistance of AlN to thermal shock (5, 6) is paralleled by the absence of phase transformations and by a low thermal expansion of the lattice of the nitride.

**Gallium nitride.**—Gallium nitride was obtained by firing a fine powder of GaP or GaAs<sup>2</sup> in a stream of dry ammonia. When GaP is used phosphorus vapors begin to evolve at 900°C. Quantitative conversion to GaN occurs in about 2 hr at 1000°-1100°. GaAs and NH<sub>3</sub> begin to react at 700° and quantitative formation of GaN takes place in 1-2 hr at 1000°. Because of the reported thermal instability of GaN (9), which we confirm, the products of the reactions were always cooled in an NH<sub>3</sub> atmosphere. Depending on starting material and thermal treatment the GaN obtained showed a color variation from white through pale yellow. White samples were obtained more easily from GaAs, while using GaP as starting material resulted generally in products with yellow tinges. The products were always highly crystalline materials and gave sharp x-ray patterns which contained high-angle diffraction maxima (2133; 0006;

2025; 1016) not previously observed. The calculated lattice constants were found to be in agreement with the values of Juza and Hahn (10) after correction of the wavelength of the CuK<sub>α</sub> radiation from 1.539 to 1.5405Å.

**Reciprocal solubility.**—In view of the similarities in crystal structure and lattice dimensions, AlN and GaN can be expected to be mutually soluble. However attempts at preparing (Ga,Al)N mixed crystals by heat treatment of mixtures of AlN and GaN powders in sealed quartz containers were unsuccessful. Treatments at 900° for one week in nitrogen atmospheres showed no solid solution formation, and attempts at a higher temperature treatment, 1100°, resulted in detonations due to high GaN dissociation pressures.

Similarly no mixed crystals Al(P,N), Ga(P,N), or Ga(As,N) were observed to form in the course of the preparations. This result is not surprising in view of the large differences in the values of the tetrahedral radii (11) of N(0.70Å) as compared with P(1.10Å) and As(1.18Å).

## Acknowledgments

The author is grateful to Miss J. R. Cooper, of this laboratory, and to Mr. J. Rabatin (General Electric Company, Chemical Products Plant, Cleveland, Ohio) for help in the collection of the x-ray data. He wishes to thank Dr. J. S. Saby and his colleagues for helpful discussions and for their interest in this research.

Manuscript received May 24, 1961; revised manuscript received July 17, 1961.

Any discussion of this paper will appear in a Discussion Section to be published in the June 1962 JOURNAL.

## REFERENCES

1. G. A. Wolff, I. Adams, and J. W. Mellichamp, *Phys. Rev.*, **114**, 1262 (1959).
2. H. G. Grimmeiss, R. Groth, and J. Maak, *Z. Naturforsch.*, **15a**, 799 (1960).
3. H. G. Grimmeiss and H. Koelman, *ibid.*, **14a**, 264 (1959).
4. Th. Renner, *Z. anorg. u. allgem. Chem.*, **298**, 22 (1959).
5. G. Long and L. M. Foster, *J. Am. Ceramic Soc.*, **42**, 53 (1959).
6. K. M. Taylor and C. Lenie, *This Journal*, **107**, 308 (1960).
7. E. F. Apple, Private communication.
8. H. Ott, *Z. Physik*, **22**, 201 (1924).
9. R. Juza and H. Hahn, *Z. anorg. u. allgem. Chem.*, **244**, 133 (1940).
10. R. Juza and H. Hahn, *ibid.*, **239**, 282 (1938).
11. L. Pauling, "The Nature of the Chemical Bond," 2nd ed., p. 179, Cornell University Press, Ithaca, N. Y. (1945).

<sup>1</sup> AlN prepared by thermal decomposition of Al(CH<sub>3</sub>)<sub>3</sub>·NH<sub>3</sub> at 200°-300° is very unstable and hydrolyzes rapidly in humid air giving off ammonia (7).

<sup>2</sup> The author wishes to thank Dr. F. H. Horn, General Electric Co., Schenectady, N. Y., for supplying a sample of GaP and Dr. H. T. Minden, General Electric Co., Syracuse, N. Y., for a sample of GaAs.



## The DSK System of Fuel Cell Electrodes

Eduard W. Justi and August W. Winsel

*Institute of Technical Physics, Braunschweig Institute of Technology, Braunschweig, Germany*

### ABSTRACT

Double skeleton catalyst (DSK) electrodes combine the high catalytic activity of Raney powder catalysts with the mechanical rigidity and electrical conductivity of bulk metals. They consist of a supporting macroskeleton pressed and sintered of metal grains of uniform size and Raney catalyst grains embedded in its pores. The authors have prepared more than 3000 different samples and investigated the following parameters: composition and particle size of both catalyst and macroskeleton, blending ratio of these two components, mixing process, pressing and sintering conditions, and a special potentiostatic process to leach the inactive component (Al or Zn) by KOH. This "controlled activation" provides extremely high activity and uniform pore sizes, avoiding too narrow and too large pores. Such "homeoporous" electrodes offer some  $10^{-2}$  pores with three phase boundaries, each contributing several microamperes to the total current density. Detailed recipes are given for the production of hydrogen DSK electrodes containing Raney Ni catalyst in a Ni macroskeleton and generating up to  $750 \text{ ma/cm}^2$  at 40 mv polarization at  $85^\circ\text{C}$ . Oxygen DSK electrodes contain a new brittle Ag Raney alloy in a supporting Ni macroskeleton. The open-cell polarization  $\phi-U_0$  at  $85^\circ\text{C}$  is 100 mv only and the maximum current density about  $500 \text{ ma/cm}^2$ . Such electrodes with fine pore coating layers are absolutely gas tight and show nearly 100% Faraday efficiency. Although the oxygen DSK electrodes contain but  $0.05 \text{ g Ag/cm}^2$  they reach the ideal process  $\text{H}_2 + \frac{1}{2} \text{O}_2 = \text{H}_2\text{O}$  delivering 4 electrons per  $\text{O}_2$  molecule instead of the Berl process with 2 electrons. A battery with such electrodes fed with impure  $\text{H}_2$  and  $\text{O}_2$  in uninterrupted service one year showed no deterioration. Therefore the lifetime of DSK cells is estimated to be at least  $10^3$ , perhaps some  $10^4$  amp-hr/cm<sup>2</sup>. Different types of DSK electrodes such as economy electrodes used for the dissolved fuel cell, and valve electrodes for the electrochemical storage of energy are described. They also act as electrolytic compressors without moving parts and can control catalytic reactions automatically. DSK electrodes may be used for light storage batteries. Mo- and W-DSK electrodes offer the possibility of the electrochemical oxidation of CO. DSK electrodes belong to the most promising systems disclosed hitherto and are capable of further improvement.

This meeting of The Electrochemical Society<sup>1</sup> with its many positive contributions on fuel cells is a delightful symptom of the optimism in this country concerning reversible generation of electric power. But 18 years ago when we started fuel cell research in Germany, most people were very pessimistic and disappointed after the failure of the originators of the fuel cell idea, Wilhelm Ostwald and Walther Nernst, to construct such cells. In fact it was very difficult to find a sponsor, and the only source of our optimism was the fact that all human and animal beings use direct energy conversion by electrochemical hydrogen-oxygen recombination at ambient temperature and pressure. Of course, it was not possible to imitate the very intricate coupled equilibrium and nonequilibrium reactions in living cells,

their highly effective organic catalysts, and their admirable submicroscopical structure.

We concluded that, in principle, it is possible to construct an indirect fuel cell fed by  $\text{H}_2$  and  $\text{O}_2$  at ambient temperature and pressure. In Table I are summarized ten requirements for the development of  $\text{H}_2$  and  $\text{O}_2$  diffusion electrodes as parts of a successful electrical power source.

It will be seen later that  $\text{H}_2$  and  $\text{O}_2$  electrodes satisfying these severe conditions offer further important technical possibilities:

11. High reversibility of power generation offers a high efficiency of the reverse process, *i.e.*, the electrolytic decomposition of  $\text{H}_2\text{O}$ .

12. Gas diffusion electrodes which combine fuel cell and electrolysis functions economically offer the possibility of storing energy electrochemically.

<sup>1</sup> Indianapolis Meeting, April 30-May 3, 1961.

Table I. Ten requirements for successful  $H_2$ - $O_2$  electrodes

1. Operating temperature	under 100°C
2. Operating pressure	under 4 atm
3. Insensitivity to impurities in commercial purity hydrogen and oxygen	
4. Open-cell voltage $U_o$	at least 90% of rev. emf $\phi$
5. Operating current density $i$	greater than 150 ma/cm <sup>2</sup>
6. Maximum current density $i_{max}$	greater than 400 ma/cm <sup>2</sup>
7. Performance at operating load	$U_{i=150}$ at least 70% of $\phi$
8. Sufficient lifetime $\tau$	greater than 1000 amp-hr/cm <sup>2</sup>
9. Inexpensive materials	not more expensive than Ni
10. Gas consumption efficiency	at least 90% utilized

13. High overload according to condition 7 includes a high storing capacity of electrode materials. In fact, our Ni catalysts can store about 1.2 H atoms per Ni atom and provide a high specific capacity as a storage battery.

14. Because of their low overvoltage our  $H_2$  electrode can reach an extremely high separation factor for the electrolytic enrichment of deuterium.

15. The extremely high catalytic activity of our  $H_2$  electrodes is sufficient to dehydrogenate liquid fuels such as methanol and ethylene glycol dissolved in the electrolyte and to act as high drain hydrogen electrodes. This dissolved liquid fuel cell type according to Justi and Winsel's U.S. patent (12) appears to be the most favorable future development in this country.

### DSK Electrodes for Hydrogen

To fulfill condition 1 and get a true low-temperature hydrogen electrode one needs the best metallic hydrogenation catalyst available. According to all handbooks of catalysis and to the experience of the chemical industry Raney nickel shows both maximum catalytic activity and minimum sensitivity to impurities, satisfying even condition 3. The usual method for preparing Raney nickel is to melt 50% Al with 50% Ni, cool, pulverize the very brittle alloy, and leach the Al with KOH. The grains left behind consist of very large surface area nickel. Because of their lattice defects these microskeletons are extremely active and pyrophoric. But if one tries to press and sinter such powder to get electrodes of proper shape, sufficient mechanical strength, and good electrical conductivity, the result will be common nickel with its insufficient activity and great sensitivity to poisons.

To combine the high catalytic activity and insensitivity to impurities of Raney catalyst powder with the mechanical strength and good electrical conductivity of a sintered metal electrode, we use a double skeleton (2). The supporting macroskeleton is pressed and sintered from carbonyl nickel powder of rather uniform grain size. The pores of this macroskeleton contain grains of Raney alloy, with Al as the alkali leachable component. The latter is dissolved with KOH and leaves the catalytically active microskeletons behind.

We have made and checked more than 3000 different Double Skeleton Catalyst samples and investigated the following parameters: composition and particle sizes of both the catalyst and the macroskeleton, the blending ratio of these two components, the mixing process, and the optimum pressing and sintering conditions. We have studied the process of leaching the inactive component of the Raney alloy and found that its catalytic activity is diminished by the usual technique of leaching, because at temperatures above 80°C the lattice defects of the catalyst are healed. We have found a new method of "controlled activation" consisting of the usual leaching process at ambient temperature, continued at 80°C, and finished by the application of a positive potential (-0.15 v against saturated calomel) to remove the remaining Al. The activation process is completed by saturating the electrode with  $H_2$  from the surrounding atmosphere within 24 hr or by electrolytic evolution of hydrogen within a few hours. Activated electrodes can be stored in water containing a few drops of alcohol (as hydrogen source) for several years without any deterioration. Figure 1 shows the polarization  $\eta$  (mv) of an electrode after common activation (upper curve) and additional controlled activation (lower curve) vs. current density  $i$  (ma/cm<sup>2</sup>). Polarization is diminished by about 65% and the limiting current density  $i_{max}$  increased by about 100 ma/cm<sup>2</sup>.

Figure 2 shows this improvement of performance of  $H_2$  DSK electrodes from 1953 to 1957;  $i_{max}$  in-

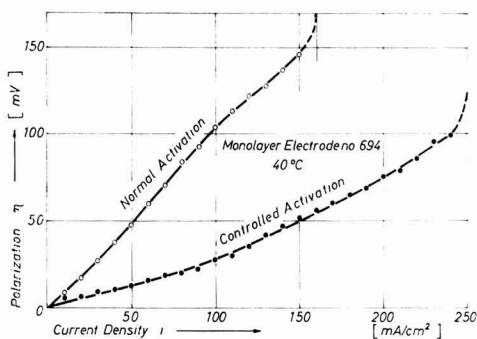


Fig. 1. Influence of activation method on the polarization vs. current density of  $H_2$  DSK electrodes. Electrolyte, 6N KOH.

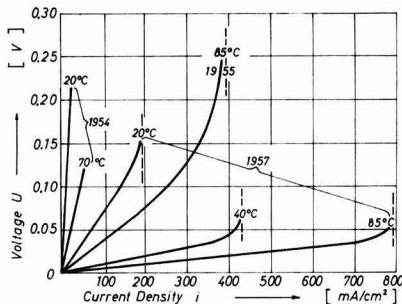


Fig. 2. Performance of hydrogen DSK monolayer electrodes, showing their voltage vs. current density; parameter: electrode temperature;  $U$  measured with Luggin capillary. The diagram shows also the progress 1954-1957.

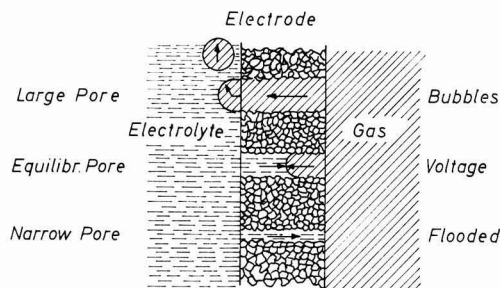


Fig. 3. Schematic cross section through a porous gas electrode, showing the different behavior of large, equilibrium, and narrow pores.

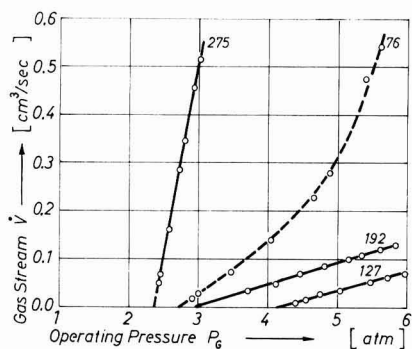


Fig. 4. Gas leakage vs. operating gas pressure of different porous electrodes. Electrode No. 76 with statistical pore size distribution gives a curved line, electrodes No. 127, 192, and 275 straight lines because of uniform pore size.

creased from 35 to 750 ma/cm<sup>2</sup> at 80°C, and polarization at  $i_{max}$  diminished from 1000 to 40 mv. This polarization is small compared with the unavoidable IR drop, and thus we have finished our efforts to improve the performance of our hydrogen electrodes.

But these first DSK electrodes were still unsatisfactory because of the statistical distribution of their pore sizes. Figure 3 shows the formation of a three-phase boundary in the middle pore, where gas pressure  $P_0$  is balanced by the capillary pressure  $P_{cap}$  because of the proper size of the pore radius. Only such "equilibrium pores" can contribute some microamperes to electrode current. If a pore is too narrow (lower pore), the capillary pressure becomes too high and the pore is drowned. If the pore is too wide (upper pore), the capillary pressure cannot counteract the gas pressure and the hydrogen escapes into the electrolyte without electrochemical reaction. By homogenizing the particle sizes carefully we can construct so-called "homeoporous" electrodes offering some 10<sup>5</sup> equilibrium pores per cm<sup>2</sup> surface, and avoiding very large pores. The homeoposity can be checked by measuring the gas bubble volume per second vs. operating pressure  $P_0$  as shown by Fig. 4. If the pore size distribution is statistical, each increase in pressure will keep dry additional pores of minor size. The result is an accelerated increase of gas throughput, such as for electrode No. 76. The homeoporous electrodes No. 127, 192, and 275 show a linear relationship

because of their uniform pore radius  $r$ . The first gas bubbles will escape exactly at  $P_0 > P_{cap} = 2\sigma \cos \theta/r$ ,  $\sigma$  being the surface tension and  $\theta$  the wetting angle. As an example, with  $\theta = 0$  and  $\sigma = 85$  dyne/cm, a pore radius of  $r = 10^{-4}$  cm needs 1.7 atm to be kept dry.

To reach higher gas consumption efficiencies than about 80% we apply double layer electrodes (6, 7) having smaller pores on the electrolyte side to prevent gas leakage. This principle seems to be simple, but it introduces some major difficulties such as additional polarization in the narrow surface pores and enrichment of inert gas impurities in the wide pores, diminishing the emf. Figure 5 shows how a 100% gas consumption efficiency could be reached with a little sacrifice of polarization and limiting current density.

### DSK Electrodes for Oxygen

The success of our hydrogen DSK electrodes encouraged us to apply the DSK system to the oxygen side too. But the technological difficulties were incomparably greater and needed many years of systematic effort. This was done by Friese (8). The first problem was to get a sufficiently brittle Raney Ag alloy. It is made by melting 35% Al under a protective coating of CaCl<sub>2</sub> in a graphite crucible and adding 65% Ag. After stirring and cooling, the regulus is pulverized and fractionated in particle size. One part of this alloy, containing 50-100 $\mu$  particles, is

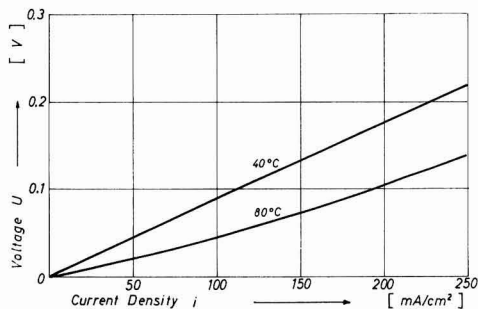


Fig. 5. Polarization vs. current density of a hydrogen DSK electrode with fine pore layer coating. Upper curve: 40°C; lower curve: 80°C operating temperature.

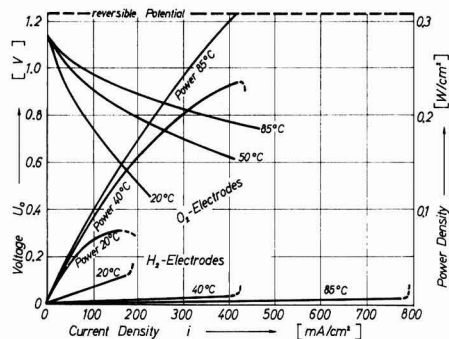


Fig. 6. Performance (left) and power density (right ordinate) vs. current density of a complete H<sub>2</sub>-O<sub>2</sub> DSK cell. Parameters: operating temperatures.



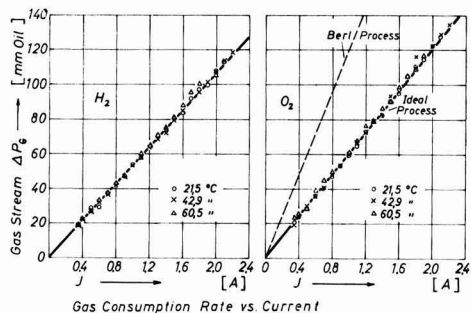


Fig. 7. Gas consumption rate ("Faraday efficiency") vs. operating current. Left, hydrogen DSK electrode; right; oxygen DSK electrode; upper line for Berl process,  $H_2O + O_2 + 2e = HO_2^- + OH^-$ ; lower line for ideal process.

blended with 1 part Ni grains of  $5\text{--}10\mu$  size and 0.5 parts of  $50\text{--}75\mu$  KCl particles. To get a 40 mm plate-shape electrode, 15 g of this mixture is hot pressed at  $370^\circ\text{C}$  with 10 tons, corresponding to  $1\text{ ton/cm}^2$ . A gas-tight double layer electrode is made by coating with 2 g of the Ni powder. Immediately after cooling the electrode is leached in 10N KOH at  $80^\circ\text{C}$ . The final weight is  $0.94\text{ g/cm}^2$  and contains only  $0.05\text{ g/cm}^2$  Ag. The performance of a complete  $H_2\text{--}O_2$  cell is shown in Fig. 6. The zero current polarization of the  $O_2$  double layer electrode is only 100 mv, increasing to 620 mv at the maximum current density of  $>500\text{ ma/cm}^2$  at  $67^\circ\text{C}$ . These new  $O_2$  DSK electrodes show remarkable progress in that they give  $>3.7$  electrons per mole  $O_2$ , compared with 2 electrons of the Berl process and 4 electrons of the ideal process, as shown in Fig. 7 (8).

#### $H_2\text{--}O_2$ DSK Cells at Ambient Temperature and Pressure

Figure 6 shows an open-circuit voltage (OCV) of 1.13 v, equal to a static efficiency of  $1.13/1.23 = 92\%$ , with the Faraday (gas consumption) efficiency of nearly 100%. Since maximum load diminishes the voltage by 50% to 0.615 v and the current density is  $250\text{ ma/cm}^2$  at  $67^\circ\text{C}$ , including an IR drop in the 1 mm KOH layer, the maximum power is  $0.154\text{ w/cm}^2$ . The weight of both electrodes and KOH is  $2.0\text{ g/cm}^2$ , and therefore the net power density  $0.154/2.0 = 0.077\text{ w/g} = 0.077\text{ kw/kg}$ , without accessories. Each electrode is 2.5 mm thick so the power density per internal volume amounts to  $0.154/0.6 = 0.256\text{ g/cm}^3$  or  $256\text{ kw/m}^3$ . This power density is somewhat lower than the 353  $\text{kw/m}^3$  which the latest model of the Bacon cell can reach at  $200^\circ\text{C}$  and 41 atm. Since the intermediate temperature system needs much more additional weight and space for automatic control, the DSK system is superior concerning power density per total volume and weight. Operating with  $i = 100\text{ ma/cm}^2$ , such as in industrial electrolyzers, the maximum overload reserve factor is 1.8. Roughly speaking, the DSK system does about the same as the intermediate temperature-high pressure system at ambient temperature and pressure. It has no intricate control problems and is always ready for use without preheating. Moreover, the DSK electrodes have the best life expectation of all known systems because the two major

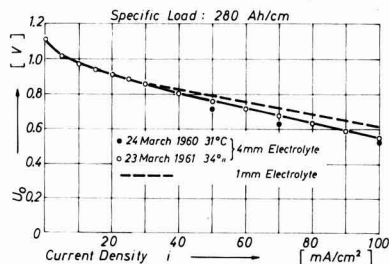


Fig. 8. Performance of a  $H_2\text{--}O_2$  DSK cell operating at ambient temperature in 1 year uninterrupted service. ● performance at 24 March 1960, ○ at 23 March 1961 after delivery of  $280\text{ amp-hr/cm}^2$  specific load. Dotted line: 1 mm electrolyte layer. Electrode size: each  $10\text{ cm}^2$ . Electrolyte 6N KOH changed.

life-limiting factors are avoided: high-temperature corrosion and hydrophobics. A 3-cell battery with a load of  $30\text{ ma/cm}^2$  at night and 50 by day has been operating since March 1960 (to 5/61 at the time). Figure 8 compares the performance curves before and after 1 year of uninterrupted service and a specific energy output of  $280\text{ amp-hr/cm}^2$ . There is no sign of deterioration, perhaps a little improvement by additional leaching of Al, and it is hoped that this cell will deliver at least  $1000\text{ amp-hr/cm}^2$ . Our collaborators, Grüneberg and Jung (10), have developed a special cleaning and regenerating process which can be applied 10 times, so a life expectation of at least some  $10,000\text{ amp-hr/cm}^2$  seems to be attainable.

#### Economy Electrodes. Dissolved Fuel Fuel Cells

If an electrode is reversible, this means that it will operate both in fuel cells and the reverse process, i.e., electrolytic decomposition, economically. In the case of the DSK electrode this is proved by Fig 9, showing its hydrogen overvoltage vs. electrolyzing current density (lower curve), which is much smaller than for a good commercial activated electrode (middle) or a bulk nickel plate (upper curve). Of course, an electrolysis electrode needs no intricate, expensive pore system, and therefore we have constructed so-called "economy electrodes" consisting of a thin DSK layer hot pressed on a cheap backing such as Ni sheet or sieve. The active layer is about 0.3 mm thick, corresponding to the measured penetration depth of

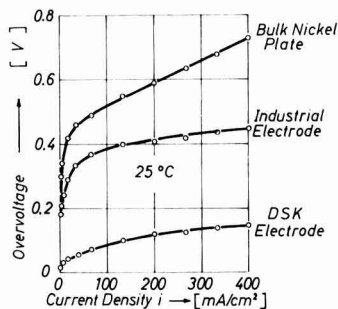


Fig. 9. Hydrogen overvoltage vs. electrolyzing current density for different nickel electrodes at  $25^\circ\text{C}$ .

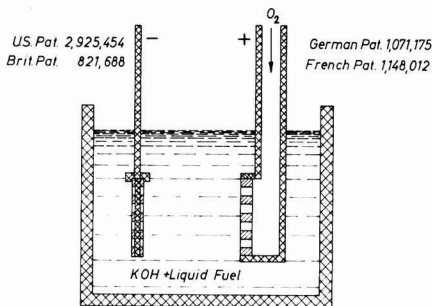


Fig. 10. Justi-Winsel fuel cell for the catalytic dehydrogenation of liquid fuel dissolved in the electrolyte. Right, common oxygen or air cathode; left, dehydrogenating electrode (f.i.DSK material) acting as  $H_{2,as}$  electrode.

current threads. Economy electrodes show the same superior performance as bulk DSK electrodes and have a long lifetime in contrast to previously known Raney nickel coatings without supporting macro-skeleton.

Such economy electrodes are also very useful for dissolved fuel fuel cells (12) as shown in Fig. 10.

Liquid fuels such as formic acid, methanol, or ethylene glycol are dissolved in the electrolyte and dehydrogenated catalytically at the economy electrode operating as a hydrogen electrode. The advantage of the Justi-Winsel process is not only its simplicity, but the high efficiency and current density. The hydrogen atoms are chemisorbed immediately after dehydrogenation without wasting energy for recombination and subsequent dissociation. Since the reaction takes place at the two-phase boundary between chemisorbed hydrogen and electrolyte, there are no geometrical limitations by three-phase boundaries. In fact, we have reached more than 1000  $ma/cm^2$  current density and 350 amp-hr at 90°C per liter in a mixture containing 15.5% ethylene glycol. Figure 11 shows a model by our collaborators, Grüneberg and Spengler, containing 2 porous carbon cathodes for air and an anode consisting of 1 mm DSK grains between two nickel microsieves. Such cells have been checked successfully with a 3  $ma/cm^2$  uninterrupted load over 1 year. Two different methods are used to regenerate the electrolyte consumed by carbon-

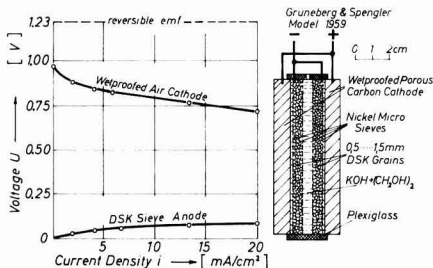


Fig. 11. Performance (left) and schematic cross section of a dissolved fuel fuel cell. Cathodes fed with air, anode containing DSK nickel between nickel microsieves. Liquid fuel: ethylene glycol, added to KOH. After Grüneberg and Spengler (13).

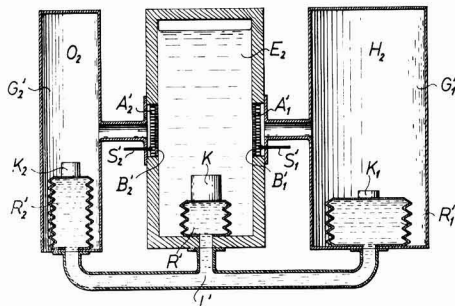


Fig. 12. Storage of electrical energy by pressure electrolysis of water (KOH) and subsequent electrochemical recombination  $H_2/O_2 \cdot A_1'$  operating equilibrium pore anode with fine pore layer  $B_1'$  of inactive material;  $A_2'$  operating equilibrium pore cathode with fine pore layer  $B_2'$  of inactive material;  $S_1'$  positive terminal;  $S_2'$  negative terminal;  $E_2$  electrolyte;  $G_1'$  hydrogen container;  $G_2'$  oxygen container;  $R_1, R_2, R_3$  metallic bellows for pressure feed back;  $K_1, K_2, K_3$  weights;  $L'$  pressurizing liquid.

atization. We were very interested to learn that our dissolved fuel fuel cell system has been checked successfully by leading laboratories such as Monsanto, Esso, Lockheed Aircraft, Engelhard, and the U.S.A. Signal Corps (14) in this country and is described as the most favorable near term development (15).

### Valve Electrodes. Storage of Energy by Pressure Electrolysis of Water and Subsequent Electrochemical Recombination of $H_2-O_2$

Another important type of DSK double layer electrodes are valve electrodes (16). They can electrolyze, separate, and compress a gas without moving parts, or can interrupt a catalytic reaction. Hydrogen valve electrodes may consist of a Raney nickel DSK electrode,  $A_1$ , with equilibrium pores (Fig. 12) coated by a copper layer,  $B_1$ , with narrow pores. Oxygen valve electrodes may consist of a Raney silver DSK electrode,  $A_2$ , coated with a fine porous titanium layer,  $B_2$ . Now if one applies at  $S_1, S_2$  a voltage exceeding the reversible emf by some 0.1 v only, no evolution of hydrogen at the copper  $B_1$  or of oxygen at the titanium  $B_2$  will be possible because of their high overvoltages.

Electrolytic decomposition can take place only in the equilibrium pores  $A_1, A_2$  because of the high catalytic activity of their walls. Hydrogen is given off at the rear side of the anode and oxygen at the rear side of the cathode, both pressurized by the capillary pressure in the narrow pores  $B_1, B_2$  of the inactive layer. The hydrogen pressure of about 3 atm is fed back to the electrolyte by metallic bellows  $R_1, R_2$  and weight  $K_1$ . In this way both hydrogen and oxygen can be compressed to about 100 atm and stored in gas containers  $G_1, G_2$ .

If energy is needed, the same cell can operate as a fuel cell. If both electrolysis and power generation is done with about 90  $ma/cm^2$ , the storing efficiency will be about 80% x 80% = 64%. This is less than the efficiency of a hypopower storing plant. But this system needs only 0.4 liter of water per kw-hr instead of 4  $m^3$  at 100 m altitude and can be placed

in a city without hills and lakes. Such storing cells can be overloaded appreciably because hydrogen and oxygen are bound in the DSK material, too. Our catalysts contain 0.68-1.2 H atoms per Ni atom in a highly reactive state. Therefore we could make good progress in constructing such DSK storage batteries (17) which can be recharged both electrically or, at least partially, by gas.

A charge can never be stored lighter than by a proton, and therefore such DSK storage batteries offer excellent chances for high capacity to weight ratio. Figure 13 shows a model delivering more than 30 amp.

In conclusion, Fig. 14 explains how to feed an oxygen valve electrode with liquid  $H_2O_2$  (8).  $H_2O_2$  solution enters the narrow pores of the inactive layer  $L_1$  and is decomposed catalytically in the large pores of the Ag DSK layer A, according to  $H_2O_2 \rightarrow H_2O + \frac{1}{2} O_2$ . The oxygen evolved will feed the  $O_2$  DSK electrode  $L_2$  with equilibrium pores being in contact with the electrolyte of a fuel cell. If more oxygen is evolved than is needed and the oxygen pressure surpasses the capillary pressure in  $L_1$ , both  $H_2O_2$  and  $H_2O$  will be pushed out at the left and decomposition will be stopped.

#### DSK Electrodes for Carbon Monoxide

About 50 years ago Hofmann (18) described a fuel cell utilizing CO as fuel. It consisted of a

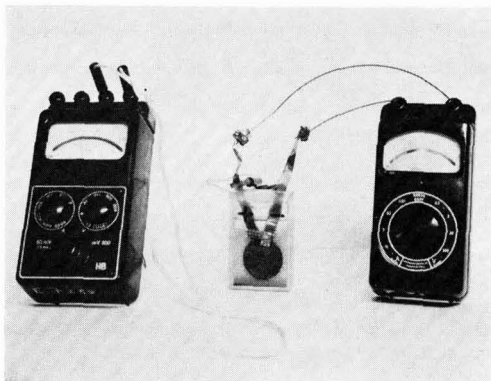


Fig. 13. Photographic view of a DSK storage battery. Ammeter (right) shows 15 amp, voltmeter (left) 0.8 v.

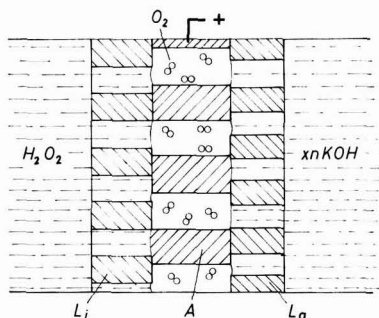
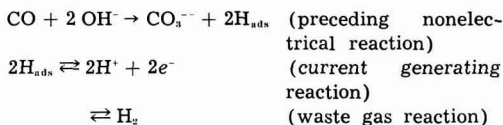
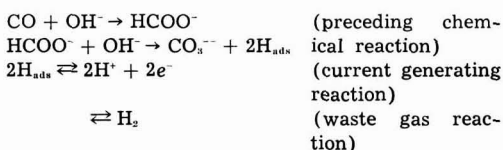


Fig. 14. Three layer electrode controlling the catalytic decomposition of hydrogen peroxide and feeding an oxygen electrode. Left,  $H_2O_2$  solution; right, electrolyte of a fuel cell.

porous copper electrode fed by CO and a common porous carbon electrode for oxygen, both immersed in a NaOH solution. Hofmann measured an OCV of 1.04 v and ascribed it to the electrochemical combustion of  $H_2$  formed in a preceding conversion reaction. We have proposed the following scheme to explain his measurement:



Furthermore, our collaborator Grüneberg (19) has observed the following reactions:



However, we disagree with Hofmann's and Grüneberg's explanation of the observed  $-0.04$  v as being an anodic hydrogen potential, since the reversible  $CO/O_2$  potential is more negative by 0.45 v. Therefore, we have pointed out (3) that the electrochemical desorption of CO must be accompanied by a cathodic hydrogen evolution at the same electrode, as illustrated by Fig. 15. According to our philosophy the material of the CO electrode should have a  $H_2$  overvoltage as high as possible. In addition, the material must show a specific ability to activate the CO molecule. This additional requirement explains why Hg shows an OCV of but  $-0.850$  v against saturated calomel, although it exhibits an extremely high hydrogen overvoltage. But Cu-DSK electrodes with a copper macroskeleton, with no Ni, reach an OCV of  $-1.17$  v, surpassing the hydro-

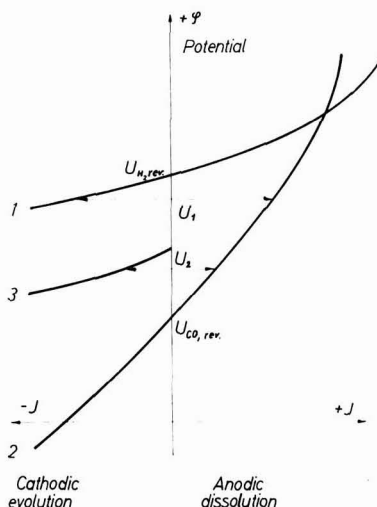


Fig. 15. Explanation of the open-cell voltage of CO diffusion electrodes as mixed potentials of a dual electrode.

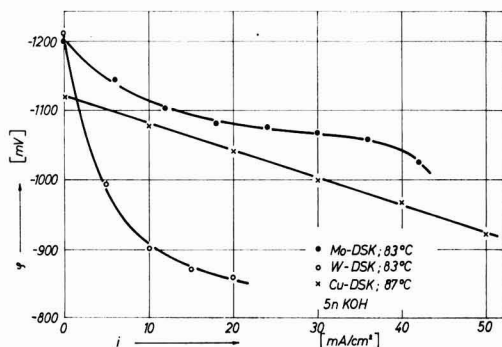


Fig. 16. Performance of CO-O<sub>2</sub> fuel cells, using fuel DSK electrodes containing Mo, W, or Cu Raney catalysts; temperature 83°C, electrolyte 5N KOH.

gen potential of  $-1.13$  v and verifying our explanation.

Best results were obtained with W- or Mo-DSK electrodes (20). In our preliminary experiments they gave an OCV of  $-1.20$  v and a current density of  $50$  ma/cm<sup>2</sup> with Raney-Mo at 83°C, Fig. 16. These results seem to be encouraging, and we shall spend forthcoming efforts to optimize such Mo- and W-DSK electrodes since we have found a new method to overcome the carbonatization of the KOH by a continuous electroalytic process consuming less than 10% of the power generated.

In conclusion we should like to mention that we have also succeeded in applying the DSK system to Pd. Such Pd-DSK electrodes operating in both acid and alkaline liquids offer new possibilities for the measurement of pH values with common, cheap voltmeters.

Manuscript received June 12, 1961. This paper was prepared for delivery before the Indianapolis Meeting, April 30-May 3, 1961.

Any discussion of this paper will appear in a Discussion Section to be published in the June 1962 JOURNAL.

#### REFERENCES

1. K. Bischoff and E. Justi, *Jahrb. Akad. d. Wiss. u. d. Lit. Mainz*, 250 (1951); *ibid.*, 200 (1955).
2. E. Justi, W. Scheibe, and A. Winsel, German Pat. 1,019,361 (1954); U. S. Pat. 2,928,891; British Pat. 806,644; French Pat. 1,132,762. A. Winsel, "Einige

Untersuchungen über den Reaktionsmechanismus von Doppelskelett-Katalysator-Elektroden (DSK-Elektroden) für Wasserstoff" doctor thesis, Braunschweig Inst. of Techn. (1957).

3. E. Justi, M. Pilkuhn, W. Scheibe, and A. Winsel, "High drain hydrogen-diffusion-electrodes operating at ambient temperature and low pressure," *Abhandl. math.-Naturw. Kl. Akad. Wiss. Lit. Mainz*, No. 8, Komm. Verlag Steiner-Wiesbaden, 1959.
4. K.-H. Friese, E. Justi, W. Scheibe, and A. Winsel, German Pat. 1,074,015 (1957); French Pat. 1,213,-191.
5. E. Justi, German Pat. 1,002,829 (1955); British Pat. 830,922; French Pat. 1,144,838.
6. A. Schmid, "Die Diffusionsgaselektrode," Enke-Verlag, Stuttgart (1923).
7. F. T. Bacon, "Fuel Cells," G. J. Young, Editor, 51, Reinhold Publishing Co., New York (1960).
8. K.-H. Friese, "Doppelskelett-Katalysator-Elektroden für die kathodische Reduktion von Sauerstoff," doctor thesis, Braunschweig Institut of Techn. (1959).
9. H. M. Dittmann, E. W. Justi, and A. W. Winsel, Paper presented at ACS Fall Meeting 1961.
10. G. Grüneberg, M. Jung, E. Justi, and H. Spengler, German Pat. applic. R 21 294 IV a/21b (1957); Austrian Pat. 199,238; French Pat. 1,207,057.
11. E. Justi and A. Winsel, German Pat. applic. R 22 829 IVa/12g (1958); Austrian Pat. 206,867; French Pat. 1,221,133.
12. E. Justi and A. Winsel, German Pat. 1,071,175 (1955); U. S. Pat. 2,925,454; British Pat. 821,688; French Pat. 1,148,012.
13. H. Spengler and G. Grüneberg, "Galvanische Brennstoffelemente bei Raumtemperatur," 75. DE-CHEMA-Monographie, 38, 579-599, Frankfurt (1960).
14. B. R. Stein and E. M. Cohn, "Second Status Report on Fuel Cells," ARO Report No. 2, Washington (1960).
15. D. R. Adams, P.-Y. Cathou, R. D. Jackson, J. H. Kirsch, L. L. Leonhard, G. S. Lockwood, W. P. Wornock, and R. E. Wilcox, "Fuel Cells, Power for the Future," The Purnell Co., Boston (1960).
16. M. Pilkuhn and A. Winsel, *Z. Elektrochem.*, 63, 1056 (1959); E. Justi, German Pat. applic. R 22 458 IVa/21b (1958); Austrian Pat. 207,430.
17. K.-H. Friese, E. Justi, and A. Winsel, German Pat. applic. R 23 720 IVa/21b (1958); French Pat. 1,229,144; Italian Pat. 611,569.
18. K. A. Hoffmann, German Pat. 310,782 (1917).
19. G. Grüneberg, "Ein Beitrag zur elektrochemischen Nutzung von CO im alkalischen Brennstoff-Element," doctor thesis, Braunschweig Inst. of Techn. (1958).
20. P. Jacob, E. Justi, and A. Winsel, German Pat. 1,071,789 (1959).

## Materials Problems in Cesium Thermionic Converters

Ling Yang and F. D. Carpenter

John Jay Hopkins Laboratory for Pure and Applied Science,  
General Atomic Division of General Dynamics, San Diego, California

The materials problems associated with cesium thermionic devices can be better understood if the discussion is preceded by a brief review of the principles of the cesium thermionic converter and the conditions under which the various components of the converter operate.

Basically, the cesium thermionic converter is a cesium-vapor-filled vacuum diode, which can be

used to convert heat (e.g., solar heat and fission heat) directly to electrical energy. The chief advantages of such a device are that (a) there are no moving parts and therefore it is completely silent; (b) an efficiency of conversion of 35% or more may be possible if the materials problems can be overcome [an efficiency of conversion of up to 15% has been achieved with materials now available (1, 2)];

(c) a power-to-weight ratio of a few pounds per kilowatt (electric) is deemed possible; and (d) fissionable and breeding materials, such as uranium, thorium, and plutonium carbides, are also excellent electron emitters, so that this device is best suited for converting fission heat directly to electrical energy.

A cesium thermionic converter consists of three principal parts: (i) a hot cathode (or emitter), which emits electrons; (ii) a cold anode (or collector), which collects the electrons emitted from the cathode; and (iii) a ceramic insulator, which separates the cathode and the anode. The system is enclosed under vacuum and filled with cesium vapor at about 1 mm Hg pressure; this vapor, when ionized either thermally or by interaction with the hot cathode surface, helps to neutralize the space charge in the vicinity of the cathode surface. To minimize the electrical impedance of the cesium plasma to the flow of current, the distance between the cathode and the anode is maintained at 1 mm or less. Figure 1 is a schematic diagram of a cesium thermionic converter.

A cesium thermionic converter can be regarded as a heat engine using electrons as the working fluid. Thermal energy is supplied to the electrons in the hot cathode to lift them out of the cathode surface. When these electrons reach the anode surface, a part of the energy carried by them is transferred to the cold anode and the rest of the energy is made available for doing useful work. Assuming complete space-charge neutralization and for  $\phi_K > \phi_A$  ( $\phi_K$  and  $\phi_A$  are electron work functions for cathode and anode, respectively),<sup>1</sup> the process can be illustrated by the potential-energy diagrams shown in Fig. 2, and the output voltage,  $V$  vs. output current,  $I$ , shown in Fig. 3.

In Fig. 2,  $e$  represents the electronic charge and  $V$  is the voltage across the load. The positions of  $M$  relative to that of  $N$  depend on the magnitude of the output voltage,  $V$ . As long as  $\phi_K \cong \phi_A + V$ , the energy barrier for electron emission from the cathode is always  $\phi_K$  (see Fig. 2 a and b), and the current reaching the anode, i.e., the output current,  $I$ , assuming zero plasma impedance and negligible back

<sup>1</sup> In general,  $\phi_K$  does not have to be greater than  $\phi_A$ , although here it is assumed to be.

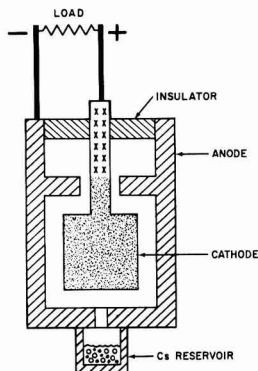


Fig. 1. Schematic diagram of a cesium thermionic converter

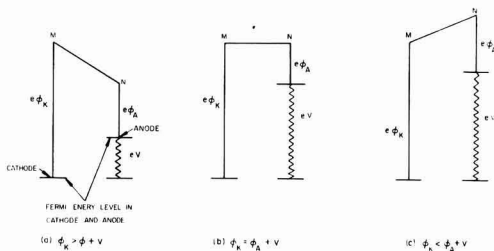


Fig. 2. Potential energy diagrams for cesium thermionic converter.

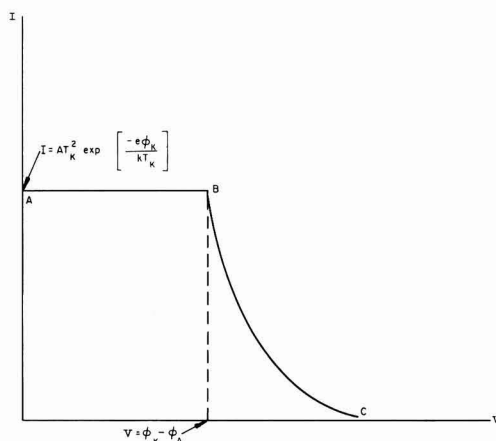


Fig. 3. Output voltage vs. output current for cesium thermionic converter at cathode temperature =  $T_K$ .

emission from the anode, is represented by the Richardson-Dushman equation

$$I = AT_K^2 \exp\left(\frac{-e\phi_K}{kT_K}\right) \quad [1]$$

where  $A$  is a temperature- and material-independent constant with a theoretical value of 120 amp/cm<sup>2</sup>-°K<sup>2</sup>;  $T_K$  is the temperature of the cathode, and  $k$  is the Boltzmann constant. Therefore, for  $V \leq \phi_K - \phi_A$ ,  $I$  is a constant at a given temperature  $T_K$ . This is represented by the section AB in Fig. 3. When  $V$  is increased so that  $\phi_K < \phi_A + V$  (see Fig. 2c), the energy barrier for cathode electron emission becomes  $\phi_A + V$ , and

$$I = AT_K^2 \exp\left(\frac{-e(\phi_A + V)}{kT_K}\right). \quad [2]$$

The output current,  $I$ , therefore decreases exponentially with the increase of  $V$ , as illustrated by the section BC in Fig. 3. At the point B,  $V = \phi_K - \phi_A$  and  $I = AT_K^2 \exp(-e\phi_K/kT_K)$ , the output power is at a maximum, and the maximum efficiency of conversion,  $\eta_{max}$ , is therefore

$$\eta_{max} = \frac{\text{power output}}{\text{power input}} = \frac{I(\phi_K - \phi_A)}{I\phi_K + Q_r} \quad [3]$$

The assumptions are that (a) there is no back emission from the anode, (b) the kinetic energy of electrons is negligible, and (c) the radiation loss,  $Q_r$ ,



from cathode to anode is the principal power loss.  $Q_r = \sigma \epsilon (T_k^4 - T_a^4)$ , where  $\sigma$  is the Stefan-Boltzmann constant,  $\epsilon$  is the emissivity factor of the system, which varies with the geometry of the electrodes and the thermal emissivities of the cathode and anode surfaces, and  $T_k$  and  $T_a$  are the temperatures of the cathode and the anode, respectively.

If Eq. [1] is substituted into Eq. [3], it can be seen that  $\eta_{max}$  increases as  $\phi_A$  decreases, so long as the anode back emission is negligible. The variation of  $\eta_{max}$  with  $\phi_K$  is more complicated;  $\eta_{max}$  first increases and then decreases with the increase of  $\phi_K$ . When  $\phi_K$  and  $\phi_A$  are kept constant,  $\eta_{max}$  increases almost exponentially with  $T_k$ . In order to achieve high efficiency of conversion, it is therefore necessary to operate the cathode at very high temperatures (e.g., 1600°-2000°C).

The unique features associated with a cesium thermionic converter, which are the causes of serious materials problems, are thus (a) high temperature, (b) partial vacuum, (c) presence of cesium vapor, (d) close spacing between the electrodes, and (e) presence of intense radiation and fission products (only for the conversion of fission heat). Special consideration must be given to the materials problems, and the proper selection of these materials must be made if the device is to deliver useful and dependable performance for long periods of time (e.g., several watts per square centimeter or more output, 25% or better efficiency of conversion, one year or longer life). The materials problems are analyzed in more detail below.

### Cathode Materials

Materials used for the cathodes have to meet the following requirements:

1. They must be chemically and mechanically stable at 2000°C in order to preserve their chemical compositions and the geometry of the electrode configurations at the operating temperature.
2. They must be immune to cesium vapor at 2000°C.
3. They must be as impermeable as possible to cesium vapor and fission products so as not to deplete or contaminate the plasma.
4. They must have the optimum electron work function in the operating temperature range, in order to provide useful power output and maximum efficiency of conversion.
5. They must have high thermal and electrical conductivities to facilitate the transfer of heat generated in the bulk to the surface and to reduce Joule loss.
6. They must be stable under irradiation so that no significant changes in dimensions and physical properties occur.

#### Type and Performance of Cathode Materials

The selection of cathode materials is greatly hampered by our lack of information on the physical and chemical properties of materials at temperatures higher than 1000°C. Present-day cathode materials are chosen mainly on the basis of their melting points and their electron emission properties. They include tungsten (2-4), thoriated tung-

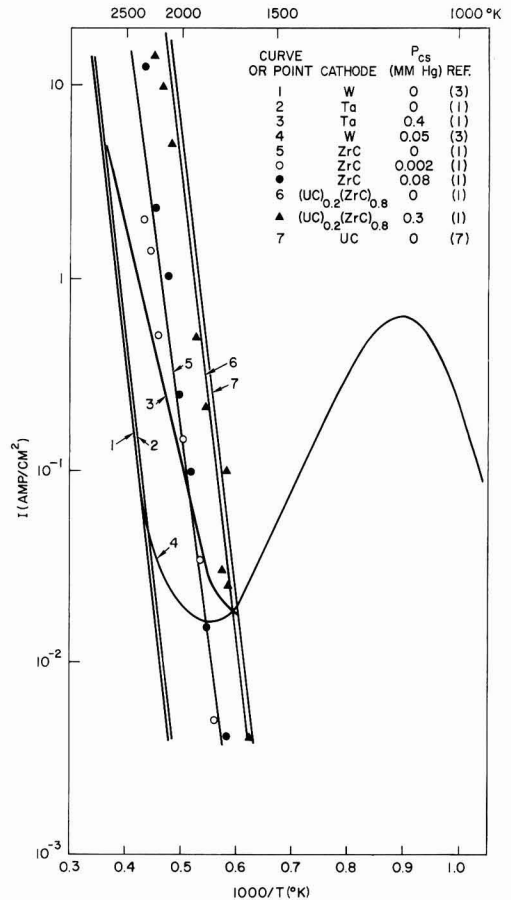


Fig. 4. Thermionic emission of various materials and the effect of cesium vapor.

sten (2), tantalum (1), molybdenum (5, 6), ZrC (1, 7), UC (7), and UC-ZrC (1, 7) solid solutions. All of these materials have melting points higher than 2400°C. Figure 4<sup>2</sup> shows the saturation emission currents at various temperatures for tungsten, tantalum, ZrC, UC, and (UC)<sub>0.2</sub>(ZrC)<sub>0.8</sub>, with and without the presence of cesium vapor. The following conclusions are evident:

1. Inherently, the carbides are much better electron emitters than the refractory metals. This is because the electron work functions of carbides are lower than those of the refractory metals.
2. For the temperature ranges indicated, the presence of cesium vapor does not seem to affect the electron emission from carbides. However, the electron emission from tungsten and tantalum is enhanced in the presence of cesium vapor. This is because the carbides do not seem to adsorb cesium at these temperatures, whereas tungsten and tantalum adsorb cesium on their surfaces, which lowers their electron work functions and facilitates electron emission.

<sup>2</sup> These are not Richardson plots, although they appear to be close to straight lines.

3. In the presence of cesium vapor, the electron emission of carbides increases exponentially with temperature; the relationship between temperature and emission current for tungsten and tantalum is represented by an S curve. At low temperatures, the tungsten and tantalum surfaces are completely covered by cesium and the electron emission increases with temperature; the electron work function is that of cesium metal. As the temperature increases, some of the adsorbed cesium atoms vaporize away and the surface coverage by cesium becomes less and less. As a result, the electron work function increases and the electron emission decreases, even though the temperature increases. At still higher temperatures, the surfaces lose all the adsorbed cesium atoms. The electron emission becomes typical of that of the metal alone and increases exponentially with temperature. The S shape is clearly shown in the curves of tungsten, whereas for tantalum it is less evident because of the limited temperature range used in the study.

On the basis of the above conclusions we can divide cathode materials into two groups: those which adsorb cesium atoms are called wet cathodes and those which do not adsorb cesium atoms are called dry cathodes. The wet cathodes are operated at temperatures lower than those for the dry cathodes (usually 1400°-1700°C) in order to keep them wet; they can provide reasonable output (7-12 watts/cm<sup>2</sup>) (2,6), at relatively low temperatures. The materials problems of the wet cathodes are less severe than those for the dry cathodes. For the dry cathodes, the only limit to their operating temperature is the durability of the materials, and therefore much higher output (30 watts/cm<sup>2</sup>) (1) has been obtained. The following discussion will be devoted mainly to the materials problems related to the dry cathodes, especially the UC-ZrC cathodes. The latter material has been demonstrated to be the most promising, and it can also serve as nuclear fuel for fission-heat conversion. Addition of ZrC to UC increases its mechanical strength and chemical stability. Up to 80 mole-% of ZrC in UC does not seem to change its electron emission characteristics (1, 7).

Studies made to date of the above cathodes have been limited to runs of less than 20 hr and most of the measurements were made outside the reactor; the only in-pile tests successfully carried out were those performed at Los Alamos Scientific Laboratory (8, 9) and at General Atomic (10), both of which used UC-ZrC cathodes. To achieve dependable performance for long periods of time, it is deemed necessary to solve the following materials problems.

*Loss of materials by vaporization.*—Although the loss of materials by vaporization is relatively unimportant at low temperatures, it becomes very serious at temperatures approaching 2000°C, especially in vacuum or low-pressure environments such as those prevailing in a cesium thermionic converter. For instance, at 2000°C in vacuum, the loss of graphite is about 1 g/cm<sup>2</sup>-yr. Loss of cathode materials by vaporization is thus one of the most serious materials problems of cesium thermionic converters.

There are a number of detrimental effects associated with the loss of materials from the cathode. First, if the cathode is also the nuclear fuel of the reactor, e.g., UC-ZrC in the case of fission-heat conversion, loss of uranium will seriously affect the performance of the reactor. Second, as the components (e.g., uranium, zirconium, and carbon) do not vaporize at equal rates from the surface of the cathode and the losses have to be replenished by diffusion from the bulk, the surface composition and therefore the electron emission properties may change with time. Although a constant sublimation composition may be reached eventually (if it does exist), large amounts of materials, especially uranium, may have been lost before this happens. Third, the vaporized materials, when condensed on the cooler anode, may increase the thermal emissivity of the anode surface and therefore increase the radiation loss from the cathode. Fourth, as the gap between the cathode and the anode is 1 mm or less, uneven condensation on the anode surface may cause an electrical short between the electrodes.

Although, in principle, it should be possible to calculate the vapor pressures of various materials from thermodynamic data, this method is difficult to apply to the present case for several reasons. First, the calculated results are often unreliable because of the uncertainties involved in estimating these thermodynamic data and the lack of information on the vaporization mechanism. Second, results calculated from thermodynamic data are equilibrium properties, whereas the loss of cathode materials in a cesium thermionic converter is a kinetic property that is determined by a combination of free evaporation and diffusion. Third, most of the carbide phases cover a wide nonstoichiometric composition range, and the surface compositions may differ widely from that of the stoichiometric composition of the bulk. It is therefore necessary to determine experimentally the vaporization losses of the cathode materials and the relative amounts of their vaporizing species as a function of temperature and time.

There has been very little experimental investigation of the vaporization of the carbides of interest in thermionic studies. To date, only a few measurements of the vapor pressure and vaporization loss of TaC (11), WC + W<sub>2</sub>C (11), ZrC (12), and UC<sub>2</sub> (13), and some rather qualitative information on the vaporization of UC (14) and (UC)<sub>0.2</sub> (ZrC)<sub>0.8</sub> (14) are available. The seriousness of vaporization loss has been clearly demonstrated by Bowman (14), who calculated the temperatures at which various cathode materials can provide 10 amp/cm<sup>2</sup> and the temperatures at which these materials lose 1 mm in thickness per year. The only material which loses less than 1 mm in thickness per year while delivering 10 amp/cm<sup>2</sup> is (UC)<sub>0.2</sub> (ZrC)<sub>0.8</sub>. As the gap between the cathode and the anode is 1 mm or less, a loss of 1 mm in the thickness of the cathode can hardly be tolerated. If the maximum allowable loss is reduced to much less than 1 mm/yr (e.g., to 0.1 mm/yr), then it remains to be answered whether (UC)<sub>0.2</sub> (ZrC)<sub>0.8</sub> can meet

this requirement without sacrificing its emission current density.

While a small amount of vaporization loss from the cathode may still be tolerable, no condensation, no matter how small the amount, of the vaporized material on the anode surface should be permitted. Even a condensate several atom layers thick may change the thermal emissivity of the anode surface so drastically that the radiation loss from the cathode to the anode becomes intolerable. To reduce evaporation loss and to keep the thermal emissivity of the anode surface low without compromising the electron emission current density is the key to the success of the cesium thermionic converters using dry cathodes. Systematic studies of the vaporization losses and vaporization mechanisms of refractory carbide systems may lead to solutions of these problems.

*Corrosion of cathode materials by cesium vapor.*—The cathode materials should be immune to cesium vapor for long periods of time at 2000°C. Previous studies have been confined to the interaction of uranium carbides with sodium (15) and some short-time tests of NbC in cesium vapor (20 mm Hg pressure) at 1150°C for 10 min (16). Studies carried out at General Atomic showed dramatic differences in the corrosion behavior of U-ZrC systems when the composition was varied (17). Although carbide cathodes immune to cesium vapor for short periods of time have been produced successfully, it is uncertain how they behave in the long run, especially after vaporization and diffusion have changed their surface compositions. Correlation between the microstructures, phase relationships, and corrosion behavior of carbides and other cathode materials in cesium vapor at high temperatures is another important materials problem to be solved.

*Compatibility of cathode and electrical lead materials.*—The current generated in the converter has to be carried out through electrical leads bonded to the cathode and the anode. For carbide cathodes containing UC, the cathode electrical leads are usually one of the refractory metals (tungsten, tantalum, molybdenum, or niobium) or their carbides. The lead material is bonded to the carbide cathode by the formation of a diffusion layer at the interface. It is very important that consideration should be given to the matching or thermal expansion coefficients and the nature of the phases formed at the interface by diffusion for long periods of time. Any formation of low-melting eutectics or voids by diffusion is detrimental. There have been no long-term tests made on the compatibility between carbide cathodes and various refractory materials. Half-hour tests made between UC and a number of refractory metals and their carbides in argon by Creagh and Drell (18) yielded the following maximum allowable temperatures: tungsten, 4400°F; tantalum, 4500°F; molybdenum, 3600°F; niobium, 4100°F; HfC, 4600°F; ZrC, 4600°F; TaC, 4500°F; Mo<sub>2</sub>C, 3700°F; NbC, 4600°F; WC, 4300°F; W<sub>2</sub>C, 4400°F; TiC, 4400°F. Results obtained at Los Alamos (19) for (UC)<sub>0.3</sub> (ZrC)<sub>0.7</sub> are tungsten, 2400°C; tantalum, 2100°C. Diffusion and phase-relationship

studies for these systems are pertinent to the selection of the electrical lead materials and the optimum operating temperatures of the bond.

*Irradiation effects.*—For fission-heat conversion, the cathode materials are subject to intense radiation, which may cause significant changes in their dimensions and in physical properties such as electrical and thermal conductivities, and may lead to the failure of the converter. To date, irradiation tests have been performed only for UC (4.6-5.2 wt-% C) at relatively low temperatures (average surface temperature, 700°-916°F; average core temperature, 1150°-1376°F) to burnups of 0.2-2 atom-% uranium and 1,000-10,000 Mw-day/ton of uranium (20). The results indicate a decrease in density of about 2% and no significant change in thermal conductivity. Cracks characteristic of thermal shock and carbon migration in hyperstoichiometric UC have been observed. Irradiation tests up to 2000°C for UC and UC-ZrC systems are needed to provide information for designing converters for fission-heat conversion.

*Fission-product release.*—The release of fission products from cathodes containing nuclear fuels contaminates the plasma and the electrode surfaces. These products may change the electron work functions of the electrodes and also cause serious back-scattering of the electrons emitted from the cathode surface. Although the above-mentioned irradiation tests on UC at low temperatures (20) indicate that the fission-gas release was small and was of the order of fission recoil from the surface, it is doubtful whether this holds true at 2000°C, even with extremely dense cathode materials. Experiments carried out at Los Alamos on UC-ZrC (19) (irradiated, then heated for 3 hr at 2400°C) showed that the diffusion rates of fission products range from 10<sup>-4</sup> to 10<sup>-6</sup>/sec, which are one to three orders of magnitude slower than those from graphite at the same temperature. In general, with the UC-ZrC cathode operating at 2000°C, it is believed that most of the fission gases will be lost. The fission products which form stable carbides, such as ruthenium, thorium, rare earths, and molybdenum, will have more chance of remaining in the cathode, while the rest, such as silver, cadmium, iodine, tellurium, strontium, barium, and antimony, will be retained only to a small extent; this was found in the Los Alamos experiments. As the fission products formed amount to a few moles per megawatt-year, their release would have serious consequences in the performance of the converter. To prevent the fission-gas pressure from building up in the converter, periodic bleeding has to be performed by incorporating carefully controlled leaks in the system. Although some cesium is lost during the bleeding, it can be shown that the amount is negligible for the size of the leaks needed for venting the fission gases.

The fission products remaining in the cathode as carbides and the fission products released from the cathode and condensed on the anode may have significant effects on the performance of the converter, but these will be evident only in in-pile tests over long periods of time.

*Dimensional change caused by thermal expansion, creep, and grain growth.*—There is practically no information available on dimensional changes of the cathode at temperatures of interest here. For carbides of interest, the linear thermal expansion coefficients have been measured mostly below 900°C ( $4$  to  $10 \times 10^{-6}/^{\circ}\text{C}$ ) (21-24), the exceptions being UC,  $\text{U}_2\text{C}_3$ , and  $\text{UC}_2$  (25). These data are pertinent to the maintenance of a small and uniform gap between the cathode and the anode.

*Heat transfer, radiation thermal loss, and joule loss.*—The heat received by the cathode (as in solar heating) or generated in the cathode (as in fission heating) has to be transferred by conduction in order to heat the emitting surface and to avoid a sharp thermal gradient in the cathode. Most of the thermal conductivities available for the carbide cathodes ( $0.03$  to  $0.08$  cal/cm-sec- $^{\circ}\text{C}$ ) have been determined at temperatures below 700°C (21-23, 26-29). The joule loss depends mainly on the electrical conductivities of the cathode materials and of the bond between the cathode and the refractory electrical leads at the temperatures of operation. For an output of several hundred amperes and a few volts, even an electrical resistance of  $0.001$  ohm can be very serious. Unfortunately, the electrical-resistivity data available for the carbide cathodes are mostly for room temperatures ( $30$  to  $150$   $\mu$  ohm-cm) (21-23). Measurements of thermal and electrical conductivities as a function of temperature up to 2000°C and compositions of the carbide cathodes [*e.g.*, the work of Kolomoets *et al.* (30) and of Samsonov *et al.* (31)] are urgently needed. Although the thermal emissivities for the carbide cathodes are known ( $0.7$ - $0.9$ ) (14), the radiation thermal loss is strongly dependent on the effect of material that condenses on the anode and on the thermal emissivity of the anode surface. The importance of preventing materials from condensing on the anode surface has been stressed under "Loss of materials by vaporization."

*Fabrication of carbide cathodes.*—The carbides of thermionic interest (UC and UC-ZrC) melt in the temperature range from 2500° to 3500°C and are extremely hard and reactive. To maintain high purity and to fabricate them into specific shapes, special techniques have to be used.

As practical examples, the fabrication techniques for two types of carbide cathodes used at General Atomic are as follows:

1. In-pile-test Mark IV cathode. The cathode consists of a drop-cast UC-ZrC cylinder (95 wt % UC, 5 wt % ZrC, 93% enrichment)  $\frac{1}{2}$  in. in diameter and  $\frac{1}{2}$  in. high, with a stem  $\frac{3}{16}$  in. in diameter and  $\frac{1}{2}$  in. high attached to it. The stem is of the same composition as the cylinder but contains only  $\text{U}^{238}$ . A niobium electrical lead is bonded to the stem by using zirconium metal as a binder, and the niobium is joined mechanically to the copper bus bar.

2. Electron-gun-heated Mark V cathode. The cathode consists of a UC-ZrC cup (10 mole % UC, 90 mole % ZrC)  $\frac{5}{8}$  in. OD,  $\frac{3}{8}$  in. ID, and  $\frac{3}{4}$  in. high, made by hot-pressing and ultrasonic drilling. It is bonded to a tantalum tube insert, with zir-

conium as a binder. The tantalum tube is welded to the copper lead by an electron beam.

### Anode Materials

The anode is usually operated between 300° and 1000°C. The materials problems involved are much less severe than those for the cathodes. The material requirements are similar to those for the cathodes, except that the requirements have to be met only in the temperature range from 300° to 1000°C.

The following materials have been used or proposed as anodes: copper, nickel, molybdenum, zirconium, Fe-Ni, AgO-Cs, and WO-Cs. All of these materials have an apparent electron work function,  $\phi_A$ , of 1.8 v ( $\phi_{\text{Cs}}$ ) or less when cesium atoms are adsorbed on them, although the electron work functions of the metals are much higher. As the optimum output voltage is  $\phi_K - \phi_A$ , and the power output and efficiency of conversion increase with the decrease of  $\phi_A$ , materials with low values of  $\phi_A$  are the most desirable for the anodes. Since  $\phi_A$  is affected by the amount of cesium adsorbed on the anode surface, and the latter depends on the anode temperature and cesium pressure, there is an optimum anode temperature for a given cesium pressure at which the amount of cesium adsorbed yields the lowest value of  $\phi_A$ . This has been demonstrated in a number of cases (2, 6).

From a metallurgical point of view, the only major problem concerning anode materials is the compatibility between cesium vapor and various promising anode materials between 300° and 1000°C for long periods of time. Studies (32) have been made on some metals and alloys with the following results: tungsten, 1830°F for 100 hr, compatible; molybdenum, 1290° and 1830°F for 100 hr, compatible; nickel, 1290°F for 100 hr, compatible; 1290°-1830°F for 100 hr, intergranular attack; Type 321 stainless steel, 1290°F for 100 hr, compatible; 1830°F for 100 hr, corroded. It would be desirable to extend such studies to other promising anode materials.

### Ceramic Insulating Seals

The ceramic insulating seal consists of a ceramic insulator bonded to two separate metal flanges, one of which is joined to the cathode electrical lead and the other to the anode material. Depending on the anode temperature, the seal is operated at 300°-1000°C.

The ceramic insulating seal should be resistant to cesium vapor at 1000°C, vacuum-tight at 1000°C, and stable under irradiation.

The seals available commercially consist mostly of  $\text{Al}_2\text{O}_3$  brazed to Fe-Ni alloys, with BT solder (72 wt % Ag, 28 wt % Cu, melting point 780°C) and are usable up to about 700°C. Special seals were made at Los Alamos (33, 35) consisting of four components in each seal. The components and their compositions were as follows: (a) ceramic insulator:  $\text{Al}_2\text{O}_3$  or CaO; (b) metallizing layer: Mo-Mn; (c) brazing alloy: BT solder (72 wt % Ag, 28 wt % Cu, melting point 780°C) or Ag-Mn alloy (85 wt % Ag, 15 wt % Mn, melting point

970°C); (d) metal flange: for  $\text{Al}_2\text{O}_3$ , Fe-Ni alloys (42, 46, or 51 wt % Ni, the balance Fe), Nb, Mo, Zr, Ta, or Cu (using a graded seal of 51 wt % Ni, 49 wt % Fe); for CaO, Ni, or Cu.

The fabrication technique consisted of the following steps:

1. A Mo-Mn metallic layer was applied to the ceramic material, and the metallized ceramic was fired at 1500°C in hydrogen.
2. The Mo-Mn layer was plated with 0.3 mil of nickel and the composite was fired at 1000°C.
3. The metal flanges were then brazed to the nickel, using the brazing alloys.

There are a number of materials problems associated with the ceramic insulating seal which need special attention. They are as follows.

**Irradiation stability.**—It has been shown by Los Alamos workers (35) that  $\text{Al}_2\text{O}_3$  seals bonded to the metals mentioned above remained intact after receiving an integrated flux of  $7 \times 10^{20}$  neutrons/cm<sup>2</sup>, as tested with a mass-spectrometer leak detector. The CaO seals disintegrated, presumably because of hydration.

**Compatibility of ceramic insulators with cesium vapor.**—The ceramic materials  $\text{Al}_2\text{O}_3$ ,  $\text{ThO}_2$ ,  $\text{ZrO}_2$ , CaO, MgO,  $\text{HfO}_2$ , and BN were exposed to cesium vapor at 20 mm Hg pressure at 1100°–1500°F for 10 min by Wagner and Coriell (16). No visible attack was observed in any of the materials. Tests for longer periods of time should be made to confirm these observations.

**Improvement of the bond between the ceramic insulator and the metal flange.**—The Mo-Mn layer was bonded to  $\text{Al}_2\text{O}_3$  mechanically. To form a better vacuum seal, a chemical bond is preferable. To achieve such a bond, modification of the metallizing layer is highly desirable.

**Exploration of ceramic materials and brazing alloys other than those mentioned above.**—This is needed to develop seals operable at temperatures higher than 700°C.

### Cesium Thermionic Converter In-Pile Test

In April 1960, an in-pile test of a cesium thermionic converter was carried out in the General Atomic TRIGA reactor (10). One of the major objectives of such a test was to learn the various materials problems associated with cesium thermionic converters for fission-heat conversion.

The cathode was in the form of a cylinder ½ in. in diameter and ½ in. high, made by drop-casting arc-melted UC-ZrC buttons (95 wt % UC, 5 wt % ZrC, 93% enrichment) around a UC-ZrC stem (3/16 in. in diameter, 1/2 in. long) of the same composition but containing only  $\text{U}^{238}$ . The stem, which served as a support as well as a thermal barrier, was bonded to a niobium rod by using zirconium as a binder. The niobium rod was joined mechanically to a copper rod heliarc-welded to the inner Fe-Ni flange of an Alite  $\text{Al}_2\text{O}_3$  seal.

The anode was OFHC copper, polished mechanically to a mirror finish. It was soldered to the outer Fe-Ni flange of the same Alite seal to which the cathode was joined. The spacing between the anode and the cathode was about 1 mm.

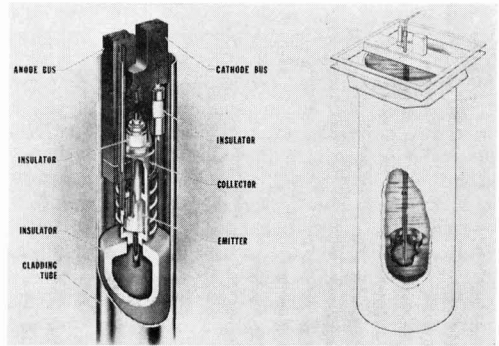


Fig. 5. Cutaway view of cesium cell and reactor

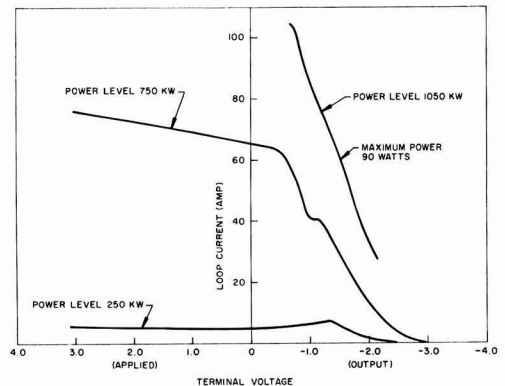


Fig. 6. Cell characteristics at 250, 750, and 1050 kw reactor power levels.

Stainless steel cooling coils were soldered to the outside of the copper anode and bus bars to keep the parts at the appropriate temperatures. Dowtherm was used as the coolant. The cesium source was located in copper tubing attached to the bottom of the anode. No provision was made to vary independently the anode temperature and the temperature of the cesium source. Thermocouples were used to monitor the anode temperature, the cesium-source temperature, and the temperature of the coolant before and after it passed through the cooling coils. From the rate of flow of the coolant and its entrance and exit temperatures, the total heat produced in the converter per unit time was calculated. The efficiency of conversion was calculated from the electric power output and the total rate of heat input. Figure 5 illustrates the arrangement of the converter assembly. Figure 6 shows the output current vs. output voltage curves for reactor power levels of 250 kw, 750 kw, and 1050 kw, respectively, at a cesium pressure of about 1 mm Hg. The optimum output for a reactor power of 1050 kw was 90 w (about 12 w/cm<sup>2</sup> of cathode surface area) at 60 amp and 1.5 v for a total power input of 900 w, and a cathode temperature of about 2000°C. The efficiency of conversion was thus 10%.

The converter was in the reactor for about ten days and operated intermittently (integral time of operation  $\approx 20$  hr) at various power levels. The carbide cathode and the niobium-to-carbide bond



stood up very well under a rapid rate of heating and cooling. Finally an electric short developed and the capsule was opened in the General Atomic hot cell. The whole cathode assembly was found to be intact, but an appreciable amount of vaporized material had collected on the anode surface. The condensate was dark and uneven, and it flaked off at certain places; this could have caused the electric short. The thermal loss by radiation from the cathode to the anode would have been much less and the efficiency of conversion would have been much higher if there had been no condensate and if the anode surface had retained its original mirror finish. These observations further illustrate the important role played by vaporization and condensation in the performance of the cesium thermionic converters.

Manuscript received May 26, 1961. This work was partially supported by the Rocky Mountain-Pacific Nuclear Research Group and by the San Diego Gas and Electric Company.

Any discussion of this paper will appear in a Discussion Section to be published in the June 1962 JOURNAL.

#### REFERENCES

1. R. W. Pidd, G. M. Grover, E. W. Salmi, D. J. Roehling, and G. F. Erickson, *J. Appl. Phys.*, **30**, 1861 (1959).
2. V. C. Wilson, American Rocket Society Conference on Space Power Systems, Preprint 1282-60, September 1960.
3. V. C. Wilson, *J. Appl. Phys.*, **30**, 475 (1959).
4. K. G. Hernquist, M. Kanefsky, and F. H. Norman, *RCA Review*, **19**, 244 (1958).
5. R. L. Hirsch and N. Razor, "Preliminary Design of a Reactor-Thermionic Space Power Plant," North American Aviation, Report NAA-SR-MEMO-5056, March 1960.
6. N. Razor, American Rocket Society Conference on Space Power Systems, Preprint 1283-60, September 1960.
7. R. W. Pidd, G. M. Grover, D. J. Roehling, E. W. Salmi, J. D. Farr, N. H. Krikorian, and W. G. Witteman, *J. Appl. Phys.*, **30**, 1575 (1959).
8. Quarterly Status Report of LASL Plasma Thermocouple Development Program, Report LAMS-2333, June, 1959.
9. G. M. Grover, *Nucleonics*, **17**, [7], 54 (1959).
10. R. C. Howard, Ling Yang, H. L. Garvin, and F. D. Carpenter, American Rocket Society Conference on Space Power Systems, Preprint 1287-60, September 1960.
11. M. Hoch, P. G. Blackburn, D. P. Dingley, and H. C. Johnston, *J. Phys. Chem.*, **59**, 97 (1955).
12. B. D. Pollock, "Vaporization of Zirconium Carbide," North American Aviation, Report NAA-SR-2124, 1957.
13. W. G. Witteman, J. M. Leitnaker, and M. G. Bowman, "Studies within the System UC-UC<sub>2</sub>," Uranium Carbide Conference, Oak Ridge National Laboratory, December 1960.
14. M. G. Bowman, American Rocket Society Conference on Space Power Systems, Preprint 1286-60, September 1960.
15. Louis Silverman, The High Temperature Chemical Reactivities of the Uranium Carbides, North American Aviation, Report NAA-SR-MEMO-4269, August 1959.
16. P. Wagner and S. R. Coriell, *Rev. Sci. Inst.*, **30**, 937 (1959).
17. Ling Yang, F. D. Carpenter, and H. E. Shoemaker, To be published.
18. "Progress in Carbide Fuels," NASA Research Program on Compatibility of Uranium Monocarbide, Second AEC Uranium Carbide Meeting at Battelle Memorial Institute, March 22 and 23, 1960, TID-7589, April, 1960.
19. Quarterly Status Report of LASL Plasma Thermocouple Development Program, Report LAMS-2396, December 1959.
20. F. A. Rough and W. Chubb, Editors, *An Evaluation of Data on Nuclear Carbides*, Battelle Memorial Institute, Report BMI-1441, May 1960.
21. L. M. Litz, "Graphite, Carbide, Nitride, and Sulfide Refractories," Asilomar Conference on High Temperature Technology, 1959, p. 134.
22. P. Schwartzkopf and R. Kieffer, "Refractory Hard Metals," Macmillan Co., New York (1953).
23. I. E. Campbell, Editor, "High Temperature Technology," John Wiley & Sons, Inc., New York (1956).
24. R. O. Elliott and C. P. Kempter, *J. Phys. Chem.*, **62**, 630 (1958).
25. W. B. Wilson, *J. Am. Ceram. Soc.*, **43**, 77 (1960).
26. C. A. Smith and F. A. Rough, *Nuclear Sci. and Eng.*, **6**, 391 (1959).
27. A. C. Secrest, Jr., E. L. Foster, and R. F. Dickerson, Preparation and Properties of Uranium Monocarbide Castings, Battelle Memorial Institute, Report BMI-1309, 1959.
28. A. Boettcher and G. Schneider, "Some Properties of Uranium Monocarbide," Proceedings of Second United Nations International Conference on the Peaceful Uses of Atomic Energy, Geneva, Vol. 6, p. 561, P/964, 1958.
29. C. A. Smith and F. A. Rough, Properties of Uranium Monocarbide, North American Aviation, Report NAA-SR-3625, June 1959.
30. N. V. Kolomoets, V. S. Neshpor, G. V. Samsonov, and S. A. Semenkovich, *Zhur. Tekh. Fiz.*, **28**, 2382 (1958).
31. G. V. Samsonov and V. P. Latisheva, *Fiz. Metal i Metalloved.*, *Akad. Nauk, USSR Ural Filial*, **2**, 309 (1956); translation AEC-tr-3321.
32. E. J. Zeilberger, Lecture Series on Materials for Missiles and Spacecraft, Lecture No. 9, University of California, LaJolla, 1960.
33. Quarterly Status Report of LASL Plasma Thermocouple Development Program, Report LAMS-2423, March 1960.
34. Quarterly Status Report of the LASL Plasma Thermocouple Development Program, Report LAMS-2473, September 1960.
35. Quarterly Status Report of LASL Plasma Thermocouple Development Program, Report LAMS-2447, June 1960.



## Nominations for Honors and Awards of The Electrochemical Society

The Honors and Awards Committee, in planning its work for the coming year, reminds the membership that their suggestions for honors and awards are solicited by the Committee. Please note the following:

### Honorary Members

*Bylaws, Article X, Section 3.*—“The Honors and Awards Committee shall make recommendations to the Board of Directors for Honorary Membership in the Society of individuals who, in the opinion of the Committee, have made valuable contributions to electrochemistry or who deserve special recognition by the Society.”

*Constitution, Article II, Section 4.*—“Honorary Members shall be those individuals who, by reason of valuable contributions to electrochemistry, deserve special recognition by the Society.”

Honorary Members are as follows:

Paul J. Kruesi  
Oliver W. Brown  
John W. Marden  
William Blum  
George W. Heise  
Frank C. Mathers  
Robert M. Burns

The number of Honorary Members is limited to ten.

Nominations must be accompanied by nine copies of a suitable biography setting forth the qualifications of the nominee.

### Acheson Medal Award

The Acheson Award can be made no oftener than every two years. The next opportunity for the Society to so honor someone is at the Boston Meeting in the fall of 1962.

The Honors and Awards Committee is charged by the Bylaws to recommend a selection to the Board. The Rules adopted by the Society, amended as of March 3, 1949, require that the Award shall be made without distinction on account of sex, citizenship, race, or residence.

In addition to the above, with regard to the selection, these Rules have the following provisos:

1. Nominations shall be accepted, also, from the membership at large. Announcement to this effect shall be made by the Secretary through the *JOURNAL* of The Electrochemical Society as promptly as possible after the appointment of the Committee, together with such instructions taken from these Rules as the Secretary may consider necessary for the guidance of the membership.

2. All nominations, whether made by a member of the Nominating Committee or by any other member of the Society, must be accompanied by a full record of qualifications of the nominee for the Award. Such supporting documents from friends of the candidate or from his organization shall be in order.

3. The nominator must assume the responsibility for providing the Chairman of the Nominating Committee with nine copies of the supporting documents, one for each member.

It is desired that such suggestions be in the hands of the Chairman *not later than February 1, 1962.*

Following is a list of Acheson Medalists since the Award was founded:

Edward G. Acheson\*—1929  
Edwin F. Northrup\*—1931  
Colin G. Fink\*—1933  
Frank J. Tone\*—1935  
Frederick M. Becket\*—1937  
Francis C. Frary—1939  
Charles F. Burgess\*—1942  
William Blum—1944  
H. Jermain Creighton—1946  
Duncan A. MacInnes—1948  
George W. Vinal—1951  
John W. Marden—1953  
George W. Heise—1954  
Robert M. Burns—1956  
William J. Kroll—1958  
Henry B. Linford—1960

\* Deceased.

Please address all nominations on both of the above subjects to the Chairman of the Honors and Awards Committee, Hans Thurnauer, Minnesota Mining & Manufacturing Co., Central Research Labs., 2301 Hudson Rd., St. Paul 19, Minn.

## Brief Communications

The *JOURNAL* accepts short technical reports having unusual importance or timely interest, where speed of publication is a consideration. The communication may summarize results of important research justifying announcement before such time as a more detailed manuscript can be published. Consideration also will be given to reports of significant unfinished research which the author cannot pursue further, but the results of which are of potential use to others. Comments on papers already published in the *JOURNAL* should be reserved for the Discussion Section published biannually.

*Submit communications in triplicate, typewritten double-spaced, to the Editor, Journal of The Electrochemical Society, 1860 Broadway, New York 23, N. Y.*



## Book Reviews



**Electro-Erosion Machining of Metals**, by A. L. Livshits. Translated from the Russian by E. Bishop; edited by R. S. Bennett. Published in association with the Dept. of Scientific and Industrial Research by Butterworths Inc., London, 1960. XI + 115 pages. \$5.75.

This recent translation of a book first published in Moscow in 1957 covers work accomplished with the direct use of electrical discharges for the machining of metals. This technique eliminates the necessity for the conventional conversion of electrical to mechanical energy.

Of the several electro-erosion processes, the U.S.S.R. has shown a particular interest in electro-spark machining. In essence, this process involves the maintenance of a gap between electrodes submerged in a dielectric fluid across which current pulses are generated by the repeated charge and discharge of a parallel capacitor. Metal removal is believed by the author to be achieved predominantly by the thermal effect of the current pulses. The process is an important supplement to conventional operations because of the ability to reproduce an electrode shape in metals regardless of hardness and thus execute a number of operations virtually impossible by mechanical means. The process has found wide use in this country, as well as in Russia, for sinking variously shaped holes into metals.

Fundamentally new techniques in circuitry were investigated in the early part of the last decade which led to development of the electro-pulse process. This process has received greatest emphasis in the book because of the manyfold increase in metal removal rate possible, and decreased tool and energy consumption. It is, perhaps, unfortunate that the ambiguous term "electro-pulse" should have been adopted since other electro-erosion processes also involve pulses of electric current. In reality, the process is differentiated from the electro-spark process mainly by the fact that the pulse waveform is independent of conditions in the erosion gap. Incidentally, the investigation of circuits for application to electro-erosion machining has led to development of a new field—"the electro-technology of low voltage unidirectional current pulses in the audio frequency range."

The chapter dealing with the evolution of the basic circuitry for the generation of current pulses is very

well presented, and charts classifying the various electro-erosion processes should be of great aid to the reader having limited familiarity with the processes. Detailed descriptions, diagrams, and electrical circuits of machines used in the Soviet Union for electro-erosion machining may be of interest to U.S. engineers concerned with this type of equipment.

Judging from the information available in the book, there is no reason to believe that American hole-piercing machines are inferior in effectiveness to Russian equipment. In fact, the comparatively low pulse frequencies used by the Russians indicate that inferior finishes are obtained. On the other hand, the electro-pulse process may offer lower relative tool wear. Accurate evaluation of the Russian processes is difficult owing to the fact that data on metal removal rate, surface finish, and relative tool wear usually are not all given for a particular machining setup.

There apparently has been little application of the spark and pulse processes to grinding operations. The anodo-mechanical method (usually classed as an electro-erosion process) is described for form-grinding of carbide-tipped tools. Electrolytic grinding is not discussed in the book because the electrochemical machining methods are considered to form a "self-contained branch of electrotechnology with their own specific features and governing principles."

The author has presented much valuable, hitherto unpublished, material on the technology and industrial applications of electro-erosion machining, which should spur widespread interest.

Fred Pearlstein  
University of Illinois  
Urbana, Ill.

**Reference Electrodes: Theory and Practice**. Edited by D. J. G. Ives and G. J. Janz. Published by Academic Press Inc., New York, N. Y., 1961. xi + 651 pages; \$20.00.

Seven of the 12 chapters in this book give comprehensive, detailed accounts of the principal electrodes and galvanic cells which have been used so widely in determining activities and other thermodynamic quantities in many electrolyte systems. The discussion ranges from the physical preparation of electrodes and cells, the precision and reliability found by different investigators, to theory and mechanism of the electrode process. Every effort is made to deduce the reasons for the good behavior of some electrodes—reversible and easily reproducible—and the poor behavior of others. These chapters include the hydrogen electrode, the mercury-mercurous salt electrodes, the silver-silver halide electrodes, the glass electrode, the quinhydrone and related electrodes, oxide-oxygen-sulfide electrodes, and electrodes reversible to sulfate ions.

Four chapters deal not so much with electrodes themselves as with their application in specific systems: systems containing membranes (the title of this chapter, Membrane Electrodes, may be compared with The Glass Electrode), nonaqueous and mixed solvents, electrodes in biological systems, and fused salts. Three fourths of the book was written by the two editors and G. J. Hills (Imperial College). The chapter on the glass electrode is by R. G. Bates (National Bureau of Standards); the one on biological systems by D. B. Cater and I. A. Silver (Cambridge); the one on fused salts by R. W. Laity (Princeton).

The first chapter (by the editors) devotes 70 pages to theory and general considerations: the nature of electrodes and galvanic cells, reversible and irreversible electrodes, conventions, experimental problems, instrumentation, etc. The authors prefer the Stockholm Convention with respect to signs and cell designations and give good reasons in detail. (Chemists will, no doubt, use "oxidation potentials" if they wish; we hope they will not call them "electrode potentials.") This chapter describes the extrapolation methods by which standard potentials are obtained and discusses the hypothetical reference states.

The chapters are very lucid and

### Notice to Members Re Voting Ballot

By now you have received your official voting ballot from Society Headquarters. If you have not already done so, please return the ballot by *December 15* so that your vote can be included in the final election count.

well written, and conform to a standard outline pattern. The book should be a valuable reference volume for students and more advanced workers, alike. Details range from the reasons why one textbook author gives 0.241 volt for the saturated calomel cell, another gives 0.246 volt, to a comprehensive discussion of the uniqueness of the hydrogen electrode. If more details are wanted, some 1900 literature references are given.

The discussions are confined to academic and theoretical research problems and do not cover, for example, the Cu-CuSO<sub>4</sub> half-cell as a reference electrode, the Ag-AgCl electrode as applied to cathodic protection, or the electrodes used in commercial rechargeable batteries (although the Pb-PbSO<sub>4</sub> and PbO<sub>2</sub>-PbSO<sub>4</sub> electrodes used in laboratory cells are described).

C. V. King  
New York University  
New York, N. Y.

**Electrolytic Dissociation**, by C. B. Monk. Published by Academic Press, Inc., London and New York, 1961. xii + 320 pages; \$10.00.

This book treats electrolyte solutions at a modern and fairly advanced level, with a minimum of elementary discussion, although there is some pretense of describing elementary experimental methods with refinements for precise work, and condensed derivations of the Debye-Hückel and other equations are given. The first chapters deal with conductance, transference numbers, interionic attraction theory, "reversible emf cells" and the determination of activity coefficients from emf, solubility, freezing points, and vapor pressures. There is a chapter on partial molal quantities and one on diffusion. The second part of the book, chapters 8-14, deals with incomplete dissociation and methods of studying it, including the more or less fringe methods such as polarography, Raman spectra, nuclear magnetic resonance, ion exchange resins, reaction kinetics.

In addition to the standard treatment of classical weak electrolytes, the difficult intermediate cases, and ion-pair formation at low dielectric constant, there is considerable emphasis on the electrolytes which show rather small deviations from the reasonable laws for complete dissociation, such as HIO<sub>3</sub>, MgSO<sub>4</sub>, AgNO<sub>3</sub>, LaFe(CN)<sub>6</sub> in dilute aqueous solution. Possible ion-pair formation to explain abnormal kinetic salt

effects is discussed; methods of treatment by the C. W. Davies school and by others are given. Complex formation and the determination of association constants are discussed. Many numerical examples are given throughout, and there is adequate reference to the literature where other examples and tabulations can be found. Several hundred references to research cited are given.

The book can be very useful to experts or semixperts in the field, but unfortunately loses much of its potential usefulness to research students and many others because it covers so much material in highly condensed form, uses so much mathematical symbolism in careless and confusing fashion (occasionally without definition), and has enough errors in text, numbers, and reference to make the reader distrustful. Printing costs are cut by writing complex equations on one line; running equations, numerical calculations, and results in the text; but, in concentrated doses, it wastes the reader's time and patience. An example of the general confusion: on pp. 32-33 the author decides to use  $N_f$ ,  $C_{\gamma}$ ,  $m_{\gamma}$  for mole fraction, molar and molal concentrations, and the corresponding activity coefficients. For some reason,  $f_{\pm}$  is defined in terms of twice the volume ionic strength. Throughout the book  $f_{\pm}$  is generally used with  $C$ , without assurance that it is different from  $\gamma_{\pm}$ ; in fact, one suspects that it isn't. In dilute solution, it does not matter; but the reader is entitled to know.  $C$  and  $c$  are used rather indiscriminately for volume concentration and, in the text,  $N$  and  $M$  often refer, apparently, to normality and molality (or molarity).

This reviewer suggests that the publishers withdraw the book from the market until the author can eliminate much of the confusion and correct some of the errors.

C. V. King  
New York University  
New York, N. Y.

### Progress in Dielectrics, Vol. III.

Edited by J. B. Birks and J. Hart. Published by John Wiley & Sons, Inc., New York, N. Y., 1961. 292 + vii pages; \$10.00.

The latest volume of this annual series will be useful to workers in dielectrics, not only as a summary of recent developments in selected areas of this field but also as a comprehensive treatment of these subjects and an excellent bibliography. Indeed, the implication of the title that the book deals with progress made over the last year or two is rather misleading, since the articles in it are quite exhaustive reviews which will make the book especially valuable both to established workers and newcomers to the field.

On the theoretical side, R. H. Cole covers theories of Dielectric Polarization and Relaxation from the Clausius-Mosotti theory up to the most recent ideas on dielectric relaxation in liquids, solids, and gases. This chapter is complemented appropriately by one by R. J. Meakins on Dielectric Absorption in Solids, in which specific chemical types are considered and interpretation of their dielectric behavior made in terms of molecular structure. Extending this theme still further is an article by J. B. Hasted on the Dielectric Properties of Water, which also treats the structure and properties of ice. The subject of dielectric breakdown is represented by a section on Breakdown in Solids by R. Stratton, dealing with theories of intrinsic breakdown, especially those of von Hippel and Fröhlich, and also treating briefly the problem of thermal breakdown.

The lead-off article in the book, Dielectric Wave-guides and Aerials, by D. G. Kiely, deals with a subject which will be new to most readers and should serve to stimulate interest in one of the less-common applications of dielectrics. The use of dielectric rods and tubes as wave guides and antennas is covered; unfortunately, no mention is made of the use of dielectric lenses for high-frequency propagation. This might be a worth-while subject to be considered for some future volume.

Other technological aspects of dielectrics are dealt with in a paper

### 1962 Bound Volume

Members and subscribers who wish to receive bound copies of Vol. 109 (for 1962) of the JOURNAL can receive the volume for the low, prepublication price of \$8.00 if their orders are received at Society Headquarters, 1860 Broadway, New York 23, N. Y., by January 1, 1962. After that date, members will be charged \$12.00, and nonmembers, including subscribers, \$24.00, subject to prior acceptance.

Bound volumes are *not* offered independently of JOURNAL subscription.

on Recent Developments in Cable Insulation by C. W. Hamilton, in which the properties of some of the newer rubbers and plastics used for wire and cable insulation are discussed.

D. Edelson  
Bell Telephone Labs., Inc.  
Murray Hill, N. J.

### Rare Metals Handbook, 2nd Ed.

Edited by Clifford A. Hampel. Published by Reinhold Publishing Corp., New York, N. Y., 1961. 715 pages; \$20.00.

This new edition of the book originally published in 1954 has been enlarged in area rather than thickness and includes six additional metals, thereby raising to 55 the number covered. The newly added elements are cesium, chromium, plutonium, rubidium, scandium, and yttrium.

The general format remains the same, but most of the chapters have been extensively rewritten and brought up to date. In many cases, this task has been facilitated by the tidal wave of information that accompanied the Geneva Conferences

on nuclear energy. In others, the beginnings of the frantic race to outer space is producing abnormally rapid development of once-rare materials. Indeed, one may question the rarity of molybdenum (production more than 50,000,000 pounds annually) or of cadmium (20,000,000 pounds annually). On the other hand, no space is given to potassium which is comparatively rare and currently is being developed as a working fluid in high-temperature engines. In fact, this Handbook covers most of the metals and semiconductors in the periodic table, excepting only the very common and the very rare.

Each chapter is not an exhaustive treatment of an individual element, but this book is an excellent "first place to look" for a brief survey of properties, production methods, statistics, and uses. In addition, nearly all of the bibliographies that terminate the chapters are extensive and modern. Like the earlier edition, this new version of the "Rare Metals Handbook" should have a place in every library on materials.

M. Kolodney  
City College  
New York, N. Y.

By action of the Board of Directors of the Society, all prospective members must include first year's dues with their applications for membership.

Also, please note that, if sponsors sign the application form itself, processing can be expedited considerably.

P. O. Box 500, Beaverton, Ore. (Electronics)

G. E. Evans, Union Carbide Consumer Products Co., P. O. Box 6116, Cleveland 1, Ohio (Battery)

D. R. Fewer, Texas Research & Electronic Corp.; Mail add: 6803 Chevy Chase Ave., Dallas 25, Texas (Electronics-Semiconductors, Theoretical Electrochemistry)

Jeremy Forten, Leesona Moos Labs.; Mail add: 308 E. 79 St., New York, N. Y. (Battery, Theoretical Electrochemistry)

C. J. Frosch, Bell Telephone Labs., Inc., Murray Hill, N. J. (Electronics-Semiconductors)

G. R. Frysinger, Arthur D. Little, Inc., 15 Acorn Park, Cambridge 40, Mass. (Theoretical Electrochemistry)

E. D. Ganz, Aerovox Corp.; Mail add: 51 Maple St., New Bedford, Mass. (Electric Insulation)

C. E. Gilbert, Continental Device Corp., 12515 Chadron Ave., Hawthorne, Calif.

B. S. Gourary, Westinghouse Research Labs., Beulah Rd., Churchill Boro., Pittsburgh 35, Pa. (Electronics)

K. F. Guenther, P. R. Mallory & Co., Inc.; Mail add: 3507 N. Parker Ave., Indianapolis 18, Ind. (Electric Insulation)

J. L. Jones, Reheis Co., Inc.; Mail add: 107 The Fellsway, Murray Hill, N. J. (Industrial Electrolytic)

H. E. Hintermann, Carl F. Norberg Research Center, Electric Storage Battery Co., 19 W. College Ave., Yardley, Pa. (Corrosion, Electrodeposition, Electronics-Semiconductors, Theoretical Electrochemistry)

H. E. Kern, Bell Telephone Labs., Inc., Rm. 1D-414, Murray Hill, N. J. (Electronics, Electrothermics & Metallurgy)

C. E. Kent, General Electric Co.; Mail add: 124 Mohawk Dr., Schenectady 3, N. Y. (Battery)

J. F. Knott, National Carbon Co.; Mail add: 564 Juniper Dr., Naperville, Ill. (Industrial Electrolytic)

J. W. Lathrop, Texas Instruments, Inc.; Mail add: 9904 Ontario Lane, Dallas 20, Texas (Electronics-Semiconductors)

## New Members

In September 1961, the following were elected to membership in The Electrochemical Society by the Admissions Committee:

### Active Members

L. L. Alt, General Electric Co., Advanced Semiconductor Lab.; Mail add: 417 S. Main St., North Syracuse, N. Y. (Electronics-Semiconductors)

R. V. Andes, Remington Rand Univac, 2750 W. Seventh Blvd., St. Paul 16, Minn. (Battery, Electrodeposition, Theoretical Electrochemistry)

H. C. Andrews, Texas Instruments, Inc.; Mail add: 10108 Harry Hines Blvd., Dallas 20, Texas (Electronics-Semiconductors)

J. A. Baumgartner, I.B.M. Corp.; Mail add: 41 Knevels Ave., Beacon, N. Y. (Electrodeposition, Electronics-Semiconductors)

H. B. Bell, Motorola, Inc., Semiconductor Products Div.; Mail add: 3252 E. Glenrosa, Phoenix 18, Ariz. (Electronics)

H. P. Bergman, Texas Instruments, Inc.; Mail add: 4520 Northaven Rd., Dallas 29, Texas (Electronics-Semiconductors)

Joan B. Berkowitz-Mattuck, Arthur

D. Little, Inc., 15 Acorn Park, Cambridge, Mass. (Corrosion)

A. E. Blakeslee, General Electric Co., Bldg. 3, Electronics Park, Syracuse, N. Y. (Electronics-Semiconductors)

R. G. Blanchette, General Instrument Corp.; Mail add: Apt. 4, 5 Richmond St., Woonsocket, R. I. (Electronics-Semiconductors and Luminescence)

E. H. Blevis, American Micro Devices Inc., 444 W. Camelback, Phoenix, Ariz. (Electronics-Semiconductors)

Gary Braunstein, Leesona Moos Labs.; Mail add: 219-30 Stewart Rd., Queens Village 27, N. Y. (Battery, Theoretical Electrochemistry)

E. G. Brush, General Electric Co., Research Labs.; Mail add: Riverside Place, Alplaus, N. Y. (Corrosion)

H. D. Cook, American Oil Co.; Mail add: 3128 Eder, Highland, Ind. (Theoretical Electrochemistry)

I. M. Croll, I.B.M. Corp., Research Center; Mail add: 116 Pierce Dr., Pleasantville, N. Y. (Electrodeposition)

M. J. Davis, Anchor Metal Co., Inc., 966 Meeker Ave., Brooklyn, N. Y. (Electronics-Semiconductors)

Jean F. Delord, Tektronix, Inc.,



- Saul Lederhandler, Micro State Electronics Corp.; Mail add: 14 Fleetwood Dr., Somerville, N. J. (Electronics—Semiconductors and Luminescence, Electrothermics & Metallurgy)
- R. H. Leet, American Oil Co., Research & Development Dept., Box 431, Whiting, Ind., (Theoretical Electrochemistry)
- M. C. Locke, Jr., Pittsburgh Plate Glass Co.; Mail add: 318 Glenmore, Corpus Christi, Texas (Industrial Electrolytic)
- A. H. Luxem, Texas Instruments, Inc.; Mail add: 13453 Shahan Dr., Dallas 34, Texas (Electronics—Semiconductors)
- G. T. Malloy, General Electric Co., Semiconductor Products Dept.; Mail add: 380 Mill St., Williamsville 21, N. Y. (Corrosion, Electronics)
- H. B. Mark, Jr., Dept. of Chemistry, University of North Carolina, Chapel Hill, N. C. (Battery)
- R. W. McJones, Cummins Engine Co.; Mail add: 319-19th St., Columbus, Ind. (Battery)
- R. P. McManus, Texas Instruments, Inc., Components Div.; Mail add: 1300 Provincetown Lane, Richardson, Texas (Industrial Electrolytic)
- R. E. Meyer, Oak Ridge National Lab., P. O. Box X, Oak Ridge, Tenn. (Theoretical Electrochemistry)

### Notice to Subscribers

Your subscription to the JOURNAL of The Electrochemical Society will expire on December 31, 1961. Avoid missing any issue. Send us your remittance now in the amount of \$24.00 for your 1962 subscription. (Subscribers located outside the United States must add \$1.50 to the subscription price for postage, and payment must be made by Money Order or New York draft, not local check.) An expiration notice has been mailed to all subscribers.

A bound volume of the 1962 JOURNALS can be obtained at the prepublication price of \$8.00 by adding this amount to your remittance. However, no orders will be accepted at this rate after January 1, 1962, when the price will be increased to \$24.00 subject to prior acceptance. Bound volumes are not offered independently of your JOURNAL subscription.

- F. F. Mikus, Sylvania Electric Products; Mail add: 305 Bridge St., Towanda, Pa. (Electronics—Luminescence)
- J. S. Mohl, Atomics International, Div. of North American Aviation, Inc.; Mail add: 10514 National Blvd., Los Angeles 34, Calif. (Battery, Electro-Organic, Electrothermics & Metallurgy, Theoretical Electrochemistry)
- W. C. Myers, Tektronix, Inc.; Mail add: 565 N.W. 257th, Hillsboro, Ore. (Electronics—Semiconductors)
- D. R. Palmer, Minneapolis-Honeywell Regulator Co.; Mail Station No. 261, 2747 Fourth Ave., S., Minneapolis 8, Minn. (Electronics—Semiconductors)
- F. A. Posey, Oak Ridge National Lab., P.O. Box X, Oak Ridge, Tenn. (Theoretical Electrochemistry)
- R. D. Richardson, Cleveite Transistor Corp.; Mail add: 20 Hudson Rd., Lexington 73, Mass. (Electronics)
- F. J. Riel, Narmco Industries, Inc., Research & Development Div.; Mail add: 1877 Lyndon Rd., San Diego, Calif. (Battery)
- Boshin Ro, Musashi Institute of Technology, 1-2334, Tamagawa Todoroki, Setagaya, Tokyo, Japan (Corrosion, Electrodeposition)
- A. B. Scott, Dept. of Chemistry, Oregon State University, Corvallis, Ore. (Theoretical Electrochemistry)
- J. E. Sandor, Fairchild Semiconductor Corp.; Mail add: 1010 Noel Dr., Apt. 17, Menlo Park, Calif. (Electronics)
- G. A. Shirn, Sprague Electric Co.; Mail add: 1 Jamieson Hts., Williamstown, Mass. (Electronics—Semiconductors)
- R. F. Stewart, Texas Research & Electronic Corp., 4439 Greenville Ave., Dallas 9, Texas (Electronics)
- P. P. Werlein, Ray-O-Vac Co.; Mail add: 1645 Sunfield St., Madison 4, Wis. (Battery)
- R. L. Yeakley, Texas Instruments, Inc., P. O. Box 5012, Dallas, Texas (Electronics—Semiconductors)

### Associate Member

- Aaron Weisstuch, Yardney Electric Corp.; Mail add: 2670 E. 7 St., Brooklyn 35, N. Y. (Battery)

### Student Members

- Gerald Aronowitz, University of Texas; Mail add: 2610 Manor Rd., Austin, Texas (Theoretical Electrochemistry)
- B. D. Guenther, University of Missouri; Mail add: 310 N. 9 St., Columbia, Mo. (Electronics—Semiconductors)

### Notice to Members and Subscribers (Re Changes of Address)

To insure receipt of each issue of the JOURNAL, please be sure to give us your old address, as well as your new one, when you move. Our records are filed by states and cities, not by individual names. The Post Office does not forward magazines.

We should have this information by the 16th of the month to avoid delays in receipt of the next issue.

- R. B. Leonard, Rensselaer Polytechnic Institute; Mail add: 25 Belle Ave., Troy, N. Y. (Corrosion, Electronics—Semiconductors)
- D. F. O'Kane, University of Michigan; Mail add: P. O. Box 88, Ann Arbor, Mich. (Electronics)

### Reinstatement to Active Membership

- Leonard Edwards, Metal & Thermat Corp., Box 471, Rahway, N. J. (Electrodeposition, Theoretical Electrochemistry)

### Transfer from Active Sustaining to Active Membership

- R. A. Peak, Transiron, Inc.; Mail add: 22 Ewell Ave., Lexington 73, Mass. (Electronics—Semiconductors)

## Division News

### Electric Insulation Symposium, Spring 1962

The Electric Insulation Division plans to hold symposia at the 121st Meeting of The Electrochemical Society to be held at the Statler Hilton Hotel in Los Angeles, Calif., during the period May 6-10, 1962. Plans are being made for sessions to be held on the following subjects:

(A) Ceramics and Integrated Circuits. Session Chairman: B. R. Eichbaum, Aeronautics, Newport Beach, Calif.

(B) Thin Film Dielectrics and Electrolytic Capacitors. Session Chairmen: C. C. Houtz, Bell Telephone Labs., Inc., Murray Hill, N. J., and R. A. Ruscetta, General Electric Co., Irmo, S. C.

(C) Reliability. Session Chairman: Hans M. Wagner, Lockheed Aircraft Corp., 3251 Hanover St., Palo Alto, Calif.

(D) Paper. Session Chairman: E. D. Eich, Anaconda Wire & Cable Co., Hastings-on-Hudson, N. Y.

As in the past, all that is required for presentation at an Electric Insulation session is that a 75-word abstract be in the hands of the Session Chairman by December 15, 1961.

B. R. Eichbaum,  
Secretary-Treasurer

### E & M Symposium, Spring 1962

As a part of the Spring 1962 Meeting of The Electrochemical Society, to be held in Los Angeles, Calif., May 6-10, the Electrothermics and Metallurgy Division will hold a symposium on "Thermodynamics and Kinetics of Gas-Condensed Phase Reactions at High Temperatures."

### Electronics Symposia, Spring 1962

For the 1962 Los Angeles Spring Meeting of The Electrochemical Society, the Electronics Division is planning four symposia. In addition to the usual sessions on Luminescence and Semiconductors, symposia on Optical Masers and on Nonconventional Electron Emitters are to be scheduled.

The Program Chairmen for these symposia are:

**Luminescence**—Dr. Henry Ivey, Research Dept., Lamp Div., Westinghouse Electric Corp., Bloomfield, N. J.

**Semiconductors**—Dr. Roger Newman, Sperry Rand Corp., Sudbury, Mass.

**Optical Masers**—Dr. Joseph Birman, General Telephone & Electronics Labs., Bayside Labs., Bayside 60, N. Y.

**Nonconventional Electron Emitters**—Dr. Charles P. Marsden, Section 14.2, National Bureau of Standards, Washington 25, D. C.

In order for a paper to be accepted in the first three of these symposia, triplicate copies of a 75-word abstract should be sent direct to the above Program Chairmen and be in their hands not later than December 15, 1961. Because of special planning required for the symposium on Nonconventional Electron Emitters, 75-word abstracts were required by October 15, 1961.

Papers will be accepted for the above symposia only with the understanding that a 1000-word extended abstract will be submitted in time for inclusion in the Electronics Division Abstracts booklet. Deadline date for extended abstracts is January 15, 1962. It is expected that this booklet will be available about one month prior to the meeting. In preparing the enlarged abstract the following points should be observed.

1. Type abstracts double-spaced on 8½ in. x 11 in. paper. Send at least one original copy.
2. Try to restrict the abstract to approximately 1000 words.
3. Keep the number of drawings or photographs to a minimum.
4. If you must submit photographs, submit only glossy prints with sharp detail. Size is preferably 5 in. x 7 in.
5. Drawings preferably should be made on tracing cloth, 8½ in. x 11 in., with India ink. Do not use larger size. Do not send carbon copy or Ditto drawings, since these would have to be redrawn.

In addition to the above special requirements, the usual Society regulation will be observed that no paper will be placed on the program

unless one of the authors or a duly qualified person designated by the authors has agreed to present it in person.

## Announcements from Publishers

"Protection of Refractory Metals for High Temperature Service. Progress Report 2—October 1, 1960—Durability of the Zinc-Base Coating for Niobium," B. F. Brown and others, U. S. Naval Research Lab., Jan. 1961. Report PB 171 159; \* 75 cents.

"Power Supplies—An ASTIA Report Bibliography," Jan. 1961. Selective Bibliography PB 171 689; \* 313 pages; \$5.00.

"Corrosion of Some Reactor Materials in Dilute Phosphoric Acid," April 1961. AEC Report ANL-6206; \* 20 pages; 50 cents.

"Film Growth on Aluminum in High-Temperature Water," April 1961. AEC Report ANL-6230; \* 25 pages; 50 cents.

"A Contribution to the Study of the Reduction of UF<sub>6</sub> to Uranium Metal," Feb. 1961. AEC Report ANL-6317; \* 38 pages; \$1.00.

"Properties of Lithium Hydride II—Lithium Hydride Corrosion Studies: 19-9DL Alloy," April 1961. AEC Report APEX-586; \* 41 pages; \$1.00.

\* Order from Office of Technical Services, Business and Defense Services Administration, U.S. Dept. of Commerce, Washington 25, D. C.

## Manuscripts and Abstracts for Spring 1962 Meeting

Papers are now being solicited for the Spring Meeting of the Society, to be held at the Statler Hilton Hotel in Los Angeles, Calif., May 6, 7, 8, 9, and 10, 1962. Technical Sessions probably will be scheduled on Electric Insulation (including sessions on Ceramics and Integrated Circuits, Thin Film Dielectrics and Electrolytic Capacitors, Reliability, and Paper), Electronics (including Luminescence, Semiconductors, Optical Masers, and Nonconventional Electron Emitters), Electrothermics and Metallurgy (including a Symposium on Thermodynamics and Kinetics of Gas-Condensed Phase Reactions at High Temperatures), Industrial Electrolytics, and Theoretical Electrochemistry.

To be considered for this meeting, triplicate copies of abstracts (*not exceeding 75 words in length*) must be received at Society Headquarters, 1860 Broadway, New York 23, N. Y., *not later than December 15, 1961. Please indicate on abstract for which Division's symposium the paper is to be scheduled and underline the name of the author who will present the paper.* No paper will be placed on the program unless one of the authors, or a qualified person designated by the authors, has agreed to present it in person. An author who wishes his paper considered for publication in the JOURNAL should send triplicate copies of the manuscript to the Managing Editor of the JOURNAL, 1860 Broadway, New York 23, N. Y.

Presentation of a paper at a technical meeting of the Society does not guarantee publication in the JOURNAL. However, all papers so presented become the property of The Electrochemical Society, and may not be published elsewhere, either in whole or in part, unless permission for release is requested of and granted by the Editor. Papers already published elsewhere, or submitted for publication elsewhere, are not acceptable for oral presentation except on invitation by a Divisional program Chairman.

"Progress in Very High Pressure Research." Edited by F. P. Bundy, W. R. Hibbard, Jr., and H. M. Strong. Published by John Wiley & Sons, Inc., New York, N. Y., 1961. XIX + 314 pages; \$12.00.

This volume contains the papers and discussions of an International Conference, held in June 1960. The editors have attempted to present the book as rapidly as possible, in order to stimulate and guide new work. Much of the data was hitherto unpublished. JOURNAL readers may be interested in the articles entitled "Research and Development on the Effects of High Pressure and Temperature on Various Elements and Binary Alloys," "State of Matter at High Pressure," "Resistance and Thermal Gap Measurements to 400,000 Atmospheres," "Properties of Semiconductors at High Pressures," "An Accurate Determination of the Equation of State by Ultrasonic Measurements," "Effect of Pressure on EMF of Thermocouples," "Effect of Hydrostatic Pressure up to 8000 Atm on the Self-Diffusion Rate in Silver Single Crystals," "Effects of Pressure on Magnetic Interactions in Metals," and "Investigations in U.S.S.R. in the Area of the Physics of High Pressures."

"Perchlorates — Their Properties, Manufacture, and Uses," ACS Monograph No. 146. Edited by Joseph C. Schumacher. Published by Reinhold Publishing Corp., New York, N. Y., 1960. XII + 257 pages; \$8.75.

JOURNAL readers will be interested mostly in the 36-page section on safety in handling these compounds. Tables of data and references are as late as 1958.

"Organo-Metallic Compounds, 2nd Ed.," by G. E. Coates. Published by John Wiley & Sons, Inc., New

York, N. Y., 1961. XIII + 366 pages; \$7.50.

This is a description of the preparation and of some of the properties of the organic compounds of each of the metals, taken by groups in the periodic table. The book is directed at the organic synthesist.

"Silicones." Edited by S. Fordham. Published by Philosophical Library, Inc., New York, N. Y., 1961. XI + 252 pages; \$10.00.

The first half of the book is an outline of the chemistry and structure

of the silicones. The second half is a discussion of possible applications.

"Interfacial Phenomena," by J. T. Davies and E. K. Rideal. Published by Academic Press, Inc., New York, N. Y., 1961. xiii + 474 pages; \$14.00.

"Solid State Physics in Electronics and Telecommunications: Proceedings of an International Conference Held in Brussels, June 2-7, 1958. Vol. III, Part I. Magnetic and Optical Properties." Edited by M. Desirant and J. L. Michiels. Pub-



## ADVANCED SOLID STATE RESEARCH & DEVELOPMENT

Senior scientists and engineers are needed to fill new positions in our rapidly expanding research and development laboratories near San Francisco. Our broadening interests have created challenging positions for individuals with significant backgrounds in the following fields:

SURFACE PHYSICS AND CHEMISTRY  
ELECTROCHEMISTRY  
ELECTRON MICROSCOPY  
MAGNETIC THIN FILMS  
EVAPORATED CIRCUITRY  
SEMICONDUCTOR MATERIALS  
ELECTRO-OPTICS  
ADVANCED CIRCUIT DEVELOPMENT  
MICROWAVE PHYSICS

A Ph.D. Degree or commensurate experience is especially desirable.

Applicants are invited to send detailed resumes, including salary history and requirements, to Mr. Donald Palmer. Palo Alto interviews for qualified applicants will be arranged from anywhere in the United States. All inquiries strictly confidential and acknowledged promptly. All qualified applicants will be considered regardless of race, creed, color or national origin.

# FAIRCHILD

## SEMICONDUCTOR

844 CHARLESTON ROAD • PALO ALTO, CALIFORNIA

### Advertiser's Index

Anaconda American Brass Co.	242C
Bell Telephone Laboratories, Inc.	241C
Eagle-Picher Co.	243C
Fairchild Semiconductor Corp.	251C
Great Lakes Carbon Corp., Electrode Div.	Cover 2
Magna Products, Inc.	252C
Olin Mathieson Chemical Corp.	252C
Sigma Press, Publishers	252C

lished by Academic Press, Inc., New York, N. Y., 1960. 557 pages; \$12.00.

"The Training, Placement, and Utilization of Engineers and Technicians in the Soviet Union." Report on the recent achievements and future goals of the Soviet Union in the field of engineering and engineering education and manpower utilization. Published by Engineers Joint Council, Inc., New York, N. Y., 1961. 112 pages. Available in limited numbers for \$1.00.

"Investing in Scientific Progress," ten-year forecast of the nation's science needs. Published by National Science Foundation, 1951 Constitution Ave. N.W., Washington 25, D. C.

#### Patent Digests Available

Patent Intelligence File Co., 187 Olive St., New Haven 11, Conn., now supplies Patent Digests as published in the Official Gazette. The annual cost on current-year patents averages under \$20.00 per subject. Five-

ten-, and seventeen-year period books on back-year patents for any of the 363 subjects are available with easy-to-use indexes.

A free brochure giving further details on the Patent Digest Service is available.

#### Employment Situations

Please address replies to box shown, c/o The Electrochemical Society, 1860 Broadway, New York 23, N. Y.

##### Position Wanted

**Chemical Engineer, B.S.**—Fifteen years' industrial experience—12 years of electrolytic background in development and production work. Supervisory experience. Married, family, 39. Reply to Box No. 372.

##### Position Available

**Research Chemist**—Opening in Magnetic Tape Division for experienced man in organic chemistry. E. M. Sears, Box 62, Bloomington, Ind.

##### Research Scientists

**Electrochemists**—experienced in the study of electrode kinetics chronopotentiometry or polarography and an understanding of the basic theories involved.

**Physical Chemists**—with strong academic background in thermodynamics and kinetics, and an interest in surface chemistry or energy transfer mechanisms.

There are research positions concerned with the study of basic phenomena involved in life processes.

Please send resume to

Mr. J. E. Rissman

Magna Products, Inc.

Research & Development Division

1001 South East Street

Anaheim, California

Affiliate of Thompson, Ramo-Wooldrige, Inc.

This is an equal opportunity employer.

--- an English Translation of

# ELECTROCHEMISTRY OF FUSED SALTS

by  
**IU. K. Delimarskii and B. F. Markov**

is at the typesetters and will be ready for publication December 15, 1961.

This comprehensive monograph published in Moscow in 1960 contains in its bibliographies references to literature as late as 1959. Not to be confused with collections of individual papers previously published and translated, this book offers not only an invaluable introduction to the extensive and significant work done in Russia in recent years in the field of fused salts, but also, since the coverage is general, it includes the major contributions in the field wherever made and published. The translation will contain approximately 375 pages including an alphabetical index of authors prepared by the editor of the translation. Hardbound.

#### ONE-MONTH PRE-PUBLICATION OFFER

Prepublication orders received before December 10, 1961—\$10.00 per copy; after that date, \$12.50 per copy. Postage and handling charges paid by publisher on prepaid orders. 25¢ additional charge on orders to be billed.



**THE SIGMA PRESS, PUBLISHERS**  
2140 K Street NW  
Washington 7, D. C.

**Olin**  
offers

opportunity

**SURFACE CHEMISTS  
or ELECTRO CHEMISTS**

Surface and Electrochemical reactions affecting the kinetics of general, localized and stress corrosion processes. Electrochemical kinetics, adsorption and oxide film structure investigations related to finishing processes. Fully-equipped modern laboratory devoted to research and development on Aluminum and Copper Alloys.

Send resume in confidence to L. C. Clancy

**OLIN MATHIESON  
CHEMICAL CORP.**

275 Winchester Ave., New Haven, Conn.

# The Electrochemical Society

## Patron Members

Aluminum Co. of Canada, Ltd.,  
Montreal, Que., Canada  
International Nickel Co., Inc.,  
New York, N. Y.  
Olin Mathieson Chemical Corp.,  
Chemicals Div., Industrial Chemicals  
Development Dept., Niagara Falls, N. Y.  
Union Carbide Corp.  
Divisions:  
Union Carbide Metals Co.,  
New York, N. Y.  
National Carbon Co., New York, N. Y.  
Westinghouse Electric Corp., Pittsburgh, Pa.

## Sustaining Members

Air Reduction Co., Inc.,  
New York, N. Y.  
Ajax Electro Metallurgical Corp.,  
Philadelphia, Pa.  
Allen-Bradley Co., Milwaukee, Wis.  
Allied Chemical Corp.  
Solvay Process Div., Syracuse, N. Y.  
General Chemical Div., Morristown, N. J.  
Alloy Steel Products Co., Inc., Linden, N. J.  
Aluminum Co. of America,  
New Kensington, Pa.  
American Metal Climax, Inc.,  
New York, N. Y.  
American Potash & Chemical Corp.,  
Los Angeles, Calif. (2 memberships)  
American Smelting and Refining Co.,  
South Plainfield, N. J.  
American Zinc Co. of Illinois,  
East St. Louis, Ill.  
American Zinc, Lead & Smelting Co.,  
St. Louis, Mo.  
American Zinc Oxide Co., Columbus, Ohio  
M. Ames Chemical Works, Inc.,  
Glens Falls, N. Y.  
Armco Steel Corp., Middletown, Ohio  
Basic Inc., Maple Grove, Ohio  
Bell Telephone Laboratories, Inc.,  
New York, N. Y. (2 memberships)  
Bethlehem Steel Co., Bethlehem, Pa.  
(2 memberships)  
Boeing Airplane Co., Seattle, Wash.  
Burgess Battery Co., Freeport, Ill.  
(4 memberships)  
Canadian Industries Ltd., Montreal,  
Que., Canada

Carborundum Co., Niagara Falls, N. Y.  
Catalyst Research Corp., Baltimore, Md.  
Consolidated Mining & Smelting Co. of  
Canada, Ltd., Trail, B. C., Canada  
(2 memberships)  
Continental Can Co., Inc., Chicago, Ill.  
Cooper Metallurgical Associates, Cleveland,  
Ohio  
Corning Glass Works, Corning, N. Y.  
Diamond Alkali Co., Painesville, Ohio  
Dow Chemical Co., Midland, Mich.  
Wilbur B. Driver Co., Newark, N. J.  
(2 memberships)  
E. I. du Pont de Nemours & Co., Inc.,  
Wilmington, Del.  
Eagle-Picher Co., Chemical and Metals Div.,  
Joplin, Mo.  
Eastman Kodak Co., Rochester, N. Y.  
Thomas A. Edison Research Laboratory, Div.  
of McGraw-Edison Co., West Orange, N. J.  
Electric Auto-Lite Co., Toledo, Ohio  
C & D Division, Conshohocken, Pa.  
Electric Storage Battery Co., Yardley, Pa.  
Engelhard Industries, Inc., Newark, N. J.  
(2 memberships)  
The Eppley Laboratory, Inc., Newport, R. I.  
(2 memberships)  
Exmet Corp., Tuckahoe, N. Y.  
Fairchild Semiconductor Corp., Palo Alto,  
Calif.  
Food Machinery & Chemical Corp.  
Becco Chemical Div., Buffalo, N. Y.  
Westvaco Chlor-Alkali Div., South  
Charleston, W. Va.  
Foote Mineral Co., Paoli, Pa.  
Ford Motor Co., Dearborn, Mich.  
General Electric Co., Schenectady, N. Y.  
Chemistry & Chemical Engineering  
Component, General Engineering  
Laboratory  
Chemistry Research Dept.  
General Physics Research Dept.  
Metallurgy & Ceramics Research Dept.  
Aircraft Accessory Turbine Dept.,  
West Lynn, Mass.  
General Instrument Corp., Newark, N. J.  
General Motors Corp.  
Allison Div., Indianapolis, Ind.  
Delco-Remy Div., Anderson, Ind.  
Guide Lamp Div., Anderson, Ind.  
Research Laboratories Div., Warren, Mich.  
General Telephone & Electronics  
Laboratories Inc., Bayside, N. Y.  
(2 memberships)  
Gillette Safety Razor Co., Boston, Mass.



(Sustaining Members cont'd)

- Globe-Union, Inc., Milwaukee, Wis.  
Gould-National Batteries, Inc.,  
Minneapolis, Minn.  
Grace Electronic Chemicals, Inc.,  
Baltimore, Md.  
Great Lakes Carbon Corp., New York, N. Y.  
Hanson-Van Winkle-Munning Co.,  
Matawan, N. J. (2 memberships)  
Harshaw Chemical Co., Cleveland, Ohio  
(2 memberships)  
Hercules Powder Co., Wilmington, Del.  
Hewlett-Packard Co., Palo Alto, Calif.  
Hill Cross Co., Inc., West New York, N. J.  
Hoffman Electronics Corp., Semiconductor  
Div., El Monte, Calif. (2 memberships)  
Hooker Chemical Corp., Niagara  
Falls, N. Y. (3 memberships)  
Hughes Aircraft Co., Culver City, Calif.  
International Business Machines Corp.,  
Yorktown Heights, N. Y.  
International Minerals & Chemical  
Corp., Skokie, Ill.  
ITT Federal Laboratories, Div. of  
International Telephone & Telegraph  
Corp., Nutley, N. J.  
Jones & Laughlin Steel Corp.,  
Pittsburgh, Pa.  
K. W. Battery Co., Skokie, Ill.  
Kaiser Aluminum & Chemical Corp.  
Div. of Chemical Research,  
Permanente, Calif.  
Div. of Metallurgical Research,  
Spokane, Wash.  
Kawecik Chemical Co., Boyertown, Pa.  
Kennecott Copper Corp., New York, N. Y.  
Leesona Moos Laboratories, Div. of Leesona  
Corp., Jamaica, N. Y.  
Libbey-Owens-Ford Glass Co., Toledo, Ohio  
Lockheed Aircraft Corp.,  
Missiles & Space Div., Sunnyvale, Calif.  
Mallinckrodt Chemical Works, St. Louis, Mo.  
P. R. Mallory & Co., Indianapolis, Ind.  
Merck & Co., Inc., Rahway, N. J.  
Metal & Thermit Corp., Detroit, Mich.  
Miles Chemical Co., Div. of Miles  
Laboratories, Inc., Elkhart, Ind.  
Minneapolis-Honeywell Regulator Co.,  
Minneapolis, Minn.  
Minnesota Mining & Manufacturing Co.,  
St. Paul, Minn.  
Monsanto Chemical Co., St. Louis, Mo.  
Motorola, Inc., Chicago, Ill.  
National Cash Register Co., Dayton, Ohio  
National Lead Co., New York, N. Y.  
National Research Corp., Cambridge, Mass.  
National Steel Corp., Weirton, W. Va.  
North American Aviation, Inc., Rocketdyne  
Div., Canoga Park, Calif.  
Northern Electric Co., Montreal, Que.,  
Canada  
Norjon Co., Worcester, Mass.  
Ovitrion Corp., Long Island City, N. Y.  
Peerless Roll Leaf Co., Inc., Union City, N. J.  
Pennsalt Chemicals Corp.,  
Philadelphia, Pa.  
Phelps Dodge Refining Corp., Maspeth, N. Y.  
Philco Corp., Research Div., Blue Bell, Pa.  
Philips Laboratories, Inc., Irvington-on-  
Hudson, N. Y.  
Pittsburgh Plate Glass Co., Chemical Div.,  
Pittsburgh, Pa.  
Potash Co. of America,  
Carlsbad, N. Mex.  
The Pure Oil Co., Research Center,  
Crystal Lake, Ill.  
Radio Corp. of America  
Tube Div., Harrison, N. J.  
RCA Victor Record Div., Indianapolis,  
Ind.  
Ray-O-Vac Co., Madison, Wis.  
Raytheon Co., Waltham, Mass.  
Remington Rand, Div. of Sperry Rand Corp.,  
New York, N. Y.  
Reynolds Metals Co., Richmond, Va.  
Rheem Semiconductor Corp.,  
Mountain View, Calif.  
Schering Corporation, Bloomfield, N. J.  
Shawinigan Chemicals Ltd., Montreal, Que.,  
Canada  
Speer Carbon Co.  
International Graphite & Electrode  
Div., St. Marys, Pa.  
Sprague Electric Co., North Adams, Mass.  
Stackpole Carbon Co., St. Marys, Pa.  
Stauffer Chemical Co., New York, N. Y.  
Tennessee Products & Chemical Corp.,  
Nashville, Tenn.  
Texas Instruments, Inc., Dallas, Texas  
Metals and Controls Corp.,  
Attleboro, Mass.  
Three Point One Four Corp., Yonkers, N. Y.  
Titanium Metals Corp. of America,  
Henderson, Nev.  
Tung-Sol Electric Inc.,  
Newark, N. J.  
Udylite Corp., Detroit, Mich.  
(4 memberships)  
United States Borax & Chemical Corp.,  
Los Angeles, Calif.  
Universal-Cyclops Steel Corp.,  
Bridgeville, Pa.  
Upjohn Co., Kalamazoo, Mich.  
U. S. Steel Corp., Pittsburgh, Pa.  
Victor Chemical Works, Chicago, Ill.  
Western Electric Co., Inc., Chicago, Ill.  
Wyandotte Chemicals Corp.,  
Wyandotte, Mich.  
Yardney Electric Corp., New York, N. Y.